

# AI-Based Federated Learning for 6G Mobile Networks

Lead Guest Editor: S. Vimal

Guest Editors: Danilo Pelusi, Shahid Mumtaz, and Alireza Souri





---

# **AI-Based Federated Learning for 6G Mobile Networks**

Wireless Communications and Mobile Computing

---

## **AI-Based Federated Learning for 6G Mobile Networks**

Lead Guest Editor: S. Vimal

Guest Editors: Danilo Pelusi, Shahid Mumtaz, and  
Alireza Souri




---


Copyright © 2021 Hindawi Limited. All rights reserved.

This is a special issue published in “Wireless Communications and Mobile Computing.” All articles are open access articles distributed under the Creative Commons Attribution License, which permits unrestricted use, distribution, and reproduction in any medium, provided the original work is properly cited.

# Chief Editor

Zhipeng Cai , USA

## Associate Editors

Ke Guan , China  
Jaime Lloret , Spain  
Maode Ma , Singapore

## Academic Editors

Muhammad Inam Abbasi, Malaysia  
Ghufran Ahmed , Pakistan  
Hamza Mohammed Ridha Al-Khafaji ,  
Iraq  
Abdullah Alamoodi , Malaysia  
Marica Amadeo, Italy  
Sandhya Aneja, USA  
Mohd Dilshad Ansari, India  
Eva Antonino-Daviu , Spain  
Mehmet Emin Aydin, United Kingdom  
Parameshchhari B. D. , India  
Kalapaveen Bagadi , India  
Ashish Bagwari , India  
Dr. Abdul Basit , Pakistan  
Alessandro Bazzi , Italy  
Zdenek Becvar , Czech Republic  
Nabil Benamar , Morocco  
Olivier Berder, France  
Petros S. Bithas, Greece  
Dario Bruneo , Italy  
Jun Cai, Canada  
Xuesong Cai, Denmark  
Gerardo Canfora , Italy  
Rolando Carrasco, United Kingdom  
Vicente Casares-Giner , Spain  
Brijesh Chaurasia, India  
Lin Chen , France  
Xianfu Chen , Finland  
Hui Cheng , United Kingdom  
Hsin-Hung Cho, Taiwan  
Ernestina Cianca , Italy  
Marta Cimitile , Italy  
Riccardo Colella , Italy  
Mario Collotta , Italy  
Massimo Condoluci , Sweden  
Antonino Crivello , Italy  
Antonio De Domenico , France  
Floriano De Rango , Italy







Antonio De la Oliva , Spain  
Margot Deruyck, Belgium  
Liang Dong , USA  
Praveen Kumar Donta, Austria  
Zhuojun Duan, USA  
Mohammed El-Hajjar , United Kingdom  
Oscar Esparza , Spain  
Maria Fazio , Italy  
Mauro Femminella , Italy  
Manuel Fernandez-Veiga , Spain  
Gianluigi Ferrari , Italy  
Luca Foschini , Italy  
Alexandros G. Fragkiadakis , Greece  
Ivan Ganchev , Bulgaria  
Óscar García, Spain  
Manuel García Sánchez , Spain  
L. J. García Villalba , Spain  
Miguel Garcia-Pineda , Spain  
Piedad Garrido , Spain  
Michele Girolami, Italy  
Mariusz Glabowski , Poland  
Carles Gomez , Spain  
Antonio Guerrieri , Italy  
Barbara Guidi , Italy  
Rami Hamdi, Qatar  
Tao Han, USA  
Sherief Hashima , Egypt  
Mahmoud Hassaballah , Egypt  
Yejun He , China  
Yixin He, China  
Andrej Hrovat , Slovenia  
Chunqiang Hu , China  
Xuexian Hu , China  
Zhenghua Huang , China  
Xiaohong Jiang , Japan  
Vicente Julian , Spain  
Rajesh Kaluri , India  
Dimitrios Katsaros, Greece  
Muhammad Asghar Khan, Pakistan  
Rahim Khan , Pakistan  
Ahmed Khattab, Egypt  
Hasan Ali Khattak, Pakistan  
Mario Kolberg , United Kingdom  
Meet Kumari, India  
Wen-Cheng Lai , Taiwan

Jose M. Lanza-Gutierrez, Spain  
Pavlos I. Lazaridis , United Kingdom  
Kim-Hung Le , Vietnam  
Tuan Anh Le , United Kingdom  
Xianfu Lei, China  
Jianfeng Li , China  
Xiangxue Li , China  
Yaguang Lin , China  
Zhi Lin , China  
Liu Liu , China  
Mingqian Liu , China  
Zhi Liu, Japan  
Miguel López-Benítez , United Kingdom  
Chuanwen Luo , China  
Lu Lv, China  
Basem M. ElHalawany , Egypt  
Imadeldin Mahgoub , USA  
Rajesh Manoharan , India  
Davide Mattera , Italy  
Michael McGuire , Canada  
Weizhi Meng , Denmark  
Klaus Moessner , United Kingdom  
Simone Morosi , Italy  
Amrit Mukherjee, Czech Republic  
Shahid Mumtaz , Portugal  
Giovanni Nardini , Italy  
Tuan M. Nguyen , Vietnam  
Petros Nicolitidis , Greece  
Rajendran Parthiban , Malaysia  
Giovanni Pau , Italy  
Matteo Petracca , Italy  
Marco Picone , Italy  
Daniele Pinchera , Italy  
Giuseppe Piro , Italy  
Javier Prieto , Spain  
Umair Rafique, Finland  
Maheswar Rajagopal , India  
Sujan Rajbhandari , United Kingdom  
Rajib Rana, Australia  
Luca Reggiani , Italy  
Daniel G. Reina , Spain  
Bo Rong , Canada  
Mangal Sain , Republic of Korea  
Praneet Saurabh , India







Hans Schotten, Germany  
Patrick Seeling , USA  
Muhammad Shafiq , China  
Zaffar Ahmed Shaikh , Pakistan  
Vishal Sharma , United Kingdom  
Kaize Shi , Australia  
Chakchai So-In, Thailand  
Enrique Stevens-Navarro , Mexico  
Sangeetha Subbaraj , India  
Tien-Wen Sung, Taiwan  
Suhua Tang , Japan  
Pan Tang , China  
Pierre-Martin Tardif , Canada  
Sreenath Reddy Thummaluru, India  
Tran Trung Duy , Vietnam  
Fan-Hsun Tseng, Taiwan  
S Velliangiri , India  
Quoc-Tuan Vien , United Kingdom  
Enrico M. Vitucci , Italy  
Shaohua Wan , China  
Dawei Wang, China  
Huaqun Wang , China  
Pengfei Wang , China  
Dapeng Wu , China  
Huaming Wu , China  
Ding Xu , China  
YAN YAO , China  
Jie Yang, USA  
Long Yang , China  
Qiang Ye , Canada  
Changyan Yi , China  
Ya-Ju Yu , Taiwan  
Marat V. Yuldashev , Finland  
Sherali Zeadally, USA  
Hong-Hai Zhang, USA  
Jiliang Zhang, China  
Lei Zhang, Spain  
Wence Zhang , China  
Yushu Zhang, China  
Kechen Zheng, China  
Fuhui Zhou , USA  
Meiling Zhu, United Kingdom  
Zhengyu Zhu , China

# Contents


## **Multimedia Concepts on Object Detection and Recognition with F1 Car Simulation Using Convolutional Layers**

Amutha Balakrishnan, Kadiyala Ramana , Gaurav Dhiman , Gokul Ashok, Vidhyacharan Bhaskar, Ashutosh Sharma , Gurjot Singh Gaba , Mehedi Masud , and Jehad F. Al-Amri   
Research Article (21 pages), Article ID 5543720, Volume 2021 (2021)









## **Sixth Generation (6G) Cognitive Radio Network (CRN) Application, Requirements, Security Issues, and Key Challenges**

Muhammad Muzamil Aslam , Liping Du , Xiaoyan Zhang , Yueyun Chen , Zahoor Ahmed , and Bushra Qureshi   
Research Article (18 pages), Article ID 1331428, Volume 2021 (2021)

## **Image Recognition Method for Pitching Fingers of Basketball Players Based on Symmetry Algorithm**

Wanquan Chen   
Research Article (12 pages), Article ID 2242222, Volume 2021 (2021)




## **An Enhanced Secure Deep Learning Algorithm for Fraud Detection in Wireless Communication**

Sumaya Sanober , Izhar Alam , Sagar Pande , Farrukh Arslan , Kantilal Pitambar Rane , Bhupesh Kumar Singh , Aditya Khamparia , and Mohammad Shabaz   
Research Article (14 pages), Article ID 6079582, Volume 2021 (2021)







## **Hierarchical Coordinated Control Method for Multiload DC Microgrid Units**

Zhigang Zhang  and Jinping Mo   
Research Article (13 pages), Article ID 4427750, Volume 2021 (2021)






## **Prediction of Traffic Generated by IoT Devices Using Statistical Learning Time Series Algorithms**

Shilpa P. Khedkar , R. Aroul Canessane , and Moslem Lari Najafi   
Research Article (12 pages), Article ID 5366222, Volume 2021 (2021)





## **Design and Simulation of Capacitive MEMS Switch for Ka Band Application**

Vinay Bhatia , Sukhdeep Kaur , Kuldeep Sharma , Punam Rattan , Vishal Jagota , and Mohammed Abdella Kemal   
Research Article (8 pages), Article ID 2021513, Volume 2021 (2021)



## **Location and Layout of Common Storage and Multichannel Common Distribution considering Time Windows**

Biqin Hu , Bin Yang , Wei Jiang , Zhe Yang , and Mohammed Abdella Kemal   
Research Article (9 pages), Article ID 2150293, Volume 2021 (2021)

## **Scalable and Storage Efficient Dynamic Key Management Scheme for Wireless Sensor Network**




Vipin Kumar , Navneet Malik , Gaurav Dhiman , and Tarun Kumar Lohani   
Research Article (11 pages), Article ID 5512879, Volume 2021 (2021)

**Nonholonomic Wheeled Mobile Robot Trajectory Tracking Control Based on Improved Sliding Mode Variable Structure**

Hua Cen  and Bhupesh Kumar Singh 

Research Article (9 pages), Article ID 2974839, Volume 2021 (2021)

**Hybrid Resource Environmental Value Chain Model Based on a Discrete Time Algorithm**

Wenting Cao , Melkamu Teshome Ayana , and Rongwei Gao 

Research Article (11 pages), Article ID 9993833, Volume 2021 (2021)

**A New Hybrid Deep Learning Algorithm for Prediction of Wide Traffic Congestion in Smart Cities**

G. Kothai , E. Poovammal, Gaurav Dhiman , Kadiyala Ramana , Ashutosh Sharma , Mohammed A. AlZain, Gurjot Singh Gaba , and Mehedi Masud 

Research Article (13 pages), Article ID 5583874, Volume 2021 (2021)

**CPIDM: A Clustering-Based Profound Iterating Deep Learning Model for HSI Segmentation**







Kriti Mahajan , Urvashi Garg , and Mohammad Shabaz 

Research Article (12 pages), Article ID 7279260, Volume 2021 (2021)



## Research Article

# Multimedia Concepts on Object Detection and Recognition with F1 Car Simulation Using Convolutional Layers

**Amutha Balakrishnan,<sup>1</sup> Kadiyala Ramana ,<sup>2</sup> Gaurav Dhiman ,<sup>3</sup> Gokul Ashok,<sup>1</sup> Vidhyacharan Bhaskar,<sup>4</sup> Ashutosh Sharma ,<sup>5</sup> Gurjot Singh Gaba ,<sup>6</sup> Mehedi Masud ,<sup>7</sup> and Jehad F. Al-Amri <sup>8</sup>**

<sup>1</sup>*School of Computing, SRM University, Chennai, India*

<sup>2</sup>*Department of Artificial Intelligence & Data Science, Annamacharya Institute of Technology and Sciences, Rajampet, Andhra Pradesh, India*

<sup>3</sup>*Department of Computer Science, Government Bikram College of Commerce, Patiala, India*

<sup>4</sup>*Department of Electrical and Computer Engineering, San Francisco State University, San Francisco, CA 94132, USA*

<sup>5</sup>*Institute of Computer Technology and Information Security, Southern Federal University, Russia*

<sup>6</sup>*School of Computer Science, Mohammed VI Polytechnic University, Ben Guerir 43150, Morocco*

<sup>7</sup>*Department of Computer Science, College of Computers and Information Technology, Taif University, P. O. Box 11099, Taif 21944, Saudi Arabia*

<sup>8</sup>*Department of Information Technology, College of Computers and Information Technology, Taif University, P. O. Box 11099, Taif 21944, Saudi Arabia*

Correspondence should be addressed to Mehedi Masud; [mmasud@tu.edu.sa](mailto:mmasud@tu.edu.sa)

Received 8 February 2021; Revised 7 May 2021; Accepted 10 November 2021; Published 9 December 2021

Academic Editor: Dafeng Hong

Copyright © 2021 Amutha Balakrishnan et al. This is an open access article distributed under the Creative Commons Attribution License, which permits unrestricted use, distribution, and reproduction in any medium, provided the original work is properly cited.

This paper presents a framework for detecting objects in images based on global features and contours. The first step is a shape matching algorithm that uses the background subtraction process. Object detection is accomplished by an examination of the oversegmentation of the image, where the space of the potential boundary of the object is examined to identify boundaries that have a direct resemblance to the prototype of the object type to be detected. Our analysis method removes edges using bilinear interpolation and reestablishes color sensors as lines and retracts background lines from the previous frame. Object contours are generated with clustered lines. The objects detected will then be recognized using the extraction technique. Here, we analyze the color and shape characteristics with which each object is capable of managing occlusion and interference. As an extension of object detection and recognition, F1 car simulation is experimented with simulation using various layers, such as layer drops, convolutionary layers, and boundary elimination, avoiding obstacles in different pathways.

## 1. Introduction

Object detection is the primary functionality needed by most computer and robot vision systems. The new study in this field has advanced significantly in many respects. Computer vision technology has rapidly and effectively developed. These results have been achieved with computer vision methods and with the development of new representations and models for specific computer vision issues. In machine

vision, we have seen great progress. It includes the details of object detection science. To detect objects, the system tracks objects in a scene and organises them into categories. The purpose of an object detector is to detect objects regardless of size, location, position, view with respect to the camera, partial occlusion, and illumination conditions.

Object detection is the first task of many computer vision systems to learn more about the object. Once a face has been identified, more details can be gathered. This

includes (i) recognizing the face in a photograph, (ii) tracking it as it moves through an image sequence, and (iii) collecting more information on the face (i.e., the gender of the person). Global features usually are some characteristics of regions in images such as area (size), perimeter, Fourier descriptors, and moments. Global features can be obtained either for a region by considering all points within a region, or only for those points on the boundary of a region [1].

Contours can be explained simply as a curve joining all the continuous points (along with the boundary), having the same color or intensity. The contours are a useful tool for shape analysis and object detection and recognition.

Object detection has been used in many applications, including (i) phone call from human computers, (ii) robotic systems, (iii) smartphones, (iv) protection systems, (v) image and video analysis and (vi) search engines, (vii) picture management, and (viii) transportation (search) (e.g., autonomous and assisted driving). Each of these applications has different specifications. This means processing time, robustness of occlusions, rotational invariance and pose shift detection. A number of applications are not assuming detection of just one class (for example faces), and some other applications are not assuming the detection of just one class from multiple viewpoints (e.g., side and frontal view of vehicles). Most systems can typically detect one object class from a restricted view set [2].

Finding meaningful regions in images has been a research topic in computer vision for many years. Researchers studied patterns at different scales, including local features like patterns on corners or intersections and long-range patterns over objects. Regions serve as the fundamental building blocks for a variety of vision applications [3–6]. For example, due to its robustness against image changes, a local region detector is critical for image matching and object recognition.

*1.1. Local Features.* Regions with high local prominence have made a major contribution to object detection and image recovery. Their methods provide robustness to image formation and distortion. If the objects are extracted and/or at several scales, the data will be good for recognizing algorithms [7–9]. Shape are mainly derived from high-profile texture/strength patterns, but are often fixed as triangles, ellipses, or rectangles. Eliminating the complexity of identification reduces the problem. Due to the lack of shape, the extracted features lose their representative power and generate noisy features [10]. We would like to identify types of parts and objects, so that a full-anthropoc identification can be made. Multiple segmentation tries to find new segments using different criteria or by integrating neighbouring areas. Unfortunately, larger populations of voxels often produce noisy segments, and the current methods lack an accurate model of the object. Instead, bottom-up methods use past experiences with categories to create their own correct category by using fragment pieces of knowledge. We usually extract regions at both object and local level without requiring category-specific information. New regions are obtained at the local and object level, then combined in a data-driven way to make a new image-based region. In order to scale

up exemplary recognition, we use the AWTV process, which uses the hierarchical structure of regions across different spatial boundaries.

## 2. Literature Survey

*2.1. Local Region Detection.* Local features are important for detecting and recognizing patterns in local regions. The extraction function combines a detection step that specifies the locations of the images to be extracted (positions, scales, shapes) and a description stage that creates a local descriptor [11]. Boundary Protection Local Area Detector and those to be tested with regional detection use various descriptors to demonstrate their applicability. Therefore, the focus of this section is type description and correspondence. Local region identification is a long-term topic of computer vision research and is important for broad baseline stereo matching. The invariant properties under image variations provide repeatability of certain instances of objects. On the other hand, generic object categories are often too sparse to capture rich visual information. Densely sampled patches provide a high level of coverage and provide reliable measurements for far higher costs [12]. Recent research shows how one sampling technique combines advantages and balances coverage with repeatability. However, unlike the various prior methods that do not know the object boundaries and shapes, our approach does not cross objects with object and context input. Algorithms that identify places based on observable characteristics are starting to use segments as the basic unit of analysis. Segments capture the structure of the object and provide broader spatial coverage. The instability of segmentation algorithms is due to the fact that they are unstable or sensitive to parameter settings. Segments can break into texture blots depending on the lighting, environment, or other background clutter [13]. Current work is focused on how reliable predictors can be selected using existing data. Many applications are randomly subsegmented to increase the likely of finding the actual object. The present work of the paper is to propose a new method, which uses new features, to solve the segmentation problem. The proposed method is shown to be effective, robust, and state-of-the-art. The proposed method supports local features such as corners, square, ellipse, rectangle, pyramid, and line. Our method does not rely on detecting those features as required in existing works on the segmentation problem. Instead, the proposed method is not based on detecting these local objects, but combines different solutions to achieve a cohesive solution for the segmentation problem.

*2.2. Object Segmentation with Shape Priors.* Using low-level image features such as color and texture, segmentation algorithms are often found to be unsuccessful when objects are present in similar-looking groups or are of a different color or have differing texture. Researchers are working on a top-down approach that uses model formats to segment the object. Top-down techniques merge the segmentation models with a bottom-up colors or textures to mark the type of the object [14]. Form-based objects work by detecting

objects in cluttered images. Cognitive architectures that use category-specific, top-down knowledge coupled with bottom-up evidence. In particular, category-specific priors make explicit assumptions about the observer's segmented point of view, for example, vehicle side views. We think about it this way: the key insight is that objects share their features, and this sharing lets one pass the features of a known class to an unknown class. We propose an exemplary transfer function for global forms [15]. Our approach ignores prior knowledge of the objects present in the scene, focusing instead on a shape descriptor that is able to accurately represent the class that the object is most likely of. The model-based design also eliminates the concerns of shapes that are difficult to pose. Mutual visual properties of groups of objects has been studied in several ways. Multi-class learning helps to employ the value of traditional item discrimination features in object detection and transfer information on newly learned items. From a signal-processing point of view, properties of the inputs are expressed in primitives, e.g., in units of symmetry [16]. Recently, efforts are directed at establishing foundational characteristics of these curves. The process, however, goes beyond local sharing to consider global style object-level predictions. Our effective nonparametric approach to sharing in 3D space brings greater flexibility to changes in object shapes and poses. There are a number of recently developed methods that work for our approach [17–19]. They also accept access to a database of segmented images, create category-independent object segmentation hypotheses and do the same thing we do. Previous methods focus on local bottom-up processing [20–22]. Multiple segments of the figure ground will provide multiple hypotheses for object regions. To reduce inconsistency, there is some work that aims to map multiple hypotheses to a single segmentation that provides a nonconflicting definition of the object. An ongoing effort is made to combine multiple segmentation [23]. They integrate an expert knowledge, a large vocabulary, and create a model from that by selecting pieces of phrases. Section 3 demonstrates the System Framework. Section 4 discusses the methods and materials. Section 5 presents the conclusions. Section 6 includes simulations for the F1 car using the system studied.

### 3. System Framework

**3.1. Image Preprocessing.** To further process, the relevant and usable image data is enhanced and distortions/noise introduced into the image is reduced in this step from low-level images. Here, in this work fault detection, feature extraction, and segmentation, image transformation is used typically. Intensity change and filtering an image are the main focus areas here as shown in Figure 1.

**3.2. Filtering.** As a preprocessing tool, noise reduction in image segmentation plays an important role.

Various methods are being developed, and almost all of them rely on the same basic method for doing this: the average. Noise is theoretically composed of other distinct pixels that are apparently apparent, and according to this informa-

tion, there are adjacent pixels. Noise can be removed using the average of the actual image data in similar areas. In fact, the actual image data can share similarities in these average areas, but there is no noise in these areas. [24]. As a result, this filtering method effectively maintains and removes noise without damaging the actual image data. It is easy to define the average, but it is not easy to determine which pixel to average. Averaging multiple pixels can result in loss of image detail. Conversely, there is no average noise reduction effect with too few pixels. The media filter replaces each pixel in the image with the median of the pixels that surround the image and uses a mask of strange length to sort the pixels in the window by output intensity.

**3.3. Intensity Adjustment.** Improvements in images can be objective (filtered) or subjective [25]. Intensity adjustment is a technique used to emphasize an image. The goal is to emphasize the image by adjusting the value of Intensity to a new area. An important way to transform the grayscale intensity is to use the  $g = \text{imadjust}(f, \text{low in; high in, low out, high out, gamma})$  syntax [26]. This function maps values in image  $f$  to new values in  $g$ , for example, map low in and high in map values to low out and high out values, low map values to low out, and high map values to high out [27]. All fully functional inputs are listed from 0 to 1 (double or 0 to 255 (unit 8), and gamma parameters determine the shape of the curve that maps the output intensity values from the inputs; so, gamma is less than 1 The smaller mapping is pushed higher (brighter). In the output value, the mapping is pushed lower (darker), and the map is linear [28] if the gamma is equal to 1.

**3.4. Interpolation.** Interpolation is the method of estimating a continuous sample function. Interpolation Image processing includes image enlargement or reduction, subpixel image register, spatial distortion correction, and image decompression. Image data is typically collected at a lower rate to reduce the noise in the image. Mapping between an unknown high-resolution image and a low-resolution image is not invertible; so, reverse mapping is not invertible [29]. The highest quality performance is needed when sampling with high-resolution cameras.

**3.5. Bilinear Interpolation.** The grey level in bilinear interpolation is calculated from a weighted average of four pixels closest to the input coordinate and assigned to the output coordinate [30]. Two linear interpolations are rendered first (horizontally); then, another linear interpolation is performed (perpendicular to the first) (in this paper). For one-dimensional linear interpolation, two grid points are required. For bilinear interpolation, the number of grid points required to test the interpolation function is four (linear interpolation in two dimensions). The interpolation kernel for linear interpolation is  $u(s) = \{0 | s| > 1$  Equation (3) and  $1 | s| | s| < 1$ , where  $s$  is the distance of the interpolated point from the grid point. Interpolation coefficients are as follows:  $ck = f(xk)$ .

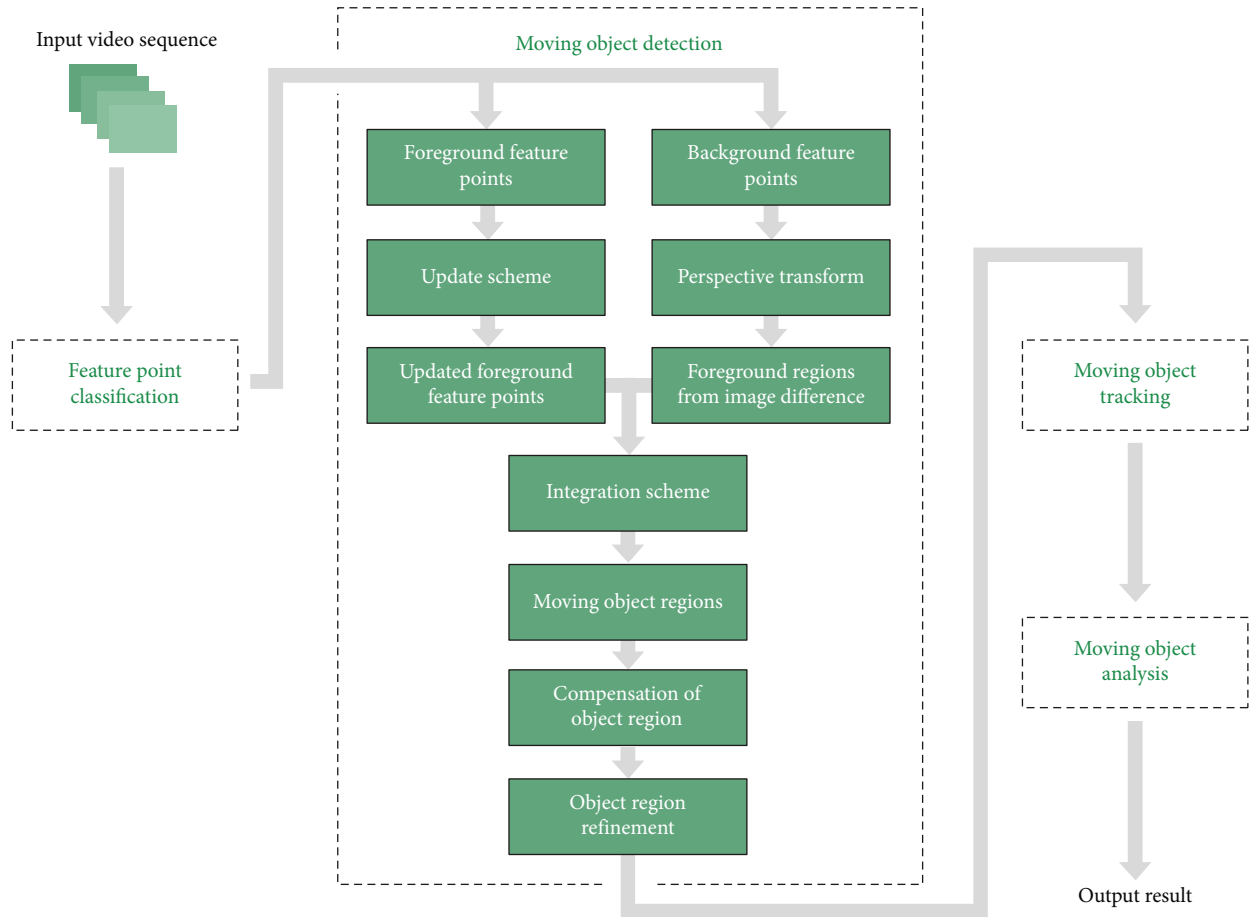


FIGURE 1: Object recognition system.

## 4. Methods and Materials

4.1. *Simulation.* Various segmentation methods have been proposed over the past few decades, and some classification is needed to properly present the method. Two very different approaches to segmentation may share properties that are contrary to a particular classification, but the classification seems impossible. Therefore, the classification described in this chapter emphasizes an approach rather than a strict division.

The subsequent categories are used:

- (i) **Threshold-based segmentation:** to segment the image, histogram thresholding and slicing techniques are used. They can be combined with pre- and postprocessing techniques that can be applied directly to images
- (ii) **Edge-based segmentation:** in this method, the edges detected in the image are used to identify the boundary of the object
- (iii) **Region-based segmentation:** area-based technology takes the opposite approach when boundary-based technology finds the boundaries of an object and then completes and searches for the object. The boundary of an object

(iv) **Clustering techniques:** it is often used as a synonym for (aggregate) segmentation, but is used here to refer to techniques used in the primary analysis of high-order, measurable tendencies of search data. In this context, clustering techniques try to group similar patterns in some sense. This is similar to what you are trying to achieve when segmenting an image, and in fact, you can use a specific clustering method to segment your image

(v) **Matching:** if you know that the object you want to define (approximately) in the image looks like a value by a characteristic such as its perimeter length, you can use this information to find the object in the image. This splitting method is called matching datasheet values

4.2. *Canny Edge Detection Algorithm.* A lot of people know that the Canny edge detection algorithm is the optimal edge detector. Canny's aim was to update the many edge detectors when he started working. He achieved his target with great success, and his principles and strategies can be found in his paper, *A Computational Approach to Edge Detection*. The first is the lowest error rate. It is important that the edges of the image are not overlooked, and that the nonedges are not addressed. The second criterion concerns

the direction of the edge points. In other words, the distance from the detector between the edge pixels and the actual edge should be at a minimum. The third criterion is that there should be only one answer to one edge (Table 1).

The Canny edge detector smoothes out the image and noise based on these parameters. The gradient of the image is then found to highlight regions with high spatial derivatives. The algorithm follows these regions and removes any non-maximum pixels. The gradient array is now further reduced by hysteresis. Hysteresis has two threshold values and is set to zero if the magnitude is below the first threshold. If the magnitude reaches the high threshold, the edge shall be drawn. And if it is between the two thresholds, it is set to zero unless the path to a pixel with a gradient above T2 is known.

**4.2.1. Step 1.** The Canny edge detector requires a number of steps to implement. It is helpful to remove the noise from the original image before locating and detecting boundaries. Which makes it easy to find the Gaussian filter's ideal frequency. Convolution can be achieved by standard means when the appropriate mask has been calculated. A mask is usually much smaller than the real image. It slides over the image, adding an extra square. The lower the sensitivity, the larger the Gaussian mask. A misaligned region increases marginally as the average size increases.

**4.2.2. Step 2.** The next step is to find the intensity of the edge by taking the gradient of the image, lightening the image and eliminating the noise. The Canny operator performs a 2D spatial gradient image measurement. The estimated absolute gradient magnitude (edge force) can then be calculated at each point. The Sobel operator uses a variety of 3x3 convolution masks, one estimating the  $x$  direction gradient (columns) and the other estimating the  $y$  direction gradient (rows) (Table 2).

The gradient's magnitude or edge intensity is approximated by the formulation:  $|G| = |G_x| + |G_y|$ .

**4.2.3. Step 3.** The position of the edge is defined by the gradient  $x$  and  $y$ . However if the sum  $X$  is equal to zero, an error occurs. There must also be a restriction in the code if this occurs. Whenever the gradient in the direction of  $x$  is 0, the direction of the edge must be  $90^\circ$  or  $0^\circ$ , depending on the value of the gradient in the direction of  $y$ . If  $G_y$  has a zero value, the direction of the edge is 0 degrees. If not, the direction of the edge is 90 degrees. The formula for finding the direction of the edge is correct:

$$\text{Theta} = \text{invtan}(G_y/G_x). \quad (1)$$

**4.2.4. Step 4.** When the direction of the edge is known, the next step is to link the direction of the edge to the direction of the image. Thus, the pixels of the  $5 \times 5$  image are aligned (Table 3).

Now, we can see the pixel "a" when identifying the surrounding pixels, and there are only four possible directions-0 degrees, 45 degrees, 90 degrees, and 135 degrees. The orientation of the edge in one of the four directions must therefore be resolved on the basis of the direction nearest to zero degrees shown in Figure 2.

TABLE 1

+1	+2	+1
0	0	0
-1	-2	-1
$G_y$		

TABLE 2

-1	0	+1
-2	0	+2
-1	0	+1
$G_x$		

TABLE 3

$x$	$x$	$x$	$x$	$x$
$x$	$x$	$x$	$x$	$x$
$x$	$x$	$a$	$x$	$x$
$x$	$x$	$x$	$x$	$x$
$x$	$x$	$x$	$x$	$x$

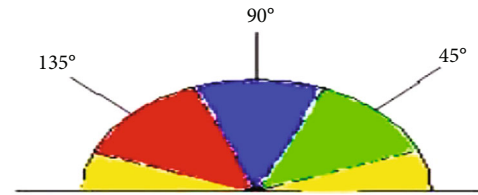


FIGURE 2: Edge detection based on angular coloring.

Any position of the edge within the yellow range is thus set to 0 degrees (0 to 22.5 and 157.5 to 180 degrees). Any direction of the edge falling within the green range (22.5 to 67.5°) shall be set at 45°C. The route at the edge of the blue (67.5 to 112.5°) is set at 90°. At the end, each path on the edge that falls into the red range (112.5 to 157.5°C) is set at 135°C.

**4.2.5. Step 5.** No full deletion must now be enforced after the edge directions have been known. Nonmaximal suppression is used to map the edge in the direction of the edge and to delete a pixel value set to 0 that is not called the edge. This gives a thin line to the output image.

**4.2.6. Step 6.** Hysteresis is used to clear a streak. In streaming, the edge is caused by an output that fluctuates above and below the threshold. A threshold will be applied to the image, and the edge will fall below the threshold due to noise. It is above the level, so that the rim appears dotted. Hysteresis uses two thresholds to prevent this from occurring. Any pixel with a value greater than 1 is to be an edge pixel and be labelled as such. Any pixels whose value is greater than T2 will also be selected as edge pixels. To follow a border, you need to start with a T2 gradient, but you will

not stop until you hit a T1 gradient.

$$G \text{ function with Gaussian } \sigma = 1.4. \quad (2)$$

Hence, the simple Gaussian is considered in a discrete grid a particular case of the  $G(x, y)$  for narrow Gaussians.

**4.3. Adjacent Weighted Threshold Variation (AWTV) Method.** The goal is to minimize the error associated with classifying a background pixel as a front pixel or vice versa, and the threshold is determined by weight. This is accomplished by minimizing the area beneath the histogram for a region on the other side of the threshold. The issue is that each region lacks an AWTV; only combined regions have a weighted threshold value [31]. Understand that there is typically no minimum overlap (where the distribution's misclassified areas are equal) when the valley occurs in the combined pixel  $(k - 1, k)$ , for example, when one cluster has a large distribution and the other a narrow distribution. One way to do this is to consider the values of both regions as two clusters; they are weightless or weightless. In other words, the mean of all pixels below the threshold may be  $\mu_B(T)$ , and all pixels above the threshold may be equal to  $\mu_O(T)$ . We want to set the threshold as follows:

$$\begin{aligned} \forall g < T : |g - \mu_B(T)| < |g - \mu_O(T)|, \\ \forall g \geq T : |g - \mu_B(T)| > |g - \mu_O(T)|. \end{aligned} \quad (3)$$

This is a variation of AWTV's clustering pattern recognition algorithm. The basic idea is to measure the mean  $\mu_B(T)$  for pixels at four corners (assumed to be the background) and the other one to measure  $\mu_O(T)$ . Set the threshold between  $\mu_B(T)$  and  $\mu_O(T)$  (so that the pixels are split according to the proximity between  $\mu_B(T)$  and  $\mu_O(T)$ ). Update the  $\mu_B(T)$  and  $\mu_O(T)$  estimates by actually measuring the pixel mean at both of the current thresholds. This method continues until the algorithm converges.

**4.4. Clustering (The AWTV Method).** Another approach that produces comparable results is to minimize duplication by clustering each cluster as closely as possible. Of course, we cannot alter the distributions themselves, but we can alter the distances between them (thresholds). When the threshold is changed in one direction, it enlarges the diffusion on one side and reduces the diffusion on the other side [32]. The goal is to choose a threshold to minimize the combined distribution. Internal distribution may be defined as the sum of the distribution weights for each cluster:

$$\begin{aligned} \sigma_{\text{within}}^2(T) &= n_B(T)\sigma_B^2(T) + n_O(T)\sigma_O^2(T), \\ n_B(T) &= \sum_{i=0}^{T-1} p(i), \\ n_O(T) &= \sum_{i=0}^{N-1} p(i), \end{aligned}$$

$$\begin{aligned} \sigma_B^2(T) &= \text{The variance of the pixels in the background (below threshold),} \\ \sigma_O^2(T) &= \text{The variance of the pixels in the background(above threshold).} \end{aligned} \quad (4)$$

$[0, N - 1]$  is the range of intensity levels. For both groups, the difference in this class of potential each threshold requires a lot of computation, but it is easier to do so. Subtracting the variance within a class from the total variance of the combined distribution gives us the variance of

$$\sigma_{\text{Between}}^2(T) = \sigma^2 - \sigma_{\text{within}}^2(T) = n_B(T)[\mu_B(T) - \mu]^2 + n_O(T)[\mu_O(T) - \mu]^2, \quad (5)$$

where  $\sigma^2$  is the sum of the variances, and  $\mu$  is the sum of the means. Take note that the variance between classes is simply the weighted variance of the cluster means in relation to the overall mean. We obtain by substituting  $\mu = n_B(T)\mu_B(T) + n_O(T)\mu_O(T)$  and simplifying.

$$\sigma_{\text{Between}}^2(T) = n_B(T)n_O(T)[\mu_B(T) - \mu_O(T)]^2. \quad (6)$$

So, for every potential threshold  $T$ , it is as follows:

- (a) Splits the pixels into two AWTVs according to a weighted threshold
- (b) Calculate the mean of each cluster
- (c) Square the difference between the means
- (d) Multiply the number of pixels in one cluster by the number of pixels in the other cluster

$$\begin{aligned} n_B(T+1) &= n_B(T) + n_T, \\ n_O(T+1) &= n_O(T) - n_T, \\ \mu_B(T+1) &= \frac{\mu_B(T)n_B(T) + n_T T}{n_B(T+1)}, \\ \mu_O(T+1) &= \frac{\mu_O(T)n_O(T) - n_T T}{n_O(T+1)}. \end{aligned} \quad (7)$$

I have noticed that the optimal threshold is to maximize the variance between classes (or minimize the variance between classes), but the calculations when switching to the threshold are not independent. As  $T$  increases, the average  $\mu_B(T)$  and  $\mu_O(T)$  with  $n_B(T)$ ,  $n_O(T)$  of each cluster can be updated as pixels move from one group to another. I can do it.

**4.5. Simulation Results.** A variation of the AWTV-based object recognition in any particular vehicle image is to train the features with the image, then use it to recognize the particular vehicle of the image by different structure element. This should provide more accurate recognition, as it corrects for different image features that is mean, perimeter, etc. Figure 3 shows the resulted images that are implemented using MATLAB. Following Figure 3 is the first image which is the input to this program that was designed using MATLAB graphical user interface (GUI) (Table 3).

The following Figure 4 shows background subtraction module resultant image, Figure 5 shows Canny edge detection image, and Figure 6 shows binary image conversion;



FIGURE 3: Car designed using MATLAB graphical user interface.



FIGURE 4: Background substruction module resultant image.

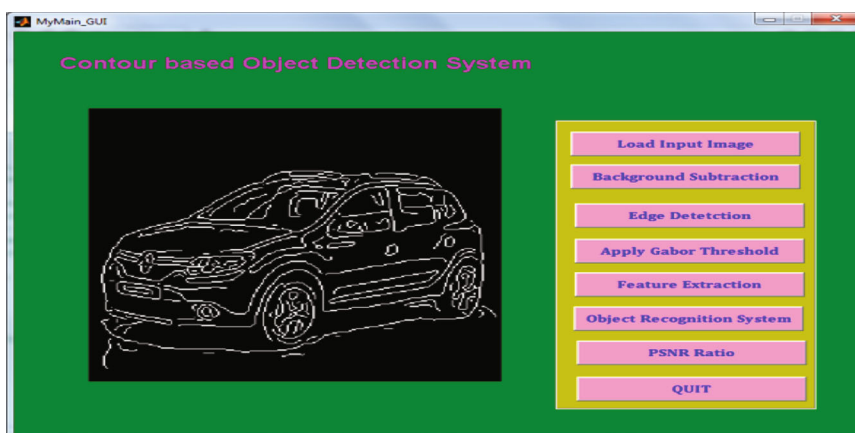


FIGURE 5: Canny edge detection image.

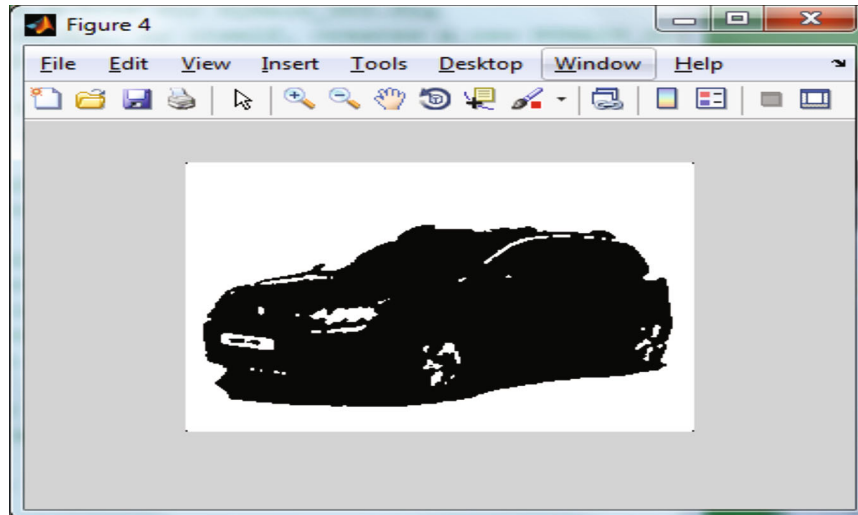


FIGURE 6: Binary image conversion.

then, Figures 7 and 8 represent object recognition result is shown in message box.

In Figure 9, features are shown in command window.

## 5. Inferences

We presented a new contour-based model for object detection. A 3D model is created by using the AWTV Method and its geometric relations. Objects are found in the test images using the most suitable object shapes. Partial occlusion is an object detection problem that is not seen in the data. The model offers geometric information for each pair of shapes; so, we expect it to handle partial occlusion. At least some samples are hardly affected by object instances in the sample dataset. The SHAPE model can handle large orientation changes, since relative rather than absolute geometric attributes are used. We can test the model with proper direction adjustments. All internal contour fragments inside the boundary are modeled, and those on the boundary are modeled as well. We will use unconnected fragments to identify patterns. Both SHAPE and relationship parameters are manually set in all experiments. For various objects, such as apples and swans, their shape and parameters may not fulfill this requirement. Our future goal is to build a machine that can determine these images automatically. We can also establish richer relationship types between type and form such as shape orientation.

## 6. Need for a Racing Simulator

This section deals with developing a software application or a simulator, that essentially simulates an environment for the user. The simulator developed here will be a Formula One Simulator that will enable users to experience a real-world action-packed racing environment in which the users will be able to get into a Formula One car and drive around a track or take part in several races against tough computer opponents. These races are held in some of the world renowned race tracks of the world. For example, we have

reconstructed the Autodromo Nazionale Monza Race Track which is located in the city of Monza, North of Milan, Italy. In any typical racing scenario, a driver cannot simply jump into a vehicle and race around. It requires immense amounts of training and dedication [32]. The same applies for a Formula One driver. These drivers belong to an elite class of world-class drivers competing for the coveted title of “Best Driver In The World.” The Formula One drivers are essentially tremendously fit athletes and hard trained to endure the many forces and stresses applicable to this form of motorsport [33]. First, reference images of an dimensionally accurate F1 car are set and arranged as shown in Figure 10:

Then, a primitive rectangular polygon is added superimposing the reference images on all of the different views as shown in Figure 11:

Then, this rectangle mesh is further sculpted by using modifiers (such as extrude, chamfer) and by moving, rotating, or scaling the vertices, edges, and faces of the mesh to bring about a rough outline of the body of the vehicle as shown in Figures 12 and 13.

Then, this rough outline is further sculpted to bring about a relatively low polygon model of a F1 car body. Generally, low polygon models are used in games to meet the resource constraint of the game [34–36]. The rough edges of low polygon models are covered by using normal mapping, a type of texturing which gives the illusion of depth as shown in Figure 14.

The other objects in the game are modeled similarly to Autodesk 3ds Max, formerly a 3D Studio Max, is a 3D graphics computer programme for 3D animations, models, and photographs. It was developed and produced by Autodesk Media and Entertainment. It has models, a modular plugin architecture, and can be used on Microsoft’s Windows platform. It is also used by video game makers, several TV studios, and architectural visualisation studios. It is also used for film effects and film previews. The latest version of 3ds also includes shaders (e.g., ambient and subsurface dispersal), dynamic simulation, particle systems, radiosity, normal mapping and



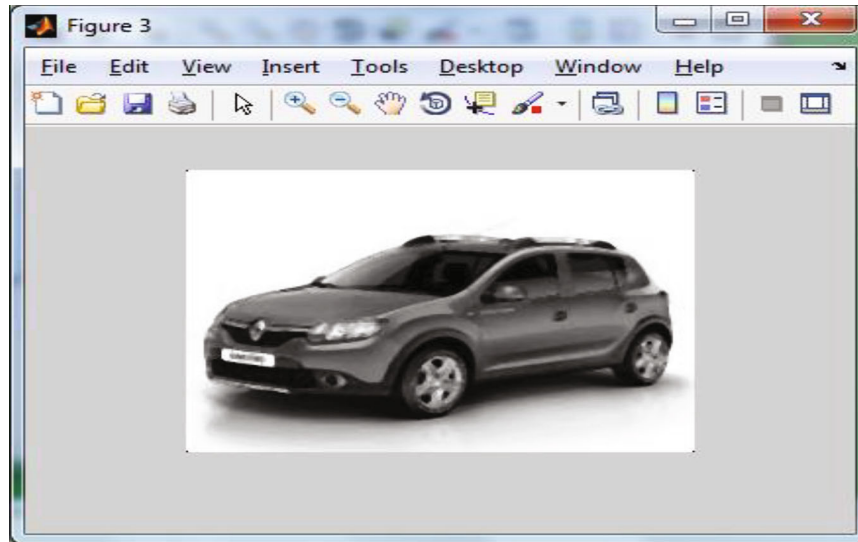


FIGURE 7: Object recognition result.

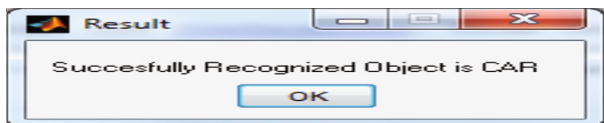


FIGURE 8: Object recognition result message box.

rendering, global lightset, flexible user interface, and its own scripting language, along with its modeling and animation tools. Some of the academy award winning movies designed in 3ds Max are Avatar, The Curious Case of Benjamin Button, 2012, Shutter Island, The Mummy, etc. Some of the highest grossing games designed in 3ds Max are Mass Effect, Unreal Tournament, Need For Speed, Call of Duty, etc.

Once these models are sculpted, then they are imported to the Unity3D game engine. The Unity3D game engine is a crossplatform with built in IDE. It is used to develop video games for web plugins, desktop platforms, consoles, and mobile devices. It was initially used to design games for the iOS but as of now, it can be used for multiple platforms. It is a free game engine which has a variety of powerful tools to effectively build a game. The levels in Unity are called scenes with each scene having multiple objects put together along with shader effects, lighting, scripts, cameras, activators, etc. The level building part deals with the placement of different objects with the help of the transformation, rotational, and scale modifiers. The development of the Autodromo Nazionale Monza track is illustrated below. Initially, a new empty scene is created. Then, the reference image of the Monza circuit is set as shown in Figure 15.

With the reference image set, the track is then placed superimposed on the reference image. The track consists of smaller pieces of roads that are first placed on the scene and then transformed, rotated, or scaled to fit the track in the reference image. The pieces of the track must be exactly aligned with one another. Otherwise, collision errors might

be seen later when dynamic objects are added to the scene. The track is progressively built as seen in the next two illustrations represented in Figures 16 and 17.

This piece is duplicated, and the duplicated piece is placed alongside the original. If there is a corner, then the appropriate piece is used. This continues until the track is complete. Minor adjustments have to be made at the end to close of the circuit to get the completed track as shown in Figure 18.

Once the track is completed, then a terrain is added to the scene. On the terrain, other props are added (like crowd stands) to populate the scene as shown in Figure 19.

Once that is done, then the terrain tools are used to generate a landscape. The terrain tools can be used to increase or decrease particular areas of the terrain. Then, the terrain tools are used again to generate vegetation for the terrain and add the bounds of the scene as represented in Figure 20.

Lastly, the visual effects are added to the scene. A directional light is added to light the scene. Then, a skybox is added to add depth to the scene. Advanced effects like fog, ambient occlusion, and antialiasing are adjusted to the finest detail. Then, the scene is finally baked before any of the dynamic game objects are added. The final scene is illustrated below as shown in Figure 21.

The modules related to the F1 car is illustrated below:

**6.1. End-User Car Handling.** This module basically deals with controlling of the car by the end-user and also assigns a trailing viewing camera relative to the position of the car in the game world (generally behind car model). This enables the user to switch the camera views from first-person viewpoint to third-person viewpoint. First-person viewpoint refers to the graphical perspective that is rendered from the viewpoint of the player, which is the cockpit of the vehicle in this case. Third-person viewpoint refers to the graphical perspective that is rendered from a fixed distance behind and slightly above the player. This viewpoint allows

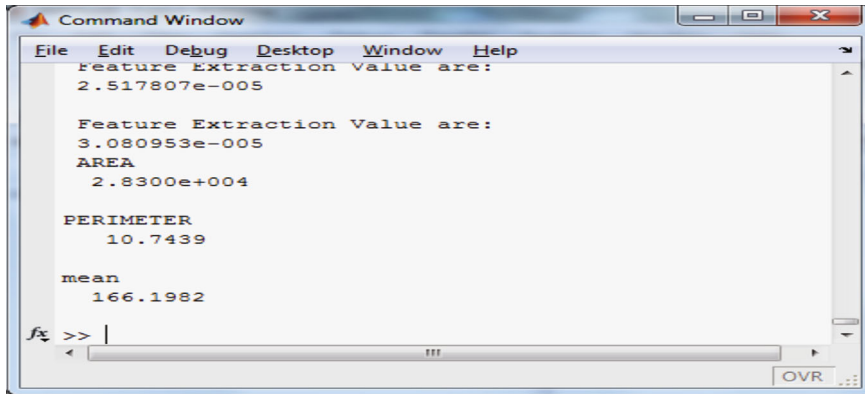


FIGURE 9: Image features.

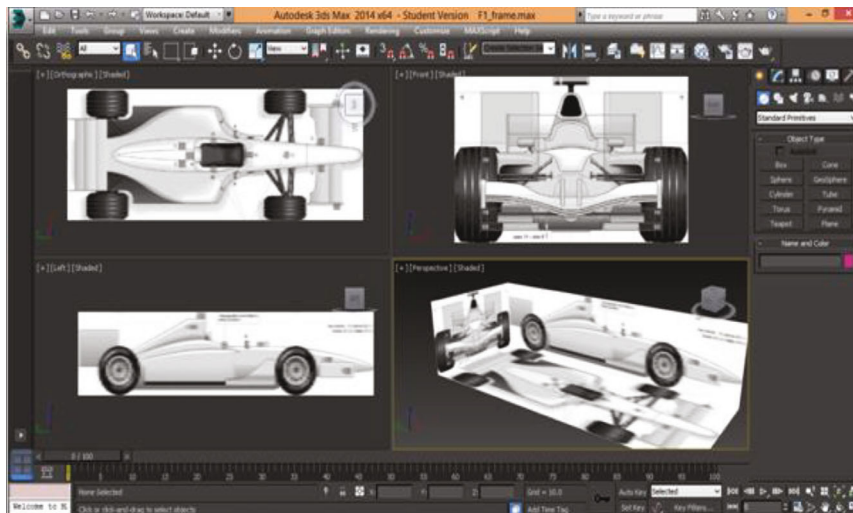


FIGURE 10: Reference images.

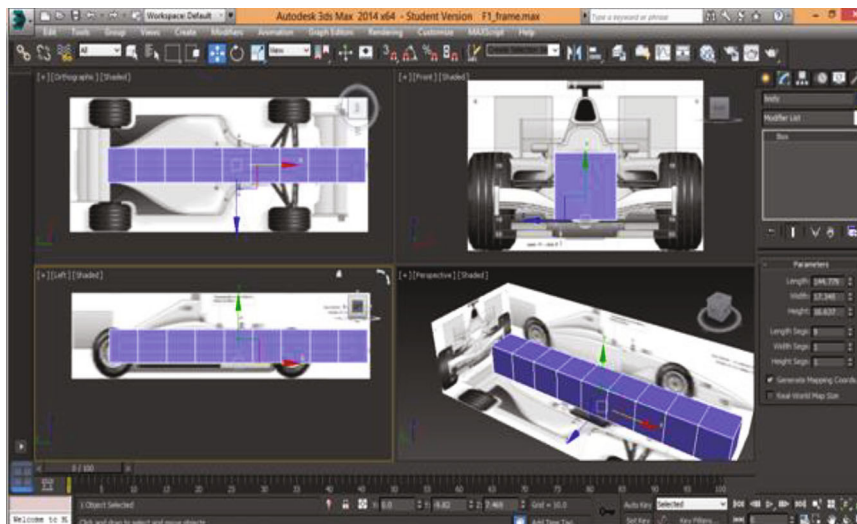


FIGURE 11: Adding rectangular primitive.

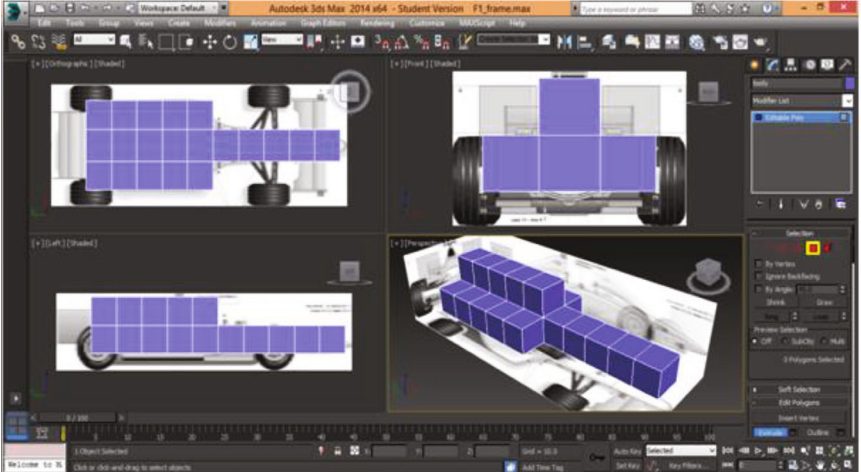


FIGURE 12: Selected faces are extruded.

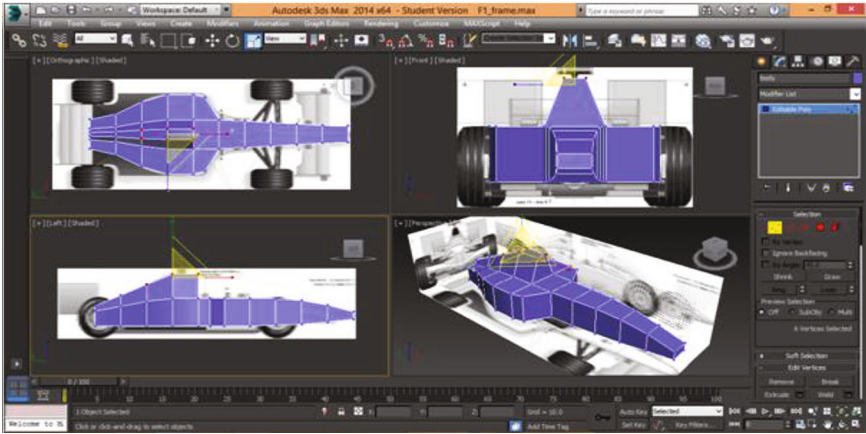


FIGURE 13: Vertices aligned with reference image.

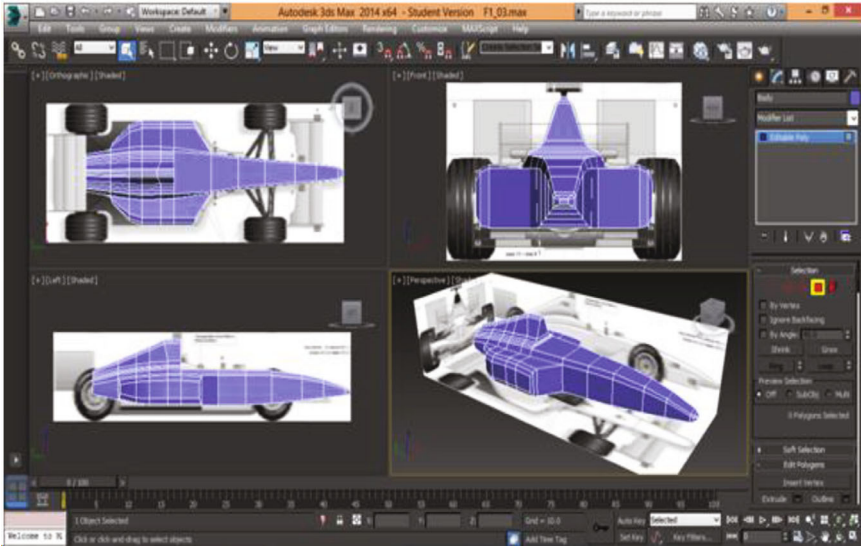


FIGURE 14: Fine tuning the mesh.

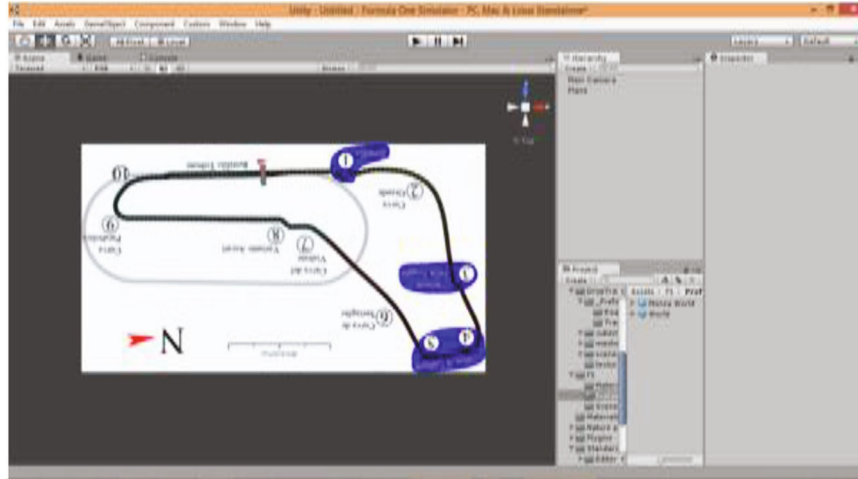


FIGURE 15: Adding reference image.

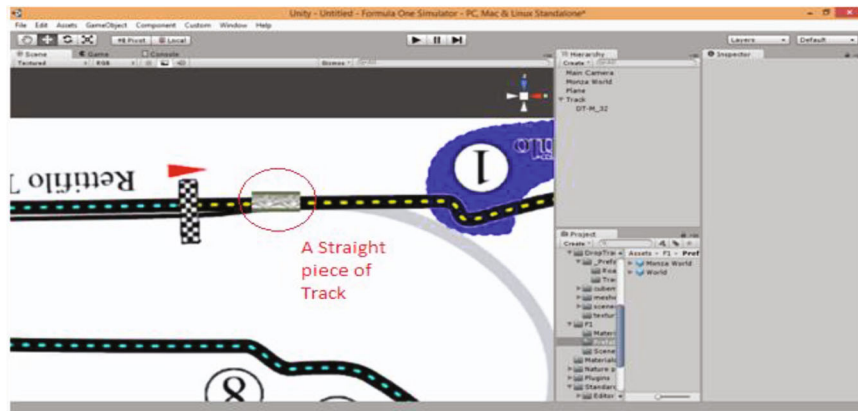


FIGURE 16: A piece of the track.

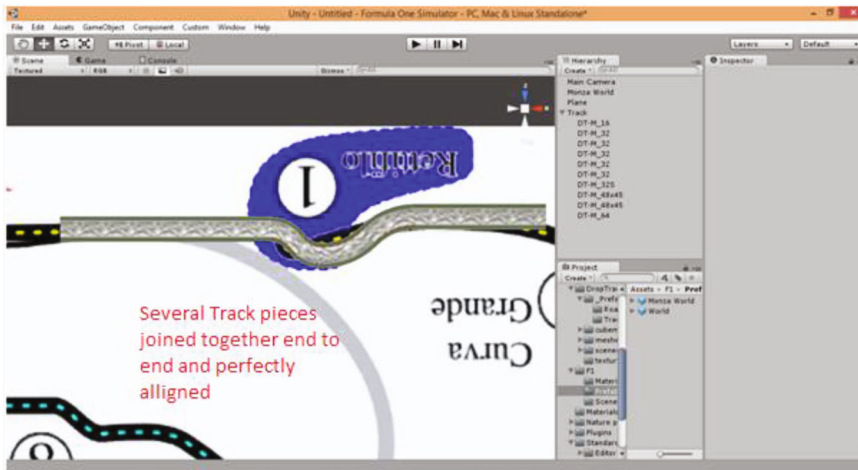


FIGURE 17: Adding more track pieces.

the user to see a more strongly characterized vehicle. Now, in order to make the car move, with the input from user, key mapping of various keys on keyboard is done which translates the car forward, backward or sideways. For example, we bind the forward movement of the car with “up arrow” key. When the key is pressed, the coordinates of

the car are updated in the game world from say (0,0,0) to (10,0,0) which translates a forward movement. In this way, it can be done to manipulate any behavior of the car. We have added many more parameters to further enhance the handling of the end-user car to bring about more realism. For example, it is no longer possible to do cornering at high

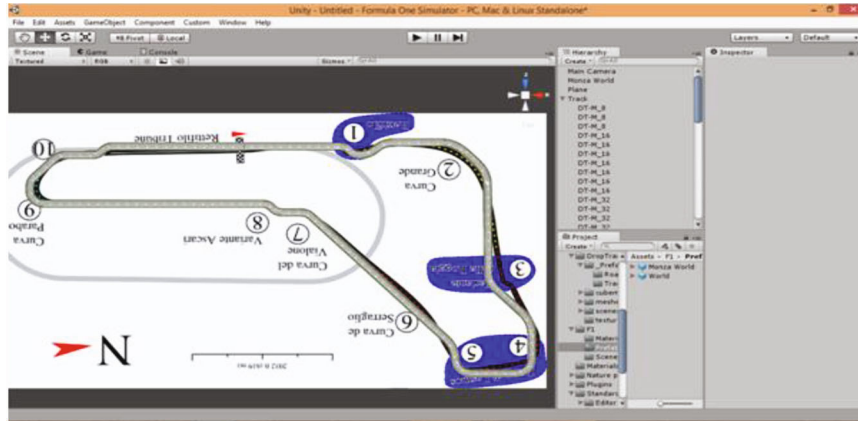


FIGURE 18: Completed track.

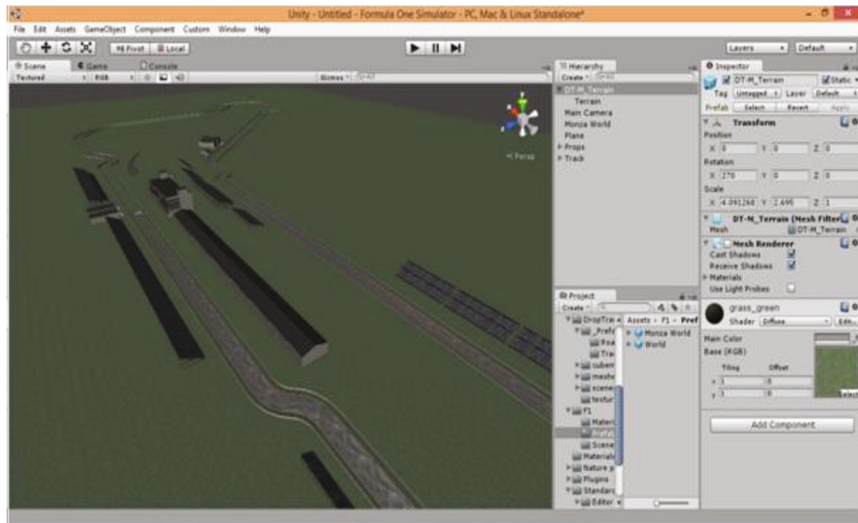


FIGURE 19: After adding terrain and props.

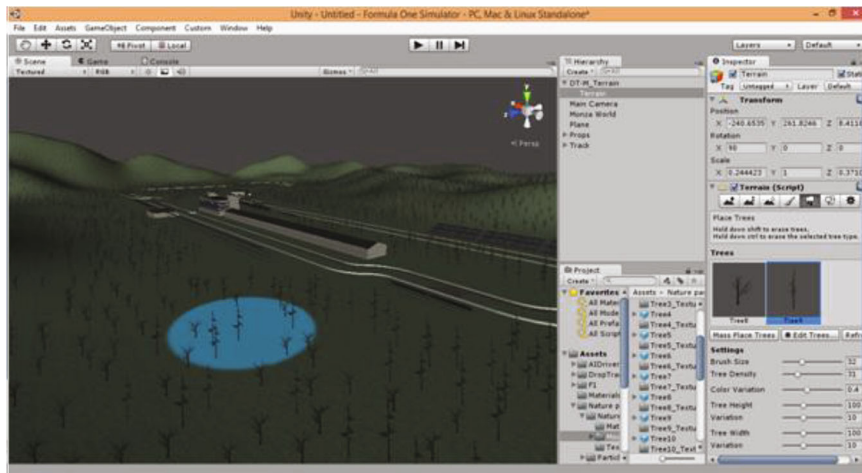


FIGURE 20: Adding terrain modifiers.

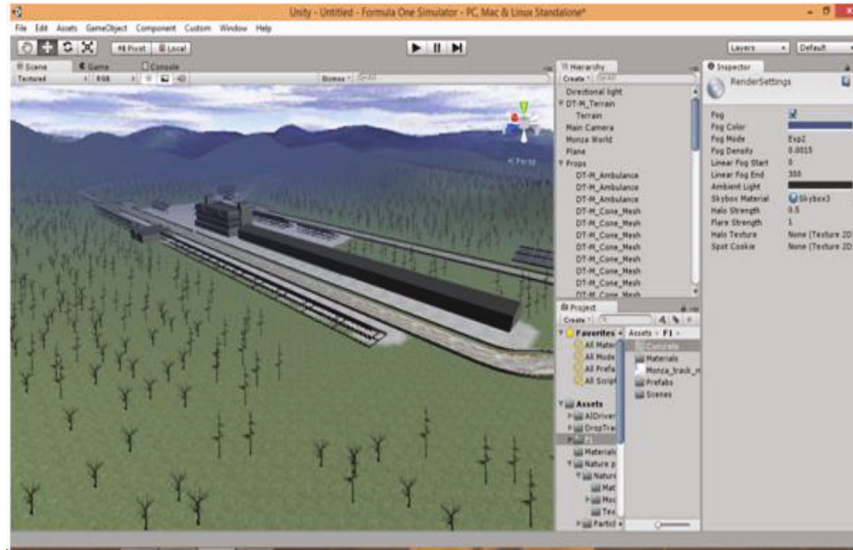


FIGURE 21: Adding visual effects.

speeds, and the car will skid. So, this ensures that the driver that is the end-user drives around the track in a disciplined manner. Also, collision mechanics have been added to every car; so, the user cannot simply go around hitting every other vehicles on track. Some of the parameters used here are the following:

- (a) Inertia-as in example given above, due to inertia, the car will not take turns at high speed
- (b) Gear ratio-the ratio of velocity applied to the car based on current gear
- (c) Antiroll bar-in the unlikely chance of a vehicle flipping over, this parameter will put the vehicle back on track
- (d) Collision-damage mechanics have been added to the user controlled car. So, whenever a collision occurs, the vertices of the car gets rearranged to show the aesthetics of the damage
- (e) GUI-enhanced graphical user interface like speedometer and RPM meter is provided to the end user to better understand the behavior of their vehicle

**6.2. AI Car Handling.** This module deals with the throttle, steering, braking, and cornering of the computer or AI controlled vehicles. We shall essentially examine the behavior of the AI on a race track represented in Figure 22. More importantly its behavior with the respect to the end-user vehicle. The throttle and steering of the AI-controlled cars are taken care of with the help of scripting. The implementation language used here is the C# programming language. The AI Driver Controller script is being used to take care of the throttle and steering of the AI-controlled vehicles. For braking and cornering purposes, there are detector lines at various angles around the bot vehicle (AI controlled). The faster the car

moves, the further are the range of detection lines. When these lines encounter an obstacle, then the AI will change its course accordingly. This is basically how the AI detects an obstacle on its course. As an example in the following slide, the black rectangle represents the car, the yellow lines represents the detector lines running at  $0^\circ$  with the axis of the car, and the brown squares depicts a unit of an obstacle. In the following example, the detection lines (colored lines) of AI driver vehicle detects another racer. When this happens, the AI driver checks the side using the angled detection lines if there is any obstacle. If one or both the sides are free of obstacles, it will then change its steer angle and deviate from its current path to avoid colliding with the other racer.

- (a) Rigid body-this parameter is mostly used in the translation of the car and to provide mass
- (b) Drag-the force acting against the forward motion of the car
- (c) Wheel alignment-this is used to turn the wheels when the vehicle makes a turn
- (d) Waypoints-the waypoints corresponds to specific coordinates in the map which defines the racing line. These waypoints are used by the AI vehicles as described below
- (e) Current heading-this is used by the AI vehicles to keep track of the waypoint it currently crossed. Target heading-this is used by the AI to move to the next waypoint
- (f) Waypoint container-an array where all the waypoints, installed on the track, are stored
- (g) Engine torque-the force that propels the vehicle towards the next waypoint. Gear ratio-the ratio of velocity applied to the car based on current gear

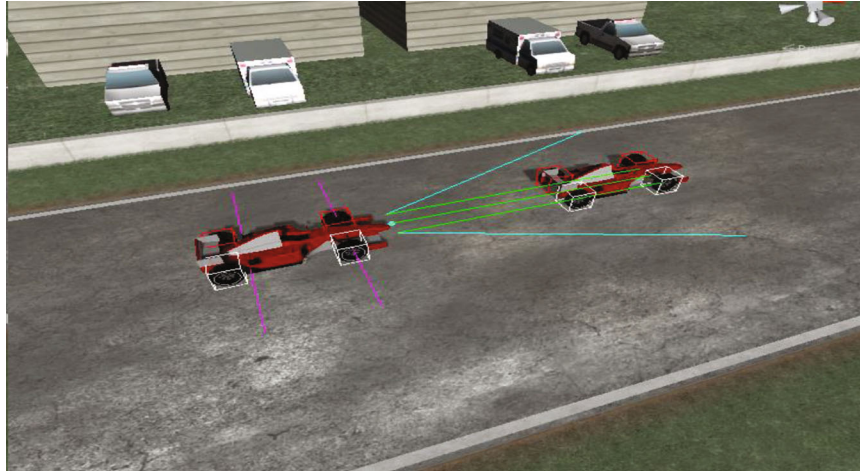


FIGURE 22: Detection lines of AI driver.

- (h) Center of mass-this parameter is used to hold the car on the road so that it does not flip. Also, it is used to show the animations of turning. Center of mass is calculated from the rigid body parameter
- (i) Wheel collider-this parameter keeps the car from falling through the track and also uses for the wheel alignment parameter for rotation
- (j) Steering sharpness-this parameter decides how the AI vehicles will quickly turn around in a corner

6.3. *AI Behavior.* This module covers the behavioral aspects of the bots vehicles like collision, overtaking, slipstreaming, and aggression. Collision spheres or cubes which defines collision range of that vehicle will be assigned to vehicles to check for collision with vehicles or objects. In the following Figure 23, the green rectangles depicts two racing vehicles.

The bots vehicle will check for empty spaces around another race vehicle using the generated detection lines (yellow lines). If the detection lines does not register another vehicle or object (like a wall), then the bots will generate temporary overtake paths (red lines) around the vehicle in front. The bots will then determine the safest overtake path, increase its speed, temporarily divert from its racing line (blue line) to the overtake path, and attempt an overtake (in this case, path B). Alternatively, the bots can slipstream behind another vehicle and use the extra burst of speed for an overtake. Aggression will define how likely is an AI controlled bots to overtake or block an overtake attempt. All the bots will be assigned an aggression factor which will define the aggression level of a bot. Higher aggression factor means that the bots are more likely to overtake or block an overtake attempt.

6.4. *Racing Lines.* The racing line is the most optimized path the driver can use to conserve speed during cornering with as little braking as possible. The entire racing line was constructed and placed on the Monza track. This line provides the AI cars the most optimized guideline so they can finish the race as quickly as possible. The bots will have a path cov-

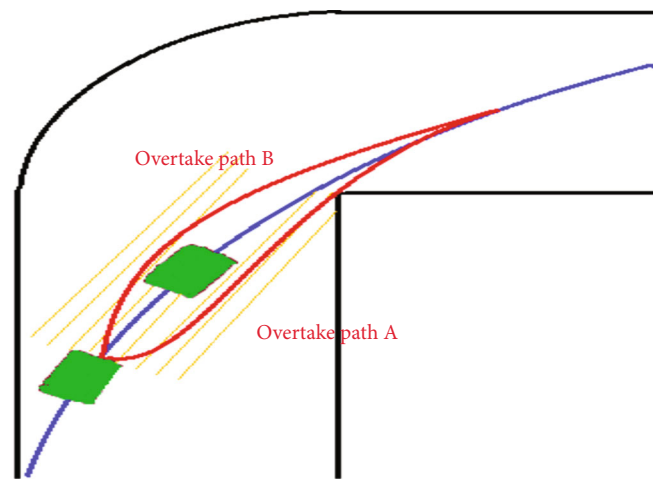


FIGURE 23: The AI behavior.

ering the length and width of the entire track in which it will have full freedom of movement (gray area).

Each track will be set up with a racing line (colored line). The racing line is the route the vehicle must take in order to minimize the time taken to complete the course. The bots will follow the racing line unless it encounters a difficulty such as an obstacle.

The racing line can even provide visual aid to the player car so as to drive optimally. The opponent cars or AI controlled vehicles will follow the designated racing line and complete laps till the finish line. Braking zones are added to the track at necessary or critical points on the track, and the AI will break the vehicle whenever it encounters a corner as shown in Figure 24.

6.5. *Obstacle Avoidance, Viewpoints, and Waypoints.* The AI-controlled Formula One vehicles are modeled and programmed with the help of obstacle avoidance, viewpoint, and waypoint techniques. Obstacle avoidance techniques are used by the AI-controlled vehicles to steer away from obstacles in front and to their sides. This is done with the help of collision detectors placed on the vehicles. This helps them to avoid collision with other vehicles on track.

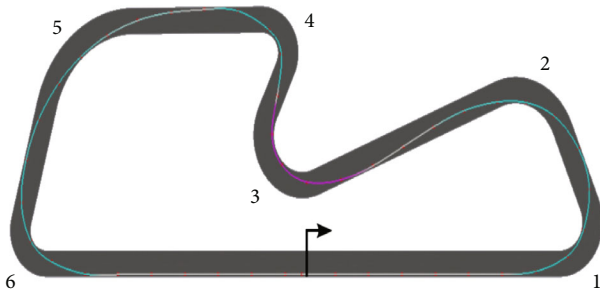


FIGURE 24: Racing line.

Viewpoints are essentially “eyes” for all the AI-controlled vehicles. This helps the vehicles to move forward and tackle corners. The dot at the nose of the vehicle in the picture below is a viewpoint while the colored lines are the collision detector lines. Waypoints are essentially points on the race track that are assigned individually to each AI vehicle. The vehicles may or may not follow these points. The waypoint system is mainly implemented to help the AI-controlled vehicles to recover after it has go off the race course. These techniques are implemented to recreate the actual Formula One driver behavior as an extension of object detection and recognition.

## 7. Implementation

Once all of the sculpting and the World Design is completed, the AI drivers and the player car must be implemented into the scene. To achieve this purpose, we again use the Unity3D game engine.

*7.1. Player Car Setup.* Initially, the player car is implemented into the scene. At first, the Formula One model sculpted in 3ds Max is imported into Unity3D. The axis of the F1 model must be adjusted so that it does not cause any problems in Unity3D. Also, the textures of the model have to be manually adjusted. The F1 car model will be constructed of separate parts, i.e., 4 individual wheel models and a body model that will be children of parent F1 car model. Once the model is completely imported, it is placed in the starting grid of the scene. First order of business is to assign the various collider meshes to the body and wheels of the car. Two rectangular collision meshes are placed on the car as illustrated in Figure 25. These two meshes make sure that the car does not fall through the road or go through walls and other cars. These meshes are also used to register collision between two cars or collision with the limits of the road.

Then, the wheel colliders are added to each of the individual wheels as shown in Figure 26. The wheel colliders are used to animate the wheels (like rotating). Hence, the wheel colliders must be precisely aligned to the wheel meshes otherwise the car will look like its floating during runtime.

Once all the colliders are in place, then an empty game object is created and named as center of mass. This is later used to define the centre of mass of the car. This object is placed roughly on the middle of the car. Then, the rigid body

modifier is added to the Player Car. This modifier gives mass to the vehicle which is used by the code to calculate the acceleration and velocity of the car. Now, the code for the movement is assigned to the Player Car. During runtime, the code first checks for the coordinates of the player car’s initial position. When the key responsible for forward movement is tapped, then the code propels the car in a particular axis by updating the position of the car. For example if the car initially is at (0,0,0), after tapping the forward movement key, the code updates the coordinates of the car to (10,0,0). Then, between the initial and the final position, the animation for the wheel rotation is applied to the wheels. Hence, it gives the impression of a forward movement of a car. When the key for sideways movement is tapped, then a parameter called steer angle calculates how long the key is tapped. Based on the duration, the steer angle parameter rotates the axis of the car according to the direction. For example, if the car is aligned at 0 degrees with global  $x$  axis and the turn right key is pressed, then the steer angle parameter will rotate the car along with the axis by say 30 degrees. During that time, the wheels will also be animated to turn by a 30 degree angle. Thus, the rotation of the car along with the turning of the wheels give the impression of the turning of a car. First, the wheels turn, then the car is rotated to provide a smooth looking turn. This is illustrated in the following Figures 27–29.

Finally, the viewing camera needs to be assigned to the Player Car. To accomplish this, the camera main object is transposed/rotated/scaled until the view of the camera is behind the player car or on the cockpit of the car as required. Then, the camera is inserted into the hierarchy of the Player Car. In this way, whenever the Player Car moves, so will its children. Hence, the camera will follow the car. Thus, the basic setup of the player car is complete. After this, the handling parameters of the car like max speed, gear ratios, forward and sideways friction, and braking force are fine tuned so as to bring the feel of the handling of a F1 vehicle.

*7.1.1. AI Driver Setup.* The car models for the AI’s are first imported from 3ds Max into Unity and placed at their starting grid alongside the player car. These also contain separate meshes for the body and wheels. Next, the various colliders, rigid body, and center of mass are assigned to the AI driver similar to the Player Car. Then, the waypoints are assigned for each vehicle. The AI car uses these waypoints to roughly navigate through the track. Also, the AI car respawns at the last checkpoint it passed through should it go off track or collide with another vehicle. Hence, the waypoints are a very important aspect of the AI drivers. The curve drawn by these waypoints represents the racing line shown in Figure 30.

Next, the viewpoint or just view is assigned to the AI vehicle as shown in Figure 31. The view contains the detection lines which detects if an obstacle is in front or side of the car. It behaves like the eyes of the vehicle. The view must be assigned to the nose of the vehicle. These lines detect objects in front of the Player Car. Then, views have to also be placed on both sides of the car to detect objects on the side. These are placed near the wheels so as to relay the most accurate



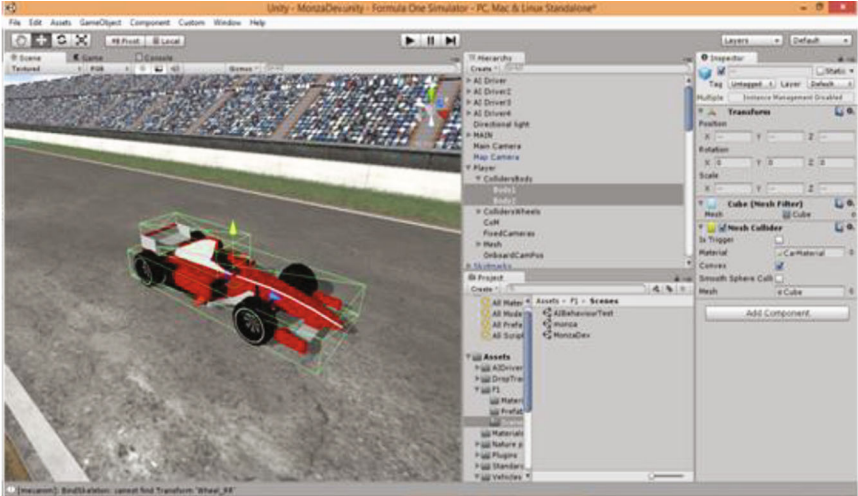


FIGURE 25: Rectangular colliders (green boxes).

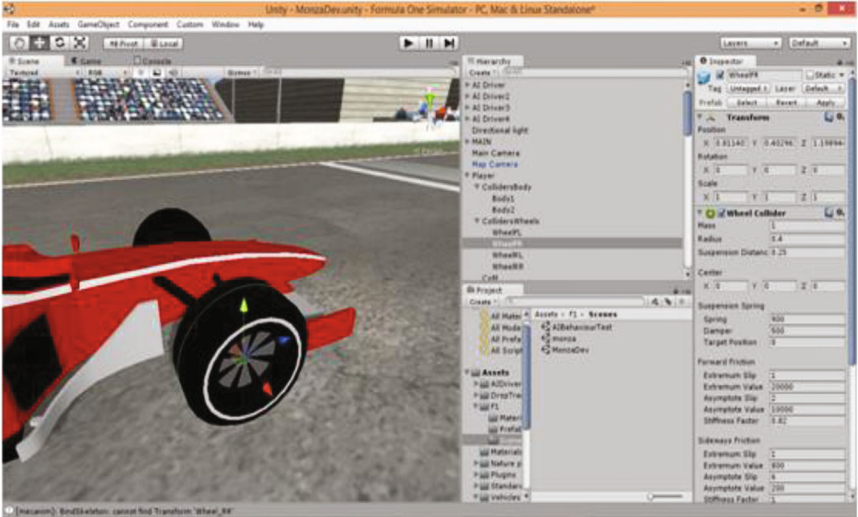


FIGURE 26: Wheel colliders (green circle around FR wheel).

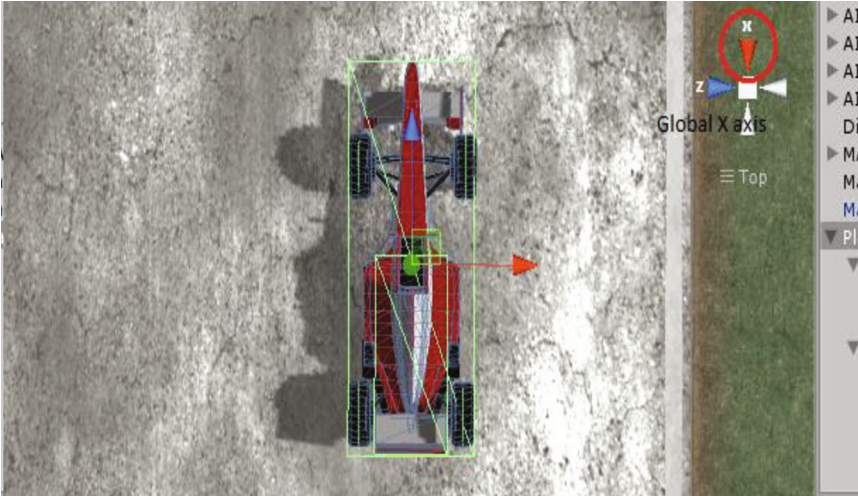


FIGURE 27: Aligned to global x axis.

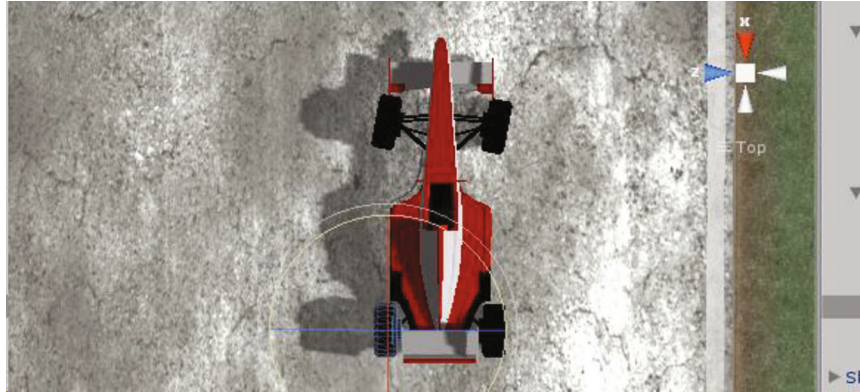


FIGURE 28: Turning of wheels.

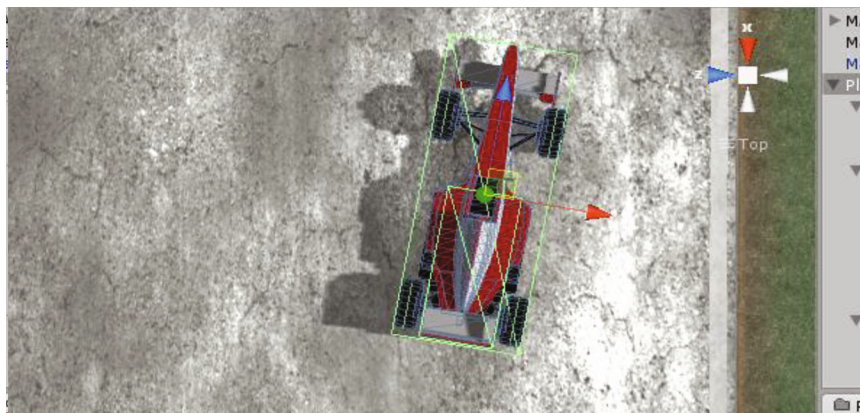


FIGURE 29: Turning of whole car.

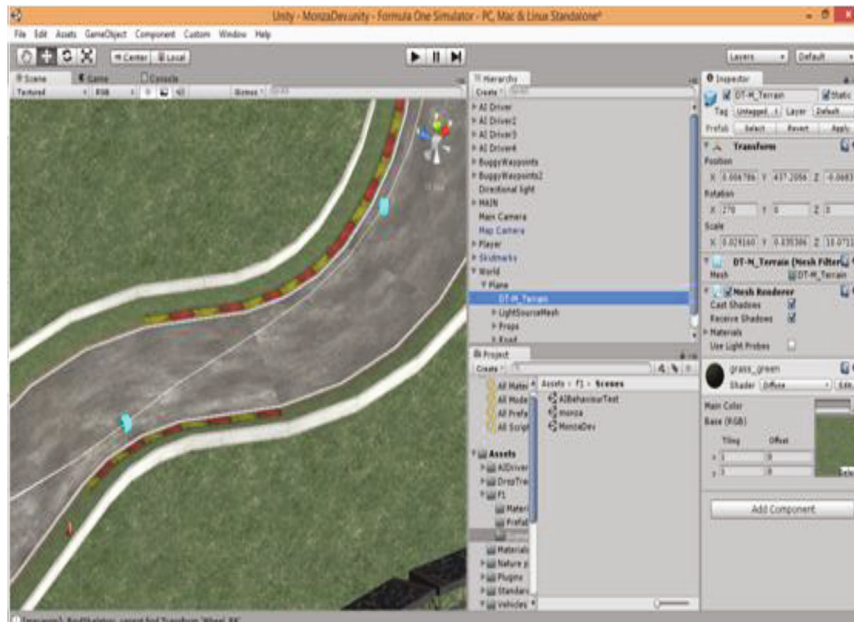


FIGURE 30: The small blue boxes represent waypoints and the white line represents the racing line.

position of objects at the sides and also since the wheels are used to turn the car.

Then, the code for the movement of the AI car is assigned. It works similar to the movement of the Player

Car code but in this case, the velocity, acceleration, and turning of the car depends upon another piece of code. This code tells the car its speed or turn bounds. The code for the AI controller is assigned next. This code uses the detection lines

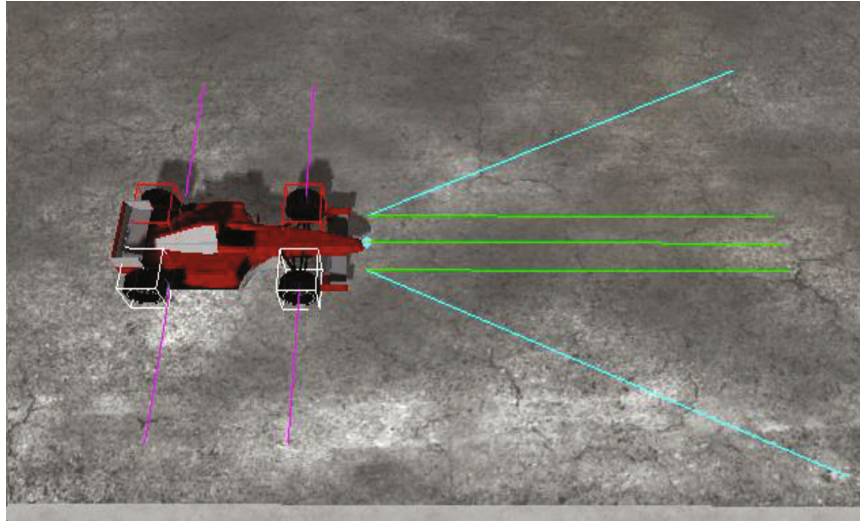


FIGURE 31: Viewpoint/view.

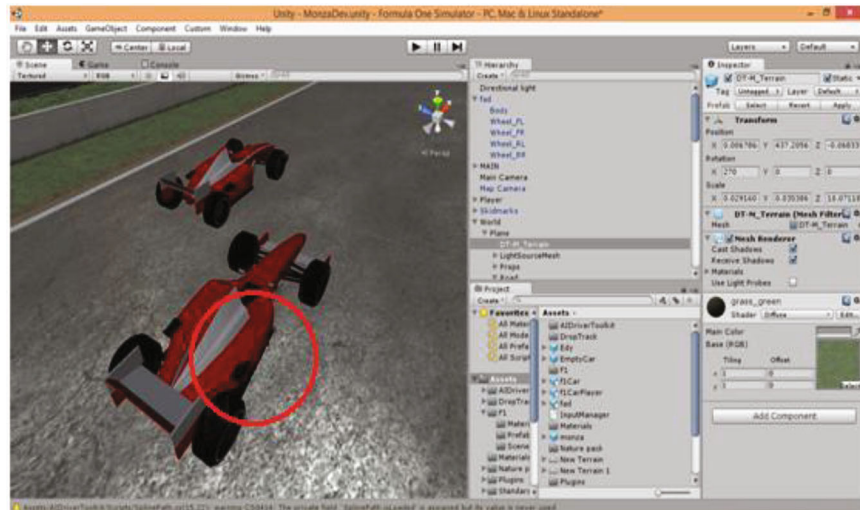


FIGURE 32: Deformation of mesh due to collision.

of the Viewpoint to steer the AI vehicle around the track. When the detection lines does not detect any object in its path, then the velocity of the car is set to its speed limit. Whenever there is a corner, the AI car detects the boundary, reduces its velocity by using the brake parameter, and accordingly turns itself. When it encounters another vehicle or object, it brakes and deviates from current path to avoid collision.

**7.1.2. Collision Damage.** After setting up all the cars, the damage mechanics are added. The code for damage is assigned to both the Player and the AI cars. When the collider meshes of two cars come in contact (occupy the same world space), then it is registered as a collision. The code then effectively rearranges the vertices of the mesh by a small factor to show the damage to the car. Even in the case of a collision with a wall the vertices of the car mesh are deformed a little. However, the vertices of the wall are not deformed as shown in Figure 32. This is due to performance reasons. The collision mechanics uses a lot of system resources. The track has separate modular

meshes that are arranged to form the track. So, adding the damage code to all of the separate meshes could result in a significant drop in FPS during runtime. The damage mechanics also effects the performance of the Player Car. The more the damage it takes, the harder it becomes to effectively control the car. For example, if the front left wheel takes damage, then the car will turn a little towards the right even when the “turn right” key is not tapped. This adds some depth to the handling of the Player Car.

**7.1.3. Final Game Build.** Once all the game objects are integrated with their respective codes, these are then added all together to the scene. The scenes exist only inside the game engine that is Unity. So, the next order of business is to make it into a stand-alone software application. To achieve this, we use the inbuilt build feature of the Unity engine. The build feature takes in all the separate scenes and along with the visual effects generates an executable file of .exe format.

There are two modes available to operate the simulator: training mode and automatic mode. In training mode, the user uses virtual control to drive the car using the steering angle, the throttle, and the brakes. You can do this with a keyboard or a mouse. During training mode, the simulator will start saving driving data to a specific spot. Driving data consists of each image on the left, right, and front sides of the vehicle and the corresponding steering, throttle, and brake measurements.

In order to collect training data, the car was driven in training mode around the virtual track for five full laps using the centre lane driving behavior, in order to avoid reaching the road boundaries on both sides. The data was further improved by numerous selective driving acts around corners to account for oversteer and understeer, with several obstacles in different directions approaching to hit the vehicle at different angles. A total of 5,000+ data points were collected from the training run. After the rise, the total number of data points was more than 10,000. We used Keras deep learning library. The control angle was the only measure used as the output for the model; the convolutionary neural networks (CNNs) were used to map raw pixels from the front-facing camera to the steering controls for the self-driving car. Training data was 80% and 20% of the data used for validation. As expected, the mean squared error loss of both the training and validation sets decreased with the number of iterations. At the end of the training process, the model was able to steer the vehicle on the track without leaving the route, thus avoiding road obstacles.

## 8. Conclusion and Future Scope

The final build of the scenes has produced a simulation program for Formula One cars. In this simulator, the end user will be able to take the wheel of one of the F1 cars. The AI cars will run along with the Player Car and behave like a real world Formula One car. It will try to overtake the player whenever it sees an opportunity. It will also avoid collision with other objects or vehicles. The simulator will contain with several racing circuits all of them providing various racing challenges for the budding racer. The circuits contains various type of corners like hairpin bends and U-turns. The circuits will also contain visual aids for the player to drive effectively in the track-like kerbs. To get the actual feel of the F1 car, there will also be a cockpit camera so that the users can view the track from the eyes of a racer.

While designing F1 simulator, we should make a note of behavior of virtual traffic and weather conditions, and the road layout can be manipulated (offline or in real time) as a function of the training needs or research aims in the future. We have to consider “safety” related features in the future research.

## Data Availability

The data used to support the findings of this study are available from the corresponding author upon request (mmasud@tu.edu.sa).

## Conflicts of Interest

The authors declare that they have no conflicts of interest to report regarding the present study.

## Authors' Contributions

Amutha Balakrishnan contributed to the conceptualization, data curation, formal analysis, methodology, writing-original draft, and software. Kadiyala Ramana contributed to the data curation, writing-original draft, investigation, resources, validation, and software. Gaurav Dhiman contributed to the supervision, writing-review and editing, project administration, and visualization. Gokul Ashok contributed to the conceptualization, investigation, resources, validation, and software. Vidhyacharan Bhaskar contributed to the supervision, writing-review and editing, and visualization. Ashutosh Sharma contributed to the supervision and writing-review and editing. Gurjot Singh Gaba contributed to the writing-review and editing and investigation. Mehedi Masud contributed to the writing-review and editing and funding acquisition. Jehad F. Al-Amri contributed to the writing-review and editing and funding acquisition.

## Acknowledgments

Taif University Researchers Supporting Project number (TURSP-2020/211), Taif University, Taif, Saudi Arabia.

## References

- [1] B.-H. Chen and S.-C. Huang, “An advanced moving object detection algorithm for automatic traffic monitoring in real-world limited bandwidth networks,” *IEEE Transactions on Multimedia*, vol. 16, no. 3, 2014.
- [2] X. Bai, Q. Li, L. Latecki, W. Liu, and Z. Tu, “Shape band: a deformable object detection approach,” in *IEEE Conference on Computer Vision and Pattern Recognition*, Miami, FL, 2009.
- [3] S. Bhattacharya, P. K. R. Maddikunta, I. Meenakshisundaram et al., “Deep neural networks based approach for battery life prediction,” *CMC-COMPUTERS MATERIALS & CONTINUA*, vol. 69, no. 2, pp. 2599–2615, 2021.
- [4] A. Kaur and G. Dhiman, “A Review on Search-Based Tools and Techniques to Identify Bad Code Smells in Object-Oriented Systems,” in *Harmony search and nature inspired optimization algorithms*, pp. 909–921, Springer, Singapore, 2019.
- [5] M. Garg and G. Dhiman, “Deep convolution neural network approach for defect inspection of textured surfaces,” *Journal of the Institute of Electronics and Computer*, vol. 2, no. 1, pp. 28–38, 2020.
- [6] D. S. Rajput, A. P. Singh, Y. Agarwal, P. K. Reddy, and G. T. Reddy, “Feature selection analysis for multimedia event detection,” in *IOP Conference Series: Materials Science and Engineering*, vol. 263, no. 4p. 042004, IOP Publishing, 2017.
- [7] O. Danielsson, S. Carlsson, and J. Sullivan, “Automatic learning and extraction of multi-local features,” in *International Conference on Computer Vision*, Kyoto, Japan, October 2009.
- [8] V. Ferrari, F. Jurie, and C. Schmid, “From images to shape models for object detection,” *International Journal on Computer Vision*, vol. 87, no. 3, pp. 284–303, 2009.

- [9] J. Shotton, A. Blake, and R. Cipolla, "Multiscale categorical object recognition using con-tour fragments," *IEEE Transactions on Pattern Analysis and Machine Intelligence*, vol. 30, no. 7, pp. 1270–1281, 2008.
- [10] J. De Winter and J. Wagemans, "Perceptual saliency of points along the contour of everyday objects: a large-scale study," *Perception & Psychophysics*, vol. 70, no. 1, p. 50, 2008.
- [11] P. Felzenszwalb and J. Schwartz, "Hierarchical matching of deformable Shapes," in *Computer Vision and Pattern Recognition*, pp. 1–8, Minneapolis, MN, USA, June 2007.
- [12] V. Ferrari, T. Tuytelaars, and L. Van Gool, "Object detection by contour segment networks," *Lecture Notes in Computer Science*, vol. 3953, p. 14, 2006.
- [13] J. Shotton, A. Blake, and R. Cipolla, "Contour-based learning for object detection," in *International Conference on Computer Vision*, pp. 503–510, Beijing, China, 2005.
- [14] S. Hermann and R. Klette, "Global curvature estimation for corner detection," *Image and Vision Computing New Zealand*, 2005.
- [15] D. Martin, C. Fowlkes, and J. Malik, "Learning to detect natural image boundaries using local brightness, color, and texture cues," in *IEEE Transactions on Pattern Analysis and Machine Intelligence*, pp. 530–549, 2004.
- [16] T. Sebastian, P. Klein, and B. Kimia, "Recognition of shapes by editing shock graphs," *IEEE International Conference on Computer Vision*, pp. 755–762, 2001.
- [17] R. Kumar and G. Dhiman, "A comparative study of fuzzy optimization through fuzzy number," *International Journal of Modern Research*, vol. 1, no. 1, pp. 1–14, 2021.
- [18] I. Chatterjee, "Artificial intelligence and patentability: review and discussions," *International Journal of Modern Research*, vol. 1, no. 1, pp. 15–21, 2021.
- [19] P. K. Vaishnav, S. Sharma, and P. Sharma, "Analytical review analysis for screening COVID-19 disease," *International Journal of Modern Research*, vol. 1, no. 1, pp. 22–29, 2021.
- [20] G. Jianhong, H. He, Z. Wenxuan, and Y. Liang, "Research on real-time collision detection for vehicle driving in the virtual environment," in *IEEE international conference on information and automation*, China, June 2008.
- [21] C. I. Tan, C.-M. Chen, W.-K. Tai, and S.-J. Yen, "An AI-tool: Generating paths for racing game," in *Seventh International Conference on Machine Learning and Cybernetics*, Kunming, July 2008.
- [22] T. P. Hartley and Q. H. Mehdi, "In-game adaptation of a navigation mesh cell path," in *17th International Conference on Computer Games*, Louisville, KY, USA, 2012.
- [23] V. Sezer and M. Gokasan, "A novel obstacle avoidance algorithm: "follow the gap method"," *Robotics and Autonomous Systems*, vol. 60, no. 9, pp. 1123–1134, 2012.
- [24] J. Oroko and B. Ikua, "Obstacle avoidance and path planning schemes for autonomous navigation of a Mobile robot: a review," *Sustainable Research and Innovation Proceedings*, vol. 4, 2012.
- [25] Y. Zhu, T. Zhang, J. Song, and X. Li, "A new hybrid navigation algorithm for mobile robots in environments with incomplete knowledge," *Knowledge-Based Systems*, vol. 27, pp. 302–313, 2012.
- [26] A. Sgorbissa and R. Zaccaria, "Planning and obstacle avoidance in mobile robotics," *Robotics and Autonomous Systems*, vol. 60, no. 4, pp. 628–638, 2012.
- [27] C. L. Kumari, "Building algorithm for obstacle detection and avoidance system for wheeled mobile robot.," *Global Journal of Research Engineering*, vol. 12, no. 11-F, 2012.
- [28] S. K. Kalmegh, D. H. Samra, and N. M. Rasegaonkar, "Obstacle avoidance for a mobile exploration robot using a single ultrasonic range sensor," in *2010 International Conference, Emerging Trends in Robotics and Communication Technologies (INTERACT)*, pp. 8–11, Chennai, India, December 2010.
- [29] A. Yufka and O. Parlaktuna, "Performance Comparison of Bug Algorithms for Mobile Robots," in *Proceedings of the 5th international advanced technologies symposium*, Karabuk, Turkey, May 2009.
- [30] <http://www.fritz-hut.com/vector-field-histogram-vfh/>.
- [31] I. Ulrich and J. Borenstein, "Vfh\*: local obstacle avoidance with lookahead verification," in *Proceedings 2000 ICRA. Millennium Conference. IEEE International Conference on Robotics and Automation. Symposia Proceedings*, pp. 2505–2511, San Francisco, CA, USA, 2000.
- [32] G. Li, A. Yamashita, H. Asama, and Y. Tamura, "An efficient improved artificial potential field based regression search method for robot path planning," in *2012 IEEE International Conference on Mechatronics and Automation*, pp. 1227–1232, Chengdu, China, August 2012.
- [33] K. H. Chen and W. H. Tsai, "Vision-based obstacle detection and avoidance for autonomous land vehicle navigation in outdoor roads," *Automation in Construction*, vol. 10, no. 1, pp. 1–25, 2000.
- [34] T. R. Gadekallu, N. Khare, S. Bhattacharya, S. Singh, P. K. R. Maddikunta, and G. Srivastava, "Deep neural networks to predict diabetic retinopathy," *Journal of Ambient Intelligence and Humanized Computing*, pp. 1–14, 2020.
- [35] Y. Liu, Q. Sun, A. Sharma, A. Sharma, and G. Dhiman, "Line monitoring and identification based on roadmap towards edge computing," *Wireless Personal Communications*, pp. 1–24, 2021.
- [36] T. Reddy, R. M. SP, M. Parimala, C. L. Chowdhary, S. Hakak, and W. Z. Khan, "A deep neural networks based model for uninterrupted marine environment monitoring," *Computer Communications*, vol. 157, pp. 64–75, 2020.

## Research Article

# Sixth Generation (6G) Cognitive Radio Network (CRN) Application, Requirements, Security Issues, and Key Challenges

Muhammad Muzamil Aslam <sup>1,2,3</sup> Liping Du <sup>2,4</sup> Xiaoyan Zhang <sup>5</sup> Yueyun Chen <sup>2</sup>  
Zahoor Ahmed <sup>6,7</sup> and Bushra Qureshi <sup>1</sup>

<sup>1</sup>Department of Electronics and Communication Engineering, University of Science and Technology China (USTC), Hefei, Anhui 230026, China

<sup>2</sup>School of Computer & Communication Engineering, University of Science and Technology Beijing, Beijing 100083, China

<sup>3</sup>Department of Information Sciences, University of Education (UoE), Multan, Pakistan

<sup>4</sup>Shunde Graduate School of University of Science and Technology Beijing, Beijing 100083, China

<sup>5</sup>State Radio Monitoring Center, Beijing 100037, China

<sup>6</sup>Department of Automation, Shanghai Jiaotong University, Shanghai 200240, China

<sup>7</sup>Department of Electronics, Government College University (GCU) Lahore, Pakistan

Correspondence should be addressed to Liping Du; [dlp2001@ies.ustb.edu.cn](mailto:dlp2001@ies.ustb.edu.cn) and Zahoor Ahmed; [zahoorqu10@sjtu.edu.cn](mailto:zahoorqu10@sjtu.edu.cn)

Received 28 July 2021; Revised 13 September 2021; Accepted 29 September 2021; Published 13 October 2021

Academic Editor: VIMAL SHANMUGANATHAN

Copyright © 2021 Muhammad Muzamil Aslam et al. This is an open access article distributed under the Creative Commons Attribution License, which permits unrestricted use, distribution, and reproduction in any medium, provided the original work is properly cited.

Recently, 5G installation has been started globally. Different capabilities are in the consistent procedure, like ultrareliability, mass connectivity, and specific low latency. Though, 5G is insufficient to meet all the necessities of the future technology in 2030 and so on. Next generation information and communication technology is playing an important role in attraction of researchers, industries, and technical people. With respect to 5G networks, sixth-generation (6G) CR networks are anticipated to familiarize innovative use cases and performance metrics, such as to offer worldwide coverage, cost efficiency, enhanced spectral, energy improved intelligence, and safety. To reach such requirements, upcoming 6G CRNs will trust novel empowering technologies. Innovative network architecture and transmission technologies and air interface are of excessive position, like multiple accesses, waveform design, multiantenna technologies, and channel coding schemes. (1) To content, the condition should be of worldwide coverage, there will be no limit on 6G to global CR communication networks that may require to be completed with broadcast networks, like satellite communication networks, therefore, attaining a sea integrated communication network. (2) The spectrums overall will be entirely travelled to the supplementary rise connection density data rates in optical frequency bands, millimeter wave (mmWave), sub-6 GHz, and terahertz (THz). (3) To see big datasets created because of tremendously varied CR communication networks, antenna rush, diverse communication scenarios, new provision necessities, wide bandwidth, and 6G CRNs will allow an innovative variety of intelligent applications with the assistance of big data and AI technologies. (4) Need to improve network security when deploying 6G technology in CR networks. 6G is decentralized, intended, intelligent innovative, and distributed network. In this article, we studied a survey of current developments and upcoming trends. We studied the predicted applications, possible technologies, and security issues for 6G CR network communication. We also discussed predicted future key challenges in 6G.

## 1. Introduction

From 2020, 5G cognitive radio networks (CRNs) [1] are playing a key role in global communication and spectrum sharing. The main part of 5G CR communication is massive machine-type communication, enhanced mobile broadband, and low

latency ultrareliable communication. The main features of 5G are about 0.1 Gbps data rate, the peak data rate is about 20 Gbps, end-to-end latency is about 1 ms, device connectivity is approximately 1 million/km<sup>2</sup>, thrice spectrum efficiency, 500 km/h supporting mobility, traffic capacity by area 10 Mbps/m<sup>2</sup>, and several times energy efficiency as compared

to 4G CRN communication [2]. Several essential technologies, such as ultradense network, millimeter-wave, and MIMO, have been studied to gain 5G CRN communication.

Although, fifth-generation is insufficient to meet the necessities of 2030 and so on. Scientists, institutes, and researchers focus on 6G CRN communication [3, 4]. An essential point of fifth-generation (5G) is low latency, which requires a deterministic network to ensure point-to-point inactivity with the requirement and precision of incoming future mandate. Authors studied in [5] that 6G must be capable to pursue high synchronization than 5G. Furthermore, there will be about maximum geographical coverage, millisecond geographical location updating accuracy, and subcentimeter geographical accuracy in 6G [6].

In some cases, 5G is still complicated, e.g., villages, remote areas, and roads are not fully covered by 5G that confines few applications, like driverless vehicles. Specific communication satellite and nonterrestrial networks must fulfill broadcast networks for ubiquitous services surety, seamless, and cost-effectiveness. The communication network of the unmanned aerial vehicle is essential for quick reply in any complication of surroundings. Although millimeter-wave can offer Gbps data transmission in 5G, it will require a Tbps data rate in 6G for applications [7, 8] such as 3D high-quality videos, virtual reality, augmented reality, alternative frequency bands, and THz may be contender bands [9, 10]. With the use of extraordinary heterogeneous networks, number of antennas in large amount, new service diverse communication situation, and wide bandwidth, there will be new access of smart applications in 6G with the assistance of machine learning [11, 12] and artificial intelligence technologies. There is an automation level for network performance improvement in several forms, such as quality of security, quality of services, fault management, experience quality, and energy efficiency [13–15].

In 5G, network traffic is dominated by streaming or video applications. Except for all the applications mentioned above and requirements, we can study from 5G physical information communication [16, 17] which CR networks are robotics controlled. Factory logistics and automated driving are fresh cellular technology applications, but still, there are some new challenges. Using such applications for network traffic analysis, several mobile objects transfer control and sensor information overload the central network in control system. Artificial intelligence used distributed control systems is developing research focus for future technology and demand. It is to be supposed that artificial intelligence and such application networks will dominate CR network traffic requirement of 6G. This area of research is untouched that makes its presence challenging [18].

To see 5G CR networks, 6G CR networks will provide maximum higher spectral, cost efficiency, energy, maximum data rate about in Tbps, about ten-time lower latency, connection density about 100 times improved, and maximum intelligence for automation. Latest transmission and spectrum sensing technologies and air interference are mandatory to gain energy efficiency and high spectrum efficiency with fresh waveforms, channel coding methods, multiple access approaches, and multiantenna technologies are the

proper combination of all such techniques. Meanwhile, such network architecture requires dynamic network slicing, software-defined network, cognitive service architecture, service-based architecture, and free of cell architecture. Although, the software comes at a point as we acknowledged from 5G progress. A commercial use server versus domain particular chips in the virtualized radio access network (VRAN) suggests a massive amount of energy consumption enhancement and measure to better energy efficiency. The current statistic shows that power consumption in 5G is more than 4G networks but at higher bandwidth.

Contrary to this, we should provide a network that is stimulatingly of its start does not cross the limits of previous generation power requirement. So, in 6G, we need a new computing paradigm to provide all advantages of notarization deprived of energy consumption cost. Some computing technologies like fog computing, edge computing, and cloud computing are key in network flexibility, processing, lower latency, synchronization, and distributed computing. To overcome the limitations and drawback of 5G short packet, the network should provide low latency service using high data rate, delivery of high reliability, internet of everything, and system coverage. To overcome the requirements of CRN communication in 2030 and beyond [19], 6G CR network should develop the data rate or human-centric [20]. To acquire such supplies, 6G CR network communication will shift to a new paradigm.

We will illustrate the 6G CR network vision in this paper. The first 6G CR networks will be sea integrated space air-ground networks for global network communication coverage. UAV communication, satellite communication, and naval communication will encompass vast areas for CR network communication coverage. All spectrums will be evident for providing a high data rate. For full application enabling, machine learning and artificial intelligence technologies will be competently combined with 6G CR networks communication for better automation and network management [21]. Besides, artificial intelligence technology can enable dynamic arrangement of a network, resource computing for performance betterment, and caching of 6G networks. Last but not least, high network security is required for the physical and network layer during development. Industry verticals like the internet of things (IoT) [22, 23], virtual cloud reality, industry automation, digital body area network, cellular vehicle to everything, energy-efficient CR network, and central acknowledged system would boost the progress of 6G CR network communication. 6G CR network overview is shown in Figure 1. There is detailed intuition of 6G in Figure 2. Table 1 is for the acronyms used in the paper.

## 2. Background, 6G Artificial Intelligence CR Network

In this work, we focused that artificial intelligence that will empower 6G in all forms, network management and composition, signal processing and physical layer, service-based communication, and data mining [24]. Researchers have started planning and envisioning the essential technologies

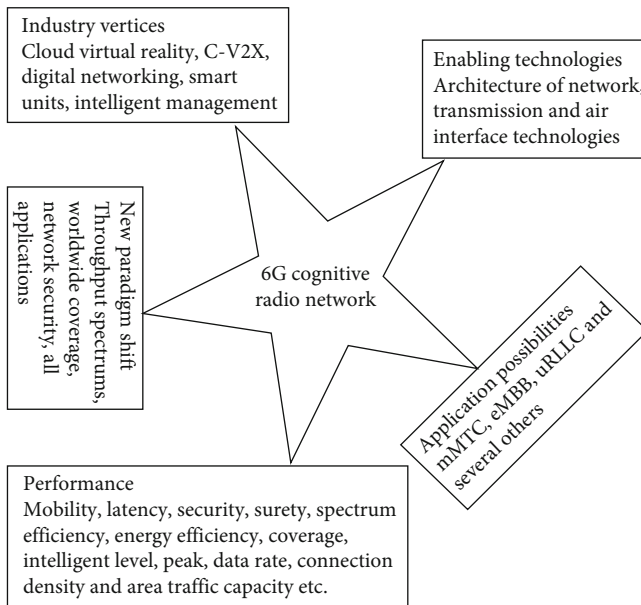


FIGURE 1: An overview on 6G cognitive radio networks.

supporting 6G CR network communication in various ways like beyond 5G+. To gain 1 ms latency order, uRLLC was introduced in 5G for critical applications latency. Mobile edge computing and computing models defined in 5G for delay reduction and network overcrowding are classically met in user equipment to integrate base station CR network communication. Although, fog nodes are unable to act as freely relay and cloud data center on basic cloud. Another derivative of cloud computing is the cloud radio access network (CRAN), in which already present base stations are swapped with distributed remote radio heads and middle baseband unit (BBU). In the cloud radio access network architecture, signal processing computations are performed at the baseband unit. Although this cloud access radio network may complete the 5G requirements, service heterogeneously, communication overhead, and BBU performed computation, six generation 6G network will improve computational complexity and latency [25]. A progressing notation to focus on this is the open radio access network (O-RAN) that holds openness and intelligence as its key idea. O-RAN supplies clearly defined open boundaries between elements applied on universal purpose hardware and the integration of RRHs and BBUs from different retailers. Cell compaction is a primary enabler for accomplishing amplified network capacity [26]. 6G intentions at ultradense network distributions relating to multiple cells within a microcell. Diverse 6G use, such as high accuracy engineering, intelligent homes, and vehicle-to-everything, will involve various devices functioning in a microcell. Though, these 6G applications will include addressing numerous key challenges. The high-frequency operation, heterogeneity, mobility, and dense operation will present a different dimension of propagation, radio resource allocation, spectrum access, security concerns, and scheduling. Such sprints will be worsened with the intended 3D communication infrastructure [27] for 6G joining mobile ground

and aerial platforms. Large-scale dense placement strategic for 6G, intelligent physical layer schemes will play a vital role in satisfying the provision requirements.

Furthermore, machine learning (ML) study at an advantage will become the leading enabler for 6G CR network communications. Deep learning (DL) explanations for CR network communication with MIMO beamforming, channel estimation and equalization, coding, error correction, signal recognition, etc., are computationally composite demanding controlling computational platforms. Though, DL architectures' proficient learning aptitude inspires the need to integrate them for future CR networks. Also, meaningful innovations in artificial intelligence have admonished it to be part of 5G yet organized only in services with substantial training data and commanding computing platforms. Though, to ease ML at an advantage, igniter operations of DL solutions will require to be established. Moreover, the black-box nature of neural networks reduces them unintelligible and erratic as it is challenging to increase vision into the educated function from network architecture.

Consequently, neural networks (NNs) present three main challenges: black-box nature, computational complexity, and resource constraint. Baseband tactile layer signal processing techniques will track the UE and base stations [28]. To see in a generation to generation of communication standard is bottlenecked by the UE's aptitude. Therefore, performing these DL explanations in the present UE stands will be impracticable as they do not own controlling computational platforms as obligatory by such tactics. Subsequently, intelligent baseband signal processing intended for 6G CR networks must be personalized for unimportant embedded computational daises with ruthless energy efficiency, latency objectives, and reliability. Combining domain information into the DL architectures embraces huge potential to rush the training process and model junction though attractive the model effectiveness. Table 2 is representing 5G to 6G evaluation.

### 3. Cognitive Radio and Wireless Sensor Network (CR and WSN)

With time, WSN used in IoT is increasing in the intelligent industry and almost covering all sectors of life such as e-health, traffic, smart homes, smart grids, intelligent stations, smart industry, monitoring purpose, and smart agriculture. WSN and CR can be in profit by sharing the process. Progressing installation of WSN can be oppressed by CR by PU channel monitoring, e.g., the new business model of spectrum sensing as a service (SSaaS). In another way, a large number of WSN usage increases the requirement of spectral resources. In this, CR is to be supposed as the solution to spectrum sharing.

*3.1. For WSN Communication Dynamic Spectrum Sharing.* Progressing the use of WSN devices requires improved use of limited frequency resources. For WSN, dynamic spectrum sharing WSN node is taken as SUs by CR. Keeping an eye on the PU channel, extra work is beard by WSN nodes, and good energy use requires SS task completion because energy



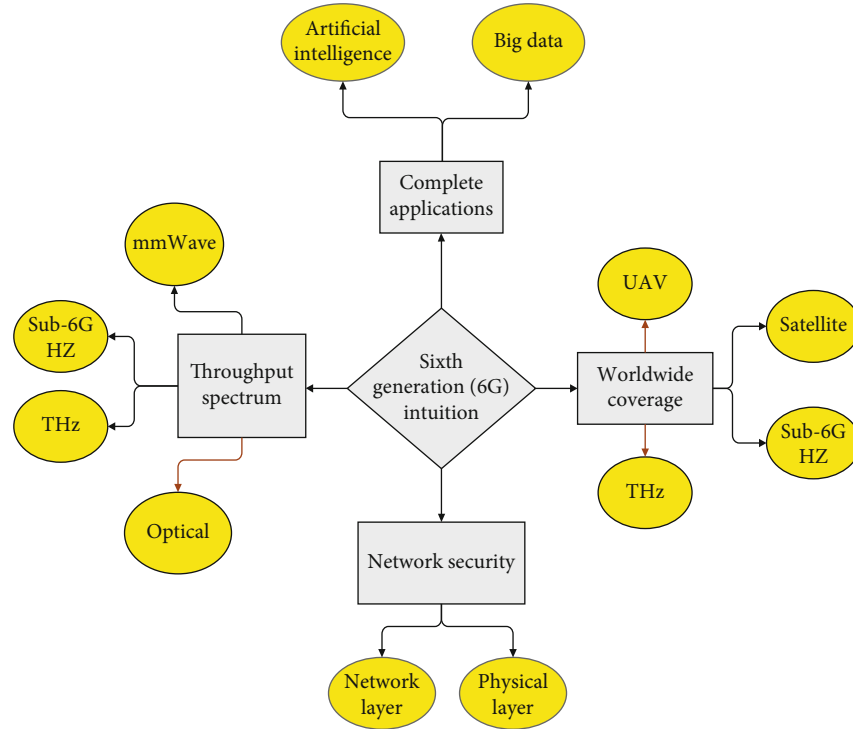


FIGURE 2: Sixth generation (6G) intuition.

consumption for WSN is vital since under protocols nodes are working for many years extension of a lifetime [29].

The CR procedure is complicated and challenging to WSNs because of many problems like spectrum sensing capability installation, sensing nodes with present frequency band, and node responsibility selection for nodes responsible for spectrum sensing.

CR's progressing technique is looking high requirement for frequency resource WSNs. Still, CR-WSN should give spectral efficiency and energy efficiency for industrial usage and applications. Transmission protocols and installation patterns play an essential role in reducing interference and lessing energy consumption between node assisting to improve the energy efficiency of CR-WSN networks. Although, different challenges have been seen as two ways exchange of data in suitable protocols, central object transmitting, and using SU data. The central object should be aware of the sensing channel SUs to be sensed and then give a decision response by these SUs. It executes frequency and time sync, such as the control channel. After detection of the present channel, transmission requires nodes or SUs should be aware by satisfactory channel for circuit configuration.

#### 4. Performance and Applications of CRN in 6G

6G CR networks are projected to attain superior performance compared to 5G and possess high-performance matrices [30–32]. For 6G, the peak data rate is expected 1-10 Tbps with optical frequency band and THz assistance, while this data rate in 5G is 20 Gbps. User utilized data rate can gain a Gbps level with such maximum frequency bands. Traffic capacity by zone may be more than 1 Gbps/m<sup>2</sup>. There

is the possibility to increase the spectrum efficiency from 3 to 5 times, and energy efficiency should also increase several times (about 100 times) compared to 5G. This is possible to attain by applying artificial intelligence to attain better network automation and management. The connection density will increase about a thousand times because of tremendously heterogeneous networks, huge antennas, wide bandwidth, and diverse communication situations. Mobility will be approximately 500 km/h because of satellite movements, high-speed trains, and UAVs. The predicted latency for the selected set of applications is less than 1 ms. Furthermore, some key matrices include security capacity, cost efficiency, intelligence level, and capacity. There is the primary support for human-centric CRNs communication notation in 2030 consisting of wearable device communication, implantable sensors, integrated headsets, smart industry 4.0, intelligent cars, human bonds communication, and robotics [33–35].

Furthermore, conventional CR users' devices such as laptops, mobile phones, and taking health-related intelligent devices into our consideration, frequency band and transmit power used in such devices should be under strict restrictions. Such devices will function on the human body and gather required data; security and weight of the device should be considered during the manufacturing and designing process. In 5G, about 256-1024 antennas realized massive MIMO. While comparing to 5G, 6G will deploy several times more antennas, in 6G, about 10000 antennas will be deployed such as ultramassive spatially massive MIMO where information is transmitted on few antennas by transmitter, and it decreases active antenna element. umMTC and feMBB are to offer massive connectivity, high data rates, and low latency. Figure 3 is showing an overview

TABLE 1: Used abbreviations and explanation.

Serial no.	Abbreviation	Explanation
1	4G	Fourth generation
2	5G	Fifth generation
3	6G	Sixth generation
4	CRNs	Cognitive radio networks
5	CR	Cognitive radio
6	THz	Terahertz
7	MIMO	Multiple-input multiple-output
8	VRAN	Virtualized radio access network
9	UAV	Unmanned aerial vehicle
10	uRLLC	Ultrareliable low latency communication
11	CRAN	Cloud radio access network
12	BBU	Base band unit
13	O-RAN	Open access radio network
14	RRHS	Remote radio heads
15	ML	Machine learning
16	DL	Deep learning
17	NNs	Neural networks
18	UE	User equipment
19	WSN	Wireless sensor network
20	IoT	Internet of things
21	PU <sub>s</sub>	Primary users
22	SU <sub>s</sub>	Secondary users
23	SSaaS	Spectrum sensing as a service
24	u/mMTC	Ultra/massive machine type communication
25	eMBB	Enhanced mobile broadband
26	feMBB	Further enhanced mobile broadband
27	LDHMC	Long-distance and high-mobility communications
28	ELPC	Extremely low-power communications
29	uHSLLC	Ultrahigh speed with low latency communication
30	uMUB	Ubiquitous mobile ultrabroadband
31	uHDD	Ultrahigh data density
32	ITU	International telecommunication union
33	ITU-T	International telecommunication union-technology
34	MR	Mixed reality
35	AR	Augmented reality
36	XR	Extended reality
37	M2M	Machine to machine
38	M2H	Machine to human
39	H2M	Human to machine
40	BCI	Brain computer interface
41	ORT	Optical radio technology
42	RF	Radio frequency
43	FSO	Free-space optical communication
44	LiDAR	Light detection and ranging
45	ITU-R	International telecommunication union-radio communication
46	OF	Optical fiber
47	LPWAN	Low-power wide-area network
48	SRS	Smart reflecting surface

TABLE 1: Continued.

Serial no.	Abbreviation	Explanation
49	IoE	Internet of everything
50	SS	Spectrum sensing
51	QoS	Quality of service
52	VR	Virtual reality
53	CPS	Cyber physical systems
54	E2E	Everything to everything
55	AI	Artificial intelligence

TABLE 2: 6G evaluation in CR networks communication from 5G to 6G.

Problem	5G	6G
Per device speed	20 GBps	1 terabytes per second (Tbps)
Latency E2E	10 ms	1 millisecond (ms)
AI	Partial	Fully
XR	Partial	Fully
Mobility support	500 km/hr	1000 kilometer per hour (km/hr)
Higher spectral efficiency	30 bps/HZ	100 bit per second/hertz (bps/HZ)
Haptic communication	Partial	Fully
Autonomous vehicle	Partial	Fully
Delay jitter	NA ms	$10^{-3}$ millisecond (ms)
Energy efficiency	NA	1 terabyte/joule (Tb/J)
Packet error rate	$10^{-5}$	$10^{-9}$
Higher channel bandwidth	1 GHz	100 gigahertz (GHz)

of 6G CRN communication. 5G focused on uRLLC, mMTC, and eMBB, while 6G CRNs will widely improve also spread the application situations. There are three situations discussed mMTC, mMTC, and enhanced uRLLC in [20, 36]. Many other application situations like ELPC and LDHMC are auspicious. Given three situations were called the ultrahigh speed with low latency communication (uHSLC), ubiquitous mobile ultrabroadband (uMUB), and ultrahigh data density (uHDD) in [37]. Authors in [38] also studied several other applications and situations like the mobile ultrawideband, super IoT, and AI. International Telecommunication Union (ITU) worked on initial research on 6G in February 2020. Its sixth-generation technology and dreams are predicted to accomplish in 2023 [27, 39]. Technology group of ITU focused for 2030 networks researched by ITU-T network group 13 at Geneva meeting 2018. It aims to research the aptitudes of networks for 2030 and beyond. In short, 6G applications of CR networks contain three 5G situations/scenarios and some new scenarios [40, 41]. Some basic applications of 6G CR networks are studied below. Figure 4 is showing possible predicted CR network communication [33, 42, 43].

**4.1. Reality Extended.** Reality extended or extended reality facilities containing mixed reality (MR), augmented reality (AR), and virtual reality (VR) are key features of the 6G CR network communication system. Such features use 3D objects, and AI is the basic element of such features. In

addition, they are providing perceptual needs of cognition, human sense, computing, physiology, and storage. 6G will avail guaranteed immersive VR/AR/MR understanding by joint high quality and designed integration of 6G CR network system. Live view of the physical world is possible by augmented reality (AR), that is, parts are amplified by different sensor inputs by way of visuals, video, audio, and worldwide aligning data system. Present reality uses and makes addition by some sort of devices. While computer-simulated 3D experienced is virtual reality (VR), where computer technology uses authorized headsets to generate realistic feelings and imitate actual surroundings and create the unreal world. VR surroundings engage five human senses. In the end, MR merAR and VR generate a new atmosphere and visualization to attract in the actual period. Mixed reality (MR) is also called hybrid reality. Its key characteristics are fundamental, and artificial world contents can reply to each other in real-time. XR is a combination of natural and virtual surroundings and human-machine communication generated by wearable computer technology. It consists of all forms like VR, AR, and MR. XR brings these under a single term. Low latency, reliable, and high data rate CRN systems connectivity given in 6G system are significant for original XR experience [44].

**4.2. Smart Housing Societies.** The key role of 6G will rush life quality improvement, automation, and surrounding monitoring with the use of artificial intelligence-based machine-

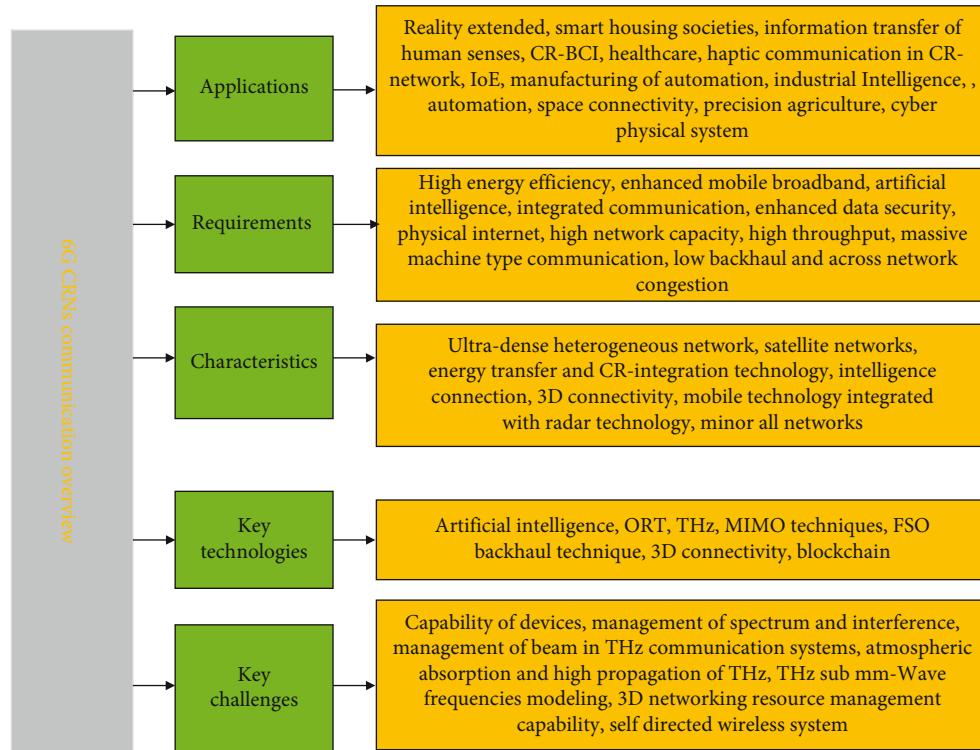


FIGURE 3: Overview of 6G CRN network communication.

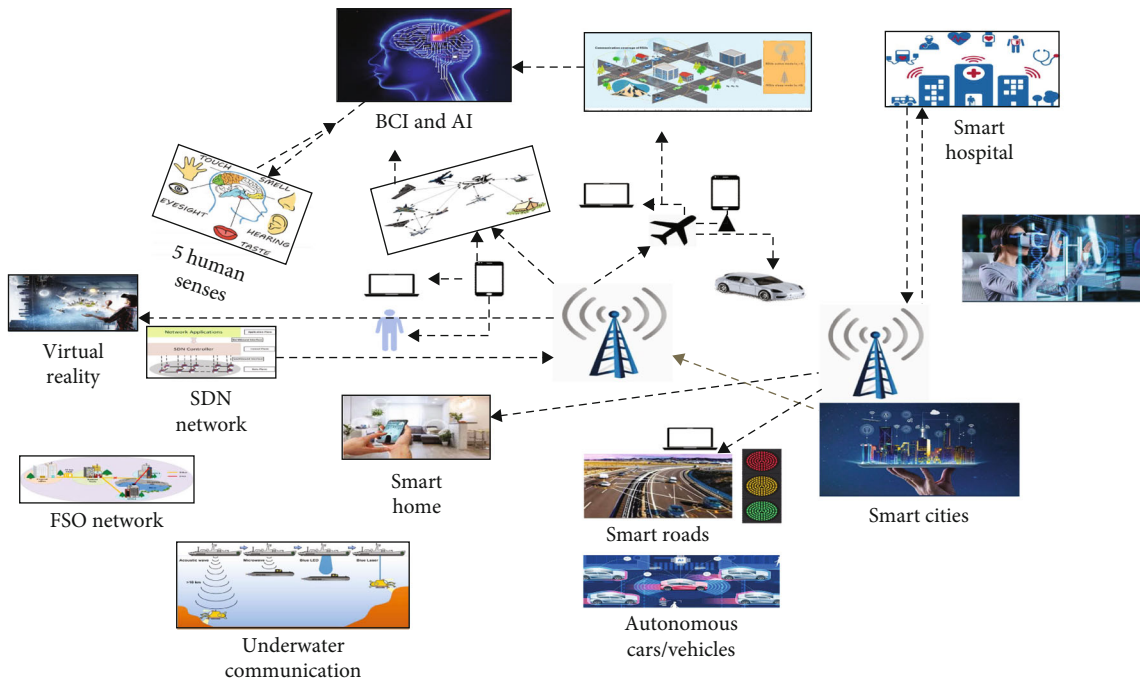


FIGURE 4: Predicted 6G CR network communication.

to-machine (M2M) communication by building intelligent societies. The 6G CR network connection will make our living standards and society super bright by using autonomous vehicles, robotics, mobile devices, etc. Furthermore, the large num-

ber of significant and rushed capitals in the globe will organize flying taxis based on 6G CR network connectivity. There will be a reality in intelligent homes because a smart device-provided command will control devices in remote access.

*4.3. Information Transfer of 5 Human Senses.* To experience the world's surroundings, there are five human senses: sight, touch, hearing, smell, and taste. These five senses received data will be remote transfer in 6G CR network communication. The neurological process by sensory integration is used in this process that detects sensation from the environment and the human body and effectively uses the body in the atmosphere and local environments. Brain-computer interface (BCI) technology will excellently boost this application.

*4.4. CR Brain-Computer Interaction (CR-BCI).* BCI controls daily used appliances in innovative societies, specifically medical systems and home used appliances. It represents direct communication between external devices and the brain. It acquires brain signals which send to the digital devices, interpret, and examine the signals into other movements. Topographies of 6G CRN communication will provision actual BCI execution for quality of living standards.

*4.5. Healthcare.* Medical technology will benefit from 6G CR technology because innovation in VR, XR, MR, AR, mobile edge computing, telepresence, holographic, and artificial intelligence will assist in building intelligent healthcare systems. In the healthcare system, a satisfied remote-control system will be served by 6G technology. With the use of 6G technology, there is the possibility of remote surgery. Low latency, high data rate, and feasible 6G CR network will assist fast and promising transport large volume of medical data, which may progress both quality and access to care.

*4.6. Haptic Communication in CR-Network.* It is the branch of nonverbal communication in which touch sense is being used. Considered 6G CR network communication will care such haptic communication, e.g., the remote user will feel feasibility and happy haptic in actual-time activity. Such system applications and implementation are predicted to be supported by the higher features of 6G CRN communication [45, 46].

*4.7. Internet of Everything (IoE).* IoE is autonomous coordination and unified integration among many elements (computing elements), people, objects, devices or sensors, and the internet using data and processing. There will be full support of IoE in 6G CR network communication [47]. It is a form of the internet of things (IoT) [22]. Still, a covered-up period that participates following features people, data, physical devices, and processes in a single form. IoT is about objects and communication with each other and physical devices. At the same time, IoE presents an intelligence network to gather all physical objects, data, processes, and people in a single system. IoE in the future will be helpful for innovative health, intelligent societies, and intelligent cars [21, 48].

*4.8. Manufacturing and Automation.* AI-based automation will be available in 6G technology. Automation term suggested to processes automated control systems and devices. The automation system in 6G will provide secure, scalable, highly reliable, and feasible CR communication using low latency and high data rates.

*4.9. Industrial Intelligence Automation.* For several years, 4.0 industry is working behind the automation industry based on supply chain optimization notation, additive manufacturing, autonomous equipment, IoT, and data analytics [49]. Still, such notations are treated as storage tower functioning in separation and boundary the real industry automation. In another way, the next feature, industry X.0, seems to feel interactions between different gradations of industrial automation by AI usage. Modern industrial floor with 6G CR communication is expected to need feasible high throughput connectivity across millions of devices with submillisecond delay/response. They are making it suitable for the upcoming 6G CR communication [50, 51].

*4.10. Space Connectivity.* Deep space connectivity near the earth is still budding with 5G; several use forms range from remote sensing and radio astronomy to backhauling and navigation, which will advance from universal connectivity supported by 6G technology. Furthermore, such application contains terrestrial cellular offloading, freight tracking, UVA long-range condition, and atmosphere monitoring, to a few names. At the end of this, the internet of space will serve as the main prospects technology for beyond connectivity for 6G CRN technology [52].

*4.11. Precision Agriculture.* Soil humidity measurements have been a backbone in irrigation verdicts for periods now inside the larger precision agriculture domain. Though, real-time extents and irrigation automation keys still face challenges curtailing strong CR communication coverage deficiency. Working beyond modest automated irrigation explanations, high-performance accuracy agriculture is principally centered around bringing data-driven visions to address the precise needs of farms, customers, soil, and crop. Simultaneously, scalable and appropriate access to such data is a crucial challenge due to breaches in rural connectivity. Consequently, there is a consideration that 6G CR network systems, with their attention on ubiquitous CR, will play a key role in attracting 6G technology in the agricultural invention.

*4.12. Cyber-Physical Systems (CPS).* UAVs and autonomous cars are about the most auspicious CPS in the present day. Such autonomous system process is characterized by the conversation of significant amounts of data amid the integral nodes, i.e., UAVs and cars, concerning high-resolution real-time planning of the topography, optimization, route, and traffic, and security information. Though the resulting bulky volumes of data must be transported inside firm deadlines in an error-free means, this is also authoritative to note that such nodes characteristically work at speeds in surplus of 100 km/h. Furthermore, to provide very high reliability, sub-millisecond latency and the connectivity solution that allows autonomous CPS necessity also bid healthy processes at high speeds, which seems impossible with present 5G systems and technology [53].

Some other applications are as follows

- (i) 3GPP technologies
- (ii) Inclusive sensing

## (iii) Communication-based on beam forming

Figure 5(a) is representing CR network environment, (b) is representing 5G CR Network requirements, (c) is representing features or advantages of 5G CR network, and (d) is representing 6G intelligent network applications. It is showing connectivity of various applications, usage, and control in one hand. Everything is connected with internet. There seems access of internet and connectivity in 6G intelligent applications.

## 5. Security Issues of CR Network in 6G Technology

In CR networks, privacy protection is a basic need in 6G technology. In CRNs, data can be lost or stolen and can be physically attacked. CRNs are more sensitive in security threats than traditional wireless networks, because in CRNs, there seems no proper cooperation in between PU and SU communication. Several security issues caused by CR, because CRN environment is sensing information based, can vary node behavior. As learning is one of the basic characters of CR, because of this having wrong supposed environment, may cause to give error in new decision. In resultant, malicious attack will take advantage for long-term effect on behavior.

Data gathered by CR can be destroyed, sniffed, or change by illegal entities. Furthermore, attackers may disturb transmission of PUs or protect channel usage by SUs by spectrum sensing data falsification. There must be acceptable level of security robustness against attacks and threats in CRNs. There are further security issues in 6G CRNs, some of issues are following, modification of data, private data access, and improper interruption to PUs, barring use of common control channel by artificially yielding blockage issue, barring use of idle channel for unlicensed users, and false data injection. We studied about 5G and 6G CR networks. In 5G, some technologies are helpful in 6G areas. 5G technologies give low latency, high reliability, efficient transmission, and secure services to 6G CR networks. In 6G, an extremely large number of small amounts of data connections may cause a high risk of people's security and privacy with comprehensive care attracted by commerce, business, and governmental entities. The more prominent risk they may execute on securing client protection and causing regulatory problems. So here, we study some fundamental security issues and possible attacks in 6G CRN technology.

**5.1. Artificial Intelligence.** In 5G CR networks, artificial intelligence works in separate areas where a huge quantity of robust and training data and hidden nodes also exist. AI will play an important role in 6G wireless networks. There is a greater impact of machine learning and AI technologies on privacy in two ways. First, the right applications of machine learning may improve 6G privacy, while second, on machine learning attacks, privacy defilements may occur. When AI transfers to the network edge, more sophisticated applications will work on devices, increasing attack threats. Although, integrating privacy-protecting mechanisms in

resource-constrained devices will be stimulating. While in 6G, AI can be divided among several layers, such as computing layers (network function virtualization, software design network, and edge computing) and physical layer (data link and network architecture devices). There may be security issues of malicious behavior, control access, communication, and authentication, etc.

**5.2. Molecular Communication.** In molecular communication, communication is done by using molecules in an aqueous environment or chemical signals—enhanced technology for 6G in several healthcare applications such as wearable body sensors and telemedicine. The use of CR wearable body wireless sensors [54] may mitigate such issues because of global operability, bandwidth, and jamming and enhance consistency. Highly sensitive information is tackled by molecular communication with many privacy concerns related to the encryption process, authentication, and communication. However, providing safe molecular communication is important. In [55], biochemical cryptography has been introduced in which a biological structure and macromolecule composition have been used as a medium to maintain information integrity. In diffusion-based channels, physical layer security and primary benefits are studied in [56, 57], where privacy ability has been discussed to gain insights on protecting symbols a diffusion-based channel can afford. For molecular communication, security needs more research and practical work. In 6G molecular communication, there are several attack methods such as de synchronization, flooding, and jamming attacks. CR implementation requirements in wireless medical networks have been discussed in [7, 58, 59].

**5.3. Blockchain Privacy.** Blockchain privacy and security problems are associated with the communication process, access control, and verification. Recently, in the telecommunication industry, blockchain gained much more attention. Benefits of blockchain like nonreputation, disintermediation, proof of provenance, immutability, pseudonymity, and integrity are particularly important to enable various facilities in 6G technology with privacy and security. The use of AI and some analytic technologies may cause attacks such as evasion attacks in the testing process and poisoning attacks in the training process. Blockchain can guard against protecting the reliability of AI data via distributed trust and immutable records between various shareholders, with assurance in the AI system in multitenant. In 6G networks, this trust gives the required confidence for clients to adopt AI-based security management systems, and it may be insufficient in preventing their failure and breach in AI systems. Blockchain-based projects can be used in trust-level agreements in the liability of each party. In [60], authors studied blockchain radio access network architecture to effectively manage and secure network verification and access between trustless objects. In [61], authors studied to enhance the security of CRNs by a blockchain method to contact vacant license spectrum. In addition, to support blockchain role to adjust with 6G necessities, several current 5G models need active involvement. Blockchain plays an important role in

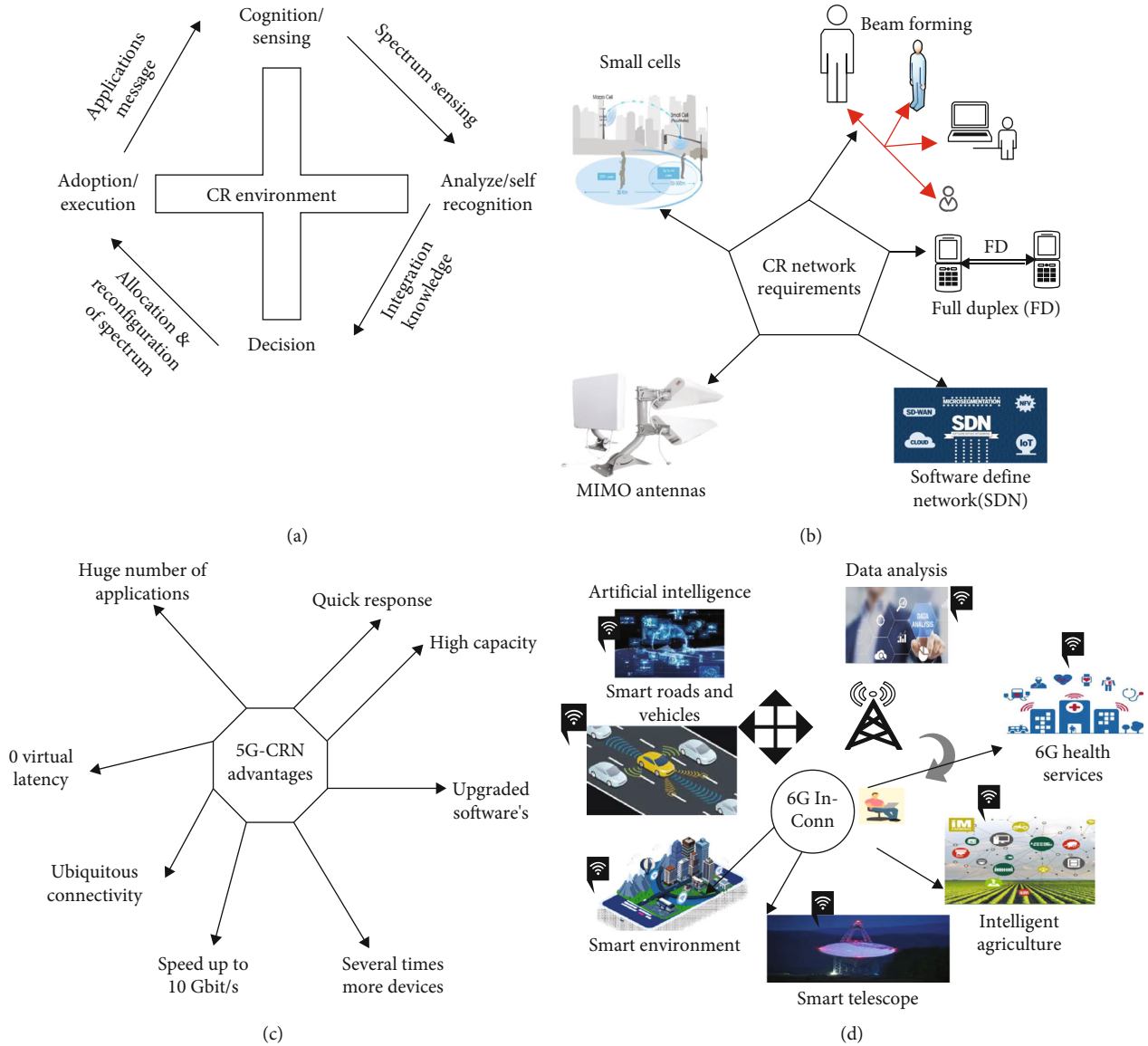


FIGURE 5: CR network environment, requirements, 5G features, and applications. (a) CR network environment. (b) CR network requirements in 5G. (c) Advantages of 5G CRNs. (d) Applications of 6G intelligent network.

privacy protection in 6G networks. In blockchain, having mutual communication channel may permits users to be recognized by pseudoname instead of personal identities.

**5.4. Security Concerns in THz.** THz communication such as GHz to 10THz is intended as an important technology for 6G. In these frequencies, improved directionality of transmitted signal is present, limiting illegal clients for signals interrupting and providing high security at the physical layer. Interception of signals by eavesdroppers has been proved in [62]. In 6G CRNs, THz also has security issues focus on malicious and authentication behavior. In [63, 64], authors studied THz frequency electromagnetic signature and can be used for verification procedure of physical layer. [27, 28] authors studied that an eavesdropper could still interrupt a signal when conveyed via a narrow beam. Certainly, THz communication is disposed to access data

transmission exposure, control attacks, and malicious behavior. For the security of THz communication, new physical layer systems are needed.

**5.5. Physical Layer Attack.** On physical layer, jamming attack is known as one kind of attack. In such kind of attack opponent sends radio signals on wireless channel to interrupt CRN working position. Such opponent may have sophisticated and powerful software and hardware. If entire network is blocked by opponent, it found DoS attack on physical layer attack. On physical layer attack another kind of attack is tampering attack. Here, attackers can damage CRNs, replacing hardware parts or whole nodes.

**5.6. Routing Layer Attack.** In this type of attack, attackers misguide the packet and change information on routing packet forwarding sensors on networks. Similar may happen

to data packets as well. Sybil attack, wormhole attack, and sinkhole attacks are possible in CRNs.

**5.7. MAC Layer Attack.** In such attack, attackers violate defined rules and create disturbance in normal operation. Such as transferring unwanted packets frequently to exhaust battery power and disturb normal operation with the use of selfishly channel and present no cooperation on priority of MAC cooperative layer. This may also lead to DoS attack.

## 6. Requirements for 6G CR-Network Technology

There are many problems in the 5G trade-off, such as energy efficiency, throughput, delay, reliability, hardware complexity, and deployment cost. This is to be considered that 5G is not meeting the market and users' requirements of 2030. There is another option of 6G, which may fill such a gap of user requirements. Based on previous work and upcoming requirements, the key objectives for 6G are millions of connected devices, ultrahigh reliable connectivity, very high per-device data rate, extremely low latency, global connectivity, and reducing energy use with battery-free IoT devices [65].

**6.1. Requirements.** Future CR network communication will have the following basic requirements.

- (i) High energy efficiency
- (ii) Enhanced mobile broadband
- (iii) Artificial intelligence integrated communication
- (iv) Enhanced data security
- (v) Physical internet
- (vi) High network capacity
- (vii) High throughput
- (viii) Massive machine-type communication
- (ix) Low backhaul and access network congestion

It is to be considered that there will be 1000-time higher simulation in 6G CR networks than 5G. URLLC, a basic feature of 5G will also play an important role in 6G communication by providing less than 1 ms end-to-end E2E delay. In 6G, volume spectral efficiency will be better than 5G. There will be the capacity of extended battery life in 6G technology. There will be no need to charge mobile devices in 6G technology separately.

## 7. Characteristics of New Network

**7.1. Ultradense Heterogeneous Network [66].** Such networks will play an important role in 6G CR network communication. These networks will reduce the cost and improve the quality of services.

**7.2. Satellite Networks.** For worldwide devices, connectivity, 6G is predictable to integrate with satellite systems. Integra-

tion of satellite, air-borne networks, and terrestrial into one CR network system will be key in 6G.

**7.3. Energy Transfer and CR-Information's Integration.** In 6G technology, the CR network will send power to battery devices like sensors and devices. Since energy transfer and CR network will be integrated.

**7.4. Intelligence Connection.** Contrary to the traditional generation of CR networks systems, upcoming technology like 6G and beyond will be transformative and will update CR improvements from linked intelligence to linked things. There will be the introduction of AI in all communication steps. There will be the new paradigm of AI in the CR communication systems.

**7.5. 3D Connectivity.** In wireless communication, UAV-based devices provide suitable solution to enhance connectivity whenever traffic data is nonstationary and heterogeneous, and it is to be considered maximum varying with time or space. To get access to various UAV-assisted applications, UAV requires connection or communication with present network either Wi-Fi or cellular, in this case, UAV response as UE of network. UAVs can response as UE applications, e.g., UAV-assisted transportation network, UAV-based drones, and real-time surveillance UAV devices used as relays to provide connectivity between aerial base station and aerial UEs. Retrieving the network and central network purposes low earth orbit satellite and drones will enable super 3D connectivity in 6G technology.

**7.6. Mobile Technologies Integrated with Radar Technology.** To gain maximum precision localization with CR communication and key concept of 6G CR networks, communication 6G will be integrated with radar [67].

**7.7. Minor Cell Networks.** Basically term minor or small cell is compact to low power base stations (10 W-20 W), such as femto cells, micro cells, and Pico cells. On another hand, ultradense network (UDN) is extended form of heterogeneous network in which huge number of small cells is deployed to reduce traffic from highly dense macro cells and network performance can be enhanced. UDN technology is one of the important technology which helps in network performance like latency, capacity, and data rate. In a UD network, overdeployment of small cells increased resource management challenges with respect to energy efficiency, spectrum resource efficiency, and control overhead, e.g., comparing to macrocells base station small cell microstation uses less energy on communication and operation. Minor cell network notation has been initiated to improve signal quality as a sign of energy efficiency, throughput, and spectral efficiency improvement on the cellular network. As a result, minor cell networks are necessary for 5G and 6G CR network communications. Figure 6 is showing mmWave massive MIMO-based ultradense network for 6G communication.



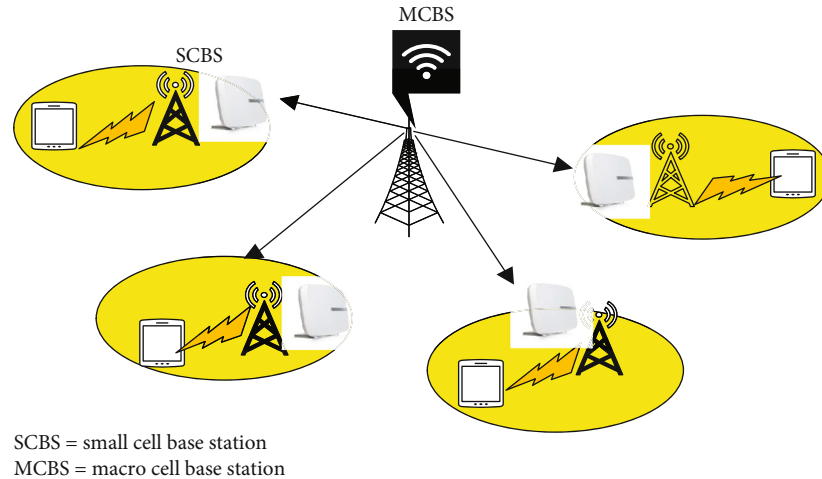


FIGURE 6: Massive MIMO-based ultradense network for 6G.

## 8. Key Technologies for 6G CR-Network

6G CR-Network will be driven by several technologies; some of the key technologies are studied below.

**8.1. Artificial Intelligence.** An essential and introduced technology in 6G CR-communication is AI [68, 69]. In 4G CR network systems, AI was not deployed. At the same time, 5G is partially supporting AI technologies. Although, 6G is predicted to support AI for automation services [33] fully. Machine learning improvements will provide a more intelligent CR network in 6G for real-time communication. In CR-communication, AI introduction will simplify and make real-time data improvement. With the use of several analytics, a complex target way can be determined by AI.

- (i) AI will be helpful in reduction of processing delay and increasing efficiency of CR-communication steps
- (ii) AI will be helpful in time-consuming tasks, like network selection and handover
- (iii) There will be the key role of AI in 6G in M2M, M2H, and H2M communication
- (iv) AI will rapid CR-communication in BCI

CR-network communication systems based on AI will be maintained by intelligent structure, intelligent devices, metamaterials, self-sustaining CR networks systems, intelligent cognitive radio, machine learning, wireless networks, and intelligent networks [70, 71].

**8.2. Optical Radio Technology (ORT).** This technology is envisioned for 6G CR communication technology [72], in addition to 6G radio frequency (RF) based communication for all predicted devices to access network, and such networks also access network to fronthaul/backhaul network connection. This technology is also functioning since 4G CR-communication systems. Although, it will be widely used for 6G CR-communication demands. ORT is like visi-

ble light communication, light fidelity, FSO communication, and optical camera communication. Researchers are focusing on overcoming challenges and enhancing performance in present technologies. Optical radio technology communication provides low latency, secure communication, and high data rates. LiDAR is also an optical band which is the key technology for 3D resolution in 6G CR network communication.

**8.3. Terahertz Communication.** Spectral efficiency can be enhanced with the bandwidth increase; it is possible to do it by sub-THz communication with max bandwidth and apply advanced MIMO networks. The radio frequency band has already been pushed, and this time, it is not sufficient to meet 6G requirements. There will be the key role of THz bands in the 6G CR-communication network [73, 74]. Such band is intended to be the next limit of maximum data rate CR communication system. THz waves are known as sub-millimeter radiation, generally state to 0.1 THz and 10 THz frequency band with 0.03 to 3 mm corresponding wavelength range [64, 69]. According to the ITU-R recommendation, the 275 GHz-3 THz band range is considered the central part of the THz band for CR communication [69]. 6G cellular communication will be enhanced by accumulation to THz bands 275 THz-3 THz still have not been assigned for any purpose globally, while such band can approach high data rate [73]. By adding this THz band with the present mmWave band, the total band capacity increased about 11.11 times. So, the 300 GHz-3 THz band represents resemblances with the radio frequency band. THz improves the potential and high-frequency challenges in CR communication systems [75].

There are few basic properties of THz communication, such as

- (i) High frequency raised high path loss
- (ii) For support of high data rate, widely bandwidth available

Highly directional generated narrow bandwidth antennas decrease the interferences. THz small wavelength

permits a more significant number of antennas to join into devices and base stations functioning in such band. It permits the use of advanced adaptive array technologies which overcome the limitation.

**8.4. MIMO Technique.** One primary technique is the MIMO technique application [76–78]. With the improvement of MIMO techniques, spectral efficiency directly improves [79]. Therefore, massive MIMO technology will be helpful in 6G communication networks.

**8.5. FSO Backhaul Technique.** It is not possible that the backhaul network has optical fiber (OF) connectivity because of inaccessible terrestrial locations and complications. The FSO backhaul network is very encouraging for 5G CR network communication systems [80, 81]. The transmitter and receiver features of the FSO system are similar to those of OF networks. Thus, data transfer in the FSO system is analogous to the OF system. Though, laterally with the OF networks, FSO is an admirable technology to provide backhaul connectivity in 6G communication networks. With FSO, there is the possibility to have pervasive range communications even at a 10,000 km distance. FSO provisions high-capacity backhaul connection for distant and nonremote areas, like outer space, sea, isolated islands, and underwater; FSO also provisions cellular base station connectivity.

**8.6. High Visibility 3D Connectivity.** 6G CR communication will integrate airborne and ground networks for user's communication provision. The 3D base stations will be provided over UAVs and small orbit satellites. The accumulation of original proportions concerning elevation and related degrees of liberty makes 3D connectivity significantly diverse.

**8.7. Blockchain.** It will be an imperative technology to accomplish big data in upcoming communication system networks. Blockchains are objective one system of the distributed ledger technology. At the same time, a distributed ledger is defined as that it is a database that is distributed across several nodes. Each node duplicates and protects a similar copy of the ledger. Peer-to-peer networks accomplish the blockchain. It can occur deprived of being achieved by a centralized authority. Data on a blockchain is collected, organized, and structured in chunks. The chunks are linked to one another and tenable using cryptanalysis. The blockchain is fundamentally a faultless accompaniment to the vast IoT with enhanced security, interoperability, reliability, privacy, and scalability. So, such technology will afford numerous services, like traceability of massive data, interoperability across devices, autonomic contacts of diverse IoT systems, and consistency for the enormous connectivity of 6G CR communication systems.

Other key enabling technologies include quantum communication, unmanned aerial vehicles, communication, sensing integration, dynamic network slicing, access-backhaul network integration, holographic beam farming, energy transfer, wireless information integration, and cell-free communication big data.

## 9. Key Challenges and Future Discussion on 6G CR Network Communication

Nowadays, Information and Communication industry is facing worldwide challenge, such as new services development with enhanced QoS and on the spot less environmental effect. There is gap between demand and supply of wireless [82]. There seems fear that imminent spectrum crises where increase requirement from smart mobile devices will soon overcome wireless capacity may occur. Challenge is deficiency of new spectrum present in wireless data carrier. Data traffic of smartphones is increasing speedy that if nothing is done they can use present spectrum. Such thing may not affect only phones but also other used wireless equipment.

To study efficiency of spectrum usage problem, CR idea was given. This CR technology has potential of being a troublesome force within spectrum management [83, 84]. Famous example is opportunistic spectrum or opportunistic radio those rules are spatial, temporal, and geographic reuse of legal spectrum. Several use of spectrum appearing that spectrum is in use, in form that complicated responsibility of spectrum usage at unplanned geographical location and at fixed frequency is not much high. It shows that there are several holes in radio spectrum which could be oppressed. Opportunistic radio system must have ability to feat such spectrum holes by detection and use in opportunistic way. Because of such propagation in television bands with floor penetration ability and strong wall, flexible bandwidth and long range may use to permit new services and enhance bounded capacity of present systems [85, 86].

On the other hand, CR is not bounded to opportunistic spectrum access and contains heterogeneous network [87]. Present spectrum locations are not permitted for frequency bands allocation to various radio access technologies [88]. Such technology may open several new applications and available opportunities, like city and campus coverage, rural connectivity, massive wireless hotspots, and content distribution networks [89].

There are several challenges facing in CRNs in both hardware and network architecture. For CRN network, it needs several technologies, like communication pattern learning intelligence, radio environment awareness, and robustness of spectrum use. Here, CRNs must be effective in network capacity as well as spectrum utilization. Coexistence and interoperability between several communication standard challenges are present. Huge quantity of data produced by huge number of real-time device should be adjusted by CRNs, such as low latency. For enhancement of network performance, CRN architecture has been executed. Numerous technical complications want an effective solution in the 6G installation of CR networks. Possible predictable challenges in 6G are studied below [86].

- (i) Switching protocols b/w CR function protocol [90, 91] (battery power devices, e.g., LPWAN)
- (ii) Access strategy for IoT wireless sensors network. (Huge number of users are responsible for dispute b/w secondary users (SUs), so spectrum sharing

strategy is essential here for successful management of several kinds of sensors access)

- (iii) Interference sensing channel coding [91–93] (challenge of selecting optimal channel coding technique, which matches SUs QoS and not preventing primary users (PUs) simultaneously)
- (iv) Using smart reflecting surface (noncooperation situation between PU and SU, complicated to apply channel estimation. Cascade and blind channel estimation could be helping SRS applications for the help to spectrum sensing (SS)) [94]
- (v) Exchange protocol for wireless sensor networks [95] (data sending nodes should be up-to-date by a central entity about already present channel)
- (vi) For CR, sensing spatial dimension [96, 97] (in noncooperation manner with PU, estimation beam of PU become a challenge, even to know PU, SU beam adjustment is also challenging because of secondary user transmitter inevitable interference to SU receiver)
- (vii) SS binary decision complication indirection of smart spectrum sensing [98]
- (viii) In CR communication technology, there is a challenge of future public safety [99, 100] such as license plate detection, web access, and video streaming
- (ix) The primary key challenge in CRN is the demonstration of CRN technology, assess, and failure to conclusively test at real-world installation scenario and scale. Physical installation needs a high resolution, speedy signal processor, and high sampling rate for CR applications in cooperative sensing [101, 102]
- (x) Challenge when SU does not see PU [12]
- (xi) During SUs transmission, PUs can claim their licensed band, and in this process, there may be the challenge of sensing duration as studied in [12, 103]
- (xii) Economics and spectrum policy challenges [104] such as the challenge in conveying energetic spectrum standards are that of essentially progressing spectrum utilization effectiveness without losing the benefits of inactive spectrum assignment [27]. The challenge in installing wireless equipment and networks that can unscrupulously work in various frequency bands and spectrum policy domains is challenging [105, 106]

Future discussion and some more key challenges are discussed below.

*9.1. The Capability of Devices (Smartphone).* There must be several advances and improved features in upcoming technology. There should be the ability of intelligent devices to adjust to the upcoming technology and its features. It does not seem very easy to provision throughput 1 Tb, XR, inte-

grating sensing, and AI with CR network structures using specific devices. There are few chances of current-generation 5G that could not provision some upcoming generation 6G features. Also, ability enhancement in advance (6G) devices might raise the price. Billions of devices are associated with fifth-generation (5G) technology this time; so, it needs to be assured that 5G-associated devices are suitable for 6G or not [72, 106].

*9.2. Management of Spectrum and Interference.* Because of the privacy of the interfering problems and spectrum resources, there is significant to professionally accomplish 6G ranges with the sharing of spectrum tactics and advanced spectrum management techniques [27]. For attaining supreme resource operation with QoS expansion, well-organized spectrum management is significant in this case. There needs concentration of researchers towards 6G, like spectrum sharing and spectrum management procedure in various networks which harmonize communication at a similar frequency. There is a need to examine the procedure for canceling interference using standard interfering cancellation methods, like successive interference cancellation and parallel interference cancellation.

*9.3. Management of Beam in THz Communication Systems.* In a massive MIMO system, beamforming is capable technology for the provision of speedy data rate communication. But in THz, beam management is not easy, and it is complicated or challenging due to sub mmWave propagation. Though, selecting optimal beam efficiently is essential in speedy traffic management.

*9.4. Atmospheric Absorption and High Propagation of Terahertz (THz).* High THz frequencies provide high data rates. Though, there is essential for THz to defeat key problem for transferring data on comparatively extensive distances for atmospheric absorption characteristics also high propagation loss. For the THz communication network, we need a novel design for transceiver architecture. The transceiver must work at high frequencies and want to confirm the complete use of extensively existing bandwidths. Trivial effective area and gain of different THz band antennas are the alternative issues of THz communication. Safety and health anxieties associated with THz band communications are also essential to be discussed.

*9.5. THz Sub-mmWave Frequency Modeling.* Sub-mmWave (THz) and mmWave broadcast features focus on atmospheric situations; consequently, diffusing and absorptive properties have been observed. The extreme situation usually is variable and thus moderately impulsive. So, such band channel modeling is comparatively complicated also; there is no perfect channel model in this band.

*9.6. 3D Networking Resource Management Complexity.* There is speedy progress towards 3D networking. Though, there was an increase in novel addition. Furthermore, numerous opponents may interrupt truthful information that may meaningfully damage the general system performance. So, novel techniques for optimizing routing protocol

and resource management, multiple access, and mobility support are essential. Preparation desires a novel CRN project.

*9.7. Self-Directed Wireless Systems.* There will be a 6G system for self-directed or automatic technology like UAVs, self-directed car, and AI-based industry. We want to have junction of numerous assorted subsystems for autonomous wireless networks, like interoperable processes, machines of systems, autonomous computing, machine learning, systems, autonomous cloud, and heterogeneous CR networks. Therefore, general system progress becomes challenging and complex. e.g., emerging an entirely autonomous system for the driverless car will be more challenging because researchers in 6G require to project fully automated self-driving cars that achieve better than human-controlled cars [107].

In 6G CRN communication technology, it may answer the following questions

- (i) How much bandwidth assigned to each SUs, and who is willing to use the existing spectrum hole of different networks?
- (ii) What is the power assigned to SUs?
- (iii) During the switching process of SU from network to network, is the SU compatible for dynamic acceptance of network limitation variations?
- (iv) For SUs support in the CRN environment, which mobility model could be best?

## 10. Conclusion

With time, technology is progressing day by day and generation to generation. 5G CR network communication is functioning in several big cities of developed countries and spreading globally. Although, 5G is not fulfilling the requirements of industries and users for the CR network in 2030. So, 6G may cover several requirements of 2030. It is to be expected that 6G wireless network will support client's applications and enhance communication latency with high throughput and low latency. This article explained review on upcoming generation of CR network communication, mentioned mandatory cases, and detailed prospective on present and future technology improvement efforts. We studied the application and requirements for 6G CR network communication. In the end, we also highlighted the possible key challenges in 6G CR network communication and significant empowering technologies that are energetic to the achievement of 6G and beyond. Besides illuminating the visualization and goal of 6G CR network communications, we have quantified the numerous technologies that could prove helpful for 6G CR network communication.

There are also some limitations in 6G technology, such as it has been studied in this paper that 6G uses multiconnectivity and cell-less technology. For this, network requires perfect architecture. Design of new cell-less architecture is challenge. Moreover, there are challenges or limitations is

6G to use THz frequencies, visible light frequencies, and energy harvesting requirement.

We also hearten researchers, readers, and book lovers to play their role in realizing upcoming CR network communication technology.

## Data Availability

Data can be provided upon request.

## Conflicts of Interest

We hereby confirm that there is no conflict of interest between authors to declare.

## Acknowledgments

This work was supported by the National Key R&D Program of China (the major project no. 2020YFB1807900) of China.

## References

- [1] D. M. Venkatesan, D. A. V. Kulkarni, and D. R. Menon, "Role of cognitive radio in 5G," *Helix*, vol. 9, no. 2, pp. 4850–4854, 2019.
- [2] M. J. Kaur, M. Uddin, H. K. Verma, and B. R. Ambedkar, "Role of cognitive radio on 4G communications a review," *Journal of Emerging Trends in Computing and Information Sciences*, vol. 3, no. 2, pp. 272–276, 2012.
- [3] H. Yu and Y. B. Zikria, "Cognitive radio networks for internet of things and wireless sensor networks," *Sensors*, vol. 20, no. 18, p. 5288, 2020.
- [4] J. Adu Ansere, G. Han, H. Wang, C. Choi, and C. Wu, "A reliable energy efficient dynamic spectrum sensing for cognitive radio IoT networks," *IEEE Internet of Things Journal*, vol. 6, no. 4, pp. 6748–6759, 2019.
- [5] Z. Ahmed, M. M. Khan, M. A. Saeed, and W. Zhang, "Consensus control of multi-agent systems with input and communication delay: a frequency domain perspective," *ISA Transactions*, vol. 101, pp. 69–77, 2020.
- [6] A. Srivastava, M. S. Gupta, and G. Kaur, "Energy efficient transmission trends towards future green cognitive radio networks (5G): progress, taxonomy and open challenges," *Journal of Network and Computer Applications*, vol. 168, article 102760, 2020.
- [7] J. Wang, M. Ghosh, and K. Challapali, "Emerging cognitive radio applications: a survey," *IEEE Communications Magazine*, vol. 49, no. 3, pp. 74–81, 2011.
- [8] A. Srivastava and G. Kaur, "Resource management for traffic imbalance problem in green cognitive radio networks," *Physical Communication*, vol. 48, article 101437, 2021.
- [9] S. Bojja Venkatakrishnan, E. A. Alwan, and J. L. Volakis, "Wideband RF self-interference cancellation circuit for phased array simultaneous transmit and receive systems," *IEEE Access*, vol. 6, no. c, pp. 3425–3432, 2018.
- [10] V. Syrjala, K. Yamamoto, and M. Valkama, "Analysis and design specifications for full-duplex radio transceivers under RF oscillator phase noise with arbitrary spectral shape," *IEEE Transactions on Vehicular Technology*, vol. 65, no. 8, pp. 6782–6788, 2016.

- [11] A. S. Musleh, G. Chen, and Z. Y. Dong, "A survey on the detection algorithms for false data injection attacks in smart grids," *IEEE Transactions on Smart Grid*, vol. 11, no. 3, pp. 2218–2234, 2020.
- [12] M. M. Aslam, L. Du, Z. Ahmed, M. N. Irshad, and H. Azeem, "A deep learning-based power control and consensus performance of spectrum sharing in the CR network," vol. 2021, Article ID 7125482, pp. 1–16, 2021.
- [13] X. Li, J. Fang, W. Cheng, H. Duan, Z. Chen, and H. Li, "Intelligent power control for spectrum sharing in cognitive radios: a deep reinforcement learning approach," *IEEE Access*, vol. 6, pp. 25463–25473, 2018.
- [14] Y. Lu, P. Zhu, D. Wang, and M. Fattouche, "Machine learning techniques with probability vector for cooperative spectrum sensing in cognitive radio networks," in *2016 IEEE wireless communications and networking conference*, Doha, Qatar, 2016.
- [15] X. Qiao, Y. Huang, S. Dustdar, J. Chen, and S. Dustdar, "6G vision: an AI-driven decentralized network and service architecture," *IEEE Internet Computing*, vol. 24, no. 4, pp. 33–40, 2020.
- [16] G. Fettweis, "The tactile internet: applications and challenges," *IEEE Vehicular Technology Magazine*, vol. 9, no. 1, pp. 64–70, 2014.
- [17] M. M. Aslam, L. Du, Z. Ahmed, H. Azeem, and M. Ikram, "Consensus performance of traffic management system for cognitive radio network: an agent control approach," in *Cyberspace Data and Intelligence, and Cyber-Living, Syndrome, and Health*, Springer Singapore, 2019.
- [18] S. Filin, H. Harada, H. Murakami, and K. Ishizu, "International standardization of cognitive radio systems," *IEEE Communications Magazine*, vol. 49, no. 3, pp. 82–89, 2011.
- [19] B. Zong, C. Fan, X. Wang, X. Duan, B. Wang, and J. Wang, "6G technologies: key drivers, core requirements, system architectures, and enabling technologies," *IEEE Vehicular Technology Magazine*, vol. 14, no. 3, pp. 18–27, 2019.
- [20] S. Dang, O. Amin, B. Shihada, and M. S. Alouini, "What should 6G be?," *Nature Electronics*, vol. 3, no. 1, pp. 20–29, 2020.
- [21] M. Z. Chowdhury, M. Shahjalal, S. Ahmed, and Y. M. Jang, "6G wireless communication systems: applications, requirements, technologies, challenges, and research directions," *IEEE Open Journal of the Communications Society*, vol. 1, pp. 957–975, 2020.
- [22] M. M. Aslam, M. N. Irshad, H. Azeem, and M. Ikram, "Cost effective & energy efficient intelligent smart home system based on IoT," *Afyon Kocatepe Üniversitesi Uluslararası Mühendislik Teknolojileri ve Uygulamalı Bilimler Dergisi*, vol. 3, no. 1, pp. 10–20, 2020.
- [23] A. U. Khan, G. Abbas, Z. H. Abbas, M. Tanveer, S. Ullah, and A. Naushad, "HBLP: a hybrid underlay-interweave mode CRN for the future 5G-based internet of things," *IEEE Access*, vol. 8, pp. 63403–63420, 2020.
- [24] A. Nasser, A. Mansour, and K. C. Yao, "Simultaneous transmitting-receiving-sensing for OFDM-based full-duplex cognitive radio," *Physical Communication*, vol. 39, article 100987, 2020.
- [25] K. E. Lee, J. G. Park, and S. J. Yoo, "Intelligent cognitive radio ad-hoc network: planning, learning and dynamic configuration," *Electronics*, vol. 10, no. 3, p. 254, 2021.
- [26] A. Nasser, H. al Haj Hassan, J. Abou Chaaya, A. Mansour, and K. C. Yao, "Spectrum sensing for cognitive radio: recent advances and future challenge," *Sensors*, vol. 21, no. 7, pp. 2408–2429, 2021.
- [27] F. Qamar, M. U. A. Siddiqui, M. H. D. N. Hindia, R. Hassan, and Q. N. Nguyen, "Issues, challenges, and research trends in spectrum management: a comprehensive overview and new vision for designing 6g networks," *Electronics*, vol. 9, no. 9, pp. 1416–1439, 2020.
- [28] B. Barakat, A. Taha, R. Samson et al., "6G opportunities arising from internet of things use cases: a review paper," *Future Internet*, vol. 13, no. 6, p. 159, 2021.
- [29] H. Bin Ahmad, "Ensemble classifier based spectrum sensing in cognitive radio networks," *Wireless Communications and Mobile Computing*, vol. 2019, Article ID 9250562, 16 pages, 2019.
- [30] F. Li, K. Y. Lam, X. Li, Z. Sheng, J. Hua, and L. Wang, "Advances and emerging challenges in cognitive internet-of-things," *IEEE Transactions on Industrial Informatics*, vol. 16, no. 8, pp. 5489–5496, 2020.
- [31] X. Yan, H. Xiao, K. An, G. Zheng, and S. Chatzinotas, "Ergodic capacity of NOMA-based uplink satellite networks with randomly deployed users," *IEEE Systems Journal*, vol. 14, no. 3, pp. 3343–3350, 2020.
- [32] S. J. Nawaz, S. K. Sharma, S. Wyne, M. N. Patwary, and M. Asaduzzaman, "Quantum machine learning for 6G communication networks: state-of-the-art and vision for the future," *IEEE Access*, vol. 7, no. M1, pp. 46317–46350, 2019.
- [33] J. Jiao, Y. Sun, S. Wu, Y. Wang, and Q. Zhang, "Network utility maximization resource allocation for NOMA in satellite-based internet of things," *IEEE Internet of Things Journal*, vol. 7, no. 4, pp. 3230–3242, 2020.
- [34] Y. C. Liang, D. Niyato, E. G. Larsson, and P. Popovski, "Guest editorial: 6G mobile networks: emerging technologies and applications," *China Communications*, vol. 17, no. 9, pp. 90–91, 2020.
- [35] R. Alghamdi, R. Alhadrami, D. Alhothali et al., "Intelligent surfaces for 6G wireless networks: a survey of optimization and performance analysis techniques," *IEEE Access*, vol. 8, pp. 202795–202818, 2020.
- [36] M. M. Aslam, J. Zhang, B. Qureshi, and Z. Ahmed, "Beyond6G- consensus traffic management in CRN , applications, architecture and key challenges," in *2021 IEEE 11th International Conference on Electronics Information and Emergency Communication (ICEIEC) 2021 IEEE 11th International Conference on Electronics Information and Emergency Communication (ICEIEC)*, pp. 182–185, Beijing, China, 2021.
- [37] International Telecommunications Union, *IMT Traffic Estimates for the Years 2020 to 2030*, Electronic publishing, Geneva, 2015.
- [38] K. David and H. Berndt, "6G vision and requirements: is there any need for beyond 5g?," *IEEE Vehicular Technology Magazine*, vol. 13, no. 3, pp. 72–80, 2018.
- [39] 5G IA, *European Vision for the 6G Network Ecosystem*, 2021.
- [40] I. F. Akyildiz, A. Kak, and S. Nie, "6G and beyond: the future of wireless communications systems," *IEEE Access*, vol. 8, pp. 133995–134030, 2020.
- [41] Q. Zhang, A. B. J. Kokkeler, and G. J. M. Smit, *Cognitive Radio for Emergency Networks*, Mobile Multimedia: Communication Engineering Perspective, 2006.
- [42] Y. E. Sagduyu, Y. Shi, A. B. Mackenzie, and Y. T. Hou, "Regret minimization for primary/secondary access to satellite resources with cognitive interference," *IEEE Transactions*

- on *Wireless Communications*, vol. 17, no. 5, pp. 3512–3523, 2018.
- [43] D. H. M. Shikh-Bahaei, Y.-S. Choi, and D. Hong, “Full-duplex and cognitive radio networking for the emerging 5G systems,” *Wireless Communications and Mobile Computing*, vol. 2018, Article ID 8752749, 2 pages, 2018.
- [44] Z. Ahmed, M. A. Saeed, A. Jenabzadeh, and Z. Weidong, “Frequency domain analysis of resilient consensus in multi-agent systems subject to an integrity attack,” *ISA Transactions*, vol. 111, pp. 156–170, 2020.
- [45] X. Liu, K.-Y. Lam, F. Li, J. Zhao, and L. Wang, “Spectrum sharing for 6G integrated satellite-terrestrial communication networks based on NOMA and cognitive radio,” 2021, <http://arxiv.org/abs/2101.11418>.
- [46] Z. Xie, G. Huang, R. Zarei, Z. Ji, H. Ye, and J. He, “A novel nest-based scheduling method for mobile wireless body area networks,” *Digital Communications and Networks*, vol. 6, no. 4, pp. 514–523, 2020.
- [47] Y. Zhou, L. Liu, L. Wang et al., “Service-aware 6G: an intelligent and open network based on the convergence of communication, computing and caching,” *Digital Communications and Networks*, vol. 6, no. 3, pp. 253–260, 2020.
- [48] M. M. Aslam, M. N. Irshad, H. Azeem, and M. Ikram, “Cost effective & energy efficient intelligent smart home system based on IoT,” *Afyon Kocatepe University International Journal of Engineering Technology and Applied Sciences*, vol. 3, no. 1, pp. 10–20, 2020.
- [49] M. Nasir, M. F. Hayat, A. Jamal, and Z. Ahmed, “Frequency domain consensus control analysis of the networked multi-agent system with controller area network bus-induced delay,” *Journal of Vibration and Control*, 2021.
- [50] F. Geng, Q. Liu, and P. Zhang, “A time-aware query-focused summarization of an evolving microblogging stream via sentence extraction,” *Digital Communications and Networks*, vol. 6, no. 3, pp. 389–397, 2020.
- [51] Y. Wei, M. Peng, and Y. Liu, “Intent-based networks for 6G: insights and challenges,” *Digital Communications and Networks*, vol. 6, no. 3, pp. 270–280, 2020.
- [52] P. Zhang and X. Kang, “Similar physical entity matching strategy for mobile edge search,” *Digital Communications and Networks*, vol. 6, no. 2, pp. 203–209, 2020.
- [53] S. Rani, A. Kataria, V. Sharma et al., “Threats and corrective measures for IoT security with observance of cybercrime: a survey,” *Wireless Communications and Mobile Computing*, vol. 2021, Article ID 5579148, 30 pages, 2021.
- [54] Y. H. Robinson, T. S. Lawrence, E. G. Julie, and S. Vimal, “Development of fuzzy enabled coverage hole detection algorithm in wireless sensor networks,” *Wireless Personal Communications*, vol. 119, no. 4, pp. 3631–3649, 2021.
- [55] F. Dressler and F. Kargl, “Towards security in nano-communication: challenges and opportunities,” *Nano Communication Networks*, vol. 3, no. 3, pp. 151–160, 2012.
- [56] L. Mucchi, A. Martinelli, S. Jayousi, S. Caputo, and M. Pierobon, “Secrecy capacity and secure distance for diffusion-based molecular communication systems,” *IEEE Access*, vol. 7, pp. 110687–110697, 2019.
- [57] J. Walko, “Cognitive radio,” *IEE Review*, vol. 51, no. 5, pp. 34–37, 2005.
- [58] J. Mitola and G. Q. Maguire, “Cognitive radio: making software radios more personal,” *IEEE Personal Communications*, vol. 6, no. 4, pp. 13–18, 1999.
- [59] S. Vimal, Y. H. Robinson, M. Kaliappan, K. Vijayalakshmi, and S. Seo, “A method of progression detection for glaucoma using K-means and the GLCM algorithm toward smart medical prediction,” *The Journal of Supercomputing*, vol. 77, no. 10, pp. 11894–11910, 2021.
- [60] X. Ling, J. Wang, T. Bouchoucha, B. C. Levy, and Z. Ding, “Blockchain radio access network (B-RAN): towards decentralized secure radio access paradigm,” *IEEE Access*, vol. 7, no. c, pp. 9714–9723, 2019.
- [61] K. Kotobi and S. G. Bilen, “Secure blockchains for dynamic spectrum access: a decentralized database in moving cognitive radio networks enhances security and user access,” *IEEE Vehicular Technology Magazine*, vol. 13, no. 1, pp. 32–39, 2018.
- [62] J. Ma, R. Shrestha, J. Adelberg et al., “Security and eavesdropping in terahertz wireless links,” *Nature*, vol. 563, no. 7729, pp. 89–93, 2018.
- [63] I. F. Akyildiz, J. M. Jornet, and C. Han, “Terahertz band: next frontier for wireless communications,” *Physical Communication*, vol. 12, pp. 16–32, 2014.
- [64] M. H. Alsharif, M. A. M. Albreem, A. A. A. Solymann, and S. Kim, “Toward 6g communication networks: terahertz frequency challenges and open research issues,” *Computers, Materials & Continua*, vol. 66, no. 3, pp. 2831–2842, 2021.
- [65] P. Singh, M. Khari, and S. Vimal, “EESMT: an energy efficient hybrid scheme for securing mobile ad hoc networks using IoT,” in *Wireless Personal Communications*, Springer, 2021.
- [66] M. A. Adedoyin and O. E. Falowo, “Combination of ultra-dense networks and other 5G enabling technologies: a survey,” *IEEE Access*, vol. 8, pp. 22893–22932, 2020.
- [67] F. Nawaz, J. Ibrahim, M. Awais, M. Junaid, S. Kousar, and T. Parveen, “A review of vision and challenges of 6G technology,” *International Journal of Advanced Computer Science and Applications*, vol. 11, no. 2, pp. 643–649, 2020.
- [68] R. A. Stoica and G. T. F. de Abreu, “6G: the wireless communications network for collaborative and AI applications,” 2019, <https://arxiv.org/abs/1904.03413>.
- [69] J. Zhao, “A survey of intelligent reflecting surfaces (IRSs): towards 6G wireless communication networks with massive MIMO 2.0,” 2019, <https://arxiv.org/abs/1907.04789>.
- [70] S. Ali, W. Saad, N. Rajatheva et al., “6G white paper on machine learning in wireless communication networks,” 2020, <https://arxiv.org/abs/2004.13875>.
- [71] M. Cesana, F. Cuomo, and E. Ekici, “Routing in cognitive radio networks: challenges and solutions,” *Ad Hoc Networks*, vol. 9, no. 3, pp. 228–248, 2011.
- [72] M. H. Alsharif, A. H. Kelechi, M. A. Albreem, S. A. Chaudhry, M. S. Zia, and S. Kim, “Sixth generation (6G) wireless networks: vision, research activities, challenges and potential solutions,” *Symmetry*, vol. 12, no. 4, p. 676, 2020.
- [73] K. Tekbıyık, A. R. Ekti, G. K. Kurt, and A. Görçin, “Terahertz band communication systems: challenges, novelties and standardization efforts,” *Physical Communication*, vol. 35, article 100700, 2019.
- [74] S. Bashir, M. H. Alsharif, I. Khan et al., “Mimo-terahertz in 6g nano-communications: channel modeling and analysis,” *Computers, Materials and Continua*, vol. 66, no. 1, pp. 263–274, 2021.
- [75] W. Chen, X. Yang, S. Jin, and P. Xu, “Sparse array of sub-surface aided blockage-free multi-user mmWave communication

- systems,” *Digital Communications and Networks*, vol. 6, no. 3, pp. 292–303, 2020.
- [76] I. A. Khoso, T. B. Javed, S. Tu et al., “A fast-convergent detector based on joint jacobi and richardson method for uplink massive MIMO Systems,” in *2019 28th Wireless and Optical Communications Conference (WOCC)*, Beijing, China, 2019.
- [77] M. Akhlaq, H. Farooq, and Z. Ahmad, “Performance analysis of X-band RADAR in the presence of electronic jammers,” in *2019 International Conference on Electrical, Communication, and Computer Engineering (ICECCE)*. IEEE, pp. 1–4, Swat, Pakistan, July 2019.
- [78] M. Attarifar, A. Abbasfar, and A. Lozano, “Modified conjugate beamforming for cell-free massive MIMO,” *IEEE Wireless Communications Letters*, vol. 8, no. 2, pp. 616–619, 2019.
- [79] I. A. Khoso, X. Dai, M. N. Irshad, A. Khan, and X. Wang, “A low-complexity data detection algorithm for massive MIMO systems,” *IEEE Access*, vol. 7, pp. 39341–39351, 2019.
- [80] Z. Gu, J. Zhang, Y. Ji, L. Bai, and X. Sun, “Network topology reconfiguration for FSO-based fronthaul/backhaul in 5G+ wireless networks,” *IEEE Access*, vol. 6, no. c, pp. 69426–69437, 2018.
- [81] A. Douik, H. Dahrouj, T. Y. Al-Naffouri, and M. S. Alouini, “Hybrid radio/free-space optical design for next generation backhaul systems,” *IEEE Transactions on Communications*, vol. 64, no. 6, pp. 2563–2577, 2016.
- [82] H. Yu, M. K. Afzal, Y. B. Zikria, A. Rachedi, and F. H. P. Fitzek, “Tactile internet: technologies, test platforms, trials, and applications,” *Future Generation Computer Systems*, vol. 106, pp. 685–688, 2020.
- [83] M. S. Miah, K. M. Ahmed, M. K. Islam, M. A. R. Mahmud, M. M. Rahman, and H. Yu, “Enhanced sensing and sum-rate analysis in a cognitive radio-based internet of things,” *Sensors (Switzerland)*, vol. 20, no. 9, p. 2525, 2020.
- [84] A. Ostovar, Y. Bin Zikria, H. S. Kim, and R. Ali, “Optimization of resource allocation model with energy-efficient cooperative sensing in green cognitive radio networks,” *IEEE Access*, vol. 8, pp. 141594–141610, 2020.
- [85] M. A. Naeem, R. Ali, M. Alazab, M. Yhui, and Y. Bin Zikria, “Enabling the content dissemination through caching in the state-of-the-art sustainable information and communication technologies,” *Sustainable Cities and Society*, vol. 61, article 102291, 2020.
- [86] H. Xu, H. Gao, C. Zhou, R. Duan, and X. Zhou, “Resource allocation in cognitive radio wireless sensor networks with energy harvesting,” *Sensors*, vol. 19, no. 23, 2019.
- [87] F. Al-Turjman, E. Ever, Y. Bin Zikria, S. W. Kim, and A. Elmahgoubi, “SAHCI: scheduling approach for heterogeneous content-centric IoT applications,” *IEEE Access*, vol. 7, pp. 80342–80349, 2019.
- [88] S. Lee, J. Youn, and B. C. Jung, “A cooperative phase-steering technique with on-off power control for spectrum sharing-based wireless sensor networks,” *Sensors*, vol. 20, no. 7, 2020.
- [89] B. S. Muwonge, T. Pei, J. S. Otim, and F. Mayambala, “A joint power, delay and rate optimization model for secondary users in cognitive radio sensor networks,” *Sensors (Switzerland)*, vol. 20, no. 17, pp. 4907–4918, 2020.
- [90] H. A. Bany Salameh, M. M. Krunz, and O. Younis, “MAC protocol for opportunistic cognitive radio networks with soft guarantees,” *IEEE Transactions on Mobile Computing*, vol. 8, no. 10, pp. 1339–1352, 2009.
- [91] Y. Wang, G. Zheng, H. Ma, Y. Li, and J. Li, “A joint channel selection and routing protocol for cognitive radio network,” *Wireless Communications and Mobile Computing*, vol. 2018, Article ID 6848641, 7 pages, 2018.
- [92] H. S. Ghazi and K. Wesolowski, “Application of an interference cancellation detector in a two-way relaying system with physical network coding,” *Electron*, vol. 10, no. 11, p. 1294, 2021.
- [93] F. Brunero, D. Tuninetti, and N. Devroye, “On code design for wireless channels with additive radar interference,” in *2019 IEEE Information Theory Workshop (ITW)*, pp. 3–7, Visby, Sweden, 2019.
- [94] H. Shajaiah, A. Abdelhadi, and C. Clancy, “Resource allocation with carrier aggregation for commercial use of 3.5 GHz spectrum,” in *Resource Allocation with Carrier Aggregation in Cellular Networks*, Springer, Cham, 2018.
- [95] A. H. Moon, U. Iqbal, and G. Mohiuddin Bhat, “Authenticated key exchange protocol for wireless sensor networks,” *International Journal of Applied Engineering Research*, vol. 11, no. 6, pp. 4280–4287, 2016.
- [96] V. Pla, A. S. Alfa, J. Martinez-Bauset, and V. Casares-Giner, “Discrete-time analysis of cognitive radio networks with non-saturated source of secondary users,” *Wireless Communications and Mobile Computing*, vol. 2019, Article ID 7367028, 12 pages, 2019.
- [97] B. Zayen, A. Hayar, and K. Kansanen, “Blind spectrum sensing for cognitive radio based on signal space dimension estimation,” in *2009 IEEE International Conference on Communications*, Dresden, Germany, 2009.
- [98] Y. Arjoun and N. Kaabouch, “A comprehensive survey on spectrum sensing in cognitive radio networks: recent advances, new challenges, and future research directions,” *Sensors*, vol. 19, no. 1, 2019.
- [99] A. Abu Alkheir and H. T. Mouftah, “Cognitive radio for public safety communications,” in *Wireless Public Safety Networks*, Elsevier, 2016.
- [100] T. Bräysy, J. Lehtomäki, B. Calvet, S. Delmas, and C. Moy, *Cognitive Techniques for Finding Spectrum for Public Safety Services*, Oulu Univ (Finland), 2010.
- [101] J. Li and B. J. Hu, “Quantized cooperative spectrum sensing in bandwidth- constrained cognitive V2X based on deep learning,” *Electron*, vol. 10, no. 11, p. 1315, 2021.
- [102] Y. Cao, E. J. Sunde, and K. Chen, “Multiplying channel capacity: aggregation of fragmented spectral resources,” *IEEE Microwave Magazine*, vol. 20, no. 1, pp. 70–77, 2019.
- [103] A. Goldsmith and I. Marić, *Capacity of Cognitive Radio Networks*, Cambridge University Press, 2012.
- [104] L. F. Minervini, “Spectrum management reform: rethinking practices,” *Telecommunications Policy*, vol. 38, no. 2, pp. 136–146, 2014.
- [105] A. S. Alfa, V. Pla, J. Martinez-Bauset, and V. Casares-Giner, “Discrete time analysis of cognitive radio networks with saturated source of secondary users,” in *NETWORKING 2011 Workshops*, vol. 6827 of Lecture Notes in Computer Science, pp. 3–12, Springer, Berlin, Heidelberg, 2011.
- [106] M. Hassan, M. Singh, and K. Hamid, “Overview of cognitive radio networks,” *Journal of Physics Conference Series*, vol. 1, p. 2021, 2021.
- [107] A. Jagannath, J. Jagannath, and T. Melodia, “Redefining wireless communication for 6G: signal processing meets deep learning,” 2020, <https://arxiv.org/abs/2004.10715>.

## Research Article

# Image Recognition Method for Pitching Fingers of Basketball Players Based on Symmetry Algorithm

Wanquan Chen 

School of Physical Education, Xianyang Vocational Technical College, Xianyang 712000, China

Correspondence should be addressed to Wanquan Chen; [chenwanquan0127@163.com](mailto:chenwanquan0127@163.com)

Received 11 June 2021; Revised 2 August 2021; Accepted 10 August 2021; Published 16 September 2021

Academic Editor: Vimal Shanmuganathan

Copyright © 2021 Wanquan Chen. This is an open access article distributed under the Creative Commons Attribution License, which permits unrestricted use, distribution, and reproduction in any medium, provided the original work is properly cited.

In the basketball game, the accuracy and standardization of pitching are directly related to the score. So it is very important to analyze the pitching figure movement to have a better positioning of the fingers. There are limited techniques to recognize the movement. The human motion recognition method is one of them. It utilizes the spatiotemporal image segmentation and interactive region detection to recognize images of pitching finger movement of basketball players. This method has a limitation that the symmetrical information of the human body and sphere cannot be excavated, which leads to certain errors in recognition effect. This paper presents a method of recognizing pitching finger movement of basketball players based on symmetry algorithm, constructs an acquisition model, carries out edge contour detection and adaptive feature segmentation of images of pitching finger movement of basketball players, and uses a fixed threshold to segment finger image to extract players' hand contour and locate the middle axis of the finger. On this basis, the symmetry recognition method based on nematode recognition algorithm is used to recognize the symmetry of basketball pitching finger movement image and complete the accurate recognition of basketball pitching finger movement image. The experimental results show that the proposed method can effectively recognize the basketball player's finger movement image. The average recognition accuracy is 98%, the growth rate of recognition speed is 98%, and the maximum recognition time is 12 s. The robustness of the proposed method is 0.45.

## 1. Introduction

In the basketball game, the accuracy and standardization of pitching are directly related to the score, which is of great significance to the accurate recognition and judgment of the finger-stroke motion image of basketball pitching. When evaluating a baseball game, analysts are also interested in important game events to explore the course of a play. For example, these events can be used in systems such as those developed in [1–3] to visualize the game timeline. A human motion recognition method based on spatiotemporal image segmentation and interactive region detection is proposed [4, 5], which detects human contours in the video stream and segments them into key regions, then expands the segmentation to include nonhuman objects interacting with the human body. The spatiotemporal histogram of gradient direction (HOG) and histogram of optical flow field (HOF) descriptor were used to represent the static and dynamic characteristics of key segments, and codebook is constructed

by  $K$ -means algorithm. At the same time, local constrained linear coding (LLC) technology is used to optimize codebook. Finally, nonlinear support vector machine (SVM) is used to learn features and recognize actions, because this method cannot mine human beings. The symmetrical information of body and sphere leads to some errors in recognition effect. Another motion recognition method combines multipose estimation features [6] and uses the obtained multimotion models to estimate the posture of any image to obtain multi-group posture feature information of the image; each group of feature information includes key point information and posture scoring, because the method is based on multimotion models to recognize images, the recognition speed is slow, and the efficiency is low. A real-time motion recognition method came up with [7]. Firstly, the depth image is projected in three projection planes; then, the Gabor features are extracted from three projection maps, and finally, these features are utilized to train extreme learning machine (ELM) classifier and complete motion classification, but the



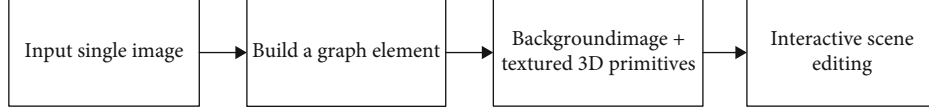


FIGURE 1: Standardized judgment process of finger throwing action in basketball throwing.

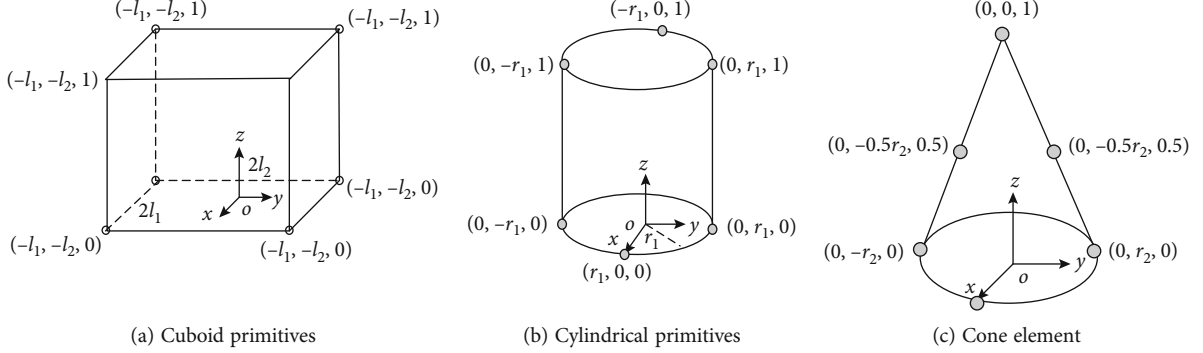


FIGURE 2: 3D modeling of finger throwing for basketball throwing.

recognition accuracy of the proposed method is less than 90% in the experiment. The data is insufficient and the usability needs to be excavated. Sun et al. [8] proposed a face recognition method based on center-symmetric local binary pattern (CS-LBP) and DBN (FRMCD). The results show that the recognition rate of FRMCD is superior to that of traditional methods; the highest recognition rate is up to 98.82%.

In view of the above problems, this paper proposes a method of recognizing the finger-stroke action image of basketball pitching based on symmetry algorithm. Firstly, the image acquisition model of finger-stroke action of basketball pitching is constructed. The edge contour detection and adaptive feature segmentation are carried out on the finger-stroke image of basketball pitching, and the hand-shape image of players is extracted. Nematode recognition algorithm identifies image of basketball players' pitching finger movement [9]. The output is measured in terms of robustness of the method which includes the judgment time and recognition accuracy. The results obtained for the proposed method are also compared with the motion recognition method fusing multipose estimation and human motion recognition method based on spatiotemporal image segmentation. The proposed method has better judgment time and recognition accuracy as compared to the other two methods and hence can be employed for real-time motion recognition.

## 2. Image Recognition Method for Pitching Finger Movement

**2.1. Image Acquisition Model of Pitching Finger Movement of Basketball Players.** Assuming that the Gauss mixture model labels the rotation of the spatial position of the pitching finger movement of the basketball players, at the multiposition points of the space of the finger movement, the body coordinates of the pitching finger movement of under the initial deformation are  $X = (x_{i0}, x_{i1}, \dots, x_{i(n-1)}, y_{i0}, y_{i1}, \dots, y_{i(n-1)})^T$ ,

and the width and height of the whole characteristic image of the basketball court are  $W$  and  $H$ . The three-dimensional spatial feature image  $I$  of pitching finger movement is divided into several subblocks, using the grid model. The coordinates of the center points along the gradient direction of the matching points on the network model are calculated to be  $X' = (x'_{i0}, x'_{i1}, \dots, x'_{i(n-1)}, y'_{i0}, y'_{i1}, \dots, y'_{i(n-1)})^T$ . Then, the sphere network model of the basketball in the player's hands is calculated separately. At the  $j$ th manual calibration point  $(x_{ij}, y_{ij})$ , the triangular partition pheromone  $p(i, j)$  of the single-frame pitching movement is obtained as given in the following equation:

$$p(i, j) = \left( i \in \left[ 0, \text{int} \left( \frac{W}{2} \right) - 1 \right], j \in \left[ 0, \text{int} \left( \frac{H}{2} \right) - 1 \right] \right). \quad (1)$$

There are  $2 \times 2$  pixels in the sampling image of pitching finger movement. The density feature of sampling points is extracted [10]. The mean square error between the standardized feature points  $(x'_{ij}, y'_{ij})$  of basketball pitching finger movement is obtained as shown in the following equation:

$$\text{err}_{ij} = \frac{1}{N} \sum_{i=1}^N \sqrt{(x'_{ij} - y'_{ij}) + (y'_{ij} - y'_{ij})^2}. \quad (2)$$

In the formula,  $N$  is the total number of evenly distributed grids for image of pitching finger of basketball players.

Considering all the pixel feature points of  $n$  spatial positions, the error vectors of basketball players' differences in lifting and pitching motions are obtained as given in the

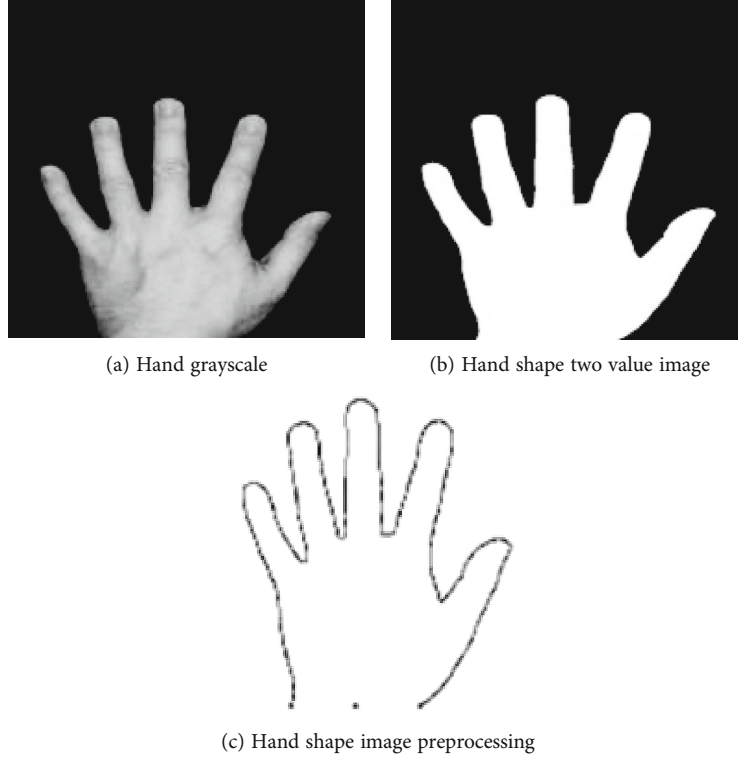


FIGURE 3: Hand image preprocessing.

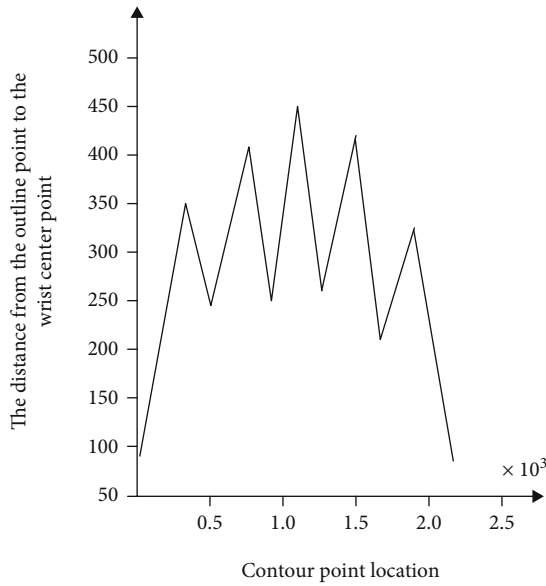


FIGURE 4: The distance from the outline point to the wrist center point.

following equation:

$$\text{ERR} = \frac{1}{n} \sum_{j=0}^{n-1} \text{err}_{ij} - \frac{1}{n} \times \frac{1}{N} \sum_{j=0}^{n-1} \sum_{i=1}^N \sqrt{(x'_{ij} - x_{ij})^2 + (y'_{ij} - y_{ij})^2}. \quad (3)$$

Thus, the sampling and feature analysis of three main

position spaces of basketball players' hands are realized, and the standardized judgment of basketball pitching action in interactive scenes is carried out employing a computer image processing method [11]. The modelling process is shown in Figure 1.

In this paper, the local reconstruction weight matrix  $A$  of the sample points' pitching motion is set up. The basketball player's motion vector is high-dimensional. The affine transformation of the pixel information features of the motion is as shown in Equation (4):

$$\begin{cases} f(G_n) = a_1 + a_2x + a_3y + a_4z + \sum_{i=0}^n \gamma_i U(g'_i, p_i), \\ g(G_n) = b_1 + b_2x + b_3y + b_4z + \sum_{i=0}^n \theta_i U(g'_i, p_i), \\ h(G_n) = c_1 + c_2x + c_3y + c_4z + \sum_{i=0}^n \omega_i U(g'_i, p_i). \end{cases} \quad (4)$$

The normalized sampling point matrix  $H$  for basketball action is a symmetric matrix and the matrix element  $h = U(g'_i, P_j) = \|g'_i - P_j\|$ :  $i, j = 0, 1, 2, \dots, n$ .  $U$  stands for matrix vectors, and  $g$  represents matrix elements. The eigenspace cost function under three-dimensional nonlinear space mapping is used to find partial differential of unknown transformation parameters  $a, b, c, \gamma, \theta$ , and  $\omega$ , so as to get the linear equations of sampling points and fixed points of network

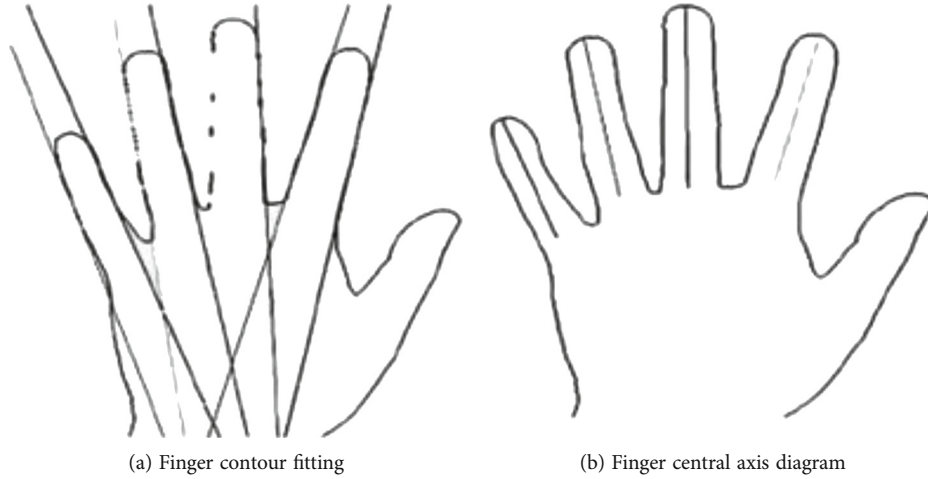


FIGURE 5: Finger localization.

P3	P2	P1
P4	P	P0
P5	P6	P7

FIGURE 6: Eight-neighborhood model.

model, and is given by Equation (5):

$$\begin{bmatrix} x & y & z \\ 0 & 0 & 0 \end{bmatrix} = \begin{bmatrix} (H + \tau \cdot I) & P \\ P^T & 0 \end{bmatrix} \begin{bmatrix} \gamma & \theta & \omega \\ a & b & c \end{bmatrix}. \quad (5)$$

The TPS transform determines the edge features of the vertex of the mesh. The cost error function of wrong pitching movement in the local coordinate system is as shown in the following equation:

$$\min \varepsilon(W) z = \sum_{i=1}^N \left| x_i - \sum_{j=1}^k w_j^i x_{ij} \right|^2. \quad (6)$$

In the formula:  $k$  vertexes of the feature space network model of basketball pitching fingers are  $x_{ij} (j = 1, 2, \dots, k)$  of  $x_i$ ,  $w_j^i$  is the weighted difference error between  $x_i$  and  $x_{ij}$ .

Through triangulation construction, the standardized characteristics of pitching motion of basketball players meet the condition  $x_{ij}$ . In order to obtain the motion vector matrix  $W$ , the edge contour segmentation errors of the  $n$ -th and  $n+1$ -th acquisition points are represented by  $P_n$  and  $P_{n+1}$ . When the elbow of the player's ball-holding hand is gradually straightened, the points of the space position in the  $P$  Euclidean space form a high-dimensional manifold [12]. With the probability of position distribution of basket-

ball in the air, a local covariance matrix  $Q_{jm}^i$  is obtained as given in the following equation:

$$Q_{jm}^i = (x_i - x_{ij})^T (x_i - x_{ij}). \quad (7)$$

Combining formula (7) with  $\sum_{j=1}^k w_j^i = 1$ , edge contour view point segmentation and the output function  $f(x) = W_x^T$  of basketball pitching motion under computer vision are used as regression function, and  $x$  is the input vector of pixel value. Based on this, the three-dimensional model visual modeling is carried out, as shown in Figure 2.

## 2.2. Hand Contour Extraction of Players

**2.2.1. Hand Image Preprocessing.** The main purpose of hand image preprocessing is to extract player's hand contour, which includes three parts: gray image, binary image, and hand contour extraction [13]. Because of the single background, uniform illumination, and obvious difference between foreground image and background, the hand image can be segmented by fixed threshold. Figures 3(a)–3(c) are gray image, binary image, and contour of the hand.

**2.2.2. Locating Fingertips and Figure End.** Locating fingertips and finger end is the basis of locating the middle axis of the finger. The commonly used location algorithm of fingertips and finger end is to find the distance from each contour point to the center of the wrist [14]. In Figure 4, the local vertex of the curve is the fingertip and the local valley is the finger end. Wrist center point, in a hand contour, is the midpoint of the vertex line of the two hand contours at the wrist (the black midpoint in Figure 3(c)).

**2.2.3. Locating the Central Axis of a Finger.** Because the player's finger contour has high stability, the finger axis positioned according to the finger contour also has high stability [15]. Firstly, the left and right contours of the finger are fitted as the edge line of the finger, and then, the midline of the two edge lines is taken as the center axis of the finger.

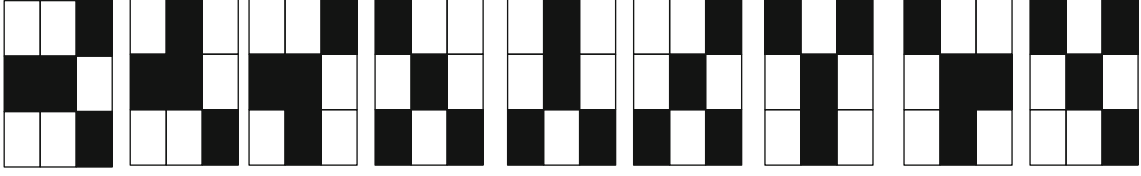


FIGURE 7: Bifurcation point model.

1	0	0	2	2	2	2	2	0	0	0	0
0	1	0	0	0	0	0	0	2	0	0	0
0	0	1	1	0	1	0	0	0	2	0	0
3	3	0	1	0	1	0	0	0	0	2	0
0	3	0	1	0	0	1	0	0	0	2	0
0	3	0	0	1	1	0	0	2	2	0	0
0	0	3	0	0	0	0	2	0	0	0	0
0	0	3	0	0	0	0	2	0	0	0	0

FIGURE 8: Sequential labeling of line segments.

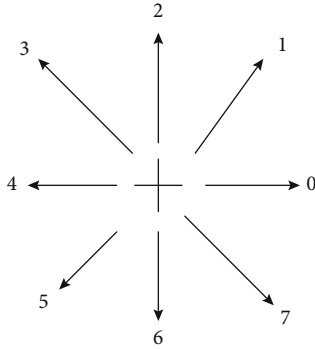


FIGURE 9: 8-unicom chain code.

For a single finger contour, the left and right contours of the finger are divided according to the fingertip points, and then, the left and right contours of the finger are fitted, respectively, by the binomial curve fitting algorithm [16]. A fitting straight line is shown below in the following equation:

$$y = k_d x + b_d, \quad (8)$$

wherein  $k_d = (\sum_{c=1}^{n_d} y_c^d \times \sum_{c=1}^{n_d} x_c^d - n_d \times \sum_{c=1}^{n_d} (x_c^d \times y_c^d)) / (\sum_{c=1}^{n_d} x_c^d)^2 - n_d \times \sum_{c=1}^{n_d} (x_c^d)^2$ ,  $b_d = (\sum_{c=1}^{n_d} y_c^d - k_d \times (\sum_{c=1}^{n_d} x_c^d)) / n_d$ ,  $\{(x_c^d, y_c^d) | c = 1, \dots, n_d\}$ ,  $d (d = 1, 2, \dots, 8)$ ,  $d$  is the finger unilateral contour label, and  $k_d$  is the fitting vector of the finger unilateral contour label.  $n_d$  is the length of the unilateral contour of the finger (from the fingertip to the end of finger),  $(x_1^d, y_1^d)$  is the fingertip,  $(x_{n_d}^d, y_{n_d}^d)$  is the figure end, and  $c$  represents the fitting parameter.

The angular bisector of the line fitted by the left contour and the line fitted by the right contour is defined as the cen-

tral axis of finger, but when the line fitted by the left contour is parallel to the line fitted by the right contour, it is considered that the line parallel to and equal to the two lines is the central axis of finger [17]. Equation (9) represents the central axis of the finger.

$$y = k_i' x + b_i' x. \quad (9)$$

In the formula,  $k_i' = \tan((\arctan k_{i \times 2-1} + \arctan k_{i \times 2})/2)$ ,  $b_i' = (k_{i \times 2-1} b_{i \times 2} - k_{i \times 2} b_{i \times 2-1}) / (k_{i \times 2-1} - k_{i \times 2}) - k_i' (b_{i \times 2-1} - b_{i \times 2}) / (k_{i \times 2-1} - k_{i \times 2})$ ,  $i (i = 1, 2, 3, 4)$ ,  $y = k_{i \times 2-1} x + b_{i \times 2-1}$  is the line fitting the left finger contour, and the intersection point between the central axis of the finger and the contour of the finger is defined as a new fingertip.

The finger length is defined as the vertical line of the finger's central axis through the left and right contour points of the finger. There are two intersections. The intersection point near the fingertip is defined as the start of finger length, and the contour length from the fingertip to the finger end is the finger length [18]. Figure 5(a) is a schematic diagram of finger contour fitting. Figure 5(b) is a sketch map of the central axis of finger.

The above process completes the effective extraction of pitching finger contour and central axis and obtains the effective pitching finger image. On this basis, the symmetry recognition of basketball pitching finger movement image based on nematode recognition algorithm is adopted to realize the accurate recognition of image.

**2.3. Symmetry Recognition of Pitching Finger Image Based on Nematode Recognition Algorithm.** The nematode body has the characteristic of high symmetry, and the human body and the basketball ball also have high symmetry. In order to accurately recognize the symmetry of the pitching finger movement image [19], the nematode recognition algorithm is used to recognize the pitching movement [20].

The biggest factor affecting nematode recognition is the bubbles in the culture medium. The length of the edge of the bubbles is similar to the length of the nematode body, and the enclosure area is similar to the nematode body area [21]. The observation showed that the body of nematode was completely symmetrical. Although the complete envelope curve of nematode edge could not be obtained after pre-treatment, the lines on both sides of the nematode body also had high similarity, and there was no similar curve around the bubble edge curve. Through this characteristic, the lines between the nematode body curve and its bubble edge curve could be distinguished [22].

Based on the nematode recognition algorithm, the image symmetry recognition method is as follows:



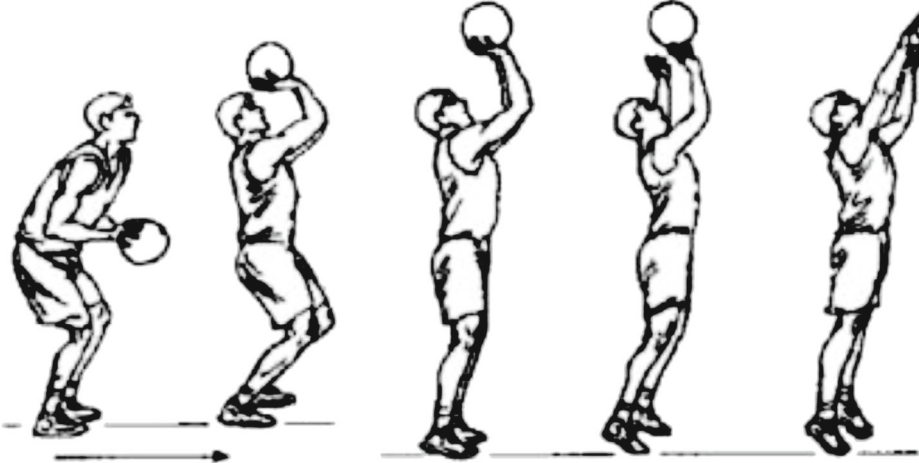


FIGURE 12: Standard mode of finger throwing in basketball bowling.



FIGURE 13: Raw information collection of basketball bowling.

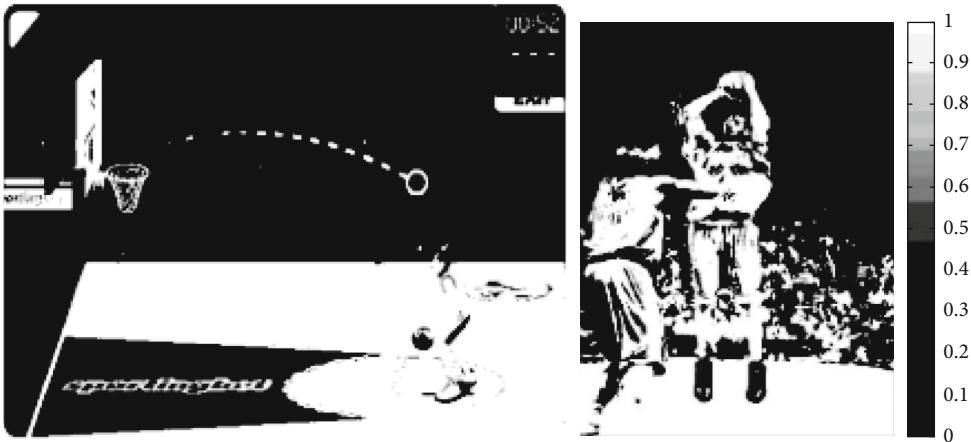


FIGURE 14: Image edge detection and adaptive feature segmentation.

TABLE 1: The results of analysis on the transformation of basketball pitching finger strokes.

Way	Topping points	Overall sampling points	Judge time (s)	Smooth time	Judgment precision (%)
Fixed point	4321	921	12.12	211	98.1
Sport	2432	1211	23.09	321	97.72

on the shorter line segment in two-line segments, the similarity of the two-line segments is calculated by using the chain code value. The formula for calculating the similarity coefficient of two lines of equal length is given in the following equation:

$$r = \frac{\sum_{i=1}^n \sum_{i=1}^n (A_i - \bar{A})(B_i - \bar{B})}{\sqrt{[\sum_{i=1}^n \sum_{i=1}^n (A_i - \bar{A})^2][\sum_{i=1}^n \sum_{i=1}^n (B_i - \bar{B})^2]}}. \quad (10)$$

In the formula:  $[A_1, \dots, A_n]$  and  $[B_1, \dots, B_n]$  are chain code values of two-line segments, respectively,  $\bar{A} = \sum_{i=1}^n A_i/n$  and  $\bar{B} = \sum_{i=1}^n B_i/n$ . The closer the similarity coefficient is to 1, the more similar the two-line character is.

In the image studied in this paper, the length of the two-line segments is not always equal (Beyer-H RTL). This is to calculate the similarity coefficient by truncating the chain code value of the same length as the chain code value of the shorter line segment from scratch in the chain code value of the longer line segment and then moving one bit backward in turn to calculate the chain code value of the same length until all the chain code values of the longer line segment have been taken. If there are  $n$  chain codes in the shorter line segment and  $m$  chain codes in the longer line segment, it is necessary to calculate the  $(m - n + 1)$ -degree similarity coefficients. Finally, all the similarity coefficients are compared, and the group with the largest value is taken as the similarity coefficients of the two-line segments. Because the players' human body and sphere are symmetrical, the similarity between the two contours of the same body and sphere is significant [31], and the similarity coefficient is large, while the similarity coefficient between the contours of different bodies and spheres or between the contours of human body and sphere and the contours of bubbles is small; this method can be used to judge whether the two contours belong to the same body or sphere [32, 33]. According to the definition of similarity, when the similarity coefficient is greater than 0.7, the similarity degree is high, so 0.7 is taken as the judgment threshold. The flow chart of the recognition algorithm is shown in Figure 11.

### 3. Results

In order to verify the effectiveness of this method, this method is used to identify and judge the standardization of pitching finger movement of a basketball player. The hardware environment of the experimental platform is as follows:

CPU is Intel Core I3 processor 3.30 GHz, memory 4GB FFR3, and the resolution of sampling image is  $320 \times 240$ . The simulation data of ball vision image express a kind of basketball throwing action. There are 100 test sample image sets in each throwing action mode, and there are  $1024 \times 1000$  test sets in the basketball throwing action image database. A simplified visual analysis model of finger pulling action of basketball throwing is established by SolidWorks, and the analysis data are imported into Adams software. The image processing and recognition analysis are carried out, and the standardized judgment of the finger pitching action is made. The standardized action mode of the finger pitching action is shown in Figure 12.

The standardized action data of basketball throwing in Figure 12 is saved as .txt text data and loaded into image data processing software. The computer vision analysis is carried out to guide the actual pitching action, and the image acquisition model of basketball pitching is constructed. The acquisition results are shown in Figure 13. The edge contour of the acquired pitching image is detected and adaptive feature segmentation is carried out, which are shown in Figure 14.

The computer vision analysis process of 20 pitching movements is averaged, and self-adaptive correction and action standardization judgment are made in the three-dimensional space of pitching movements. The results are shown in Table 1:

From Table 1, it can be seen that the accuracy of recognition and judgment is more than 95% for the proposed method and thus can be used to perform fixed-point judgment and motion of pitching motion. The accuracy of proposed method suggests that it can accurately identify the pitching action image of a basketball player and correct the pitching deviation in real-time and hence, this method realizes adaptive real-time correction.

The comparison of the proposed method with human motion recognition method based on spatiotemporal image segmentation and interactive region detection and action recognition method fused with multipose estimation features is also conducted with eight sample runs. Eight basketball pitching finger motion image recognition experiments are set up. The recognition images are set to four. The recognition accuracy of the three methods is counted. The comparison results are shown in Tables 2-4.

Tables 2-4 represent the recognition accuracy of the various methods for the same basketball pitching finger image and identical recognition times. The average recognition accuracy of proposed method is 98%; the average recognition accuracy of human motion recognition method based on spatiotemporal image segmentation and interactive region detection is 46%. The average recognition accuracy of the multipose estimation methods is 76%. This comparison shows that the accuracy of the proposed method is the largest among the three methods.

The results of the recognition growth rate of the three methods in the above experiments are statistically analyzed. The results are shown in Figure 15.

Analysis of Figure 15 shows that three methods can identify the growth rate of speed. The trend of the broken

TABLE 2: Identification accuracy of this method.

Number of experiments/times	Identification accuracy (%)				4 image recognition accuracy mean
	Image 1	Image 2	Image 3	Image 4	
1	95%	97%	99%	99%	98%
2	99%	95%	98%	98%	98%
3	97%	97%	99%	99%	98%
4	97%	97%	99%	99%	98%
5	99%	95%	99%	98%	98%
6	97%	99%	98%	98%	98%
7	99%	98%	95%	98%	98%
8	98%	99%	95%	95%	97%
8 identification accuracy mean	98%	97%	98%	98%	98%

TABLE 3: Identification accuracy of human motion recognition method based on time and space image segmentation and interaction area detection.

Number of experiments/times	Identification accuracy (%)				4 image recognition accuracy mean
	Image 1	Image 2	Image 3	Image 4	
1	45%	48%	46%	46%	46%
2	46%	48%	46%	45%	46%
3	46%	48%	45%	46%	46%
4	46%	48%	48%	45%	47%
5	46%	48%	48%	46%	47%
6	45%	48%	45%	45%	46%
7	46%	46%	45%	46%	46%
8	45%	45%	45%	48%	46%
8 identification accuracy mean	46%	47%	46%	46%	46%

TABLE 4: Identification accuracy of action recognition method for fusion of multiple posture estimation features.

Number of experiments/times	Identification accuracy (%)				4 image recognition accuracy mean
	Image 1	Image 2	Image 3	Image 4	
1	77%	76%	76%	76%	76%
2	76%	77%	78%	78%	77%
3	76%	78%	77%	77%	77%
4	76%	78%	48%	78%	70%
5	77%	77%	77%	78%	77%
6	78%	76%	76%	78%	77%
7	78%	77%	77%	78%	78%
8	75%	75%	75%	78%	76%
8 identification accuracy mean	77%	77%	73%	78%	76%

line of the growth rate of recognition speed of the proposed method is obviously above the other two methods. With the increase of the number of experiments, the maximum growth rate of recognition speed of the proposed method reaches 98%, and the recognition speed of the motion recognition method with multipose estimation features increases. The growth rate of recognition speed of proposed method is 91.8%. The highest speed of human motion recognition based on spatiotemporal image segmentation and interactive region detection is only 91.5%. From this, we can see that the

speed of recognition in this paper increases rapidly and the efficiency is high.

Statistical time-consuming data of the three methods in the above experiments are described in Tables 5–7.

Tables 5–7 show that, on the premise of identifying the same target and identical recognition times, the maximum recognition time of this method is 12 s; the maximum recognition time of human motion recognition method based on spatiotemporal image segmentation and interactive region detection is 62 s. The maximum time of the recognition of



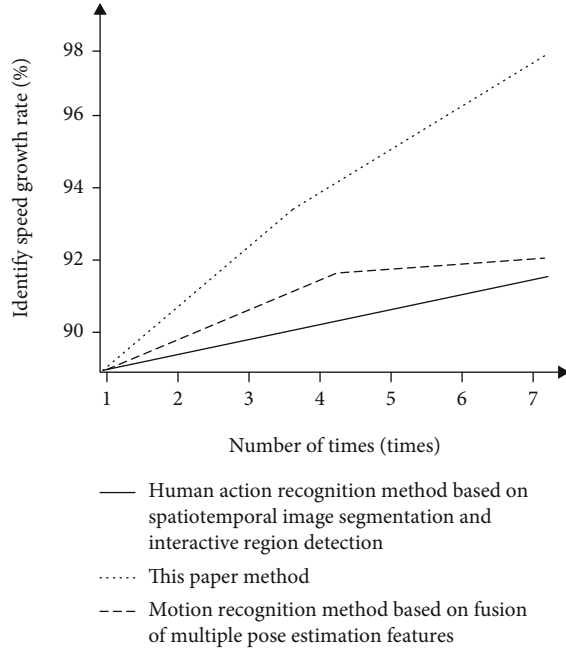


FIGURE 15: Growth rate of recognition of the three methods.

TABLE 5: Time-consuming identification of this method.

Number of experiments/ times	Time consuming (s)			
	Image 1	Image 2	Image 3	Image 4
1	10	11	11	11
2	10	11	10	10
3	12	11	10	12
4	10	11	11	11
5	12	11	10	11
6	12	10	11	10
7	12	10	10	10
8	10	12	10	10

TABLE 6: Time-consuming recognition of human motion recognition methods based on spatial and temporal image segmentation and interactive region detection.

Number of experiments/ times	Time consuming (s)			
	Image 1	Image 2	Image 3	Image 4
1	56	57	53	51
2	52	53	55	55
3	56	57	60	61
4	56	57	59	58
5	57	59	58	58
6	56	62	61	60
7	56	57	58	60
8	57	60	60	60

TABLE 7: Time consuming for recognition of motion recognition methods incorporating multiple posture estimation features.

Number of experiments/ times	Time consuming (s)			
	Image 1	Image 2	Image 3	Image 4
1	32	33	34	34
2	34	34	34	35
3	34	35	36	35
4	37	34	34	34
5	33	33	36	37
6	35	36	36	37
7	37	37	37	36
8	36	34	36	33

the action recognition method based on the fusion of multi-pose estimation features is 37 s. Through data comparison, we can see that the recognition time of this method is the shortest and the recognition efficiency is the fastest.

Statistics on robustness of the three methods are described in Figure 16.

Analysis of Figure 16 shows that with the increase of the number of experiments, the overall trend of the robust data of the proposed method is always above the other two methods. The maximum robustness and minimum robustness of the proposed method are 0.45 and 0.1, respectively. The maximum robustness and minimum robustness of the motion recognition method fusing multipose estimation features are 0.43 and 0.43, respectively. The maximum robustness and minimum robustness of the human motion recognition method based on spatiotemporal image segmentation and interactive region detection are 0.37 and 0.05, respectively, which shows that the robustness of the proposed method is higher than that of the other two methods. The experimental results show that the proposed method has higher robustness.

#### 4. Discussion

Based on the results of the previous section, this paper discusses the impact of wrist and finger movements on the percentage of hits. Firstly, the wrist backward motion during pitching directly affects the direction, rotation, and running parabola of the ball. If the wrist back is not enough, the angle of the shot is small, and the parabola of the ball is low, the possibility of entering the basket will be reduced. The correct action should be as follows: five fingers are separated naturally, the hand turns backward, the palm is empty, and the ball does not fall on the hand; the center of gravity falls between the middle finger and the index finger, so as to facilitate the control of the ball by the hand and finger. Secondly, the finger movement when the ball is released is beneficial to the control of the ball's movement route and can make the thrown ball naturally produce backspin. The backspin ball has a higher flying radian than the nonrotating ball, which enlarges the incident cross section and improves the chances of basketball entering the basket. In this case, even if the

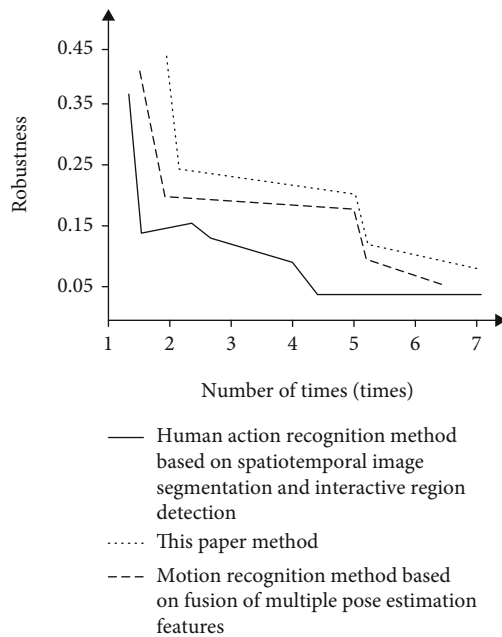


FIGURE 16: Comparison of the robustness of the three methods.

backspin ball occasionally encounters the basket, because the ball's rebound direction is upward, the ball will be more likely to score the basket again. Therefore, it is very important to pay attention to and strengthen the training of wrist and finger movements, form correct throwing techniques, and make them become dynamic stereotypes, so as to improve the shooting rate of the ball. Practice has proved that if we grasp the opportunity (condition) of pitching well, grasp the correct jump shot technology (core), give full play to good physical quality (foundation), plus a better feel, we can improve the hit rate of pitching (especially jump shot) in the fierce competition. Therefore, grasping the correct throwing wrist and finger movements is the key to improve the hit rate of jump shots.

## 5. Conclusion

In this paper, a method of recognizing basketball pitching finger movement image based on symmetry algorithm is proposed. A model of acquiring pitching finger movement image is constructed. The edge contour of pitching finger movement image is detected, and self-adapting feature segmentation is carried out. The players' hand contour is extracted. Basketball pitching based on nematode recognition algorithm is carried out. According to the high symmetry of the nematode body, the human body and sphere are also highly symmetrical. First, the chain code value on one side of the body contour is obtained by image analysis, and then, the basketball pitch is recognized by comparing the similarity coefficient of the chain code value of adjacent line segments. Based on the experimental results, it is concluded that the accuracy of recognition and judgment is more than 95% when judging the movement in basketball pitching. An accuracy of above 95% indicates that the method can be employed for time recognitions. The average recognition

accuracy for the proposed method is 98%, the growth rate of recognition speed is 98%, and the maximum recognition time is 12 s. The recognition efficiency and accuracy for the proposed method are greater than those for the other two methods. The robustness of the proposed method is 0.45, which shows that the method has high stability.

## Data Availability

Data is available on request.

## Conflicts of Interest

The authors declare no conflicts of interest.

## References

- [1] C. Dietrich, D. Koop, H. T. Vo, and C. T. Silva, "Baseball4D: a tool for baseball game reconstruction & visualization," in *2014 IEEE conference on visual analytics science and technology (VAST)*, pp. 23–32, Paris, France, 2014.
- [2] M. Lage, J. P. Ono, D. Cervone, J. Chiang, C. Dietrich, and C. T. Silva, "StatCast Dashboard: exploration of spatiotemporal baseball data," *IEEE Computer Graphics and Publications*, vol. 36, no. 5, pp. 28–37, 2016.
- [3] J. P. Ono, D. Dietrich, and C. T. Silva, "Summarizing baseball plays into a static visualization," in *Computer Graphics Forum*, vol. 37, pp. 491–501, Wiley Online Library, 2018.
- [4] J. Zhang, J. Z. Wu, and J. L. Tang, "Human action recognition method based on spatio-temporal image segmentation and interactive area detection," *Application Research of Computers*, vol. 34, pp. 302–305, 2017.
- [5] N. Wiedemann, C. Dietrich, and C. T. Silva, "A tracking system for baseball game reconstruction," *Computer Vision and Pattern Recognition* <https://arxiv.org/abs/2003.03856v1>.
- [6] H. L. Luo, Y. J. Feng, and F. S. Kong, "Fusing multiple pose estimations for still image action recognition," *Journal of Image and Graphics*, vol. 20, pp. 1462–1472, 2015.
- [7] S. Wang, J. W. Dang, and Y. P. Wang, "Research on real-time action recognition approach," *Computer Engineering and Applications*, vol. 53, pp. 28–31, 2017.
- [8] K. Sun, X. Yin, M. Yang, Y. Wang, and J. Fan, "The face recognition method based on CS-LBP and DBN," *Mathematical Problems in Engineering*, vol. 2018, Article ID 3620491, 9 pages, 2018.
- [9] B. Yang, J. Chen, and F. S. Lee, "GC-MS fingerprints for discrimination of *Ligusticum chuanxiong* from *Angelica*," *Journal of Separation Science*, vol. 31, pp. 3231–3237, 2015.
- [10] D. A. Williams, T. Kiiza, R. Kwizera et al., "Evaluation of fingerstick cryptococcal antigen lateral flow assay in HIV-infected persons: a diagnostic accuracy study: Figure 1," *Clinical Infectious Diseases*, vol. 61, no. 3, pp. 464–467, 2015.
- [11] Z. Liu, F. Li, B. Zhang, S. Li, J. Wu, and Y. Shi, "Structural basis of plant homeodomain finger 6 (PHF6) recognition by the retinoblastoma binding protein 4 (RBBP4) component of the nucleosome remodeling and deacetylase (NuRD) complex," *Journal of Biological Chemistry*, vol. 290, no. 10, pp. 6630–6638, 2015.
- [12] A. Badu-Nkansah, A. C. Mason, B. F. Eichman, and D. Cortez, "Identification of a substrate recognition domain in the replication stress response protein zinc finger ran-binding

- domain-containing protein 3 (ZNRANB3),” *Journal of Biological Chemistry*, vol. 291, no. 15, pp. 8251–8257, 2016.
- [13] M. Gruber, M. Ritchey, S. F. Wang, M. K. Doss, and C. Ranganath, “Post-learning hippocampal dynamics promote preferential retention of rewarding events,” *Neuron*, vol. 89, no. 5, pp. 1110–1120, 2016.
- [14] O. Dziadek, B. Shoup, and K. Williams, “Abstract 4: differential gene expression associated with lynch syndrome in patients less than and over 60 years of age with endometrial adenocarcinoma,” *Gynecologic Oncology*, vol. 137, no. 3, p. 592, 2015.
- [15] N. T. Zhang, K. L. Zhao, and G. L. Liu, “Thought on constructing the integrated space-terrestrial information network,” *Journal of China Academy of Electronics & Information Technology*, vol. 10, no. 3, pp. 223–230, 2015.
- [16] Q. Wei, M. Zhang, B. Ogorevc, and X. Zhang, “Recent advances in the chemical imaging of human fingerprints (a review),” *The Analyst*, vol. 141, no. 22, pp. 6172–6189, 2016.
- [17] F. Wang, D. Wang, and X. Zhang, “Study of three-level inverter carrier-based over-modulation strategy,” *Journal of Power Supply*, vol. 4, pp. 24–30, 2015.
- [18] B. Figueroa, Y. Chen, K. Berry, A. Francis, and D. Fu, “Label-free chemical imaging of latent fingerprints with stimulated Raman scattering microscopy,” *Analytical Chemistry*, vol. 89, no. 8, pp. 4468–4473, 2017.
- [19] C. J. Lin, L. Bin, and G. F. Chang, “Experimental study on internal resistance of LiFePO<sub>4</sub> batteries under different ambient temperatures,” *Chinese Journal of Power Sources*, vol. 341, pp. 1110–1123, 2015.
- [20] Y. Kominami, S. Yoshida, S. Tanaka et al., “Computer-aided diagnosis of colorectal polyp histology by using a real-time image recognition system and narrow-band imaging magnifying colonoscopy,” *Gastrointestinal Endoscopy*, vol. 83, no. 3, pp. 643–649, 2016.
- [21] J. P. Ba and J. L. Mao, “Research on the control system of rectifying device based on USS communication,” *Automation & Instrumentation*, vol. 57, pp. 43–69, 2015.
- [22] C. M. B. Evans and S. N. Baker, “Task-dependent intermanual coupling of 8-Hz discontinuities during slow finger movements,” *European Journal of Neuroscience*, vol. 18, pp. 453–456, 2015.
- [23] J. X. Du, C. S. Chen, and J. F. Tong, “Research on maintain task scheduling of armored equipment support based on queuing theory,” *Computer Simulation*, vol. 1, pp. 43–64, 2016.
- [24] H. Shidnia, N. B. Hornback, and E. M. Helveston, “Treatment results of retinoblastoma at Indiana University Hospitals,” *Cancer*, vol. 40, pp. 2917–2922, 2015.
- [25] V. Alberto, M. Bruno, and V. D. Nguyen, “Attribution of regional flood changes based on scaling fingerprints,” *Water Resources Research*, vol. 52, pp. 5322–5340, 2016.
- [26] P. K. Singh, A. K. Srivastava, D. Dalela, S. K. Rath, M. M. Goel, and M. L. B. Bhatt, “Frequent expression of zinc-finger protein ZNF165 in human urinary bladder transitional cell carcinoma,” *Immunobiology*, vol. 220, no. 1, pp. 68–73, 2015.
- [27] Z. Han and M. Ma, “Hip-hop action image recognition based on symmetric algorithm and iterative weighting of dense sampling,” *Journal of Ambient Intelligence and Humanized Computing*, 2020.
- [28] C. Yang, Z. Yang, G. Zhang et al., “Characterization and differentiation of chemical fingerprints of virgin and used lubricating oils for identification of contamination or adulteration sources,” *Fuel*, vol. 163, pp. 271–281, 2016.
- [29] K. Jairath, N. Singh, V. Jagota, and M. Shabaz, “Compact ultra-wide band metamaterial-inspired split ring resonator structure loaded band notched antenna,” *Mathematical Problems in Engineering*, vol. 2021, Article ID 5174455, 12 pages, 2021.
- [30] M. Peters, A. Scharmgga, A. van Tubergen et al., “The reliability of a semi-automated algorithm for detection of cortical interruptions in finger joints on high resolution ct compared to MicroCT,” *Calcified Tissue International*, vol. 101, pp. 132–140, 2017.
- [31] K. Beyer, L. Grabenhenrich, M. Härtl et al., “Predictive values of component-specific IgE for the outcome of peanut and hazelnut food challenges in children,” *Allergy*, vol. 70, no. 1, pp. 90–98, 2015.
- [32] B. Jiang, P. Wang, Y. Zhang, J. Zhao, and Q. Dong, “Modification of the internal suture technique for mallet finger,” *Medicine*, vol. 94, no. 6, article e536, 2015.
- [33] S. Tang and M. Shabaz, “A new face image recognition algorithm based on cerebellum-basal ganglia mechanism,” *Journal of Healthcare Engineering*, vol. 2021, Article ID 3688881, 11 pages, 2021.

## Research Article

# An Enhanced Secure Deep Learning Algorithm for Fraud Detection in Wireless Communication

Sumaya Sanober <sup>1</sup>, Izhar Alam <sup>2</sup>, Sagar Pande <sup>2</sup>, Farrukh Arslan <sup>3</sup>,  
Kantil Pitambar Rane <sup>4</sup>, Bhupesh Kumar Singh <sup>5</sup>, Aditya Khamparia <sup>6</sup>,  
and Mohammad Shabaz <sup>5,7</sup>

<sup>1</sup>Computer Science and Engineering, Prince Sattam Bin Abdul Aziz University, Saudi Arabia Wadi Aldwassir

<sup>2</sup>Computer Science and Engineering, Lovely Professional University, Punjab, India

<sup>3</sup>School of Electrical and Computer Engineering, Purdue University, USA

<sup>4</sup>KCEs COEM JALGAON, India

<sup>5</sup>Arba Minch University, Ethiopia

<sup>6</sup>Babasaheb Bhimrao Ambedkar University, Lucknow, India

<sup>7</sup>Department of Computer Science Engineering, Chitkara University, India

Correspondence should be addressed to Sumaya Sanober; [s.sanober@psau.edu.sa](mailto:s.sanober@psau.edu.sa), Sagar Pande; [sagarpande30@gmail.com](mailto:sagarpande30@gmail.com), and Mohammad Shabaz; [mohammad.shabaz@amu.edu.et](mailto:mohammad.shabaz@amu.edu.et)

Received 9 July 2021; Revised 20 July 2021; Accepted 26 July 2021; Published 15 August 2021

Academic Editor: VIMAL SHANMUGANATHAN

Copyright © 2021 Sumaya Sanober et al. This is an open access article distributed under the Creative Commons Attribution License, which permits unrestricted use, distribution, and reproduction in any medium, provided the original work is properly cited.

In today's era of technology, especially in the Internet commerce and banking, the transactions done by the Mastercards have been increasing rapidly. The card becomes the highly useable equipment for Internet shopping. Such demanding and inflation rate causes a considerable damage and enhancement in fraud cases also. It is very much necessary to stop the fraud transactions because it impacts on financial conditions over time the anomaly detection is having some important application to detect the fraud detection. A novel framework which integrates Spark with a deep learning approach is proposed in this work. This work also implements different machine learning techniques for detection of fraudulent like random forest, SVM, logistic regression, decision tree, and KNN. Comparative analysis is done by using various parameters. More than 96% accuracy was obtained for both training and testing datasets. The existing system like Cardwatch, web service-based fraud detection, needs labelled data for both genuine and fraudulent transactions. New frauds cannot be found in these existing techniques. The dataset which is used contains transaction made by credit cards in September 2013 by cardholders of Europe. The dataset contains the transactions occurred in 2 days, in which there are 492 fraud transactions out of 284,807 which is 0.172% of all transaction.

## 1. Introduction

Credit card fraud might be a significant issue which requires payment card as Mastercard as illegal supply of money in transactions. Fraud is illegal because of getting funds and goods. The objective of such unlawful transaction might be urging items without paying and also obtain an unauthorized fund from an account. Identifying such fraud might be a troublesome and must risk the company as well as business organizations. Within the world of Fraud Detection System (FDS) [1], investigators are not prepared to examine each

transactions. Here, the Fraud Detection System monitors all of the authorized transactions and alerts the foremost distrustful one. Investigator verifies these alerts and also provides FDS with responses in case the transaction was authorized and fraudulent. Verifying all of the alerts each day might be a time intensive and dear process. Hence, investigator is in a place to confirm just a number of alerts each day. The rest of the transactions stay unchecked until client identifies them and reports them to be a fraud. Also, the techniques employed for fraud, and consequently, the cardholder paying behavior changes over time. This particular alteration

in Mastercard transaction is called as idea drift [1, 2]. Thus, usually, it is hard to notice the Mastercard fraud. Machine learning is taken into consideration collectively of the foremost profitable method for fraud identification. Classification is used by it and also regression strategy for knowing fraud in Mastercard. The machine learning algorithms are split into 2 kinds, supervised [3] along with unsupervised [4] learning algorithm. Supervised learning algorithm uses labeled transactions for instructing the classifier whereas unsupervised learning algorithm uses coeval's analysis that groups customers in line with the profile of theirs and identifies fraud supported clients spending behavior.

Many learning algorithms are offered for fraud detection in Mastercard that features neural networks, logistic regression (LR), Naive Bayes (NB), Support Vector Machines (SVM), decision tree (DT), and  $K$ -nearest neighbors (KNN) as well as random forest (RF). This paper examines the functionality of above algorithms supported the ability of theirs to classify whether the transaction was authorized, and fraudulent next compares them. The comparison is created utilizing performance measure accuracy, precision, and specificity. The end result proved that random forest algorithm showed improved precision and accuracy than some other methods. Further the obtained accuracy was improved by using deep Autoencoder.

The following are the main contributions in this paper:

- (i) Novel deep learning framework is implemented using Spark for financial fraudulent detections
- (ii) Comparative analysis is performed with proposed deep architecture using various machine learning algorithms
- (iii) Performance factors like accuracy, specificity, and precision are used for comparing their performance measures
- (iv) The importance of feature selection techniques is discussed and explored with five different techniques
- (v) A stacked-based novel approach for feature selection is proposed
- (vi) Comparative analysis is performed with proposed deep architecture using various machine learning algorithms
- (vii) Novel deep learning framework is implemented using Spark for financial fraudulent detections
- (viii) Performance factors like accuracy, specificity, and precision are used for comparing their performance measures

The paper is organized as follows: review of the related papers has been done in the literature review section, and next section proposed the methodology where discussion on the dataset is provided along with its description. Further section is of result analysis where comparison of all the algo-

gorithms is done by using the performance factor. The experiment is performed on a system having the configuration of 8 gigabytes of RAM, Intel i5 8th generation quad-core processor with 1.6 GHz clock speed. In the last section, the conclusion and future scope are explained.

## 2. Literature Survey

Various papers were reviewed and are discussed as follows.

Altiti [1] states that the fast evolution of technology all around the world is more often using cards as compared to cash in their day to day life. The Mastercard becomes the highly useable equipment for Internet shopping. This increase in use causes a considerable damage and fraud cases also. It is very much necessary to stop the fraud transactions because it impacts on financial conditions over time the anomaly detection is having some important application to detect the fraud detection. This paper is mainly focused on checking if the transaction is legal or fraud. They present models like "Bidirectional Long short-term memory (BiLSTM)" and "Bidirectional Gated recurrent unit (BiGRU)." They also apply deep learning and Machine Learning algorithms. But their model shows much better results than the machine learning classifiers which is 91.37% score.

Makki et al. [2] describe that in today's era of technology especially in the Internet commerce and banking, the transactions by the Mastercards have been increasing rapidly. The Mastercard becomes the highly useable equipment for Internet shopping. This increase in use causes a considerable damage and fraud cases also. It is very much necessary to stop the fraud transactions because it impacts on financial conditions over time the anomaly detection is having some important application to detect the fraud detection. The paper mainly focused on the solution that tackles the imbalance problem of classification they explore the solution for fraud detection using machine learning algorithms. They also find the summarized results and weakness that they get using credit card fraud labeled dataset. They give us the conclusion that the imbalanced classification is ineffective when the data are highly imbalanced. In this paper, the authors found that the existing methods were costlier and show many false alarms.

Ounacer et al. [3] state that in today's era of technology especially in the Internet commerce and banking, the transactions by the Mastercards have been increasing rapidly. The Mastercard becomes the highly useable equipment for Internet shopping. This increase in use causes a considerable damage and fraud cases also. It is very much necessary to stop the fraud transactions because it impacts on financial conditions over time the anomaly detection is having some important application to detect the fraud detection. Logistic regression, decision tree, SVM, and so on are some approaches to detect anomalies. But these methods are limited because they are supervised algorithms which are trained by the labels to know whether the transactions are legitimate or not.

Benchaji et al. [4] state that in today's era of technology especially in the Internet commerce and banking, the

transactions by the Mastercards have been increasing rapidly. The Mastercard becomes the highly useable equipment for Internet shopping. This increase in use causes a considerable damage and fraud cases also. It is very much necessary to stop the fraud transactions because it impacts on financial conditions over time the anomaly detection is having some important application to detect the fraud detection. The purpose of this paper is to enhance the performance of the classified instances in the imbalanced dataset for which they proposed the unsupervised sampling method based on the genetic algorithm and  $K$ -means clustering.

Dal Pozzolo et al. [5] describe that in today's era of technology especially in the Internet commerce and banking, the transactions by the Mastercards have been increasing rapidly. The Mastercard becomes the highly useable equipment for Internet shopping. This increase in use causes a considerable damage and fraud cases also. It is very much necessary to stop the fraud transactions because it impacts on financial conditions over time the anomaly detection is having some important application to detect the fraud detection.

Zheng et al. [6] describe that with the increase of e-commerce, transactions are also increasing in which some of them were fraud. To detect the fraud transaction, it is important to extract historical transaction records on the behavior profile of the users. To represent the BPs of the user, the Markov chain model is popular. Whose transaction behaviors are stable, this will affect them. The Mastercard becomes the highly useable equipment for Internet shopping. This increase in use causes a considerable damage and fraud cases also.

Venkata Suryanarayana et al. [7] address states in today's era of technology especially in the Internet commerce and banking, the transactions by the Mastercards have been increasing rapidly. The Mastercard becomes the highly useable equipment for Internet shopping. This increase in use causes a considerable damage and fraud cases also. It is very much necessary to stop the fraud transactions because it impacts on financial conditions over time the anomaly detection is having some important application to detect the fraud detection. This paper states the overall performance of LR, RF, and DT for charge card fraud detection. The 3 methods are used for the dataset, and function is applied in the R language. The functionality of the methods is actually evaluated for diverse variables grounded on awareness, specificity, and reliability as well as error rate. The end result displays of reliability for LR, RF, and DT classifier are actually 90.0, 95.53, and 94.3, respectively. The comparative results indicate that the random forest does much better compared to the logistic regression as well as decision tree techniques.

Thennakoon et al. [8] state that in today's era of technology especially in the Internet commerce and banking, the transactions by the Mastercards have been increasing rapidly. The Mastercard becomes the highly useable equipment for Internet shopping. This increase in use causes a considerable damage and fraud cases also. It is very much necessary to stop the fraud transactions because it impacts

on financial conditions over time the anomaly detection is having some important application to detect the fraud detection. Fraud transactions are one of the major financial issues in the banks. There are 10 million transactions that are fraudulent out of 12 billion which can cause a huge loss. So to analyze these, they have predicted the fraud transaction using isolation forest and local outlier factor. They also calculated the no. of error and accuracy of both algorithms.

Shukur and Kurnaz [9] project that in today's era of technology especially in the Internet commerce and banking, the transactions by the Mastercards have been increasing rapidly. The Mastercard becomes the highly useable equipment for Internet shopping. This increase in use causes a considerable damage and fraud cases also. It is very much necessary to stop the fraud transactions because it impacts on financial conditions over time the anomaly detection is having some important application to detect the fraud detection. Such issues can also be tackling with the help of data science with the combination of machine learning. The main objective here is to find all the fraud transactions while increasing the accuracy. Mastercard fraudulent detection is actually a sample of classification. With this procedure, centering on preprocessing datasets and analyzing in addition to the deployment of several anomaly detection algorithms like isolation forest algorithm as well as local outlier factor on the PCA changed Mastercard transaction information.

John and Naaz [10] describe that in today's era of technology especially in the Internet commerce and banking, the transactions by the Mastercards have been increasing rapidly. The Mastercard becomes the highly useable equipment for Internet shopping. This increase in use causes a considerable damage and fraud cases also. It is very much necessary to stop the fraud transactions because it impacts on financial conditions over time the anomaly detection is having some important application to detect the fraud detection. Online transaction fraud detection may be the vast majority of challenging issue for financial businesses and banks. So it is much crucial for financial businesses and also banks to have highly effective fraud detection techniques to reduce the losses of theirs as an outcome of these fee card fraud transactions. Different techniques are found by many researchers till morning to be able to recognize these frauds at the same time as to take down them. After the analysis of the dataset, the reliability is ninety-seven % by LOF and seventy-six % by IF.

Yu et al. [11] state that that in today's era of technology especially in the Internet commerce and banking, the transactions by the Mastercards have been increasing rapidly. The Mastercard becomes the highly useable equipment for Internet shopping. This increase in use causes a considerable damage and fraud cases also. It is very much necessary to stop the fraud transactions because it impacts on financial conditions over time the anomaly detection is having some important application to detect the fraud detection. This algorithm detects the frauds very quickly resulting in the reduction of loss and risks.

### 3. Methodology

**3.1. Dataset Description.** The datasets consist of card purchases made by European cardholders in September 2013. This dataset describes transactions that happened in 2 days, specifically where 492 frauds beyond 284,807 transactions. The dataset is highly unbalanced; most transactions account for 0.172 per cent of the beneficial group (frauds). Figure 1 depicts the neural network architecture. The proposed framework is represented in Figure 2. Generalized block diagram is represented in Figure 3.

**3.2. Autoencoder.** AE is used to reduce input sizes to a smaller representation. They will recreate it from the compressed data if someone wants the original data. Having a similar algorithm in machine learning, i.e., PCA, performs the same task. AE is a class of unmonitored networks consisting of two main networks: Encoders and Decoders. The standard Autoencoder working can be seen in Figure 4. An AE neural network is an unsupervised learning algorithm which applies back propagation and sets target values equal to the inputs; i.e., they are using  $B(i) = A(i)$ . Simply put, an AE is made up of two parts, an encoder and a decoder. Taking into account, a data model  $A$  with samples and  $f$  attributes, the encoder output  $B$  represents a reduced representation of  $A$ , and the decoder is optimized to recreate the original dataset  $A$  from the representation  $B$  of the encoder by minimizing the gap between  $A$  and  $A_0$ . The encoder is simply a function  $f$ , which maps an input  $A$  to hidden representation  $B$ . The method is set out as [12].

$$B = f(A) = a_f(W_m A + b_x), \quad (1)$$

where  $a_f$  is a nonlinear activation function and the AE must do linear projection if it is an identity function. The encoder is parameterized by a  $W_m$  matrix of weight and a bias vector by  $b \in R^n$ .

The decoder function  $d$  maps hidden representation  $B$  back to a reconstruction  $A'$  as follows:

$$A' = d(B) = a_d(W'_m B + b_y), \quad (2)$$

where  $a_d$  is the activation function of the decoder, either the identity (rendering linear reconstruction) or a sigmoid is usually used. Parameters of the decoder are by and matrix  $W'_m$  a bias vector. In this paper, we explore only the case of bound weights where  $W'_m = W_m^T$ . Training an AE involves finding parameters like  $\Theta = (W_m, b_x, b_y)$  which minimize the loss of reconstruction on the given dataset  $X$  and the objective

$$\Theta = \min_{\Theta} L(A, A') = \min_{\Theta} L(A, d(f(A))). \quad (3)$$

For linear reconstruction, the reconstruction loss (L1) is

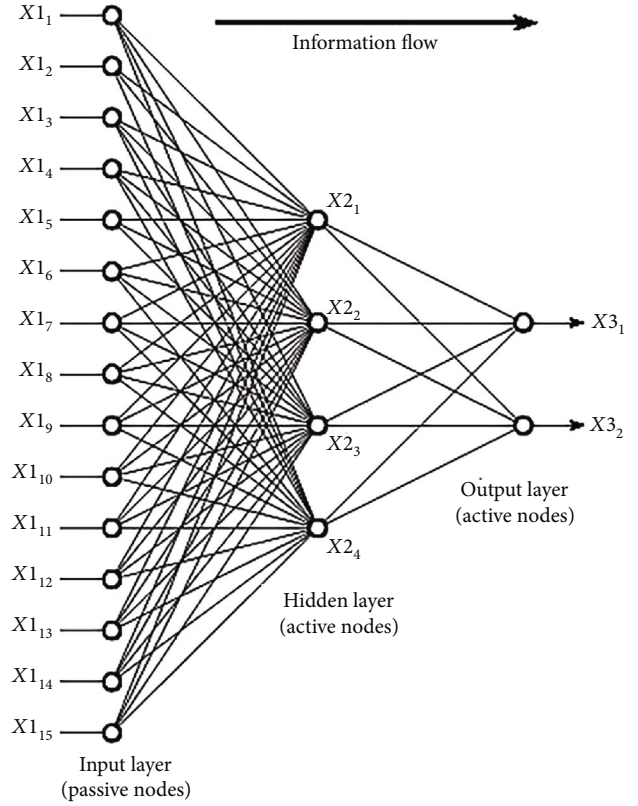


FIGURE 1: Neural network architecture [12].

generally from the squared error as follows:

$$L1(\Theta) = \sum_{i=1}^n \|a_i - a'_i\|^2 = \sum_{i=1}^n \|a_i - d(f(a_i))\|^2. \quad (4)$$

For nonlinear reconstruction, the reconstruction loss (L2) is generally from cross-entropy as follows:

$$L2(\Theta) = - \sum_{i=1}^n [a_i \log(b_i) + (1 - a_i) \log(1 - b_i)], \quad (5)$$

where  $a_i \in A$ ,  $a'_i \in A'$ , and  $b_i \in B$ .

Apache Spark3 is a streaming-enabled Map-Reduce implementation that distributes the computation automatically among the allocated resources and aggregates the results on a distributed file system. Spark offers both a deep and machine learning database and a streaming database. A strong point for Spark is its ability in the same framework to enable batch and stream analyses. The proposed framework is focused on Spark Streaming which processes data streams in minilots that trail the order of the latency of the second. Although this may be considered a downside in some streaming contexts, it is harmless in quasi-real-time setting. The Spark module of the system is written in Scala, a language that blends functional programming with object-oriented one. Scala runs atop Java VM and is fully compliant with the Java libraries. Overall, in the process, Spark fulfills two tasks: aggregating

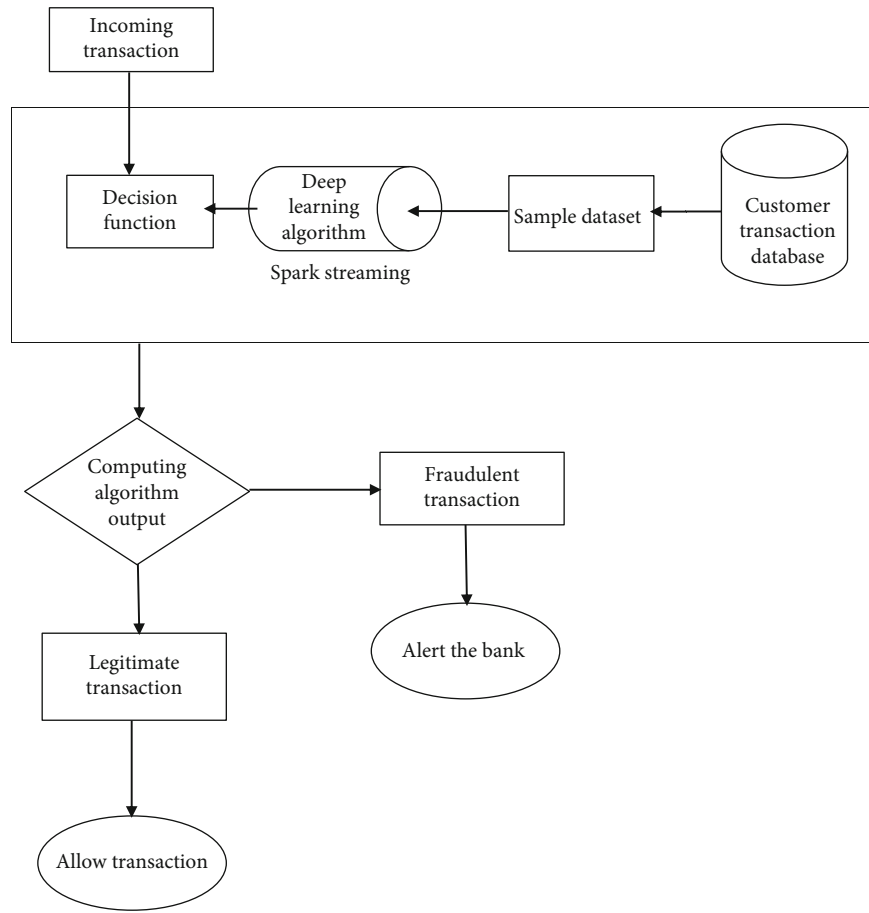


FIGURE 2: System flow.

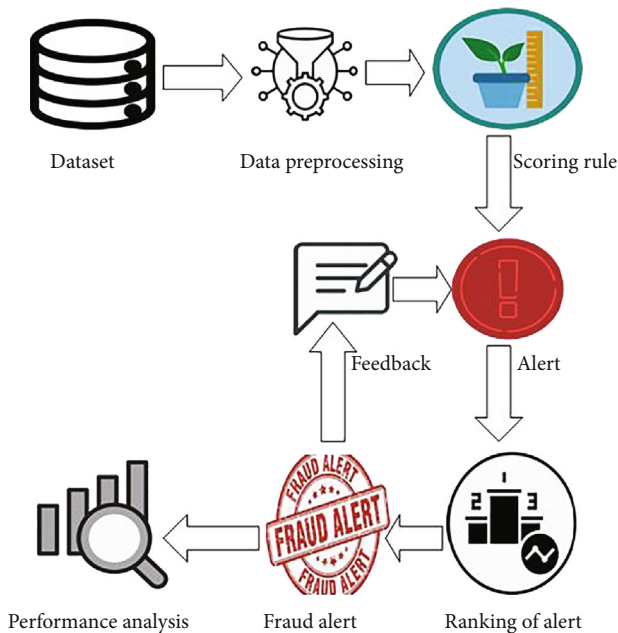


FIGURE 3: Proposed system block diagram.

historical transactions to perform design engineering and classifying transactions online that return the estimated risk of fraud.

**3.3. Random Forest (RF) Algorithm.** RF is a supervised learning algorithm, which can be used in addition to regression for both groups. But it is mainly used for classification issues. Because a forest is made up of more plants and leaves, it means a much better forest. Likewise, the RF algorithm selects trees on knowledge samples and then collects the prediction from all of them and eventually selects the optimal alternative by voting. It is an ensemble strategy that is much better than an individual choice tree because by averaging the end result it reduces the over fit.

The following is the implementation of random forest in scikit learn:

- (i)  $node_j$  = importance of node  $j$
- (ii)  $weight_j$  = weightage no. of sample reaching node $_j$
- (iii)  $C_j$  = impurity of node $_j$
- (iv)  $left_j$  = child node from left split on node $_j$
- (v)  $right_j$  = child node from right split on node $_j$



```

1: procedure AE( $T_E, B_S, a, D_S, L_R, \Theta$ ):
2:  $a = [a_1, a_2, \dots, a_j] \in R^{i \times j}$  is the input matrix, in which  $a_n \in [0, 1]^j$  ( $1 \leq n \leq j$ ) is a single input data
3:  $T_E = \text{training\_epochs} = 10$ 
4:  $B_S = \text{batch\_size} = 256$ 
5:  $D_S = \text{display\_step} = 1$ 
6:  $L_R = \text{learning\_rate} = 0.01$ 
7:  $\Theta = (W_m, b_x, b_y)$ , where  $\Theta$  is the parameter of AE
8: for 0 to  $T_E$  do
9:   for 0 to  $B_S$  do
10:     $f(A) = a_f(W_m A + b_x)$ 
11:     $d(B) = a_d(W'_m B + b_y)$ 
12:     $L1(\Theta) = \sum_{i=1}^n \|a_i - d(f(a_i))\|^2$ 
13:     $L2(\Theta) = -\sum_{i=1}^n [a_i \log(b_i) + (1 - a_i) \log(1 - b_i)]$ 
14:     $\Theta = \min_{\Theta} L(A, A')$ 
15:     $C = \text{compute the cost with respect to } \Theta$ 
16:    for  $\Theta_n, C_n$  in  $(\Theta, C)$  do
17:       $\Theta_n = \Theta_n - L_R * C_n$ 
18:    end for
19:  end for
20: end for
21: end procedure

```

ALGORITHM 1

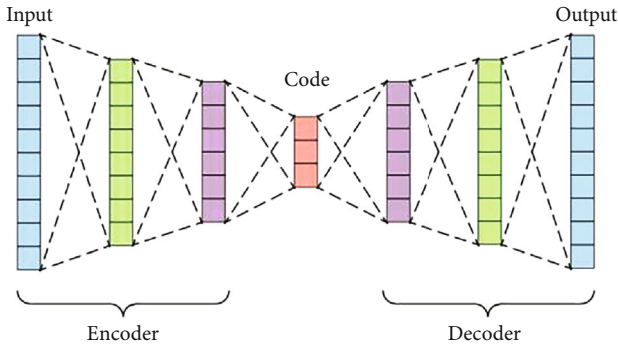


FIGURE 4: AE architecture [13].

$$\text{node}_j = \text{weight}_j C_j - \text{weight}_{\text{left}(j)} C_{\text{left}(j)} - \text{weight}_{\text{right}(j)} C_{\text{right}(j)}, \quad (6)$$

(vi)  $f_i$  = importance of feature  $i$

(vii)  $\text{node}_k$  = importance of node  $j$

$$f_i = \frac{\sum_{j: \text{node } j \text{ split on feature } i} \text{node}_j}{\sum_{k \in \text{all nodes}} \text{node}_k}, \quad (7)$$

(viii)  $\text{RF}f_i$  = importance of feature  $I$  calculated from all trees in the random forest model

(ix)  $\text{Norm}f_{ij}$  = normalized feature importance for  $I$  in tree  $j$

$$\text{norm}f_i = \frac{f_i}{\sum_{j \in \text{all features}} f_j}, \quad (8)$$

(x)  $T_{\text{all}}$  = total no. of trees

$$\text{RF}f_i = \frac{\sum_{j \in \text{all trees}} \text{norm}f_{ij}}{T_{\text{all}}}. \quad (9)$$

### 3.4. K-Nearest Neighbor

(i) *K*-nearest neighbor (KNN) algorithm is a kind of supervised ML algorithm that can be used for predictive problems in both categories and regression. Nevertheless, it is mainly used in industry for predictive classification issues. The next 2 attributes could well decide KNN [13]

(ii) *Lazy Mastering Algorithm*. *K*-nearest neighbor is a sluggish learning algorithm since it does not possess a special education phase and also requires all of the information for education while classification

(iii) *Nonparametric Mastering Algorithm*. KNN is additionally a nonparametric learning algorithm since it does not believe anything about the main information

Implementation of *K*-nearest neighbor (KNN) Algorithm.

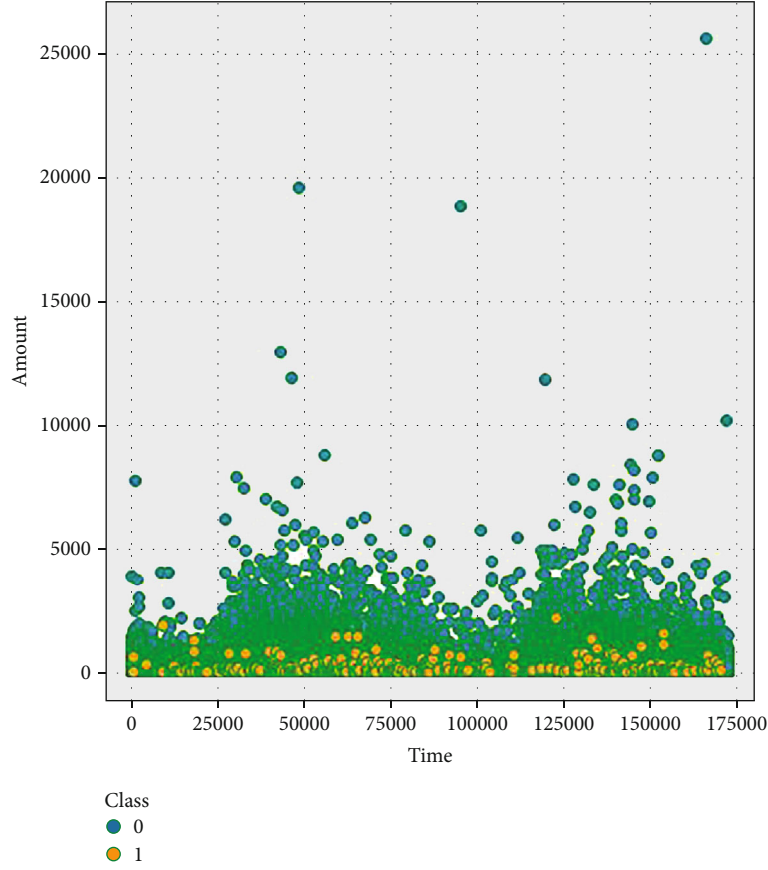


FIGURE 5: 2D scatter plot of distribution of all the cases.

We are able to know its working with the aid of pursuing steps:

*Step 1.* For applying some algorithm, we require dataset. So, throughout the initial stage of KNN, we should load the instruction and evaluation data.

*Step 2.* Next, we have to select the importance of  $K$ , i.e., probably the nearest data points.  $K$  could be any integer.

*Step 3.* For every stage within the test information do the following:

- (a) Measure the gap between the training specifics of each row and check with the help of the strategy: Euclidean, Manhattan, or even Hamming distance. The most often used method to compute distance is Euclidean

$$d(p, q) = \sqrt{\sum_{i=1}^n (p_i - q_i)^2}, \quad (10)$$

- (b) Now, dependent on the distance worth, sort them in ascending order

- (c) Next, the high  $K$  rows from the sorted array are to be chosen

- (d) Now, it is going to assign a course to the test stage based on many regular categories of these rows

*Step 4.* End.

*3.5. Decision Tree Algorithm.* The supervised learning algorithm contains decision tree. The general purpose of utilizing decision tree is creating a training type that will utilize to predict value or class of goal variables by mastering choice regulations inferred from prior data (training data). The comprehension amount of decision tree algorithm is very simple in contrast to some other group algorithms [14].

Implementation of Decision Tree Algorithm:

*3.5.1. Gini Index (GI).* It is the title of the price feature which is utilized to assess the binary splits in the dataset and also works together with the categorical target variable "Failure" or "Success." The higher the importance of GI, the higher will be the homogeneity. A great GI value is zero, and worst is 0.5 (for two class problem). Gini list for a split may be estimated with the aid of the following steps [14]:



FIGURE 6: Plot of all instances.

- (i) For starters, compute Gini index for subnodes by utilizing the system  $p^2 + q^2$  and that is the amount of the square of likelihood for failure and success
- (ii) Then, compute Gini list for split using weighted Gini rating of every node of that particular split

Classification and Regression Tree (CART) algorithm employs Gini technique to produce binary splits.

**3.5.2. Split Index.** A split is simply incorporating a characteristic in a value and the dataset. We are able to develop a split in dataset with the assistance of the following 3 parts:

- (i) *Calculating Gini Score.* We have simply talked about this particular component in the prior section
- (ii) *Splitting a Dataset.* It might be described as separating a dataset into 2 lists of rows keeping index of a characteristic along with a split worth of that feature. After getting the 2 groups, right and also remaining, from the dataset, we are able to compute the importance of split by utilizing Gini score calculated in original part. Split value is going to decide where the team the attribute will reside
- (iii) *Evaluating Almost All Splits.* Next component after finding Gini score as well as splitting dataset is

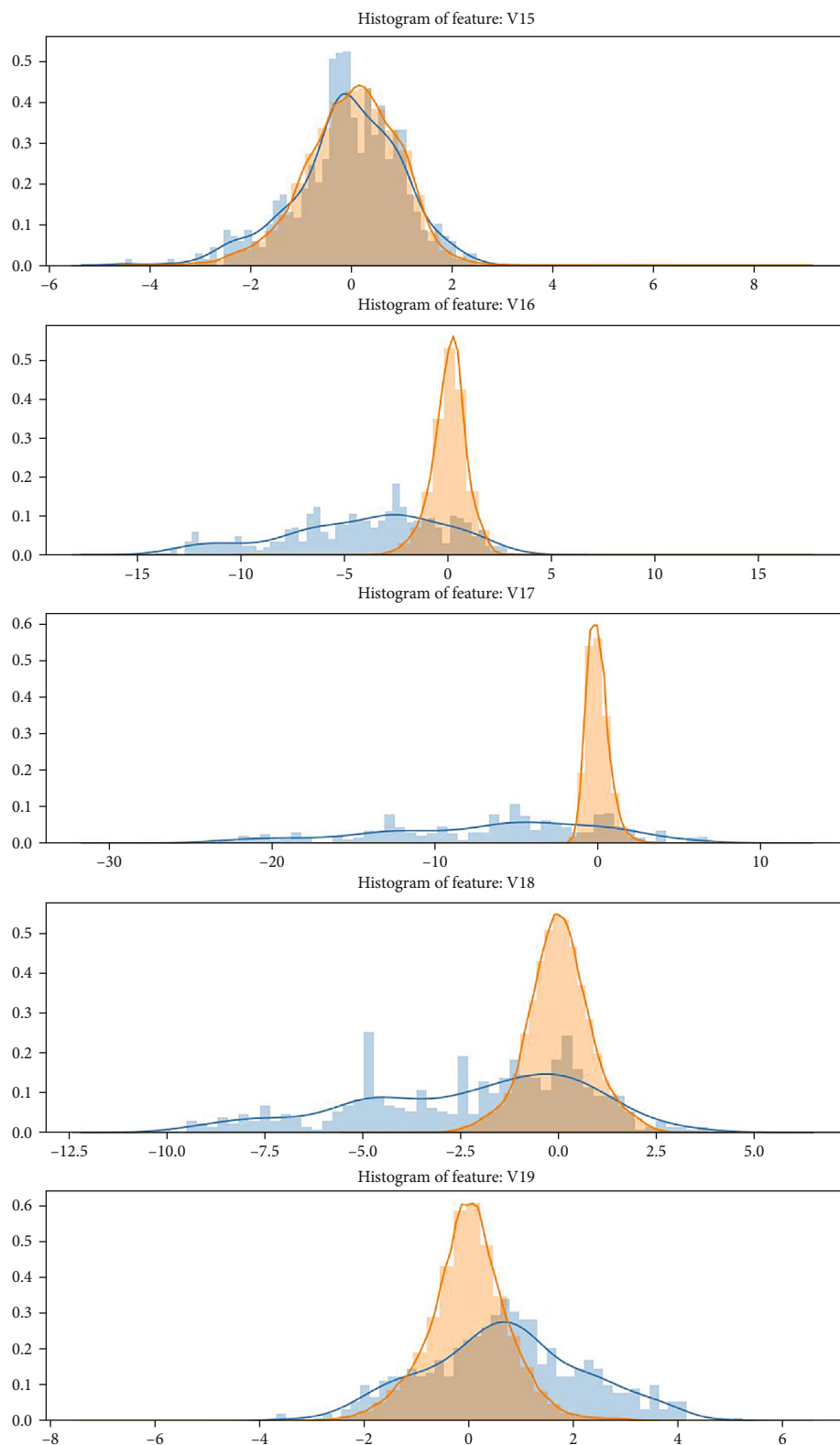


FIGURE 7: V15-V19 feature histogram.

definitely the analysis of all splits. For this particular purpose, for starters, we should examine each value connected to each feature as being a candidate split.

Next, we have to discover the absolute best split by analyzing the price of the split. The most effective split would be used as a node in the decision tree

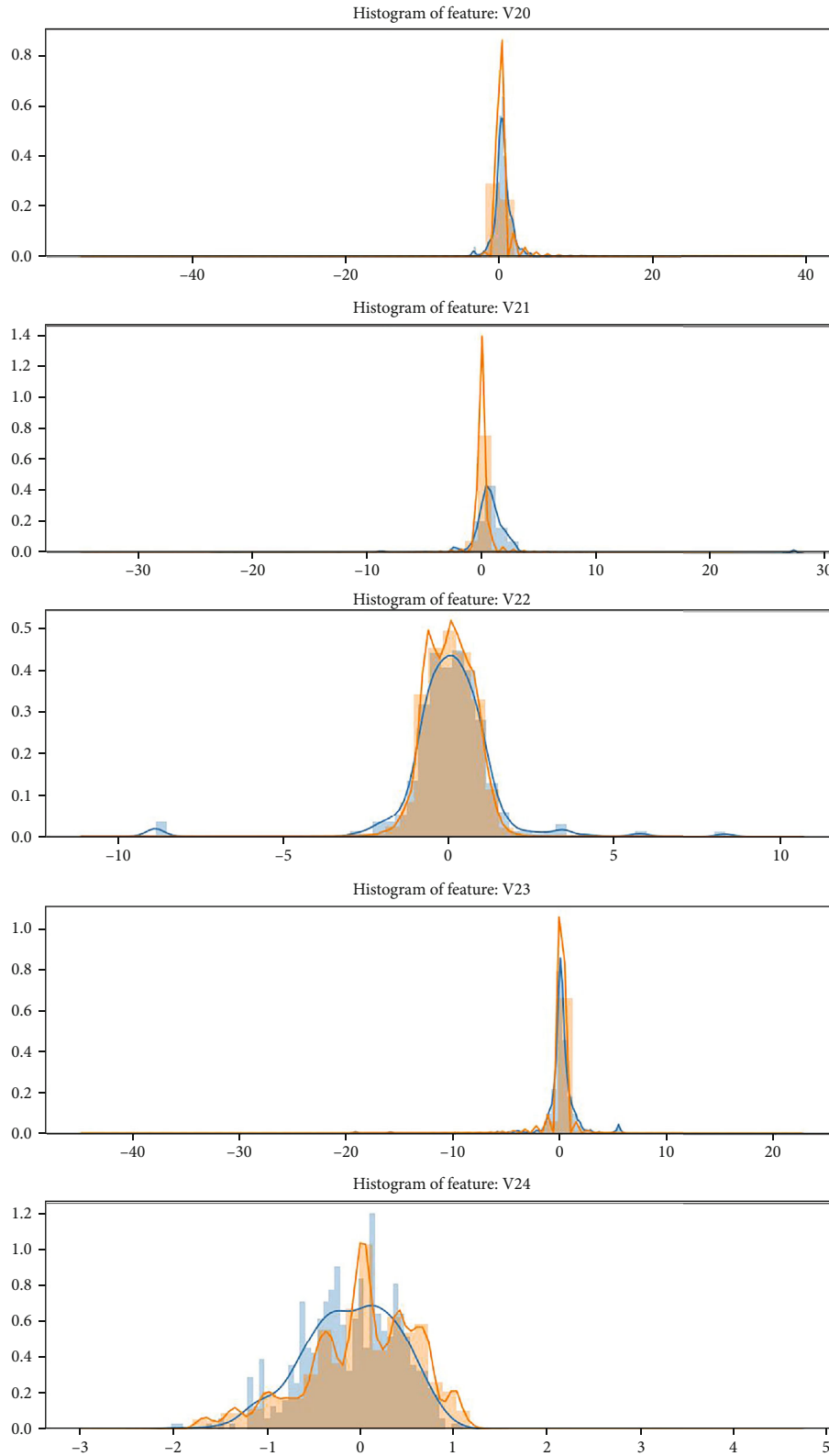


FIGURE 8: V20-V24 feature histogram.

3.6. *Logistic Regression (LR)*. LR is a supervised learning category algorithm used to predict the likelihood of an adjustable goal. The target dynamics, or maybe dependent

component, are dichotomous; meaning, there will be only 2 possible courses. In simple words, the dependent element is binary in nature to get knowledge written as

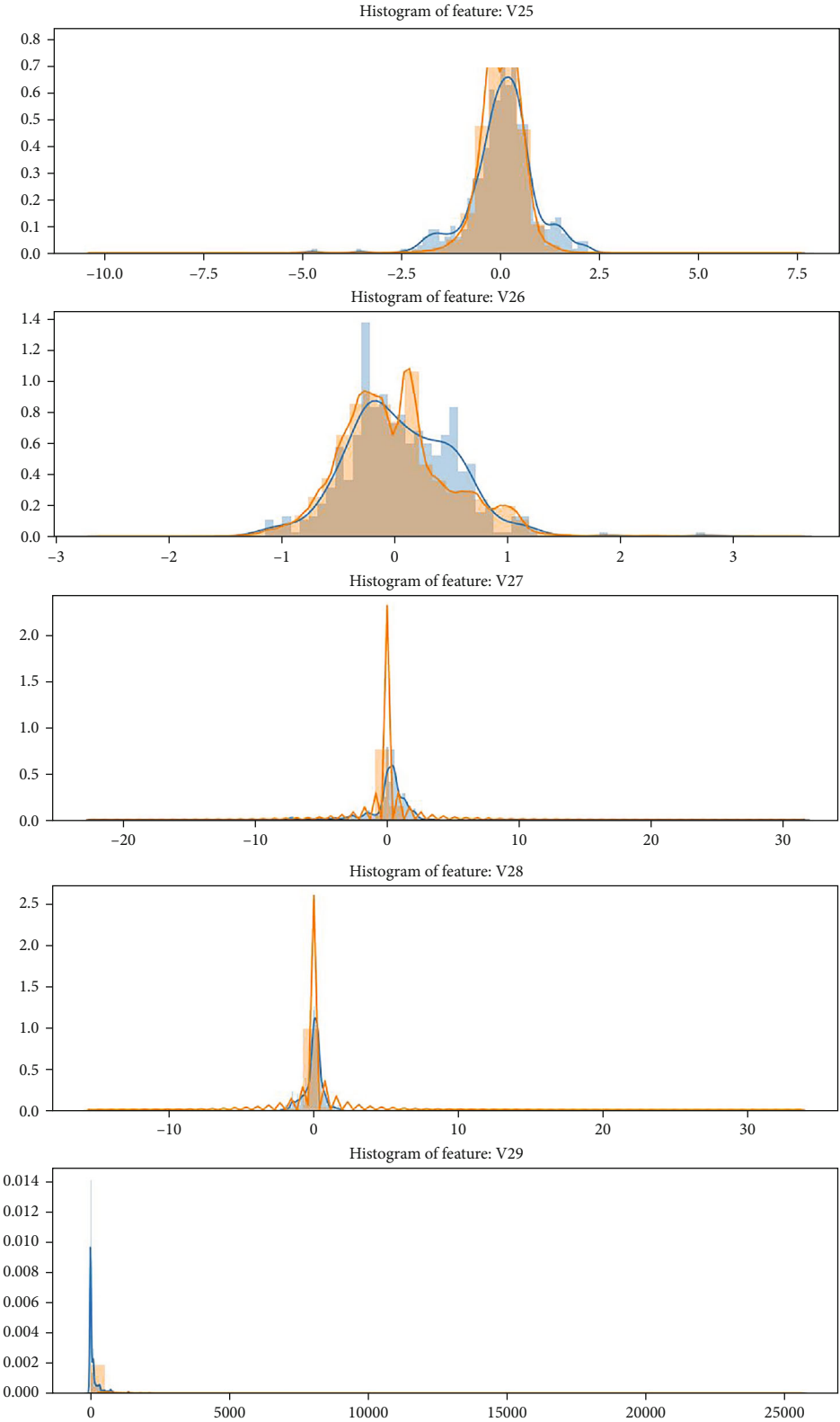


FIGURE 9: Amount and V25-V28 feature histogram.

theoretically one or even zero. Mathematically,  $P(Y = 1)$  is predicted as a characteristic of  $X$  by an LR algorithm. It is among the simplest ML algorithms that could be used to detect spam, cancer detection, diabetes prediction, etc., for various classification complications [14].

*3.6.1. Types of LR.* In general, LR suggests binary LR owning binary goal variables, but there could be 2 more types of target variables which may be predicted by it. Based upon those numbers of types, LR is split into the following types:

- (i) *Binomial.* In such a type of classification, a reliant variable is going to have just 2 possible kinds both one and zero
- (ii) *Multinomial.* In such a type of category, dependent variable should have three or maybe more potential unordered styles or even the kinds getting no quantitative significance
- (iii) *Ordinal.* In such a type of category, dependent variable should have three or maybe more feasible ordered styles or even the kinds with a quantitative significance

### 3.6.2. LR Assumptions

- (i) Before diving into the implementation of LR, we should be conscious of the coming assumptions about the same
- (ii) In case of binary logistic regression, the goal variables should be binary constantly, and the desired outcome is represented by the aspect level one
- (iii) Right now, there should not be some multicollinearity within the product; this means the independent variables should be outside of one another
- (iv) We need to have significant variables in the model of ours
- (v) We must select a big sample size for LR

*3.7. Support Vector Machine.* In 1960s, SVMs were first released, but eventually, they have enhanced in 1990. SVMs have the unique way of theirs of setup as compared to various other machine learning algorithms. Recently, they are incredibly well known due to their capability to deal with a couple of continuous and categorical variables [15].

*3.7.1. Working of SVM.* An SVM unit is simply a representation of various courses in a hyperplane in space that is multi-dimensional. The hyperplane would be created within an iterative fashion by Support Vector Machine; therefore, the mistake could be lessened. The objective of Support Vector Machine is dividing the datasets into martial arts classes to locate an optimum marginal hyperplane.

The following are important ideas in SVM:

TABLE 1: Machine learning comparison table on the basis of performance measures.

Classifiers	Accuracy %	Specificity %	Precision %	F1-score %
Random forest	96.2	98.7	99.7	92
Logistic regression	94.7	97.9	99.6	91.7
SVM	93.8	98.4	78.2	80.2
Decision tree	90.8	91.2	91	86
KNN	94.2	97.1	41.0	50.6

TABLE 2: Deep learning evaluation for training dataset.

Train data	Test data	Train instances	Train fraud cases	% of train fraud cases	Training accuracy	Time elapsed (sec)
90	10	256326	470	0.00183	0.959921	18.35
80	20	227845	417	0.00183	0.954843	17.36
70	30	199364	384	0.00193	0.957749	14.63
60	40	170884	360	0.00211	0.963300	12.54
50	50	142403	269	0.00189	0.953874	10.63

- (i) *Support Vectors.* Data points what are nearest to the hyperplane is called SVs. Separating line would be identified with the aid of these data points
- (ii) *Hyperplane.* It is a choice plane or maybe room that is split between a pair of items having various classes
- (iii) *Margin.* It might be described as the gap between 2 lines on the closet information points of various courses. It may be estimated as the perpendicular distance out of the series on the assistance vectors. Huge margin is viewed as an excellent margin, and tiny margin is as a terrible margin

The primary objective of SVM is dividing the datasets into classes which can be achieved inside the next 2 steps as follows:

- (i) First, SVM is going to generate hyperplanes iteratively that segregates the classes in most effective way
- (ii) Next, it is going to choose the hyperplane which separates the classes properly

## 4. Experiment and Result Analysis

Several machine learning algorithms are analyzed for the performance measures in the credit card fraud detection dataset. Along with this, deep Autoencoder is implemented using various training and testing split ratio. Majorly five core machine learning algorithms, namely, RF, LR, KNN, DT, and SVM algorithm, are implemented. From Figure 5, it is clearly visible that there are frauds only on the transactions which have transaction amount approximately less than 2500. Transactions which have transaction amount approximately above 2500 have no fraud. As per with the time, the

TABLE 3: Deep learning evaluation for testing dataset.

Train data	Test data	Test instances	Test fraud cases	% of test fraud cases	Testing accuracy	Time elapsed (sec)
90	10	28481	22	0.00077	0.923378	00.07
80	20	56962	75	0.00132	0.949008	00.13
70	30	85443	108	0.00126	0.939815	00.23
60	40	113923	132	0.00116	0.944843	00.32
50	50	142404	223	0.00157	0.965315	00.38

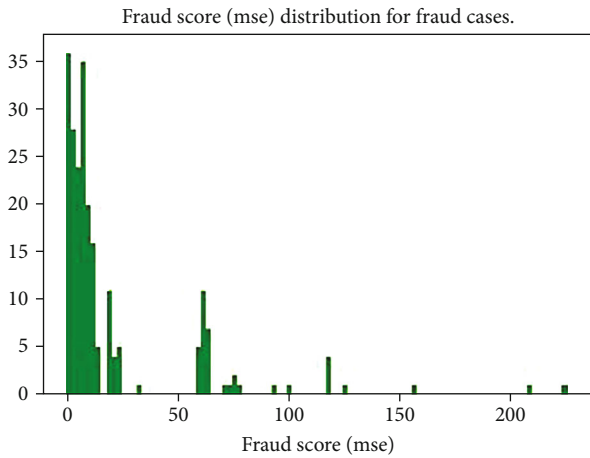


FIGURE 10: Fraud score distribution for 50-50 split ratio.

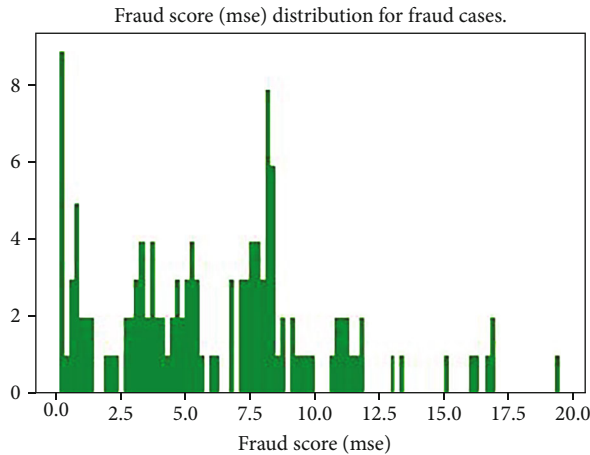


FIGURE 11: Fraud score distribution for 60-40 split ratio.

frauds in the transactions are evenly distributed throughout time. Amount and time distribution can be seen in Figure 6. Feature distribution from 15 to 30 is depicted in Figures 7–9, respectively. Table 2 narrates the obtained machine learning results. Tables 2 and 3 provide the result obtained by using Deep AE with various training and testing split ratio. Figures 10 and 11 depict fraud score distribution for 50-50 and 60-40 split ratio, respectively. Accuracy, precision, and specificity for all machine learning algorithms are

calculated as follows which is shown in Table 1:

$$\begin{aligned}
 TP = X, TN = Y, FP = P, FN = Q, \\
 Accuracy &= \frac{X + Y}{X + Y + P + Q}, \\
 Precision &= \frac{X}{X + P}, \\
 Specificity &= \frac{Y}{Y + P}, \\
 F1 \text{ Score} &= \frac{2 * (Precision * Recall)}{Precision + Recall}.
 \end{aligned} \tag{11}$$

## 5. Conclusion

As in today's era of technology, especially in the Internet commerce and banking, the transactions by the Mastercards have been increasing rapidly. The Mastercard becomes the highly useable equipment for Internet shopping. This increase in use causes a considerable damage and enhances inflation rate of fraud cases also. It is very much necessary to stop the fraud transactions because it impacts on financial conditions over time the anomaly detection is having some important application to detect the fraud detection. This paper has reviewed several algorithms to identify fraud in card transaction. Autoencoder is used to classify the alert as fraudulent or even authorized in spark environment. Next, it will aggregate every probability to discover alerts. Further, proposed model utilizes ranking approach where alert is positioned based on priority. The model is able to resolve the class imbalance. In today's era, we just detect the fraudulent transaction, but we are not able to prevent it. Preventing fraud transaction dynamically is not easy, but it is possible. The system which proposed is design to detect fraud transaction, but in future by some advancement, it can became fraud prevention system.

## Data Availability

The data shall be made available on request.

## Conflicts of Interest

The authors declare that they have no conflicts of interest.

## References

- [1] O. Altit, "Credit card fraud detection based on machine and deep learning," in *2020 11th International Conference on Information and Communication Systems (ICICS)*, pp. 204–208, Irbid, Jordan, 2020.
- [2] S. Makki, Z. Assaghir, Y. Taher, R. Haque, M. S. Hacid, and H. Zeineddine, "An experimental study with imbalanced classification approaches for credit card fraud detection," *IEEE Access*, vol. 7, pp. 93010–93022, 2019.
- [3] S. Ounacer, H. A. El Bour, Y. Oubrahim, M. Y. Ghomari, and M. Azzouazi, "Using Isolation Forest in anomaly detection: the case of credit card transactions," *Periodicals of Engineering & Natural Sciences*, vol. 6, no. 2, pp. 394–400, 2018.



- [4] I. Benchaji, S. Douzi, and B. El Ouahidi, "Using genetic algorithm to improve classification of imbalanced datasets for credit card fraud detection," *Lecture Notes in Networks & Systems*, vol. 66, pp. 220–229, 2019.
- [5] A. Dal Pozzolo, G. Boracchi, O. Caelen, C. Alippi, and G. Bontempi, "Credit card fraud detection: a realistic modeling & a novel learning strategy," *IEEE Transactions on Neural Networks & Learning Systems*, vol. 29, no. 8, pp. 3784–3797, 2018.
- [6] L. Zheng, G. Liu, C. Yan, and C. Jiang, "Transaction fraud detection based on total order relation & behavior diversity," *IEEE Transactions on Computational Social Systems*, vol. 5, no. 3, pp. 796–806, 2018.
- [7] S. Venkata Suryanarayana, G. N. Balaji, and G. Venkateswara Rao, "Machine learning approaches for credit card fraud detection," *International Journal of Engineering & Technology (UAE)*, vol. 7, no. 2, pp. 917–920, 2018.
- [8] A. Thennakoon, C. Bhagyani, S. Premadasa, S. Mihiranga, and N. Kuruwitaarachchi, "Real-time credit card fraud detection using machine learning," in *Proceedings of the 9th International Conference on Cloud Computing, Data Science & Engineering*, vol. 7no. 10, pp. 488–493, Noida, India, 2019.
- [9] H. A. Shukur and S. Kurnaz, "Credit card fraud detection using machine learning methodology," *International Journal of Computer Science and Mobile Computing*, vol. 8, no. 3, pp. 257–260, 2019.
- [10] H. John and S. Naaz, "Credit card fraud detection using local outlier factor & isolation forest," *International Journal of Computer Sciences and Engineering*, vol. 7, no. 4, pp. 1060–1064, 2019.
- [11] W. F. Yu and N. Wang, "Research on credit card fraud detection model based on distance sum," in *IJCAI international joint conference on artificial intelligence*, pp. 353–356, Hainan, China, 2009.
- [12] <https://towardsdatascience.com/logistic-regression-detailed-overview-46c4da4303bc>.
- [13] "Autoencoders tutorial : a beginner's guide to autoencoders," <https://www.edureka.co/blog/autoencoders-tutorial/>.
- [14] Q. Meng, D. Catchpoole, D. Skillicom, and P. J. Kennedy, "Relational autoencoder for feature extraction," in *2017 International Joint Conference on Neural Networks (IJCNN)*, pp. 364–371, Anchorage, AK, 2017.
- [15] F. Carcillo, A. D. Pozzolo, Y. L. Borgne, O. Caelen, Y. Mazzer, and G. Bontempi, "SCARFF: a scalable framework for streaming credit card fraud detection with spark," *Information Fusion*, vol. 41, pp. 182–194, 2018.

## Research Article

# Hierarchical Coordinated Control Method for Multiload DC Microgrid Units

Zhigang Zhang<sup>1</sup> and Jinping Mo<sup>2</sup>

<sup>1</sup>College of Management Science and Engineering, Guangxi University of Finance and Economics, Nanning 530003, China

<sup>2</sup>Ministry of Modern Educational Technology, Guangxi University of Finance and Economics, Nanning 530003, China

Correspondence should be addressed to Jinping Mo; mojinping8456@163.com

Received 24 June 2021; Revised 17 July 2021; Accepted 22 July 2021; Published 10 August 2021

Academic Editor: Vimal Shanmuganathan

Copyright © 2021 Zhigang Zhang and Jinping Mo. This is an open access article distributed under the Creative Commons Attribution License, which permits unrestricted use, distribution, and reproduction in any medium, provided the original work is properly cited.

Electricity has become not merely a source of power but also a vital component of our lives in a rapidly changing world. However, according to a World Bank report, 17% of the globe's population live without power. The key cause for such a huge population not being electrified is the proximity of the central electrical grid system or the high expenditure of installing the grid lines to such remote areas. The notion of a microgrid was first proposed more than a decade ago, but the numerous obstacles it entails have hampered its broad adoption and made it a research focus in recent years. A hierarchical control structure of the microgrid is designed, which is divided into layers according to the control objectives and control time scales of the microgrid, and the hierarchical control structure is realized by using multiagent technology. In the framework of hierarchical control, aiming at the demand of energy coordination and optimization of the microgrid, the operation strategy of the microgrid is proposed in grid-connected and/or off-grid mode. In the grid-connected mode, the large power grid is used for power supply and in the off-grid mode, the load bidding mechanism is introduced to ensure the power supply of important loads. Experiment results reveal the power quality and stability of the system.

## 1. Introduction

Due to the increasingly serious problems of power crisis and environmental issues, grid-connected power generation method by using renewable energy has become one of the imperative methods for generation of electricity [1]. The output power and the single access to distributed generation (DG) units have the limitations of high cost, small capacity, flexibility, and controllability. Therefore, in order to use multiload DC microgrids and to realize the benefits of DG units, it is important to assimilate the microgrid into the main network [2]. At present, microgrid structure mainly includes AC microgrid, DC microgrid, and hybrid microgrid. Previous research mainly focused on AC microgrid. However, with the continuous increase of DC load, DC microgrid has the benefits of less energy conversion times, cheap cost, great efficiency, and modest control structure which promotes the rapid development of DC microgrid [3–5].

DC microgrid comprises distributed generation, energy storage units, load units, and grid-connected interface converters [6]. In order to manage energy flow and coordinate the controls among the diverse units, the development of DC microgrid requires immense caution while designing the DC microgrid. To solve this problem, the researchers have proposed effective control strategies and made a lot of contributions. Meng et al. [7] proposed an energy management approach for isolated operation of DC microgrid based on wind turbine and super capacitor energy storage. The four PI controllers of energy storage system can effectively control the situation of excess energy, insufficient energy, excessive discharge of battery, and charging, respectively. Most of the traditional control methods are based on the hierarchical control strategy of DBS.

*1.1. Related Work.* Due to the considerable benefits of DC microgrids over AC microgrids and their versatile uses,

researchers and academicians are attempting to research upon DC microgrids to cut down production costs and for optimizing the usage of renewable energy.

Prajof et al. [1] have introduced three innovative nonlinear smart grid-control techniques to enhance the accuracy of load sharing between connected voltage sources, as well as to improve the regulation of DC bus voltage. The experimental data proves the efficacy of the proposed control mechanisms. Performance analysis is presented under various operating situations, of the three droop control strategies along with their advantages over conventional methods. Hamed et al. [2] have presented the optimum fuel cell (FC) and combined heat power- (CHP-) based microgrid (MG) transmission in a grid-connected mode with the inclusion of a demand response program (DRP). The proposed technique reduces the number of effective solutions to a more manageable amount compared to the ways that are currently utilized without requiring any information on the policy criteria. Keshta et al. [3] have proposed a multiagent system (MAS) to accomplish optimal energy management for voltage control and to improve system stability under various weather conditions and load disturbances for two connected microgrids. The simulation results demonstrate a high degree of efficiency in the proposed energy management system.

Martin-Ramos et al. [6] have proposed a hardware-in-the-loop (HIL) simulation system, a new mechanism for developing and testing control algorithms for DC microgrids. The platform is built on the basis of universal acceptance and adaptability. Meng et al. [7] have demonstrated how to configure and communicate with the HIL simulation system. Finally, simulation tests are performed to demonstrate that the suggested HIL simulation platform is valid. Kou et al. [8] have introduced a novel distributed load share control technique in a stable and optimum DC microgrid among many permanent magnet synchronous generators (PMSGs). The primary feature of this technique is that the rotor kinetic energy and generation ranges in the controller design are not only efficient for load sharing but also capable to maintain the steady functioning of all PMSGs. Dam and Lee [9] have proposed a new power distribution control mechanism for a DC microgrid. This technique restores the DC bus voltage when the load changes and spreads the load power proportionately to the distributed power source ratings. To do this efficiently, a shifted voltage method is developed based on the power rating and instantaneous power of dispersed generators. To validate the method's efficacy, simulations and experiments have been carried out utilizing a 2.8kW DC microgrid prototype.

Yousefizadeh et al. [10] have created an adaptive backstepping controller for a DC MG feeding nonideal CPLs, which is coupled to a 3rd-degree cubature Kalman filter (CKF). The results of the experiments reveal that the proposed adaptive controller is successful and stable. Islam et al. [11] have shown a coordinated control structure, centralized as well as distributed, which allows more flexibility in system design and better supervisory control. There are various control choices in a hierarchical approach for each level, including DC signals, droop control, and fuzzy control, for primary and secondary control such as centralized,

decentralized, and distributed control. For tertiary control, genetic algorithm (GA), particle swarm algorithms, and consensus algorithms are used. Each of these control systems has its own set of advantages and disadvantages.

There is still a scope for further improvements in the methods for DC microgrids on the basis of renewable energy and hence, we are proposing a new framework in this paper.

*1.2. Contributions of the Paper.* This paper presents a hierarchical coordinated control method for multiload DC microgrid units. Compared with the existing research methods, the main contributions and characteristics of the proposed method are as shown:

- (A) The control switching conditions of each unit are determined by DC bus voltage variation, grid-connected converter current, battery SOC, and current. The above variables are local control information and do not need communication technology
- (B) In grid-oriented operation, converter current limiting, and islanding process modes, the converters controlling DC bus voltage adopt PI control to ensure zero steady-state error regulation of DC bus voltage, which effectively avoids the instability of constant power load when DC bus voltage deviates from the ideal reference value
- (C) When the system functions in island mode and the load power is less than the DG output power, an open-loop pitch angle control method is suggested to participate in DC voltage coordinated control, which cannot achieve constant power operation above rated power but also can realize constant voltage control of fan under rated power to eliminate the fluctuation of DC bus voltage
- (D) The control configuration of the suggested method in this paper is simple, is convenient to device, and can improve the power quality and stability of the system

The paper is arranged into five sections:

- (a) Introduction with background study, literature review, and contributions of the suggested work in this paper
- (b) The proposed method is elaborated in the second section of this paper
- (c) Energy coordination model of the microgrid is discussed in the third section
- (d) Results are discussed in the fourth section
- (e) Conclusion is given in the last section

## 2. Proposed Method

*2.1. Hierarchical Control Structure of Microgrid Energy Management.* In order to coordinate the micropower generation, arrange the charging and discharging of energy storage, manage the controllable load, and maintain the system

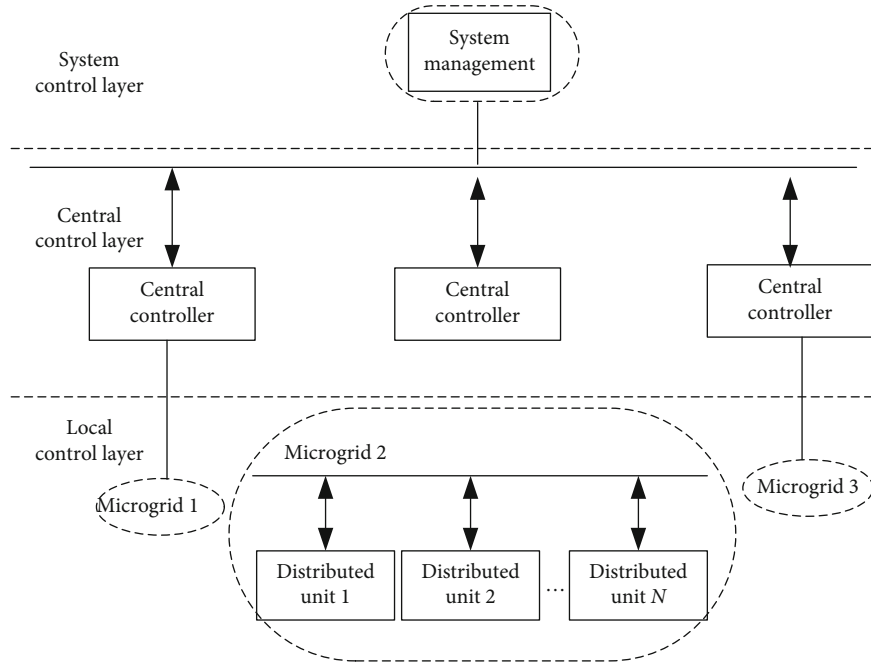


FIGURE 1: System hierarchical structure diagram.

stability, it is often necessary to introduce the microgrid energy management system [12]. In this paper, the hierarchical control method is used to stratify the microgrid system from the functional level. Each layer of control system independently completes the control objectives, and each layer of information sharing jointly achieves the control and optimization objectives of the microgrid energy management system.

As shown in Figure 1, the first layer is the local control layer, which is the primary control layer of the microgrid which comprises local devices. The local layer is responsible for the real-time control of each micropower source to ensure the power balance in the microgrid structure and the voltage and frequency stability on the bus. The voltage instability of DC bus in islanded operation mode can be intervened and controlled by this layer to reduce the interference of circulating current and maintain the power balance of DC microgrid as far as possible. In each distributed unit, the converter is configured to control the DC bus voltage stability and provide high-quality power for users.

The second layer is the central control layer. As per the current functionality of the microgrid, such as the frequency and voltage on the bus, the ultra-short-term prediction results of natural resources and loads, and the operation plan from the system layer [13], the active as well as reactive power output of the local distributed generation is adjusted in real time to ensure the stability in the operation of the microgrid. All at once, when the large grid or microgrid itself fails, it can quickly switch the system operation mode and achieve a stable transition process.

The third layer is based on the top layer of hierarchical control, that is, the system layer of energy management. Its function is to control the whole microgrid from the perspective of the overall operation of the distribution system. The

energy management system can forecast the changes of natural resources and user load in the next 24 hours and submit an operation plan of each microelectricity supply in microgrid according to the demand change of power market, so that users can participate in the market competition of the microgrid at the lowest cost and benefit from it.

*2.2. Multiagent Implementation of Hierarchical Control.* The local control layer may contain multiple generation agents, energy storage agents, and load agents; the central control layer contains energy ultra-short-term forecasting agent and real-time control agent; and the system control layer contains energy short-term prediction agent and economic dispatch agent. In addition, there are also SCDA agents (service control and data acquisition agent) which are used to monitor the real-time operation status information of the microgrid micropower supply and ensure the communication function between agents at all levels. The functional principles of each agent are as shown in Figure 2.

### 3. Energy Coordination Model of the Microgrid

The energy optimization of the second and third scheduling layers is modeled and analyzed. In order to achieve this, the particle swarm optimization (PSO) is deployed in our model.

*3.1. Secondary Scheduling Optimization Model.* In this paper, the secondary dispatch of the microgrid is aimed at coordinating the output power of each micropower source in the microgrid system based on the radical short-term prediction of wind energy, light energy, and load, so as to achieve the control objective of peak load shifting and valley filling [14]. Figure 3 is the information flow diagram of real-time dispatching agent. The real-time operation status of the

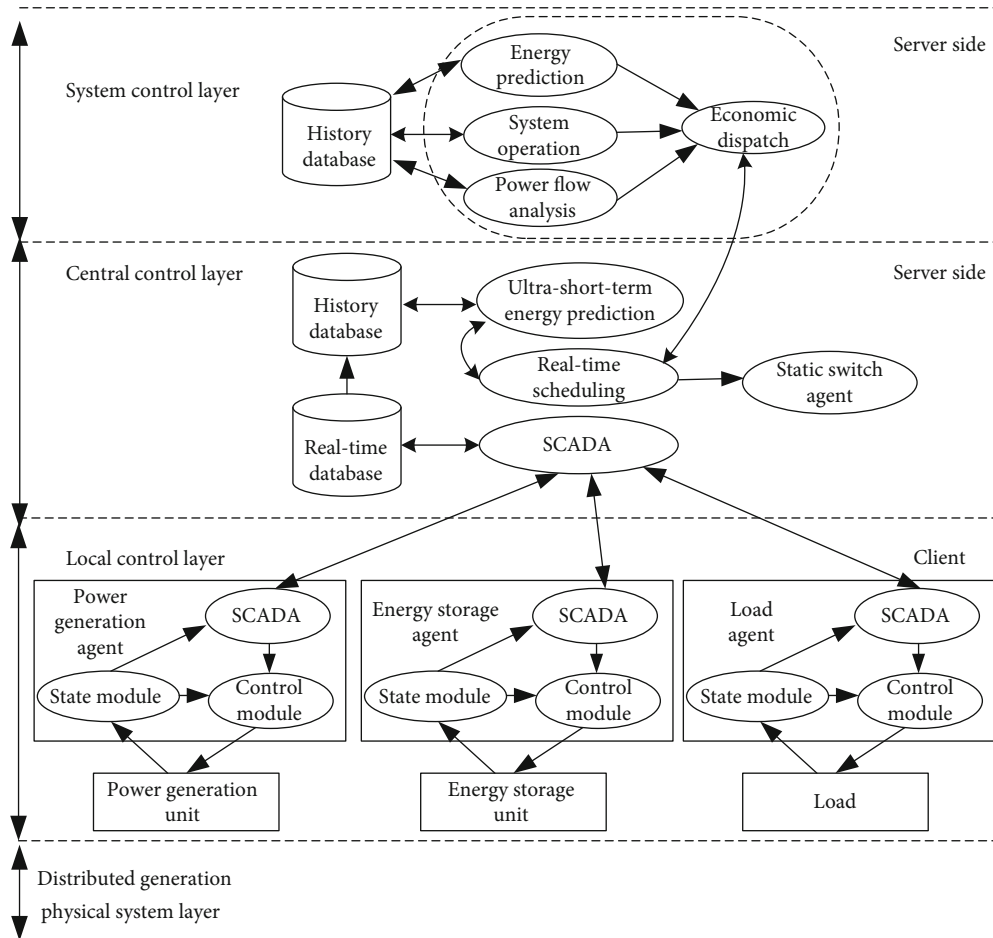


FIGURE 2: Multiagent hierarchical control structure.

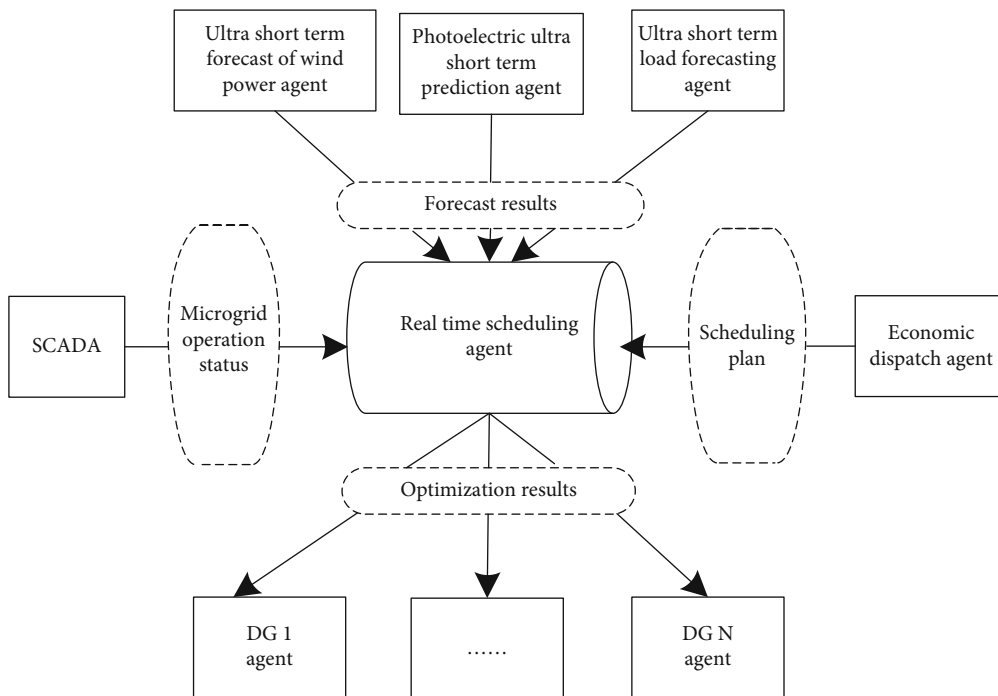


FIGURE 3: Information flow of real-time scheduling agent.

microgrid is obtained from SCADA; the prediction results of next time are obtained from radical short-term forecasting agent of wind power, photoelectric, and load; and the operation plan is obtained from economic dispatch agent. According to the current operation mode of the microgrid, the corresponding operation strategy is selected to optimize the operation state of the microgrid.

### 3.1.1. Energy Optimization Model for Connected Grid Mode.

While the microgrid is under the grid-connected mode, the mathematical model is established according to the operation strategy of peak shaving and valley filling. According to the peak and valley period and battery SOC state, different battery charging and discharging penalty numbers are determined as the operation cost of the battery. At the same time, the economic benefit, environmental treatment cost, plus reactive power production cost of the microgrid are comprehensively considered, and the energy optimization is carried out under the operation constraints of each micro-power source in the microgrid.

(1) *Objective Function.* The objective function under grid-connected mode includes the cost of power generation and operation, the cost of environmental governance, the cost of exchanging power with power grid, and the cost of reactive power production which is mentioned in the following equation:

$$F = \lambda_1 C_o + \lambda_2 C_e + \lambda_3 C_g + \lambda_4 C_r, \quad (1)$$

where  $C_o$  is the functional plus maintenance cost of the microgrid system; that is, the fuel consumption, equipment maintenance, active and reactive power grid loss, and battery charging and discharging penalty costs may be included in the operation of the microgrid system;  $C_e$  is the cost of pollutant emission treatment of the microgrid, that is, the treatment cost of carbon dioxide or other toxic gases generated due to fuel consumption during the operation of the microgrid; and  $C_g$  is when the microgrid is coupled with the grid, the cost of power conversation with the grid should be negative when the microgrid delivers more power to the grid, otherwise it is positive;  $C_r$  is the cost of reactive power production.  $\lambda_1$ ,  $\lambda_2$ ,  $\lambda_3$ , and  $\lambda_4$  are the weight proportion of the above four costs in the objective function. For attaining the purpose of economic operation of the microgrid, the value of objective function should be minimised. The different weight proportion settings will affect the optimization of objective function. Therefore, it is necessary to set the weight proportion reasonably and balance the proportion of each item.

The expression of each component of the objective function is as shown:

#### (A) System operation and maintenance cost $C_o$

In this paper, the functional plus maintenance cost of the microgrid system is defined as fuel cost, equipment maintenance cost, active and reactive power loss cost, and battery

charging and discharging penalty cost as shown in the following equation:

$$C_o = \sum_{k=1}^n (C_{\text{firel},k} + C_{\text{om},k}) + C_{\text{loss}} + C_{\text{bat}}, \quad (2)$$

where  $n$  represents the number of distributed generation units in the microgrid system;  $C_{\text{firel},k}$  is the fuel cost of the  $k$ th distributed unit. The renewable energy generation unit has no fuel cost; only the microfuel turbine and fuel cell are considered. The characteristics of fuel cost and output power have been analyzed in chapter 2;  $k$  is the equipment maintenance cost of the  $k$ th distributed unit, which mainly includes the start-up and shutdown cost of equipment and the labor cost of equipment maintenance. It is generally considered that the equipment maintenance cost of distributed generation unit has a linear relationship with its operation time; closure is the cost of active as well as reactive power loss in the microgrid system and the network loss caused by impedance of transmission lines and operating equipment of the microgrid.  $C_{\text{bat}}$  is the penalty cost of battery charge and discharge. When the battery is in peak or valley, the battery operates according to the control strategy, and its output power is constrained by constraints; when in the valley, the battery sets corresponding charge and discharge penalty according to the SOC interval and controls the battery SOC level in interval 3 as much as possible.

#### (B) $C_e$ for trade in Xingduo gas stone

In the operation of the microgrid, the units that generate electricity by fuel combustion, such as microgas turbine and fuel cell, will produce polluting gas or greenhouse gas, which will affect the environment. These gases that will affect the environment mainly include carbides, sulfides, and nitrides; appropriate gas emission treatment costs shall be formulated according to various gas emissions, so as to restrict the environmental problems caused by excessive output of the above units [15]. The calculation of the cost is based on the output of the relevant units to obtain the emissions of various gases and then calculate the corresponding treatment costs as given in the following equation:

$$C_e = \sum_{k=1}^n \sum_{j=1}^m (\alpha_{kj} P_{\text{DG},k} + \beta_{kj} P_{\text{DG},k}^2). \quad (3)$$

In the formula, the treatment cost of  $m$  gases emitted by  $n$  units in total during the operation time of the system is counted. Among them,  $\alpha_{kj}$  and  $\beta_{kj}$  are the  $j$ th gas emission coefficient of the  $k$ th distributed generation unit. It is considered that the gas emission has a quadratic relationship with the output power of the DG, and  $f_j$  is the governance cost coefficient of the  $J$ -type gas.

#### (C) Exchange power cost $C_g$ with large power grid

When the output of micropower source in microgrid (MG) meets the load of MG, surplus power can be sold to

huge power grid; when the output of micropower source in the microgrid is insufficient to meet the load of the microgrid, power can be purchased from a large grid in normal and valley. The cost expression is as shown in the following equation:

$$C_g = \begin{cases} C_{\text{buy}} P_{\text{grid-b}}, \\ C_{\text{sell}} P_{\text{grid-s}}, \end{cases} \quad (4)$$

where  $C_{\text{buy}}$  and  $C_{\text{sell}}$  are the costs of the purchased power and sold off by the MG from the grid and  $P_{\text{grid-b}}$  and  $P_{\text{grid-s}}$  represent the powers of the microgrid to buy and sell electricity from the large grid, respectively.

#### (D) Reactive power production cost $C_r$

Because reactive power itself does not produce economic benefits, the charge for reactive power is defined as the cost corresponding to the reduction of micropower generation capacity due to reactive power output. That is to say, if the micropower supply wants to generate reactive power, the limit value of its active power output will be reduced, and the active power capacity as a spinning reserve will also be reduced accordingly. Therefore, this part of the loss is defined as the cost of generating reactive power as given in the following equation:

$$C_r = \left\{ \sum_{i=1}^n \left[ C(S_{\text{DG},i}) - C\left(\sqrt{S_{\text{DG},i}^2 - Q_i^2}\right) \right] \right\} k. \quad (5)$$

Among them,  $S_{\text{DG},i}$  is the rated apparent power of the micropower supply,  $C(S_{\text{DG},i})$  is the cost of the supply when it outputs at the maximum capacity of the equipment;  $Q_i$  is the reactive power output of the  $i$ th micropower supply.  $k$  is the profit rate of active power generation of micropower source, which is generally taken as 0.05~0.1.

(2) *Constraints*. During the operation of the microgrid, for maintaining the stable functionality of the microgrid, there are many constraints, such as equipment capacity, control strategy, and other factors.

#### (A) Equality constraints

(a) Active and reactive power balance constraints in microgrid are represented in Equations (6) and (7).

$$\sum P_{G,i} = P_D + P_L + P_g, \quad (6)$$

$$\sum Q_{G,i} = Q_D + Q_L + Q_g, \quad (7)$$

where  $P_{G,i}$  and  $Q_{G,i}$  are the output active and reactive power of the  $i$  distributed generation in the microgrid;  $P_D$ ,  $Q_D$  are the load active as well as reactive power demand of the microgrid;  $P_L$  and  $Q_L$  are the active as well as reactive network losses during the operation of the microgrid;  $P_g$  and

$Q_g$  are the active versus reactive power exchanged between the microgrid system and the large grid.

(b) Power flow constraint is given in the following equation:

$$\begin{cases} \Delta P_i = P_{\text{is}} - \sum_{j \in i}^n V_i V_j (G_{ij} \cos \theta_{ij} + B_{ij} \sin \theta_{ij}) = 0, \\ \Delta Q_i = Q_{\text{is}} - \sum_{j \in i}^n V_i V_j (G_{ij} \sin \theta_{ij} - B_{ij} \cos \theta_{ij}) = 0, \end{cases} \quad (8)$$

where  $G_{ij}$ ,  $B_{ij}$ , and  $\theta_{ij}$  are the admittance and phase angle differences between node  $i$  and node  $j$ ;  $n$  is the number of microgrid system nodes;  $i$  is the node number of the microgrid system; and  $j$  is the node connected with node  $i$ .

3.1.2. *Energy Optimization Model in Off-Grid Mode*. When the microgrid is in the off-grid mode, when the power supply is surplus, the distributed generation output is reduced according to the economic principle; when the power supply is inadequate, the load is cut off according to the load bidding strategy, and the compensation cost of the interrupted load is included [16]. The energy optimization model is as shown:

#### (B) Objective function

Compared with the energy optimization model under grid-connected mode, the objective function under off-grid mode does not include the exchange cost with the grid, and the expression is as shown in the following equation:

$$F = \lambda_1 C_o + \lambda_2 C_e + \lambda_3 C_r + \lambda_4 C_1, \quad (9)$$

where  $C_o$  is the functional and maintenance cost of the microgrid system,  $C_e$  is the pollutant emission treatment cost of the microgrid,  $C_r$  is the reactive power cost of production, and  $C_1$  is the compensation cost of the interrupted load.  $\lambda_1$ ,  $\lambda_2$ ,  $\lambda_3$ , and  $\lambda_4$  are the weight proportion of the above four costs in the objective function. Except  $C_i$ , the other expressions are the same as those in grid-connected mode.  $C_1$  is calculated as shown in the following equation:

$$C_1 = \sum_i^n \delta_i P_{d,i}, \quad (10)$$

where  $P_{d,i}$  is the energy demand of the  $i$ th generator cut-off load and  $\delta_i$  is the cost compensation coefficient of the  $i$ th cut-off load.

#### (C) Constraints

The difference between the constraint conditions and the grid-connected mode is that the ninth point of the grid connection mode is the transmission power constraint interacting with the large grid, which is not considered here but

needs to be added with the rotating reserve constraint of the microgrid as shown in the following equation:

$$\sum_{i=1}^N P_{DG,i}^{\max} \geq P_{\text{load}} + P_{\text{loss}} + P_{\text{R}}. \quad (11)$$

Generally, the spinning reserve capacity of the microgrid system is a fixed value, which can be taken as 5% of the maximum load demand. The higher the spinning reserve capacity is, the more reliable the system is, but the investment and operation cost of the system will increase.

**3.2. Three-Time Scheduling Optimization Model.** The three dispatches of the microgrid system give the daily scheduling plan of the microgrid. For the preestablished scheduling strategy, based on the short-term projection of wind energy, light energy, and load, the micropower system is optimized. The start and stop state and power output of the micropower supply and the switching of reactive power compensator have to be optimized [17]. Compared with the secondary scheduling, the difference lies in the different time scales of optimization. For the third scheduling, an all-day economic optimal scheduling scheme based on microgrid is needed, and the power optimization problem in the next period is only considered in the secondary scheduling [18].

### 3.2.1. Energy Optimization Model under Grid-Connected Mode

(1) *Objective Function (ObjF).* The ObjF of the third dispatching of the microgrid system is as shown in the following equation:

$$F = \lambda_1 C_o + \lambda_2 C_e + \lambda_3 C_g + \lambda_4 C_r. \quad (12)$$

Its expression is the same as that of the secondary dispatching grid connection mode, but the calculation method of each component is different, as shown above.

(A) System operation and maintenance cost  $C_o$ .

The unit fuel consumption cost, pollution control cost, maintenance cost, active and reactive power network loss cost, and battery charging and discharging penalty cost of the microgrid are accumulated in the following equation:

$$C_o = \sum_t^T \left( \sum_{k=1}^n (C_{\text{firel},k} + C_{\text{om},k}) + C_{\text{loss}} + C_{\text{bat}} \right). \quad (13)$$

(B) Pollution gas treatment cost  $C_e$

In the same way, the total cost of pollution control is calculated:

$$C_e = \sum_t^T \left( \sum_{k=1}^n \sum_{j=1}^m (\alpha_{kj} P_{DG,k} + \beta_{kj} P_{DG,k}^2) \right). \quad (14)$$

(C) Exchange power cost  $C_g$  with large power grid

When exchanging power with large power grid, purchase power from the power grid, pay the cost, sell power to the power grid, obtain income, and calculate the total exchange cost of the whole day as depicted in the following equation:

$$C_g = \sum_t^T (C_{\text{buy}} P_{\text{grid-b}} - C_{\text{sell}} P_{\text{grid-s}}). \quad (15)$$

(D) Reactive power production cost  $C_r$

The calculation method of reactive power production cost is the same as shown in the following equation:

$$C_r = k \sum_t^T \left\{ \sum_{i=1}^n \left[ C(S_{DG,i}) - C \left( \sqrt{S_{DG,i}^2 - Q_i^2} \right) \right] \right\}. \quad (16)$$

(E) Constraints

The constraint conditions of the third dispatching mode are the same as those of the second dispatching mode.

### 3.2.2. Energy Optimization Model in Off-Grid Mode

(A) Objective function (ObjF)

The expression of the ObjF is the same as that of the secondary dispatching off-grid mode. Except for the compensation cost of the load to be cut, the other calculation expressions are the same as those of the third dispatching mode. The calculation method of compensation cost of interruptible load is given in the following equation:

$$C_1 = \sum_t^T \sum_i^n \delta_i P_{d,i}. \quad (17)$$

The compensation cost of the cut load is mainly related to the capacity of load shedding, the duration of load interruption, and the price of interruption compensation. The whole-day operation cost should be optimized in the third dispatching, so the duration of load interruption should be considered.

(B) Constraints: the constraints are the same as those of the secondary scheduling off-grid mode

**3.3. Model Solving.** In this paper, the PSO is used to simulate the predatory behavior of birds, which has the characteristics of fast convergence speed and strong global optimization ability. In the process of particle swarm optimization, a certain number of feasible solutions are generated randomly in the feasible region of the model, and any group of feasible solutions are defined as particles. The optimal solutions of particles themselves and the global optimal solutions recorded in the iterative process are updated iteratively according to formula (19), and then, they are forced to



approach or even converge to the optimal solution of the model.

In PSO, the position of particle is defined as the feasible solution of the current model, and the particle velocity is defined to represent the moving direction and speed of particles in the feasible region. The renewal equation of particle iteration is depicted in the following equation:

$$v_{iD}^{k+1} = \omega \cdot v_{iD}^k + c_1 \xi (P_{\text{best},iD}^k - x_{iD}^k) + c_2 \eta (G_{\text{best}}^k - x_{iD}^k) + R_{\text{rand}}, \quad (18)$$

$$x_{iD}^{k+1} = x_{iD}^k + v_{iD}^{k+1}, \quad (19)$$

where  $v_{iD}^k$  is the speed of the  $i$ th particle at the  $k$ th iteration,  $x_{iD}^k$  is the position of the  $i$ th particle after the  $k$ th iteration,  $P_{\text{best},iD}^k$  is the optimal solution of the  $i$ th particle itself,  $G_{\text{best}}^k$  is the ideal solution of the swarm,  $c_1$  and  $c_2$  are the learning parameters,  $\omega$  is the inertia weight coefficient, and  $\xi$  and  $\eta$  are random numbers, with the value range between 0 and 1.  $R_{\text{rand}}$  is a random number; its value range depends on the speed range. Adding random number can increase the diversity of particle population, but if the random value is too large, the stability of the algorithm may be destroyed.

The flow chart of the PSO is shown in Figure 4, and the process steps are described as shown:

- (A) Initialization: the position of the particle is the value of all the optimization variables in the model. In the initialization process, a group of solutions is generated randomly in the range of each optimization variable, and the speed is the same
- (B) Calculation of fitness: according to the modeling method, the objective function is calculated, and part of the constraint conditions is transformed into objective terms by penalty function method and added into the fitness value together with the objective function
- (C) Find individual best value and global best value: compare the fitness value of the current particle, and record the individual best value and global best value
- (D) Update the position of the particle and velocity of all particles: update according to formula (18)
- (E) Judging whether the end condition is satisfied: in the standard PSO, the common method is to set the maximum iteration algebra. Once the algorithm reaches the maximum iteration, the iteration will be stopped. However, due to the randomness of PSO in the process of optimization, the amount of calculation needed to obtain the optimal solution is not consistent when facing some complex problems, The end condition can be modified as follows: when the global optimal value does not change after a certain number of iterations, the algorithm is considered to be convergent and meets the end condition

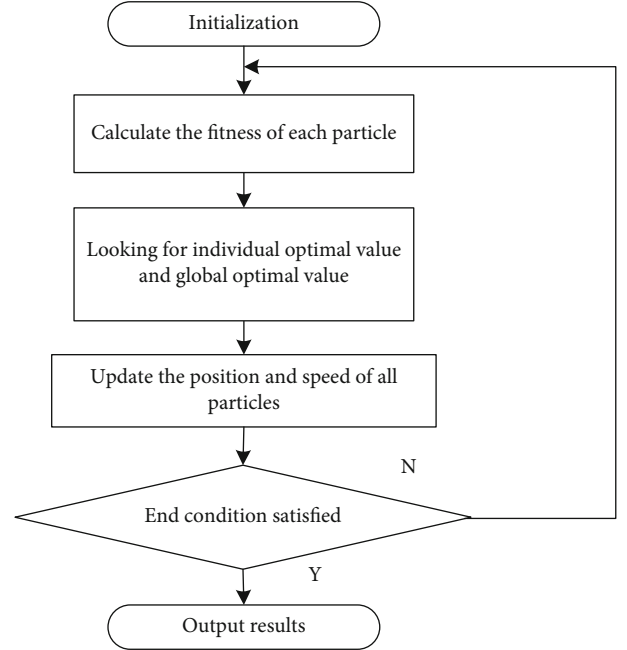


FIGURE 4: Flow chart of the PSO.

- (F) If the stopping criterion is not satisfied, return to the second step, calculate the fitness value according to the updated particles, and iterate repeatedly

## 4. Experiment

In order to verify the suggested DC microgrid control strategy in this paper, a simulation model of DC microgrid is built. In this paper, the DC bus voltage is 400 V of DC microgrid, the peak value of voltage is 160 V for grid phase, and the allowable DC side voltage variation is  $V \pm 10$  V. A grid-connected converter with a capacity of 3 kW is used as the interface unit of grid side. The DC bus is connected to a small direct drive PMSG generation system for wind power with a capacity of 6.5 kW and a photovoltaic power generation system with a capacity of 2 kW. The energy storage system considers a battery with a rated power of 3 kW, its capacity is 96 V/12 Ah, the rated discharge current is 2.4 a, and the upper and lower limits of SOC of battery are 95% and 40%, respectively. DC microgrid contains various types of loads, including 1.5 kW AC constant power load, 2 1.8 kW DC constant power load, and 2 local loads. Buck converter and resistor constitute DC constant power load 1; boost converter and resistor constitute DC constant power load 2. Local load 1 and load 2 are 100 kW and 200 kW resistive load, respectively. The simulation of grid-connected, converter current limiting, islanding load shedding, and islanding operation modes are carried out.

The overall structure of the DC microgrid is shown in Figure 3. It is mainly composed of grid-connected converter (GCC), static transfer switch (STS), DG unit, battery energy storage (BES) unit, constant power load, and local load. The grid-connected converter in Figure 5 is a three-phase two-level voltage source converter topology, and the grid side is connected with a third-order LCL filter. The main control

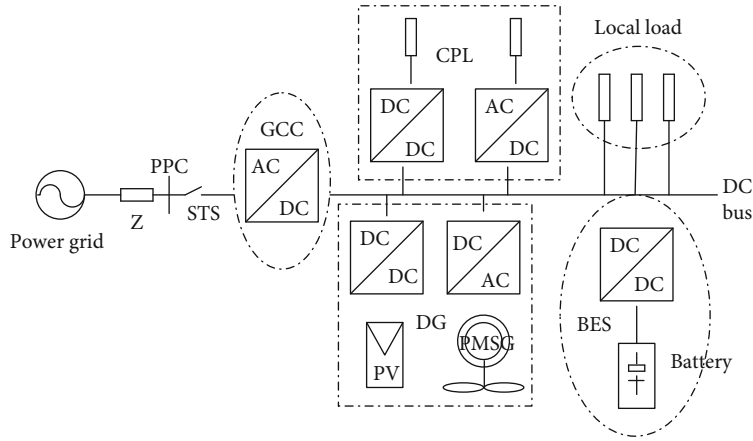


FIGURE 5: Low-voltage DC microgrid structure.

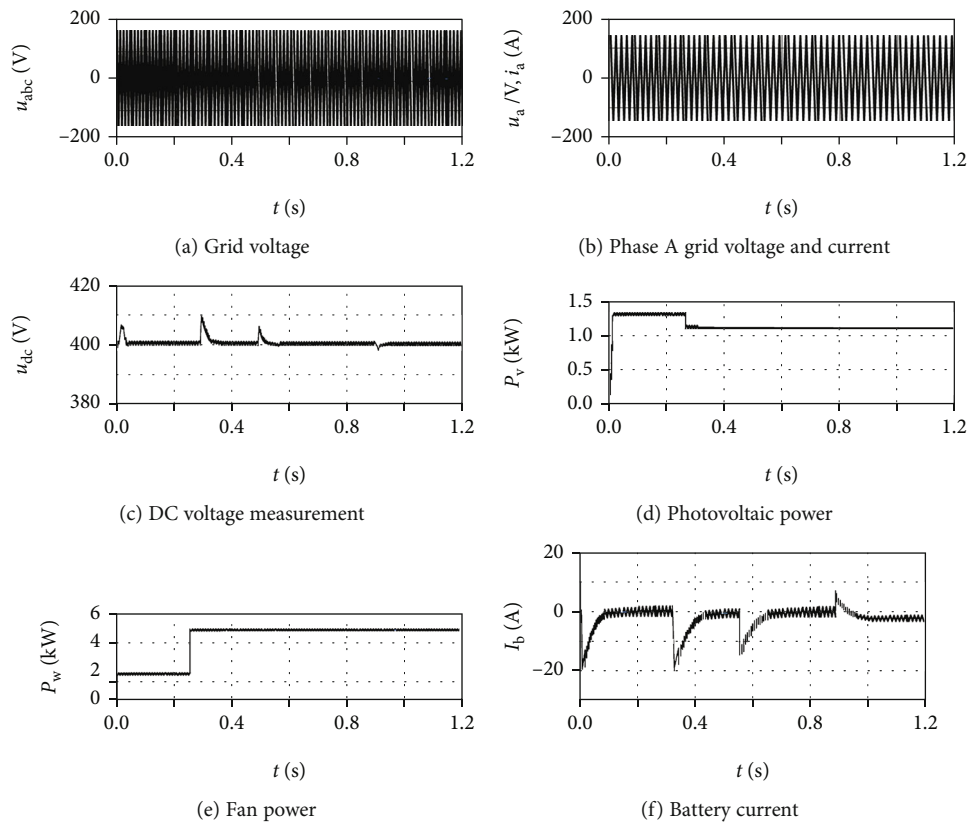


FIGURE 6: Simulation results of grid-connected operation.

objectives of grid-connected converter are to maintain the DC bus voltage constant, reduce the harmonic of grid current, and realize the unit power factor operation and bidirectional energy flow at the grid side. DG includes wind turbine and photovoltaic power generation unit. The wind turbine adopts PMSG structure, and the PV power generation system adopts double-stage single-tube boost grid-connected topology. The storage system is composed of battery and bidirectional buck/boost converter to realize the bidirectional flow of energy. The constant power load is simulated by DC/DC and DC/AC converters and resistive load, and the local load is resistive load.

**4.1. Grid-Connected Operation.** Figure 6 shows the simulation results of DC microgrid operating in grid-connected mode under normal grid conditions, which is running in energy management mode. Under the initial conditions, the light intensity is  $1.2 \text{ kW/m}^2$ , the wind speed is  $8 \text{ m/s}$ , the DC bus voltage is controlled by the grid-connected converter, the wind turbine and photovoltaic power generation system operate in MPPT state, the battery operates in standby mode, AC constant power load and two DC constant power loads are connected to the system, and the output power of DG unit is less than the load power. In order to observe the phase relationship between the grid voltage and current, the grid

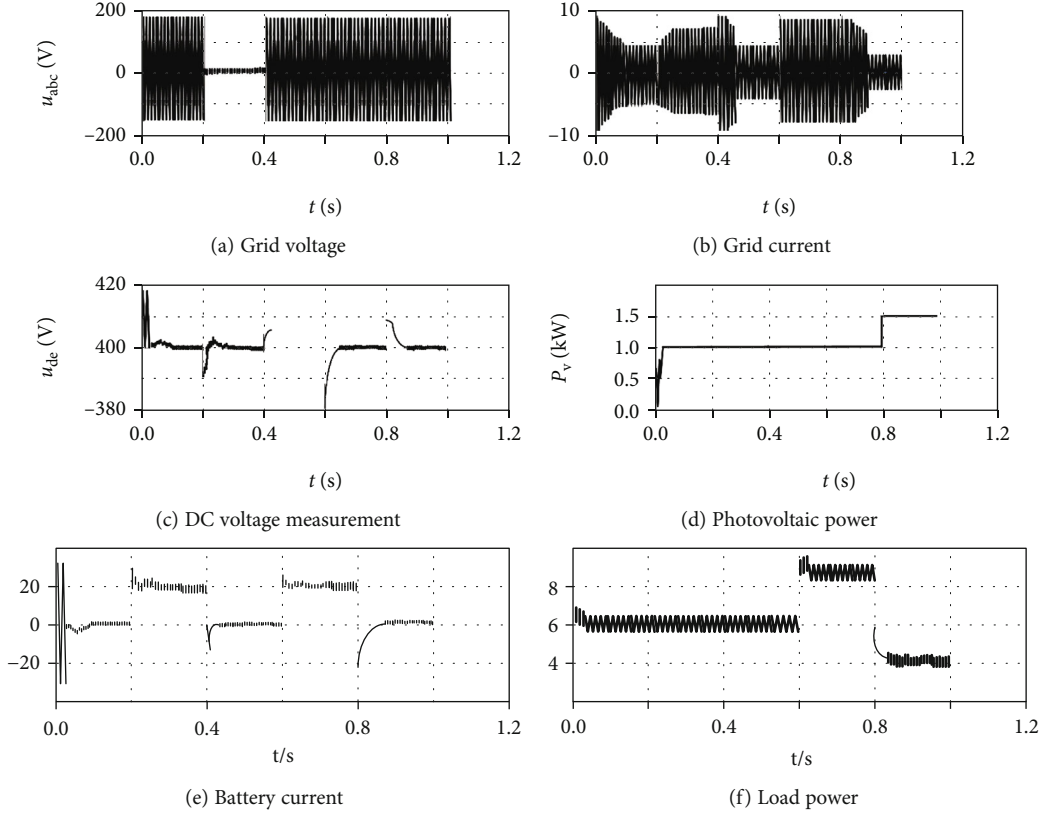


FIGURE 7: Simulation results of short-time fault and current limiting operation of converter.

current is amplified by 5 times. It can be seen from Figure 6(b) that the grid voltage and current are in the same frequency and phase, and the grid-connected converter is operating in the rectification state. At 0.3 s, the illumination intensity changes step by step from  $1.2 \text{ kW/m}^2$  to  $1 \text{ kW/m}^2$ , the wind speed changes from  $8 \text{ m/s}$  to  $11 \text{ m/s}$ , and the DC side voltage remains unchanged at  $400 \text{ V}$  after a short period of adjustment. At this time, the output power of DG unit is greater than the power absorbed by the load. The grid voltage and current are in the same frequency phase, and the grid-connected converter operates in the inverter state. At 0.5 s, when DC constant power load 1 is switched out, the total load power decreases; at 0.9 s, local load 2 cuts into the system, and the total load power increases. In the case of load cut-out/cut in disturbance, the DC voltage can be quickly stabilized through closed-loop regulation.

**4.2. Short-Time Fault of Power Grid and Current Limiting Operation of Converter.** Figure 7 shows the simulation results of DC microgrid under short-term fault and current limiting condition of converter. Under the initial conditions, the light intensity is  $1 \text{ kW/m}^2$ , the wind speed is  $9 \text{ m/s}$ , and AC constant power load and two DC constant power loads are connected to the system. In 0.2 s, three-phase short-circuit fault occurs in the power grid, which causes PCC voltage to droop at the same time. Grid-connected converter works in current limiting mode and cannot maintain constant DC bus voltage. At this time, battery switches from droop control to constant voltage control. In 0.4 s, the grid fault is cleared, the grid volt-

age is recovered, the output of the grid-connected converter voltage outer loop regulator is desaturated, and the DC bus voltage is recontrolled. The battery is switched from constant voltage control to droop control and operates in standby mode. At 0.6 s, the local loads 1 and 2 are connected to the system at the same time. At this time, the grid needs to provide more active power to maintain the power balance. Due to the limitation of rated capacity, the grid-connected converter operates in current limiting mode again. At this time, the battery changes from droop control to constant voltage control to maintain DC bus constant voltage. At 0.8 s, two  $1.8 \text{ kW}$  DC constant power loads are cut off, the light intensity changes step by step from  $\text{kW/m}^2$  to  $1.5 \text{ kW/m}^2$ , and the load power is less than the output power of DG unit, which makes the grid-connected converter controls the DC bus voltage, and the battery switches to the standby working state.

**4.3. Island Load Shedding Operation.** Figure 8 shows the simulation results of islanding and load shedding operation of DC microgrid. Under the initial conditions, the light intensity is  $0.8 \text{ kW/m}^2$ , the wind speed is  $9 \text{ m/s}$ , and AC constant power load and two DC constant power loads and local load 2 are connected to the system. In 0.3 s, three-phase short-circuit fault occurs in the power grid, which leads to the disconnection of the converter and the grid current, and the grid current drops to zero. For guaranteeing the power balance, the battery switches from droop control to constant voltage control to maintain the constant DC bus voltage. Since the

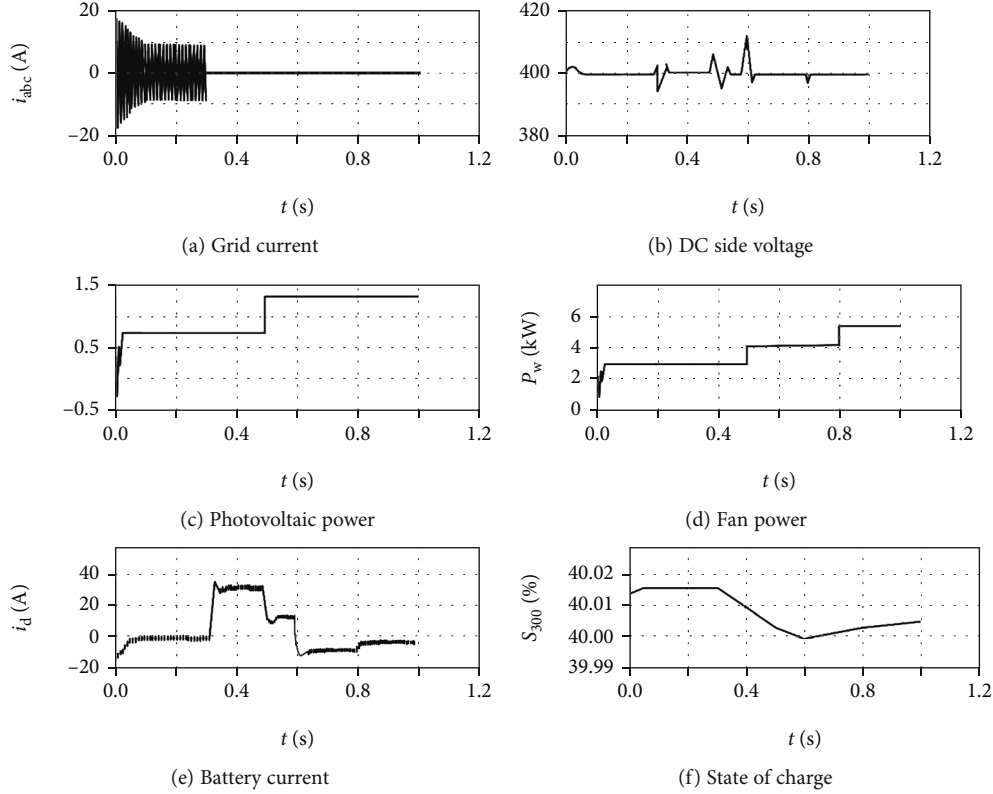


FIGURE 8: Simulation results of islanded load shedding operation.

rated discharge current of the battery is small, in order to simulate the deep discharge state of the battery, the initial SOC value of the battery is set as 40.015%. At this time, the battery current is greater than 0, and it is in continuous discharge state. In 0.5 s, the illumination intensity changes from 0.8 kW/m<sup>2</sup> to 1.2 kW/m<sup>2</sup>, and the wind speed fluctuations are from 9 m/s to 10 m/s. At this time, the output power of DG unit is still less than the load power, so the battery remains in discharge state until the SOC of the battery reaches 40% of the lower limit and lasts for a period of time. To avoid excessive discharge, the DC constant power load 1 with the lowest load priority is removed. At this time, the load power is less than the output power of DG unit, and the battery changes from discharge to charging state and controls DC bus voltage; battery SOC increases gradually. At 0.8 s, the wind speed changes from 0 m/s to 1 m/s, and local load 1 is connected to the system. Since the output power of wind power generation system is cubic with wind speed, the load power is still less than the output power of DG unit, the battery is still working in charging state, and the DC bus voltage is controlled.

**4.4. Island Operation.** Figure 9 shows the simulation results of islanding operation of DC microgrid. Under the initial conditions, the light intensity is 1.2 kW/m<sup>2</sup>, the wind speed is 10.5 m/s, and AC constant power load and DC constant power load 1 and local load 2 are connected to the system. In 0.3 s, the three-phase short-circuit fault occurs in the power grid, which leads to the disconnection between the converter and the grid. At this time, the battery switches from

droop control to constant voltage control to maintain the constant DC bus voltage. In order to simulate the deep charging state of the battery, the initial SOC value of the battery is set as 94.99%. At this time, the battery current is less than zero and it is in continuous charging state. The SOC reaches 95% due to the continuous charging of the battery. In order to avoid the deep charging of the battery, the given value of the battery current is zero. At this time, the battery is in the stop state, and the wind power generation system is switched from MPPT to constant voltage control. In order to eliminate the DC bus voltage fluctuation, the open-loop pitch angle control combined with the fan constant voltage control strategy is adopted in this paper. At 0.8 s, the local load 1 is connected to the system. Since the load power is greater than the output power of DG unit, the battery changes from stop working state to constant voltage control for discharge. At the same time, the fan is switched from constant voltage control to MPPT control. In order to improve the utilization rate of wind energy, the value of  $\beta$  is reduced from 5° to 0°. At 1 s, the wind speed changes step by step from 10.5 m/s to 9 m/s, and the light intensity changes from 1.2 kW/m<sup>2</sup> to 0.8 kW/m<sup>2</sup>. At this time, the wind turbine and photovoltaic power generation system work in MPPT (max power point tracking) state, and the battery continues to discharge to control the constant DC bus voltage.

**4.5. Discussion on Results.** This paper has presented a hierarchical coordinated control method (HCCM) for multiload DC microgrid units. The proposed HCCM is divided into layers according to the control objectives and control time

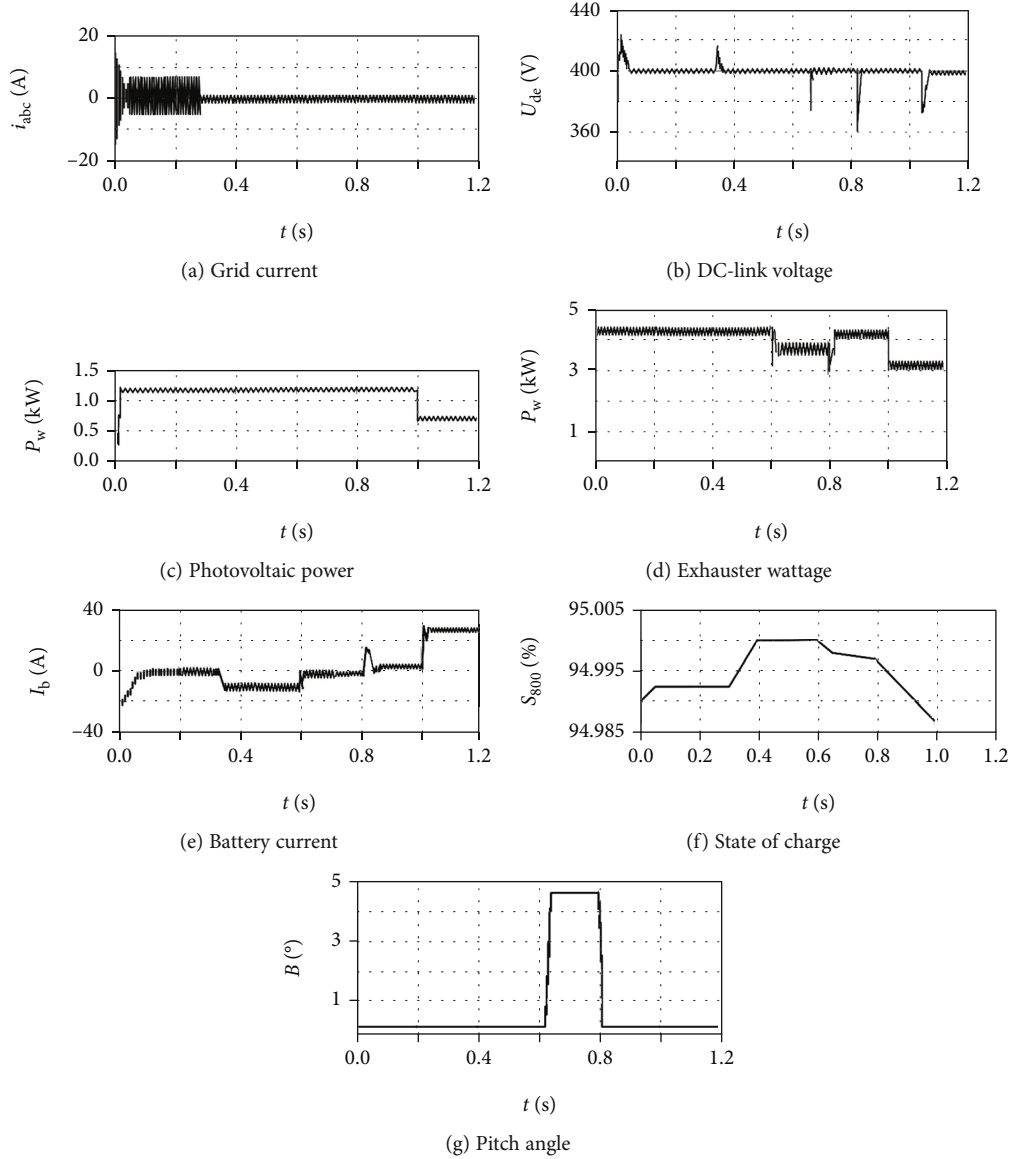


FIGURE 9: Simulation results of island operation.

scales of the microgrid, and the hierarchical control structure is realized by using multiagent technology in this paper. The proposed HCCM framework is aiming at the demand of energy coordination and optimization of the microgrid. The operation strategy of the microgrid is proposed in the grid-connected and/or off-grid mode. In the grid-connected mode, the large power grid is used for power supply, and in the off-grid mode, the load bidding mechanism is introduced to guarantee the power supply of important loads. Figure 6 shows the simulation results of DC microgrid functionality in the grid-connected mode under energy management mode. The results reveal that the proposed method saves energy and provides stable performance. Figure 7 shows the simulation results of DC microgrid under short-term fault and current limiting condition of converter. The battery changes from drop control to constant voltage control/standby working mode to maintain DC bus constant voltage. Figure 8 shows the simulation results of islanding and load

shedding operation of DC microgrid. Since the output power of the wind power generation system is cubic with wind speed, the load power is still less than the output power of DG unit, the battery is still working in charging state, and the DC bus voltage is controlled. Figure 9 shows the simulation results of islanding operation of DC microgrid. At this time, the wind turbine and photovoltaic power generation system work in MPPT state, and the battery continues to discharge to control the constant DC bus voltage. The experiment results reveal the power quality and stability of the system in result section.

## 5. Conclusion

The hierarchical control structure of a microgrid is designed and developed in this paper, and it is comprehended using multiagent technology. The operating strategy of a microgrid in the grid-connected/off-grid mode is provided within the

context of hierarchical control. The huge power grid is aided in the grid-connected mode to cut the peak and the load bidding mechanism is implemented in the off-grid mode to secure the power supply of key loads. When DC bus voltage deviates from the idyllic reference value, the converters controlling DC bus voltage use PI control to provide zero steady-state error regulation of DC bus voltage, thereby avoiding the instability of constant power load. To engage in DC voltage coordinated control, an open-loop pitch angle control approach is utilized, which can achieve constant voltage control of the fan underrated power and eliminate DC bus voltage fluctuation. According to the results of the performance study, the proposed solution is simple, is convenient to implement, and improves the system's power quality and stability. The results are presented in simulated environment under three conditions such as DC microgrid under short-term fault and current limiting condition of converter, islanding and load shedding operation of DC microgrid, and islanding functionality of DC microgrid. The experiment results depict that the power quality remains unaltered and the system remains stable under different conditions.

## Data Availability

Data is available on request.

## Conflicts of Interest

The authors declare no conflicts of interest.

## Acknowledgments

We would like to acknowledge the Experimental Training Teaching Base of Guangxi Undergraduate Colleges and Universities for providing guidance and support and for carrying out the research work presented in this paper.

## References

- [1] P. Prajof, Y. Goyal, and V. Agarwal, "Novel nonlinear droop control techniques to overcome the load sharing and voltage regulation issues in DC microgrid," *IEEE Transactions on Power Electronics*, vol. 33, no. 5, pp. 4477–4487, 2018.
- [2] P. D. Hamed, S. Nojavan, R. Nourollahi, and K. Zare, "Optimal economic-emission performance of fuel cell/CHP/storage based microgrid," *International Journal of Hydrogen Energy*, vol. 44, no. 13, pp. 6896–6908, 2019.
- [3] H. E. Keshta, A. A. Ali, E. M. Saied, and F. M. Bendary, "Real-time operation of multi-micro-grids using a multi-agent system," *Energy*, vol. 174, no. 1, pp. 576–590, 2019.
- [4] K. Jairath, N. Singh, V. Jagota, and M. Shabaz, "Compact ultra-wide band metamaterial-inspired split ring resonator structure loaded band notched antenna," *Mathematical Problems in Engineering*, vol. 2021, Article ID 5174455, 2021.
- [5] B. Wang, X. Yao, Y. Jiang, C. Sun, and M. Shabaz, "Design of a real-time monitoring system for smoke and dust in thermal power plants based on improved genetic algorithm," *Journal of Healthcare Engineering*, vol. 2021, Article ID 7212567, 2021.
- [6] J. A. Martin-Ramos, O. Pardo-Vaquero, J. Diaz, F. Nuno, P. J. Villegas, and A. Martin-Pernia, "Modelling a multilevel LCC resonant AC-DC converter for wide variations in the input and the load," *IEEE Transactions on Power Electronics*, vol. 34, no. 6, pp. 5217–5228, 2019.
- [7] J. Meng, Y. Wang, C. Wang, and H. Wang, "Design and implementation of hardware-in-the-loop simulation system for testing control and operation of DC microgrid with multiple distributed generation units," *IET Generation, Transmission and Distribution*, vol. 11, no. 12, pp. 3065–3072, 2017.
- [8] P. Kou, D. Liang, J. Wang, and L. Gao, "Stable and optimal load sharing of multiple PMSGs in an islanded DC microgrid," *IEEE Transactions on Energy Conversion*, vol. 33, no. 1, pp. 260–271, 2018.
- [9] D.-H. Dam and H.-H. Lee, "A power distributed control method for proportional load power sharing and bus voltage restoration in a DC microgrid," *IEEE Transactions on Industry Applications*, vol. 54, no. 4, pp. 3616–3625, 2018.
- [10] S. Yousefzadeh, J. D. Bendtsen, N. Vafamand, M. H. Khooban, F. Blaabjerg, and T. Dragicevic, "Tracking control for a DC microgrid feeding uncertain loads in more electric aircraft: adaptive backstepping approach," *IEEE Transactions on Industrial Electronics*, vol. 66, no. 7, pp. 5644–5652, 2019.
- [11] S. Islam, S. Agarwal, A. B. Shyam et al., "Ideal current-based distributed control to compensate line impedance in DC microgrid," *IET Power Electronics*, vol. 11, no. 7, pp. 1178–1186, 2018.
- [12] E. Hossain, R. Perez, A. Nasiri, and R. Bayindir, "Stability improvement of microgrids in the presence of constant power loads," *International Journal of Electrical Power & Energy Systems*, vol. 96, pp. 442–456, 2018.
- [13] S. Gunter, G. Buticchi, G. De Carne et al., "Load control for the DC electrical power distribution system of the more electric aircraft," *IEEE Transactions on Power Electronics*, vol. 34, no. 4, pp. 3937–3947, 2019.
- [14] H. Farzin, F.-F. Mahmoud, and M.-A. Moein, "Role of outage management strategy in reliability performance of multi-microgrid distribution systems," *IEEE Transactions on Power Systems*, vol. 33, no. 3, pp. 2359–2369, 2018.
- [15] X. Liu, B. Gao, Z. Zhu, and Y. Tang, "Non-cooperative and cooperative optimisation of battery energy storage system for energy management in multi-microgrid," *IET Generation Transmission & Distribution*, vol. 12, no. 10, pp. 2369–2377, 2018.
- [16] E. Shahryari, H. Shayeghi, B. Mohammadi-Ivatloo, and M. Moradzadeh, "A copula-based method to consider uncertainties for multi-objective energy management of microgrid in presence of demand response," *Energy*, vol. 175, no. 15, pp. 879–890, 2019.
- [17] M. Katayama, T. Ohno, H. Obara, and A. Kawamura, "Application of multi-level converter for fast current control in small-scale DC power network," *IEEE Transactions on Industry Applications*, vol. 55, no. 3, pp. 2902–2909, 2019.
- [18] B. Blanco-Contreras, J. Meneses-Silva, P. Mendoza-Araya, and G. Jiménez-Estévez, "Effect of constant power load models on the stability of isolated microgrids," in *CHILECON 2019: IEEE CHILEAN Conference on Electrical, Electronics Engineering, Information and Communication Technologies (CHILECON)*, pp. 1–6, Valapraiso, Chile, 2019.

## Research Article

# Prediction of Traffic Generated by IoT Devices Using Statistical Learning Time Series Algorithms

Shilpa P. Khedkar <sup>1</sup>, R. Aroul Canessane <sup>1</sup> and Moslem Lari Najafi <sup>2</sup>

<sup>1</sup>Department of Computer Science and Engineering, Sathyabama Institute of Science and Technology, Chennai, India

<sup>2</sup>Pharmaceutical Science and Cosmetic Products Research Center, Kerman University of Medical Sciences, Kerman, Iran

Correspondence should be addressed to Moslem Lari Najafi; [m.larinajafi@kmu.ac.ir](mailto:m.larinajafi@kmu.ac.ir)

Received 19 June 2021; Accepted 19 July 2021; Published 2 August 2021

Academic Editor: VIMAL SHANMUGANATHAN

Copyright © 2021 Shilpa P. Khedkar et al. This is an open access article distributed under the Creative Commons Attribution License, which permits unrestricted use, distribution, and reproduction in any medium, provided the original work is properly cited.

An IoT is the communication of sensing devices linked to the Internet in order to communicate data. IoT devices have extremely critical reliability with an efficient and robust network condition. Based on enormous growth in devices and their connectivity, IoT contributes to the bulk of Internet traffic. Prediction of network traffic is very important function of any network. Traffic prediction is important to ensure good system efficiency and ensure service quality of IoT applications, as it relies primarily on congestion management, admission control, allocation of bandwidth to the system, and the identification of anomalies. In this paper, a complete overview of IoT traffic forecasting model using classic time series and artificial neural network is presented. For prediction of IoT traffic, real network traces are used. Prediction models are evaluated using MAE, RMSE, and *R*-squared values. The experimental results indicate that LSTM- and FNN-based predictive models are highly sensitive and can therefore be used to provide better performance as a timing sequence forecast model than the conventional traffic prediction techniques.

## 1. Introduction

The Internet of Things (IoT) are communicating devices with sensing capability that are connected to the Internet which enables collecting and sharing of data without human intervention. Initially, RFID tags were added to devices to help track their location, and this was one of the first IoT applications. As things are made to communicate with one another, such kind of communication is called Machine-to-Machine (M2M) communication. Communication can be short range with mobile networks like 3G, 4G, LTE, and 5G, such as Wi-Fi, Bluetooth, and broad range [1]. The main tasks to be performed by IoT devices are data collection, M2M communication, and application processing. IoT devices are meant to handle massive amount of data; therefore, its infrastructure needs to implement methods that can manage, hold, and evaluate large data. In order to enable Machine-to-Machine (M2M) communication, IoT platforms are used along with protocols such as MQTT and CoAP [2–4]. IoT devices may include services like monitoring, node managing, data storage and evaluating capabilities, etc. IoT

devices are mainly used in applications such as Health Care Systems, Home Appliances, Transportation, Monitoring of Environmental Conditions, Logistics Management, Security services, and many more. The IoT infrastructure consists of (1) IoT nodes which are mainly called the IoT devices which consists of sensors and actuators; (2) servers which are otherwise called Fog nodes that facilitate storage, computing, and networking; (3) data centers called cloud nodes that store data using machine learning techniques and help in data sharing; and (4) IoT applications that make use of the computed data to provide services to the end user. In the Internet of Things (IoT), individuals, systems, data, and objects have been predominantly linked to and connected with the Internet. The effectiveness of any IoT ultimately depends on how easily it can interact with other IoT devices. Their performance is assessed. Speed increase helps to minimize delays and enhance the communication of data between devices. For any IoT system, which relies on real-time updates, having consistent and stable network conditions is extremely essential. The network's ability to deal with more connected devices will help the devices become more reliable.

IoT will contribute to the major part of Internet traffic. Research contributions related to IoT and network traffic are limited to modeling IoT traffic and characterizing its properties. IoT traffic characteristics depend on the types of sources, hardware devices, and services provided as it is the combination of different devices at different environments. Traffic generators, for instance, Iperf and D-ITG, are used in evaluating network performance and characterizing traffic. Different types of interfaces and transport protocols are used by the traffic generators. A traffic generator injects traffic into the network for utilization by other devices. Traffic generator facilitates in evaluating device performance. The IoT usage is rapidly increasing, but a few research studies have been carried out regarding traffic characterization. By visualizing IoT traffic with the  $t$ -distributed stochastic neighbor embedding ( $t$ -SNE) technique, flowing data analytics to perceive anomalous IoT traffic by visually observing the traffic through sensing devices with the BS graphs are some of the techniques used in traffic characterization [5]. Machine learning algorithms are employed for identifying and classifying IoT devices. Artificial intelligence (AI) is used in the prediction of network traffic for data networking. Traffic size is predicted on the basis of the count of input and output bytes during communication at various network levels. For network operations, management, and other network functionalities and roles, traffic prediction is mandatory. IoT traffic can be broken down into three forms of traffic: deterministic, probabilistic, and facilitated. The traffic from the IoT devices and other communications networks can be transported. Although the traffic from M2M connections was historically smaller than that from end users. Currently, traffic has grown faster than the number of connections as video applications on M2M connections have been deployed quickly, and IoT applications have become more frequent and demand more bandwidth and lower latency.

Devices and their connectivity have increased enormously as well as people and Internet users. This leads to a rise in average per household and per capita devices and connections. Each year, new devices are launched and implemented on the market from a variety of sources and heterogeneous hardware components with increased capacities and intelligence. The development of these devices and connections is greatly influenced by an increasing number of M2M applications. Therefore, the shifting mix of devices and connections must be monitored, and their various ownership affects the traffic patterns differently. One of the main contributors to global mobile traffic growth is the ever-changing combination and increase in wireless devices accessing mobile networks worldwide. Enhancing system capabilities through faster, higher bandwidth, and smarter networks will allow broad experimentation and the expansion of new multimedia applications to help increase mobile and Wi-Fi traffic. The rise in the usage of mobile apps and the growth of mobile access in scope are increasing the number of end users. The need for optimized bandwidth management and new network monetization models has been brought about. This is why the growth of mobile IoT brings individuals, systems, data, and items together to improve the relevance and value of network connections and thus to increase network

traffic contribution [6]. Most of the infrastructure of IoT devices consists of sensors, processors, network software, and different vendors' applications. A gateway often comprising products of several suppliers controls the endpoints. The endpoints are different for different applications. The basic functions of each application produce different types of traffic in return. Different variables such as whether a processing gateway is passed through, how much intelligence it includes, and the applications run on the gateway depends on traffic. Intelligent gateway awareness can react locally and process most generated data while dumb devices need more connectivity to a data center or to a cloud service. The characteristics of traffic depend on flow, data collection, transmission of data, and communications amongst actuators and sensors.

There are several IoT devices linked by wireless. Rising online device volumes would require more bandwidth. As IoT grows, ensuring it can handle its devices and traffic through the network is compulsory. As the number of devices increases, IoT can increase its effect on the bandwidth needs. As the technology develops more, the amount of data linked to IoT devices will increase, which in turn will help to improve the bandwidth requirement. Bandwidth will still be sufficient for the end users. The major problem of effective IoT technology deployment is related to the speed and coverage of wireless networks available (Wi-Fi). Another important factor to IT traffic is the rise in broadband speed. The network demands are far higher than IP voice and video. The distribution of bandwidth in a congested network is difficult to handle. Improvements to broadband speed result in increased usage and use of content and software with high bandwidth. The global average speed of broadband is still growing and will double from 45.9 Mbps to 110.4 Mbps from 2018 to 2023. Implementation and use of fiber to the home (FTTH), high-speed DSL, and broadband cable adoption as well as broadband penetration in general are key factors influencing the broadband fixed forecast [6].

As mentioned earlier, IoT is liable for the interaction amongst different devices. With the rise in smartphones, IoT traffic on the Internet has significantly increased, and a lot of research has been done to enhance the end user's connectivity experience. The component to predict traffic has crucial effects on dynamic negotiation of bandwidths. Two independent sections of the method are normally sampled and predicted. To ensure good system efficiency, traffic prediction is vital. To use network resources efficiently, traffic prediction is essential. Congestion management, induction control, network assignment of bandwidth, and detecting malicious applications are based on accurate predictions of traffic at end points. This allows for effective distribution of resources to ensure consistent service quality. Network abuses are preventing and detecting increasingly difficult with increasing traffic and network complexity. The adequacy of traffic forecast is directly linked to this. The quality of service provided by wireless sensor networks depends on the supply of power. A precise traffic prediction is needed to speed up these nodes and to maximize energy savings. With rising requirements for demands in traffic and computational needs, power consumption is increased [7].



The contributions of the paper are listed as follows:

- (i) The related techniques for traffic prediction are explored and implemented for comparative study of the existing methods with the proposed LSTM method and feedforward neural networks (FNN) prediction method
- (ii) To use the network bandwidth optimally, to reduce the over consumption of the IoT channels, FNN and LSTM are proposed which are more efficient than the existing ARIMA- and VARMA-based techniques
- (iii) The problem of insufficient data of IoT devices and unavailability of historical data, a time series-based learning model has also been introduced in this paper. By learning from the accumulated data from similar domains, the LSTM and FNN methods allow the predictive models to get trained from accumulated data and application of time series-based learning model in the local domain

The rest of the paper is structured accordingly. Section 2 outlines the previous work on the forecasting of IoT traffic. In Section 3, the IoT traffic forecasting models used are presented in brief. Section 4 describes the evaluation methodology with the experimental findings. In Section 5, concluded with future trends.

## 2. Related Work and Research Gap

The rapid growth of network traffic leads to enormous research contributions based on prediction of the network traffic, but the Internet of Things requires improved and efficient approaches to handle huge and dynamic data as shown in some recent study [2, 7]. We have surveyed the different techniques used in network traffic prediction in this section to provide insights into the research contributions made by others in the area of our research work.

The author proposes a model which uses spatiotemporal features from neighboring cellular stations to target base station. Traffic prediction is done with the help of these features over time using deep learning algorithms like 3D convolutional networks. The methodology used showed promising results that outperformed other traffic prediction systems [8]. Essien et al. proposed a model for urban traffic prediction using deep learning architecture which works on features extracted from traffic and weather-related tweets. This model helps in multistep traffic prediction which includes deep Bidirectional Long Short-Term Memory (LSTM) stacked autoencoder (SAE) architecture. The results obtained showed to be effective in improving prediction accuracy when compared to other traditional statistical and machine learning models. This model was found to be useful to reduce frustration due to heavy road traffic, low cost and increased savings for businesses, and environmental sustainability [9].

Volkov et al. proposed an IoT traffic prediction model using NARX neural network with a single step ahead and multistep ahead prediction. The evaluation of prediction was done

using Traincrgf, Traincgp, and Trainlm neural network training algorithm along with forecasting accuracy measures like mean square error (MSE) and mean absolute percentage error (MAPE) [10]. Meena et al. proposed a tool used for accurate traffic flow prediction. They used machine learning, genetic, soft computing, and deep learning algorithms to build a model which does big-data analysis with reduced complexity for the transportation system [11]. Feng et al. proposed a traffic prediction end-to-end model using deep-learning approaches. The model uses spatial-dependent and long-period cellular traffic for forecasting traffic. The model comprises a feature extractor that models spatial dependencies and encodes the external information. It also models complicated temporal variations using a sequential module. Spatial modeling is done using a correlation selection mechanism, and encoding of external information is done by embedding mechanism. The attention mechanism is applied to the seq2seq model to build the sequential model. The observation of results shows that this model outperforms other traditional prediction models by more than 12.31 percent [12].

Hua et al. proposed the Random Connectivity LSTM, an LSTM-based deep learning model (RCLSTM). RCLSTM is used to forecast traffic and confirm the satisfactory efficiency of the RCLSTM with even 35% neural connectivity, and its prediction accuracy is even higher than the basic LSTM [13]. Wang et al. [14] suggest an optimized model for prediction of space-temporal traffic flow. In comparison to traditional coevolutionary neural networks, the GCN's applications have a more robust and accurate capacity to learn spatial features of the road system and the use of LSTM with the introduction of weather and regular features as additional knowledge increases its strength in temporary feature extraction. The test results showed the model's capacity to capture spatial and temporal features [14]. Zhang et al. suggest a way of bridging the gap between deep learning and mobile and wireless networking research by the adoption of a systematic crossover of the two fields. This survey reveals the issues facing currently and the potential of wireless network research [15].

In the time series NARX feedback neural networks with multistep ahead prediction, Abdellah et al. proposed an IoT-prediction model traffic time series. The prediction was assessed using reliability assessment functions such as MSE, SSE, MAE, and the mean absolute percentage of error (MAPE) [16]. Essien et al. proposed a method for single-step time series prediction using a combination of deep study methods, such as Wavelet Transforms (WT) and 2-dimensional CNN's and Long Short-Term Memory (LSTM) stacked autoencoders (SAE). In the univariate time series prediction, the model had positive results [17]. Kamble and Kounte proposed to use machine learning algorithms (ML) to identify traffic congestion using parameters such as difficult timing limitations and the speed available via GSP trajectory. This paper shows that approaches to machine learning (ML) can be useful for prediction of current and historical data in real-time traffic and future traffic and short-term traffic. There were three separate time slots used for tracking traffic congestion that contributed to the assessment of vehicle average speed [18].

Tang et al. proposed to predict future TL and network involvement with a new deep learning system with a TL prediction algorithm. A new intelligent channel assignment algorithm was considered to be a deep learning-based predictive method with partially overlapping channel assignments. The proposed algorithm smartly prevents future congestion and helps to rapidly allocate appropriate channels for SDN-IoT. It is observed that the results were much better than other traditional channel algorithms [19]. A traffic congestion control system was suggested by Nguyen et al. Different functions of the proposed model include collection of data, building-up of structures, modelling of traffic flow, congestion prediction, and congestion services. The use of a verification method based on the Rankine-Hugoniot condition minimizes false predictions. The experimental model analyses showed that traffic congestion can be effectively tracked in terms of precision and network response time [20].

In deep learning methods, Polson and Sokolov suggested a combined architecture. The architecture combines a linear model that is equipped with  $\ell_1$  regularization with a series of tanh layers. In order to capture spatio-temporary effects and short-term traffic forecasts, the proposed model was followed [21]. Huang et al. introduced a multitask learning architecture using mobile traffic prediction deep learning networks. Three traditional algorithms for deep learning, RNN, and 3D CNN have been used. The CNN-RNN algorithm was designed with different purposes to collect mobile traffic resources. The experimental observation shows that the customized CNN and RNN can be used effectively to obtain geographic and time traffic characteristics. The comparative study shows that CNN-RNN reliably track traffic with an accuracy of 70% to 80% [22]. Li et al. introduced a methodology which used traffic big data analysis. There was a systematic analysis of the modelling and estimation of mobile network traffic. A new traffic prediction has been created to incorporate and explore more of these characteristics using a dictionary learning-based alternative direction method system. Experimental results of the established model showed that the modelling and forecasting problems in application-level learning of traffic and prediction were significantly solved [23].

Luo et al. suggested a model with more than 9 layers of a deep convolutive neural network. The proposed models with the support of a deep convolution neural network have shown to be more powerful in terms of prediction accuracy than other typical vehicle recognition systems based on machine learning algorithms [24]. Xu et al. proposed a method for mobile traffic extraction and modelling. It has developed, implemented, and assessed the model using a time series analysis method that decomposes mobile large-scale traffic based on component regularity and randomness. The experimental proves that the regularity variable is highly predictable and does not predict the average component [25].

Though much research explores different methodologies for predicting, classifying network traffic for the Internet of Things is still to be explored. Traditional prediction and classification techniques to forecast IoT-based traffic and provide data security and integrity will not be able to give satisfying performance and accurate results. This leads to the use of

newer AI-based intelligent techniques which are suitable to the IoT environment. Therefore, we are proposing machine learning methods to predict the IoT-based traffic.

### 3. Data Preparation

Data has to be prepared as per the model selected. The two steps for data preparation are by firstly considering the quality of the data and then organizing the data in a particular way for a time series forecasting context. These two steps of data preparation are elaborated below and process see in Figure 1.

*3.1. Data Preprocessing.* Abnormal measurements (e.g., due to problems with a measuring sensor) has to be removed. The abnormal measurements might trick the model into learning patterns that it should not, which results in overfitting the training data. Hence, it is imperative to visualize the data in different ways to find abnormal measurements and fix it. Data has to be normalized as per the ML models used. For example, all features of the dataset may to be normalized to a particular scale (e.g., all values between 0 and 1) as shown in

$$x_{\text{std}} = \frac{x - x_{\min}}{(x_{\max} - x_{\min})}, \quad (1)$$

$$x_{\text{scaled}} = x_{\text{std}} * (x_{\max} - x_{\min}) + x_{\min}. \quad (2)$$

Recent studies focus on applying machine learning techniques to time series forecasting through supervised learning. For this purpose, the data has to be prepared before feeding it as input to some machine learning model. Also, predicting a value in a time series is based on many previous values in the same time series, e.g.,  $y_T = f(x_1, x_2, \dots, x_{T-h})$ . Therefore, in order to give the model some temporal context, the inputs must be sequences of feature vectors and not just a single feature vector. The moving window approach is applied during the learning phase as the machine learning model expects many pairs of inputs and outputs, the number of sets  $n$  be contingent on the number of windows the time series is split up into which is evaluated to be  $T - s - h + 1$ , where the window size is represented as “ $s$ ” and forecasting horizon as “ $h$ .” The direct strategy for multistep forecasting is applied by training different models for each value of  $h$  [26].

The model will iterate through the mappings window by window and learn the temporal patterns throughout the time series. By the end of the learning phase, the model will be an approximation of the function  $f$  as shown below:

$$y(t+h) = f(x_{(t-n+1)}, x_{(t-n+2)}, \dots, x_{(t)}), \forall t \in \{n, n+1, \dots, T-h\}, \quad (3)$$

where  $f$  requires new inputs to also be sequences of size  $n$ . The output similar to the trained sequence during the learning phase will be produced when the new sequence of  $n$  inputs is fed into the model. The output will not be accurate if the input sequence does not resemble the learning phase inputs. This shows that the training data which was used

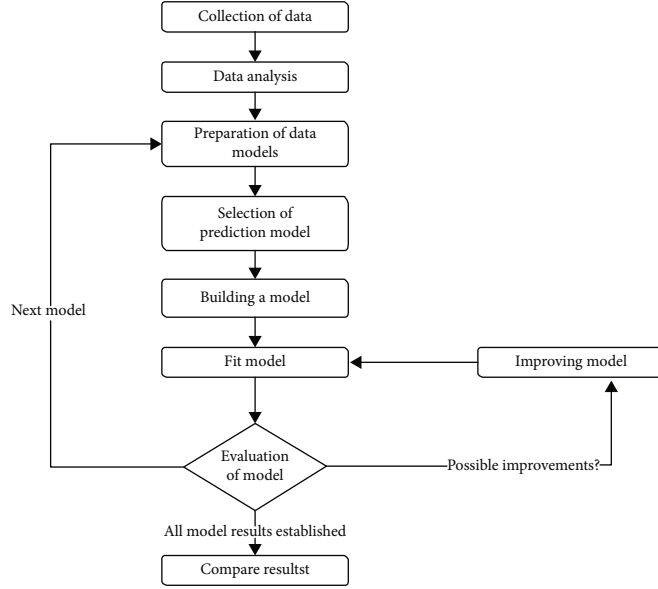


FIGURE 1: Flow of the proposed model.

for generalizing to the data in the test set has abnormal measurements. Machine learning models depend on many fixed parameters which do not directly belong to the model itself and remain constant throughout the learning phase. These are called hyperparameters. Tuning the hyperparameters helps in avoiding a poorly performing model. Optimization requires a trial-and-error approach which is usually a difficult task. A technique called grid search is often used to automate the process of empirically finding the best combination of hyperparameters [27].

### 3.2. Forecasting Models

**3.2.1. ARIMA.** ARIMA is one of the most commonly used time series prediction models and is a widely used statistical technique. Exponential smoothing is also used in time series forecasting in addition to the ARIMA model. Exponential smoothing model relies on trend and seasonality in data while ARIMA is responsible for describing the auto correlation in the data and for predicting future values for a prediction based on past time series values. The Auto-Regressive Integrated Moving Average (ARIMA) model, it is a linear model of regression using its own lags as predictors.

There are two kinds of ARIMA model that can be used for forecasting which are seasonal and nonseasonal. The ARIMA model norm is given as an  $ARIMA(x, y, z)$ , where  $x$  is the order of the AR term,  $y$  is the order of the Moving Average term, and  $z$  is the number of differentials that are necessary to stabilize the time series [28]. A time series property like mean and time variance is known stationary. The time series must be stationary in the ARIMA model. This concerns the disadvantage of using this prediction model because extremes, typical in traffic data sets, appear to be missed [29]. The previous value must be removed from the current value to make the sequence stationary. The complexity of the series therefore determines how many differences are necessary. Thus, the  $d$  value is the minimum number of

differences needed to stabilize the series, and if the time series is already stationary, then  $z = 0$ . The series should be over-differentiated, because it affects the parameter of the model. The “ $x$ ” parameter is the lag order that shows the number of lag observations in the model. The parameter “ $y$ ” is called the order that shows the moving average window size.

This model is defined by the differencing

$$C_t = \phi_1 c_{t-1} + \phi_2 c_{t-2} + \dots + \phi_x c_{t-x} + a_t - \theta_1 a_{t-1} + \dots - \theta_y a_{t-y}. \quad (4)$$

The model’s Equation (4) describes predicted  $C_t =$  Constant + Linear grouping Lags of  $C$  (upon  $x$  lags) + Linear Forecast error grouping (upon  $y$  lags),

where  $c$  is an overall sequence of times,  $C_t$  marks the time series forecast  $t$ ,  $c_{t-1} \dots c_{t-p}$  is the previous time series  $p$  values,  $\phi_1 \dots \phi_p$  is the coefficients for model fitting to be defined,  $a_t \dots a_{t-x}$  zero indicates white noise and is the stirring avg. term,  $\theta_1 \dots \theta_{t-x}$  is the coefficient for model fitting to be determined,  $x$  is the autoregression term numbers, and  $y$  is stirring avg. term numbers.

The combination of AR and MA with their respective  $x$  and  $y$  parameters defines the operation, known as  $ARIMA(x, y)$ , and is defined in Equation (5) as follows:

$$C_t = AR(x) + MA(y). \quad (5)$$

A pure AR model is where  $C_t$  relies only on its own lags, while  $C_t$  relies exclusively on the lagged prediction errors.

**3.2.2. VARMA.** For the production of linear forecasts for sets of time series variables, vector autoregression moving average models (VARMA) are used. ARIMA is generalized to several parallel time series. Linear forecasts are used in the assessment of nonlinear characteristics as a benchmark.

Consider  $K$  associated time series,  $y_t = (y_{1t}, \dots, y_{kt})$ : the vector autoregressive (VAR) form [30] in Equation (6) can

be a model for the conditional mean of data generation process (DGP) of the observed series.

$$y_t = A_1 y_{t-1} + \dots + A_p y_{t-p} + u_t, \quad (6)$$

where the coefficient matrices of  $A_i (i = 1, \dots, p)$  is  $(k \times k)$  and  $u_t$  is a term  $k$ -dimensional error. If  $u_t$  is time independent, the conditions of  $y_t$  are in Equation (7) given past observations

$$y_{t|t-1} = E(y_t | y_{t-1} \dots) = A_1 y_{t-1} + \dots + A_p y_{t-p}. \quad (7)$$

This model is therefore suitable for  $y$  for forecasting a time ahead and repetitively measuring predictions with wider horizons.

The VARMA modelling technique allowed for the modelling of many dependent time series, both cross-relationships and intercorrelations. Assume that  $z_t$  is a stationary  $k$ -dimensional presentation sequence, then the VARMA( $x, y$ ) models used in the forecast for each group can be defined as Equation (8) [31].

$$\phi(B)z_t = \phi_0 + \theta(B)a_t, \quad (8)$$

where “ $t$ ” represents period and  $\phi_0$  is a constant vector

$$\phi(B) = I_k - \sum_{i=1}^q \phi_i B_i, \quad (9)$$

$$\Theta(B) = I_k - \sum_{i=1}^q \theta_i B_i. \quad (10)$$

Two polynomial matrices of the  $x > 0$  and  $y > 0$  order, respectively, are represented by Equation (7). In Equations (9) and (10),  $B$  is an operator of a back-shift defined by  $B_{xt} = x_t - x_{t-1}$ , and  $a_t$  has an independent, equally distributed random sequence with a midnull covariation matrix and a positive-defined matrix  $\sum a$ .

VARMA can be expressed as Equation (11) for any two-time series  $z_{1t}$  and  $z_{2t}$ ,

$$\begin{bmatrix} z_{1t} \\ z_{2t} \end{bmatrix} - \begin{bmatrix} \phi_{11} & \phi_{12} \\ \phi_{21} & \phi_{22} \end{bmatrix} + \begin{bmatrix} z_{1t-1} \\ z_{2t-1} \end{bmatrix} = \begin{bmatrix} a_{1t} \\ a_{2t} \end{bmatrix} - \begin{bmatrix} \theta_{11} & \theta_{12} \\ \theta_{21} & \theta_{22} \end{bmatrix} * \begin{bmatrix} a_{1t-1} \\ a_{2t-1} \end{bmatrix}. \quad (11)$$

**3.2.3. Recurrent Neural Networks/LSTM.** Neural networks are a collection of algorithms designed for patterns to be identified by means of the interpretation of sensory data through interpretation, marking or grouping of raw data as shown in Figure 2.

The first phase in an advancing propagation is a neural network. The output is forecast by the network when an input is applied. The second stage is backpropagation, where the real learning takes place. Clanking fits well with conventional feedforward neural networks, but rather than evaluating input sequences, it is restricted to individual instances. Recurrent neural networks are based on neurons like feedfor-

ward neural networks, but, as shown in Figure 3, there are additional connections between layers.

The RNN architecture is depicted in Figure 3. There are one or more neurons in each square in the architecture, and each arrow is corresponding to a completely connected layer between the neurons on either side of the arrow. The left side shows the cyclically weighed RNN whereas the right side shows the over time, and the same network unrolls. Recurrent neural networks (RNN) are recurrent, as the functions used for every data input are the same, and the current input output is dependent on the last one. The output is copied into the recurrent network and returned as an input. It takes into account the present input and the output of the previous input. When using tanh as an activation method, RNN does not process very long sequences.

Long-term Short-Term Memory (LSTM) networks are an improved variant of recurring, deliberately designed to prevent the long-term issue of reliance. One of the inconveniences of RNN is also corrected here as a vanishing gradient problem. In view of time lags of uncertain length, LSTM is used to define, process, and forecast time series. In sequence prediction problems, it is able to learn order dependence [32].

LSTM architecture is shown in Figure 4.

The architecture, as shown in Figure 4, includes three cell gates—the forgotten gate, the input gate, and the output gate. These gates represent sigmoid functions which take values within the [0,1] range and transfer information to and from the cell. By descending the gradient, weight of the gates is balanced. Forget gate the sigmoid feature produces a 0 to 1 value which defines the amount of information to keep from the previous hidden state and current input. The sigmoid feature is used. In the cell state,  $C_{t-1}$  for each number is the predecessor state ( $h_{t-1}$ ) and the input ( $i_t$ ) and the output number between 0 and 1. The input gate selects the new data to be stored in the memory cell. A vector of new candidate values can be applied to the state in the tanh layer. The input gate is combined with the tanh layer to construct a state change. The tanh function weighs values between -1 and 1 to identify their significance. The old state is multiplied by  $f_i$  and the information we have forgotten before. Then, we add  $i_t * C_{new}^t$ . This is the current values of the candidate by how often each state value has been modified. The performance is finally dependent on the cell condition. The sigmoid function selects the values by [0,1], and the tanh function measures the values, so that their significance can be determined between -1 and 1 and multiplied by the sigmoid output.

Equations (12) to (17) of LSTM are as follows:

$$f_t = \sigma(W_f [h_{t-1}, X_t] + b_f), \quad (12)$$

$$i_t = \sigma(W_i [h_{t-1}, X_t] + b_i), \quad (13)$$

$$o_t = \sigma(W_o [h_{t-1}, X_t] + b_o), \quad (14)$$

$$C_t = f_i * C_{t-1} + i_t * C_{new}^t, \quad (15)$$

$$h_t = o_t * \tanh * C_t, \quad (16)$$

$$C_{new}^t = \tanh(W_c [h_{t-1}, X_t] + b_c). \quad (17)$$

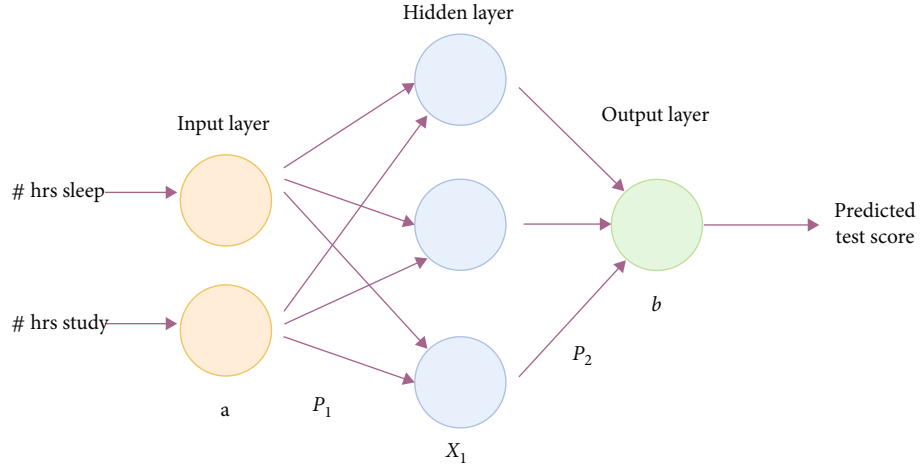


FIGURE 2: An example of a neural network.

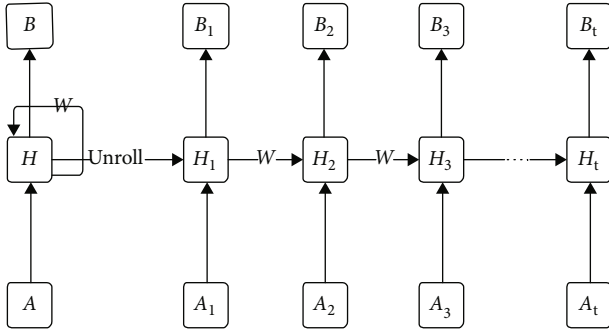


FIGURE 3: RNN architecture.

LSTM contains an actual memory that is not in the RNN architecture. When backed by depth, LSTM also retains a consistent error. It is anticipated that the LSTM network can yield the best results because it is suitable to time sequence problems. It is proposed that only if simpler conventional approaches fail can LSTM networks apply. LSTM is one of the most common methods for the prediction of time series statistics and machine learning.

**3.2.4. Feedforward Neural Network.** Any number of layers, units per layer, network inputs, and network outputs can be available for a neural network. Neural feedforward network (FNN) and the related training algorithm for backpropagation (BP). Neurons (i.e., processing units) are placed in the form of layers in a feedforward neural network.

In Figure 5, this is a 3-layer feedforward network, which consists of 4 units in the first (layer A), 3 units in second (layer B), known as hidden layers, and 3 units (layer C) known to be a layer known as output layer. There are four network inputs and one network output in the respective network.

A unit is equivalent to the inputs of network inputs. As shown in Figure 5, weight is altered in each network-input/unit-to-unit and unit-to-unit relation. Each unit has one additional input and one constant. The bias is the weight that modifies this additional data. It is called feeding as all data

propagates from the network inputs to the network outputs along the connections [33].

$$O_c = h\text{Hidden} \left( \sum I_c, p Wc, p + bc \right), \quad (18)$$

$$h\text{Hidden}(x) = \frac{1}{(1 + e^{-yx})}. \quad (19)$$

In Equations (18) and (19),  $O_c$  is the latest hidden layer unit  $c$  output, either  $P$  is number of units in the past hidden layer or in the number inputs of network,  $I_c, p$  is an input to  $c$  from either the hidden unit  $p$  of the previous layer or the network input  $p$ ,  $Wc, p$  is the weight by which either unit  $p$  to unit  $c$  or  $p$  to unit  $c$  is altered, and  $b_c$  is the bias.  $H$   $\text{Hidden}(x)$  is the unit's sigmoid enhancer. The  $y$  controls the slope of the feature constantly. Equation (20) gives the network input to the  $j$  processing unit

$$\text{net}_j = \sum_i x_i w_{ij} + \theta_j, \quad (20)$$

where  $x_i$ 's is the output of the previous layer,  $w_{ij}$  is the weight, which specifies the position of the sigmoid, of the relation unit  $i$  to  $j$ , and  $\theta_j$  is the weight of the bias.

A neural feed network primarily operates with established examples by forming the network. Based on the difference between  $o_p$  and  $y_p$ , a performance criterion function is defined. The sum of the squared error (SSE) function in Equation (21) is a widely used criterion function

$$F = \sum_p F_p = 1/2 \sum_p \sum_k \left( y_{pk} - o_{pk} \right)^2, \quad (21)$$

where  $p$  is the model index and  $k$  the output unit index. The output layer error is restored via the network, and the

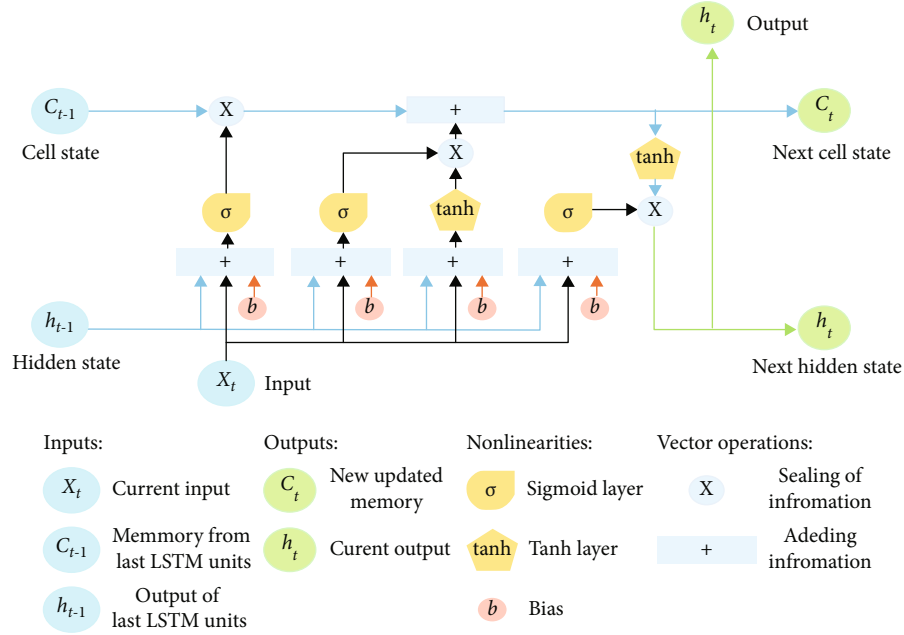


FIGURE 4: Architecture of LSTM.

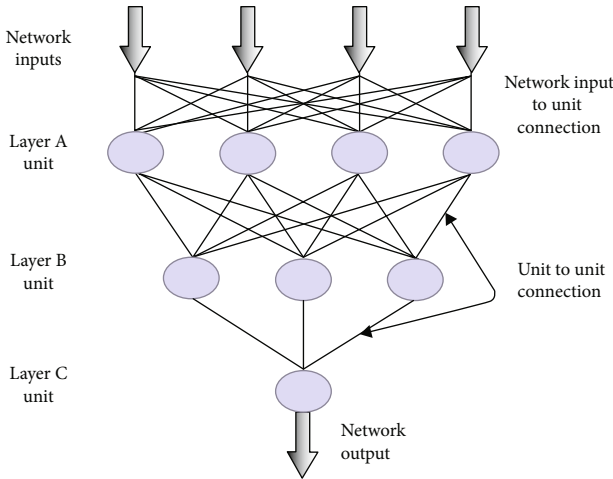


FIGURE 5: Architecture of feedforward network.

weights ( $w_{ij}$ ) are updated based on their contribution to the error function shown in

$$\Delta w_{ij} = -\frac{\eta \delta F}{\delta w_{ij}}, \quad (22)$$

where  $\eta$  is called learning rate; the phase size of the weight is determined during the update.

#### 4. Experimental Results Analysis and Discussion

In this section, we carry out experimental research to examine the efficiency in real traffic data sets of ARIMA and LSTM driven prediction models. Network service provider and traffic data from the UCI library were collected in 11 cities.

TABLE 1: Results of Dickey-Fuller test.

Test statistic	-1.025742e+01
$p$ value	4.324537e-18
#lags used	3.100000e+01
Number of observations used	4.968000e+03
Critical value (1%)	-3.431667e+00
Critical value (5%)	-2.862122e+00
Critical value (10%)	-2.567080e+00
dtype	Float64

**4.1. Experimental Setup.** With varied durations of training sets, lengths of future predictions, feature sets used in learning and prediction, and so on, the suggested methodology is implemented on a single computer using Python. By utilizing Python to create a time series model, we can capture more of the data's complexity and incorporate all of the data pieces that are relevant. Adjustments to different measurements are also made possible which makes it potentially more accurate.

**4.2. Experimental Results.** In this section, we present the traffic forecasting performance results in following subsections, including time series collection at regular intervals, converting the time series into stationary time series, converting to supervised and then applying time series algorithm, evaluating the performance accuracy by using root mean square error (RMSE),  $R$ -squared score, mean absolute error (MAE), and mean absolute percent error (MAPE) performance indicators.

In linear forecasts of fixed time series variables, vector autoregression moving averages (VARMA) can be used. Several time series based on each other are modelled. The

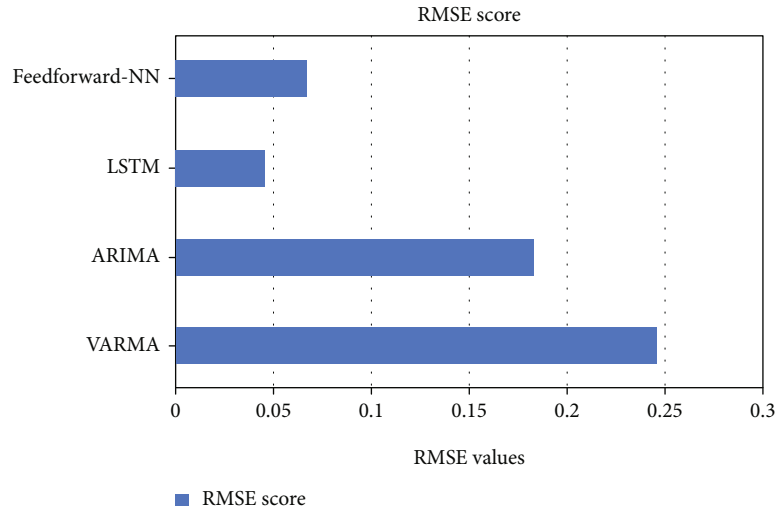


FIGURE 6: Comparing the RMSE scores of all the applied models.

interrelationships of the series are accounted for both. In the following step, each time series with an ARIMA model is modelled. Therefore, for multivariate stationary sequences, this model can be called the generalization of ARIMA. The vector autoregression moving average (VARMA) is a mixture between VAR and VMA and a generalized ARIMA model for stationary multivariate time sets. It is defined by parameters “ $x$ ” and “ $y$ .” It is similar to ARIMA, which is able to behave as an AR model by setting “ $y$ ” as 0 and “ $x$ ” as 0 as an MA model. Thus, VARMA is also able of interim like VAR model by setting “ $y$ ” to 0 and as a VMA model by setting “ $x$ ” to 0.

When we work with LSTM, the series data can be used as it is or can be converted to supervised learning data using “`shift()`” function of the Pandas. Both the methods mentioned above are applied in our project. Hence, we have used two implementations of LSTM.

The DataFrame is created by inserting columns from the front and assigning NaN values to the inserted columns or inserting columns at the end and filling NaN values at the end. This process is accomplished using the `shift()` function. The `shift()` function will produce lag observation columns and prediction observation columns for the time series data set in a controlled learning format. Once all the comments are passed down, a new row is added to top. The new inserted row does not have information, so NaN represents “zero.” The moved column with the aid of the shift feature is inserted next to our original sequence. New time series problem frameworks are generated using the `shift()` function on Pandas from the desired input and output sequence length. Pandas are a helpful tool in that it helps us to explore various framings of a time series problem using machine learning algorithms for model performance.

The data points obtained are called time series at constant intervals. Time series are analyzed to assess the long-term patterns in order to predict the future or do some other research. The two factors which distinguish a time series from a normal regression problem are as follows: (1) The lin-

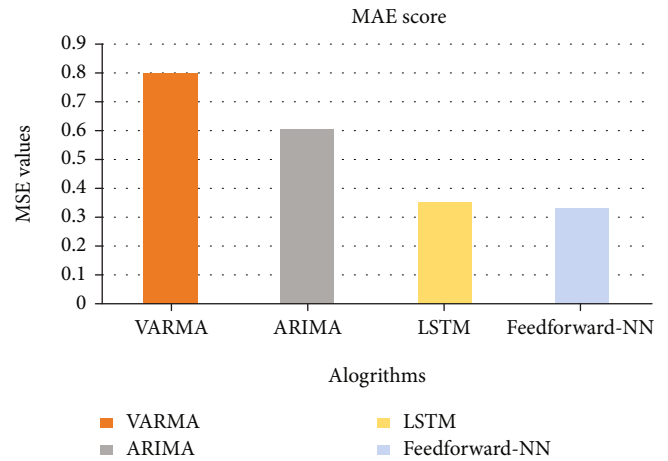


FIGURE 7: Comparing the MAE scores of all the applied models.

ear model of regression is time-independent, and the time series depends on the time. (2) Time series have certain seasonal trends that are unique to a specific timing. By constructing a time series model using Python, we can understand the dynamics of the data more easily and include all the important data elements. Adjustments are often made to various dimensions which can make it more precise.

The time series must be converted into a time series (TS). It says that time series is stationary because of their statistical properties, such as average and variation according to their ability to stay continuous overtime. Most models of the time range presume that the time range is stationary [34]. If the time series plans to carry out a specific action over an era, it is likely to be the same in the future. Many studies in connection with stationary series often claim queer and simpler to deploy stationary time series in comparison with other non-stationary series. Stationary behavior is determined using certain fixed criteria’s. However, practically the time series is assumed to be stationary if it has constant statistical

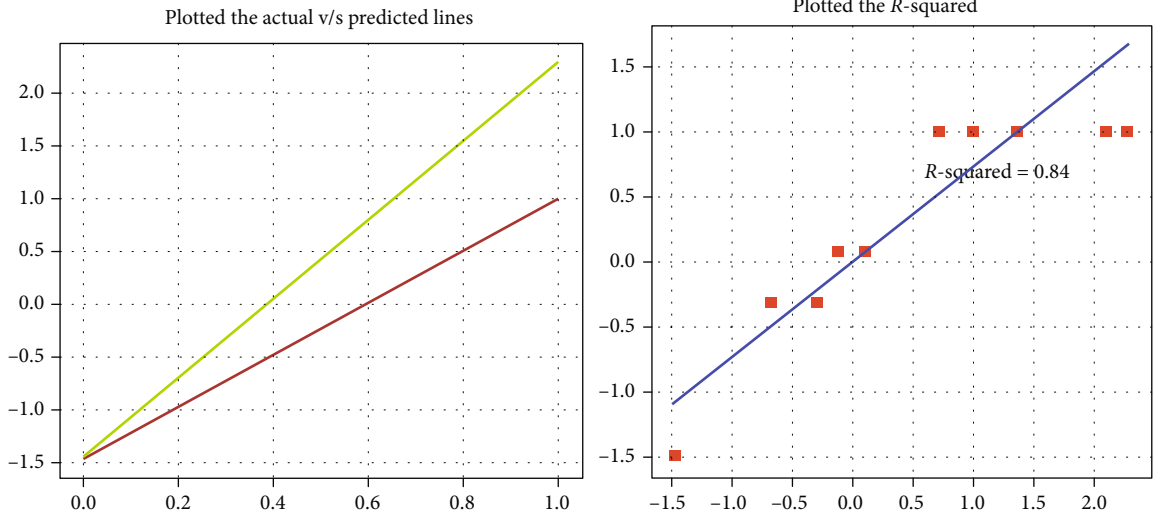


FIGURE 8: The predicted traffic values and R-squared values for ARIMA.

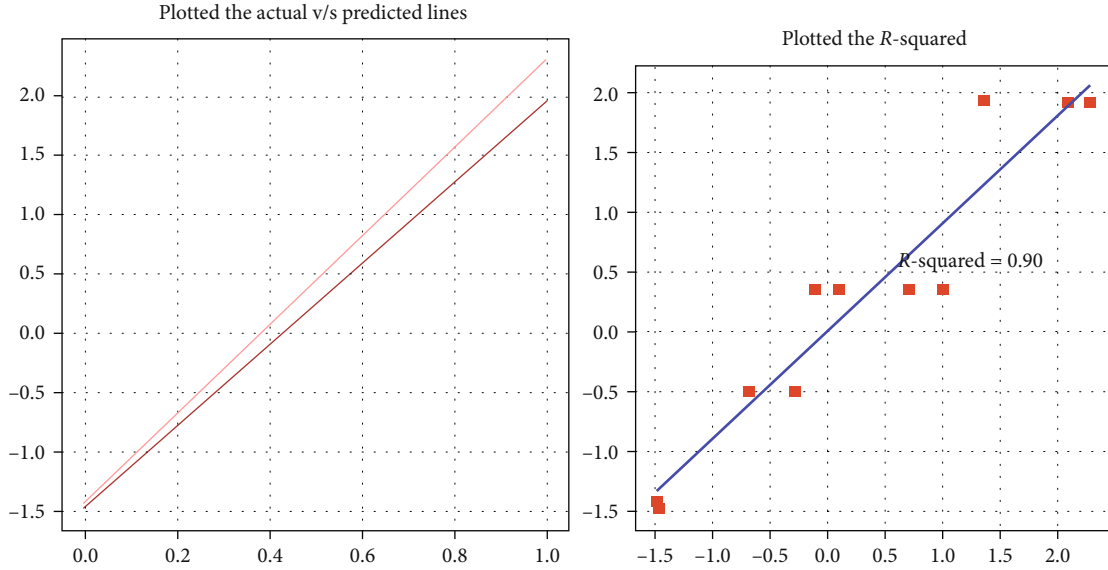


FIGURE 9: The predicted traffic values and R-squared values for LSTM.

properties that does not change overtime and that does not depend on time. In order to determine the statistical properties considered are as follows: (1) constant mean, (2) constant variance, and (3) self-covariance. Consequently, most time series used in the forecast models are stationary, or the time series must be stationary in order to suit a model. Visualization and the Augmented Dickey-Fuller (ADF) test are the two typical methods for the control of the time series stationarity.

As shown in Table 1, according to an interpretation of the results of the time series statistical analysis, there have been even fewer differences in the mean and standard deviation in magnitude in the time series listed. From the observation, it is shown that the test statistic is smaller than the 1% critical value. There are no missing values in the data observed as all

values from starting are given weights. Therefore, this data will work even with fresh values.

4.3. *Statistical Performance Evaluation.* The accuracy of the traffic prediction models has been evaluated by mean absolute error (MAE), rooted mean squared error (RMSE), and R-squared values.

$$\begin{aligned} \text{MAE} &= 1/\xi \sum_{i=1}^{\xi} |y_i - Y_i|, \\ \text{RMSE} &= \sqrt{1/\xi \sum_{i=1}^{\xi} (y_i - Y_i)^2}, \end{aligned} \quad (23)$$



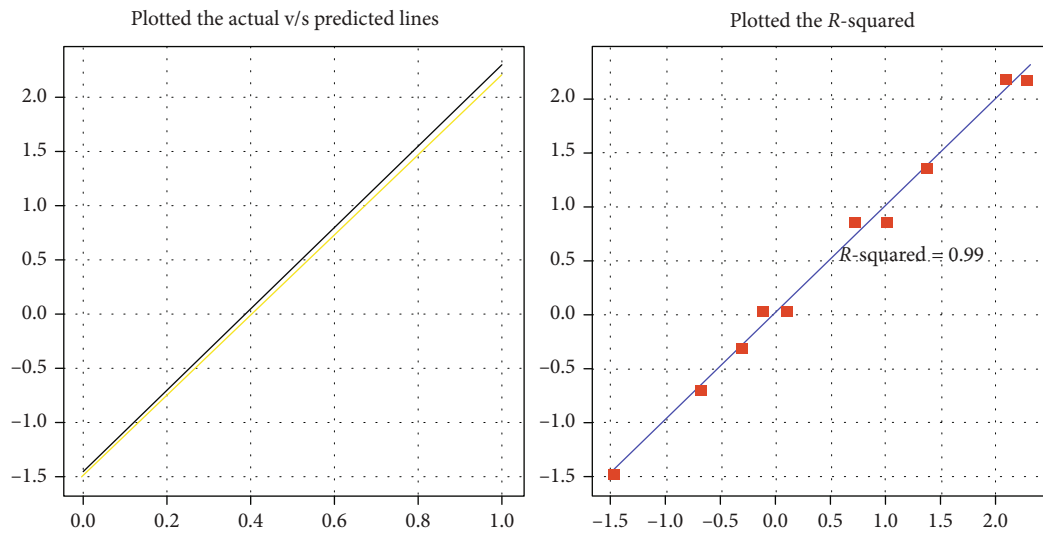


FIGURE 10: The predicted traffic values and R-squared values for feedforward-NN.

where  $y_i$  and  $Y_i$  denote the predicted value and the ground truth of region  $i$  for predicted time step and  $\xi$  is the total number of samples.

Figure 6 shows the RMSE values attained by various algorithms taken up for the research study for prediction of IoT traffic. The scores reveal that LSTM and feedforward-NN give better accuracy over ARIMA and VARMA.

The prediction results clearly show that the accuracy of prediction strongly depends on the training dataset, standardization of data, statistical evaluation, and the feature set used in the learning scheme. The results in Figure 7 indicate that the reframed LSTM and feedforward-NN are performing significantly better than other forecasting models such as VARMA and ARIMA.

It can be observed from Figures 8–10 that the highest accuracy in predicted and actual values is given by feedforward-NN, then at slight difference by reframed LSTM over the accuracy produced by ARIMA.

## 5. Conclusion and Future Scope

Prediction of IoT traffic in the recent years has attracted an insightful attention for enhancing resource and bandwidth utilization. This paper is focusing on the study of the problem of IoT traffic prediction by employing machine learning, deep learning, and statistical time series-based prediction methods including LSTM, ARIMA, VARMA, and feedforward neural networks. In the different traffic intervals and architecture parameters, a comparative study of prediction models on the basis of statistical learning has been performed. In the prediction of futuristic IoT-based traffic, the LSTM model and FNN model have shown the considerable accuracy over the conventional models such as VARMA and ARIMA. Our experiment results demonstrate that the LSTM and feedforward neural networks (FNN) exhibit more accurate predictions as compared to the other methods considered for comparative study on the basis of statistical parameters such as RMSE score, MAE score, and R-squared

values. The future scope of the research is to design algorithms which can consider all dynamic parameters of IoT environment and can predict the upcoming traffic with more accuracy.

## Data Availability

Data are available on request.

## Conflicts of Interest

The authors declare no conflicts of interest.

## References

- [1] I. A. T. Hashem, V. Chang, N. B. Anuar et al., "The role of big data in smart city," *International Journal of Information Management*, vol. 36, no. 5, pp. 748–758, 2016.
- [2] N. Naik, "Choice of effective messaging protocols for IoT systems: MQTT, CoAP, AMQP and HTTP," in *2017 IEEE International Systems Engineering Symposium (ISSE)*, pp. 1–7, Vienna, Austria, 2017.
- [3] G. K. Saini, H. Chouhan, S. Kori et al., "Recognition of human sentiment from image using machine learning," *Annals of the Romanian Society for Cell Biology*, vol. 25, no. 5, pp. 1802–1808, 2021.
- [4] A. Dogra, A. Kaur, and M. Shabaz, "Data collection for classification in IOT and heart disease detection," *Annals of the Romanian Society for Cell Biology*, vol. 25, no. 4, pp. 2954–2964, 2021.
- [5] N. Hung, S. Thomas, Y. Taku, and M. Takumi, "Generating IoT traffic: a case study on anomaly detection," in *Proceedings of the IEEE International Symposium on Local and Metropolitan Area Networks (LANMAN)*, pp. 1–6, Orlando, FL, USA, 2020.
- [6] U. Cisco, *Cisco Annual Internet Report (2018–2023)*, White Paper, 2020.
- [7] S. Wu, W. Mao, C. Liu, and T. Tang, "Dynamic traffic prediction with adaptive sampling for 5G HetNet IoT applications,"

- Wireless Communications and Mobile Computing*, vol. 2019, 11 pages, 2019.
- [8] J. Mejia, A. Ochoa-Zezzati, and O. Cruz-Mejia, "Traffic forecasting on mobile networks using 3D convolutional layers," *Mobile Network and Applications*, vol. 25, no. 6, pp. 2134–2140, 2020.
  - [9] A. Essien, I. Petrounias, P. Sampaio, and S. Sandra, "A deep-learning model for urban traffic flow prediction with traffic events mined from Twitter," World Wide Web, 2021.
  - [10] A. Volkov, A. R. Abdellah, A. Muthanna, M. Makolkina, A. Paramonov, and A. Koucheryavy, "IoT Traffic Prediction with Neural Networks Learning Based on SDN Infrastructure," in *Distributed Computer and Communication Networks. DCCN 2020*, V. M. Vishnevskiy, K. E. Samouylov, and D. V. Kozyrev, Eds., vol. 12563, pp. 64–76, Springer, 2020.
  - [11] G. Meena, D. Sharma, and M. Mahrishi, "Traffic prediction for intelligent transportation system using machine learning," in *2020 3rd International Conference on Emerging Technologies in Computer Engineering: Machine Learning and Internet of Things (ICETCE)*, pp. 145–148, Jaipur, India, 2020.
  - [12] J. Feng, X. Chen, R. Gao, M. Zeng, and Y. Li, "DeepTP: an end-to-end neural network for mobile cellular traffic prediction," *IEEE Network*, vol. 32, no. 6, pp. 108–115, 2018.
  - [13] Y. Hua, Z. Zhao, Z. Liu, X. Chen, R. Li, and H. Zhang, "Traffic prediction based on random connectivity in deep learning with long short-term memory," in *2018 IEEE 88th Vehicular Technology Conference (VTC-Fall)*, pp. 1–6, Chicago, IL, USA, 2018.
  - [14] Y. Wang, Y. Guo, Z. Wei, Y. Huang, and X. Liu, "Traffic flow prediction based on deep neural networks," in *2019 International Conference on Data Mining Workshops (ICDMW)*, pp. 210–215, Beijing, China, 2019.
  - [15] C. Zhang, P. Patras, and H. Haddadi, "Deep learning in mobile and wireless networking: a survey," *IEEE Communications Surveys & Tutorials*, vol. 21, no. 3, pp. 2224–2287, 2019.
  - [16] A. R. Abdellah, O. A. K. Mahmood, A. Paramonov, and A. Koucheryavy, "IoT traffic prediction using multi-step ahead prediction with neural network," in *2019 11th International Congress on Ultra Modern Telecommunications and Control Systems and Workshops (ICUMT)*, pp. 1–4, Dublin, Ireland, 2019.
  - [17] A. Essien and C. Giannetti, "A deep learning framework for univariate time series prediction using convolutional LSTM stacked autoencoders," in *2019 IEEE International Symposium on INnovations in Intelligent SysTems and Applications (INISTA)*, pp. 1–6, Sofia, Bulgaria, 2019.
  - [18] S. J. Kamble and M. R. Kounte, "Machine learning approach on traffic congestion monitoring system in Internet of Vehicles," *Procedia Computer Science*, vol. 171, pp. 2235–2241, 2020.
  - [19] F. Tang, Z. M. Fadlullah, B. Mao, and N. Kato, "An intelligent traffic load prediction-based adaptive channel assignment algorithm in SDN-IoT: a deep learning approach," *IEEE Internet of Things Journal*, vol. 5, no. 6, pp. 5141–5154, 2018.
  - [20] D.-B. Nguyen, C.-R. Dow, and S.-F. Hwang, "An efficient traffic congestion monitoring system on Internet of Vehicles," *Wireless Communications and Mobile Computing*, vol. 2018, 17 pages, 2018.
  - [21] N. G. Polson and V. O. Sokolov, "Deep learning for short-term traffic flow prediction," *Transportation Research Part C: Emerging Technologies*, vol. 79, pp. 1–17, 2017.
  - [22] C. Huang, C. Chiang, and Q. Li, "A study of deep learning networks on mobile traffic forecasting," in *2017 IEEE 28th Annual International Symposium on Personal, Indoor, and Mobile Radio Communications (PIMRC)*, pp. 1–6, Montreal, QC, Canada, 2017.
  - [23] R. Li, Z. Zhao, J. Zheng, C. Mei, Y. Cai, and H. Zhang, "The learning and prediction of application-level traffic data in cellular networks," *IEEE Transactions on Wireless Communications*, vol. 16, no. 6, pp. 3899–3912, 2017.
  - [24] X. Luo, R. Shen, J. Hu, J. Deng, L. Hu, and Q. Guan, "A deep convolution neural network model for vehicle recognition and face recognition," *Procedia Computer Science*, vol. 107, pp. 715–720, 2017.
  - [25] F. Xu, Y. Lin, J. Huang et al., "Big data driven mobile traffic understanding and forecasting: a time series approach," *IEEE Transactions on Services Computing*, vol. 9, no. 5, pp. 796–805, 2016.
  - [26] G. Bontempi, S. B. Taieb, and Y. A. L. Borgne, "Machine Learning Strategies for Time Series Forecasting," in *European business intelligence summer school*, M. A. Aufaure and E. Zimányi, Eds., vol. 138, pp. 62–77, Springer, 2013.
  - [27] A. Géron, *Hands-On Machine Learning with Scikit-Learn and TensorFlow*, O'Reilly Media, Inc., 2017.
  - [28] K. Li, C. Zhai, and J. Xu, "Short-term traffic flow prediction using a methodology based on ARIMA and RBF-ANN," in *2017 Chinese Automation Congress (CAC)*, pp. 2804–2807, Jinan, China, 2017.
  - [29] C. Giannetti, A. Essien, and Y. O. Pang, *A Novel Deep Learning Approach for Event Detection in Smart Manufacturing*, CIE49 proceedings, 2019.
  - [30] L. Helmut, "Chapter 6 Forecasting with VARMA Models," *Handbook of Economic Forecasting*, vol. 1, pp. 287–325, 2006.
  - [31] P. Aboagye-Sarfo, Q. Mai, F. M. Sanfilippo, D. B. Preen, L. M. Stewart, and D. M. Fatovich, "A comparison of multivariate and univariate time series approaches to modelling and forecasting emergency department demand in Western Australia," *Journal of Biomedical Informatics*, vol. 57, pp. 62–73, 2015.
  - [32] F. I. Facultit, Y. Bengio, P. Frasconi, and J. Schmidhuber, "Gradient flow in recurrent nets: the difficulty of learning long-term dependencies," in *A Field Guide to Dynamical Recurrent Neural Network*, IEEE Press, 2001.
  - [33] Z. Tang and A. F. Paul, "Feedforward neural nets as models for time series forecasting," *INFORMS Journal on Computing*, vol. 5, no. 4, pp. 374–385, 1993.
  - [34] M. Abbasi, A. Shahraki, and A. Taherkordi, "Deep learning for network traffic monitoring and analysis (NTMA): a survey," *Computer Communications*, vol. 170, pp. 19–41, 2021.

## Research Article

# Design and Simulation of Capacitive MEMS Switch for Ka Band Application

Vinay Bhatia <sup>1</sup>, Sukhdeep Kaur <sup>1</sup>, Kuldeep Sharma <sup>1</sup>, Punam Rattan <sup>2</sup>,  
Vishal Jagota <sup>3</sup> and Mohammed Abdella Kemal <sup>4</sup>

<sup>1</sup>Department of Electronics and Communication Engineering, CGC-CEC Landran, Punjab, India

<sup>2</sup>Punjab Technical University, Punjab, India

<sup>3</sup>Department of Mechanical Engineering, Madanapalle Institute of Technology & Science, AP, India

<sup>4</sup>Arba Minch University, Ethiopia

Correspondence should be addressed to Mohammed Abdella Kemal; [abdella.kemal@amu.edu.et](mailto:abdella.kemal@amu.edu.et)

Received 13 May 2021; Revised 13 June 2021; Accepted 29 June 2021; Published 13 July 2021

Academic Editor: Vimal Shanmuganathan

Copyright © 2021 Vinay Bhatia et al. This is an open access article distributed under the Creative Commons Attribution License, which permits unrestricted use, distribution, and reproduction in any medium, provided the original work is properly cited.

In this paper, RF MEMS switch with capacitive contact is designed and analyzed for Ka band application. A fixed-fixed beam/meander configuration has been used to design the switch for frequency band 10 GHz to 40 GHz. Electromagnetic and electromechanical analysis of three-dimensional (3D) structure/design has been analyzed in multiple finite element method (FEM) based full-wave simulator (Coventorware and high-frequency structure simulator). A comparative study has also been carried out in this work. The high resistivity silicon substrate ( $\tan \delta = 0.010$ ,  $\rho > 8 \text{ k}\Omega\text{-cm}$ ,  $\epsilon_r = 11.8$ ) with a thickness of  $675 \pm 25 \mu\text{m}$  has been taken for switch realization. The designed structure shows an actuation voltage of around 9.2 V. Impedance matching for the switch structure is well below 20 dB, loss in upstate, i.e., insertion loss  $>0.5 \text{ dB}$ , and isolation of  $>25 \text{ dB}$  throughout the frequency band is observed for the aforesaid structure. Furthermore, to increase the RF parameters, AlN dielectric material has been used instead of  $\text{SiO}_2$  resulting in capacitance in downstate that increases hence improved the isolation. The proposed switch can be utilized in various potential applications such as any switching/tunable networks phased-array radar, reconfigurable antenna, RF phase shifter, mixer, biomedical, filter, and any transmitter/receiver (T/R) modules.

## 1. Introduction

The Micro-Electro-Mechanical-System (MEMS) is an agglomeration of submicron mechanical moving parts and electronics components/elements on a single module/chip [1]. In the last 20 years, MEMS has spread into the RF regime also. RF MEMS switches are building blocks for this technology, without the existence of these switches; RF MEMS seems to be unimaginable [1, 2]. Nowadays, RF MEMS capacitive shunt switch has a major role for designing in an advanced communication application. RF MEMS switches are preferable to design filters, reconfigurable microwave antenna, and space communication than solid-state switch like field-effect transistor (FET) and PIN diode. RF MEMS switches based on MEMS technology offer many advantageous over

solid-state switches, for example, high isolation, low insertion loss, zero DC power consumption, low noise, more linearity, and used up to millimeter wave [2–4]. MEMS technology-based RF switches have the advantages of miniaturization, monolithically integrated with other IC using batch processing technology as compared to other conventional switches. The performance of the RF MEMS shunt switch depends upon the material used for the membrane and also depends upon return loss, pull-in voltage, insertion loss, isolation, and switching time [1]. Metal-metal contact in the switch creates the stiction problem in the switch. Based on MEMS technology, RF MEMS switches have two types such as shunt switch and series switch [3]. These series and shunt configuration further classified as a capacitive switch and resistive switch base upon contact [2]. Series switches are used for a

low-frequency application due to poor isolation, while for a higher frequency of application, capacitive switches are used. In capacitive type contact MEMS switch, a dielectric layer is used between the top beam and bottom electrodes for isolation. The structure of the membrane can be bridge type or cantilever type or dip harm type [3–6]. The actuation voltage of the switch structure can be minimized with bridge structure supporting meanders and step type [1–4]. MEMS-based switches are superior in terms of their RF performances over conventional electromagnetic relays and solid-state switches [5–8]. As per the configuration, the switch can be broadly classified into two categories, i.e., series and shunt [1, 2]. Generally, series switch utilizes metal-metal contact, while shunt switches are mostly capacitive in nature [9]. Some sort of actuation force is needed to make these switches work. Although several actuation mechanisms are there, the electrostatic actuation technique is extensively used due to its negligible DC power consumption, short switching time, and compatibility with IC technology [1, 2, 10]. The reliability of space systems is of utmost importance for their smooth operation over a period of 10-15 years of satellite life. A single point failure may cause catastrophe for the whole mission. So, each and every component, be in launch vehicle or communication systems need to be highly reliable [8, 11, 12]. Metal contact reliability in series switches has always been a concern during long-term reliability tests [13]. A switch based on metal-metal contact normally suffers from various issues like electromigration, stiction, metal creep, dielectric charging, and fatigue over a period of time [12, 14]. Stiction issue in MEMS switch occurs, when surface adhesive forces are larger than the restoring force of the beam structure [15]. Electromigration is a high current density phenomenon which causes voids in metal lines. While creep describes the trends of a material to deform or to move permanently to relieve stresses, resulting in a long-term revelation to levels of stresses due to material deformation, which are below the yield or final strength of the material [8, 14]. Keeping in mind all the abovementioned issues associated with metal contact switches, capacitive contact switch was taken into consideration [8]. A MEMS capacitive shunt switch serves as a two-state digital capacitor: a smaller capacitance (fF) is obtained while the switch is in up position, while a larger capacitance value of capacitor (pF) results in downstate of the switch [1, 2]. Generally, RF MEMS capacitive switch uses silicon nitride as dielectric layer due to its medium dielectric constant ( $\epsilon_r = 7.5$ ), which provides the isolation between both electrodes [16]. Other dielectric material such as  $\text{TiO}_2$  ( $\epsilon_r = 32$ ), strontium titanate oxide ( $\epsilon_r = 120$  [16]), hafnium dioxide ( $\text{HfO}_2$ ,  $\epsilon_r = 25$  [17]), piezoelectric lead zirconate titanate (PZT,  $\epsilon_r = 190$  [18]), and aluminium nitride (AlN,  $\epsilon_r = 9.8$  [19]) can also be utilized because of high dielectric constant in place of silicon nitride layer for impressive RF performance.

Many researchers and industries around the globe have reported various RF MEMS switches using different materials with various technologies and by varying the electromechanical and RF parameters. Somayye et al. developed the shunt switch with reduced air gap using step structure, and AlN dielectric layer is used instead of  $\text{SiO}_2$  and  $\text{Si}_3\text{N}_4$  for

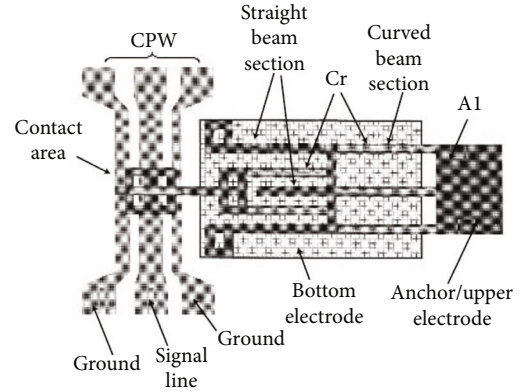


FIGURE 1: Fabricate capacitive shunt switch National Taiwan University [1].

improved isolation, i.e., -58 dB. Chan et al. have developed the DC contact switch using GaAs substrate at National Taiwan University as shown in Figure 1. In this switch, the coplanar waveguide (CPW) line and center conductor are fabricated using gold material and  $\text{SiO}_2$  was used as a dielectric layer. The authors reported the return loss  $>20$  dB, isolation of  $>20$  dB, and actuation voltage around 26-30 V [15–23].

Furthermore, Guo et al. [24] developed the low actuation voltage MEMS switch by utilizing aluminum alloys for movable beam. The designed switch shows the low pull-in voltage of 5 V for alloy instead of gold material, i.e., 45 V. Rao et al. fabricate the MEMS switch using the clamped-clamped structure of gold beam having thickness  $500 \text{ \AA}$ , and the dielectric layer of AlN is deposited by plasma-enhanced chemical vapor deposition (PECVD) process. The authors reported the actuation voltage of 5.5 V and behaviors of dielectric charging to characterize by the capacitance-voltage (CV) curve method. Goel et al. developed the MEMS series switch having low actuation voltage, improved RF performance for reconfigurable antenna, and sufficient switching speed. The authors reported the pull-in voltage of 5 V with return loss  $>20$  dB and insertion loss  $>0.4$  dB from DC to 60 GHz. Further, the capacitive shunt switch was fabricated on a four-mask silicon wafer by utilizing surface micromachining process technology to report the low actuation voltage. The PECVD is used to deposit a thin AlN dielectric layer to improve isolation in the downstate due to a high dielectric constant. Therefore, Thelluir et al. developed the low pull-in voltage MEMS switch using gold as a beam material with improved RF performance. Chu et al. fabricate the MEMS switch on GaAs substrate using a pull-in electrode and inline cantilever beam to achieve “On” and “Off” states as shown in Figure 2. In this train, spaced holes are etched into cantilever beam to achieve the lower pull-in voltage. The measured insertion loss of  $>3$  dB and isolation of  $>20$  dB in the frequency range 1-40 GHz was reported.

## 2. RF Actuation Mechanism

Mechanical actuation and electrical actuation are two parts of the RF MEMS switch. Mechanical movement can be realized

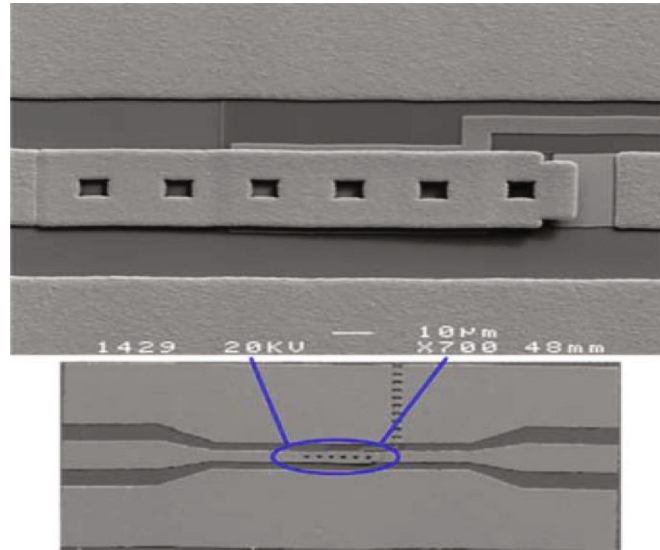


FIGURE 2: Scanning electron microscope image of DC contact switch developed by Chu et al. [17].

TABLE 1: Different actuation techniques for MEMS switch.

Technology	Contact force ( $\mu\text{N}$ )	Current (mA)	Size	Voltage (V)	Switching time ( $\mu\text{s}$ )	Power (mW)
Magnetostatic	50-200	20-150	Medium	3-5	400-1000	0-100
Thermal	500-3500	5-100	Large	3-5	200-10,000	0-200
Piezoelectric	50-250	0	Medium	3-20	50-500	0
Electrostatic	50-1500	0	Small	20-80	1-200	0

by piezoelectric, electromagnetic, electrostatic, and thermal mechanisms. The common approach used now days is electrostatic actuation mechanism, due to its advantages like low DC power consumption, low switching speed, thin layers of material, wide range of contact forces of 50–200  $\mu\text{N}$ , and most importantly tiny electrode size. Its ON-OFF capacitance ratio is also very high, but a higher actuation voltage is required. In comparison to electromagnetic actuation, voltage requirement is low but current consumption is high. Coil and ferromagnetic armature are used as an electromagnetic actuator in electromagnetic actuation. In this type of mechanism, semihard magnetic materials or permanent magnets allow the addition of a self-latching mechanism. The example of MEMS device that uses this mechanism is a micromechanical relay. A thermal actuator can also be used to simplify the relay. Thermal actuators include the armature of a soft magnetic material, permanent magnets, and thermo-sensitive magnetic materials stators. The piezoelectric mechanism depends upon the piezoelectric effect, and it provides exceptional material characteristics, where elastic deformation is generated by electrical field stimulation. To actuate ON or OFF conditions, a downward force is created by attaching a designed piezoelectric actuator to switch the membrane. Reduced pull-in voltage may be obtained by enabling the switch to have a high force by using this mechanism. This high force permits the air gap height to be increased with no reduction in another parameter of the

switch such as critical stress and switching speed. The switch can also be actuated by using a thermal actuation mechanism. This actuation mechanism includes the thermal microactuators. For example, two thick metal posts are linked with the two thermal actuators which act as the centerline of the CPW transmission line, and the MEMS switch may be trigger ON and OFF by utilizing current or voltage pulses. A very few researchers had been developed the MEMS switch using thermal actuation with a huge contact force and large beam spring constant to achieve the low contact resistance and hence enhance the power handling capacity. Table 1 shows the comparisons between four actuation technologies, which are used to actuate the RF MEMS switch.

### 3. Design and Working Principal

A high resistive silicon wafer (thickness of  $675 \pm 20 \mu\text{m}$ , dielectric constant and 11.8) has been used for the development of MEMS switch using fixed-fixed beam configuration. Figures 3(a) and 3(b) show the cross-section view of the proposed MEMS capacitive switch in upstate position and downstate position, respectively. The coplanar waveguide transmission line with dimension (G/W/G) of 90/120/90 (all in  $\mu\text{m}$ ) is designed to support the RF MEMS switch whose characteristics impedance is  $50 \Omega$ . The grounds of the CPW line are connected to both ends of the MEMS

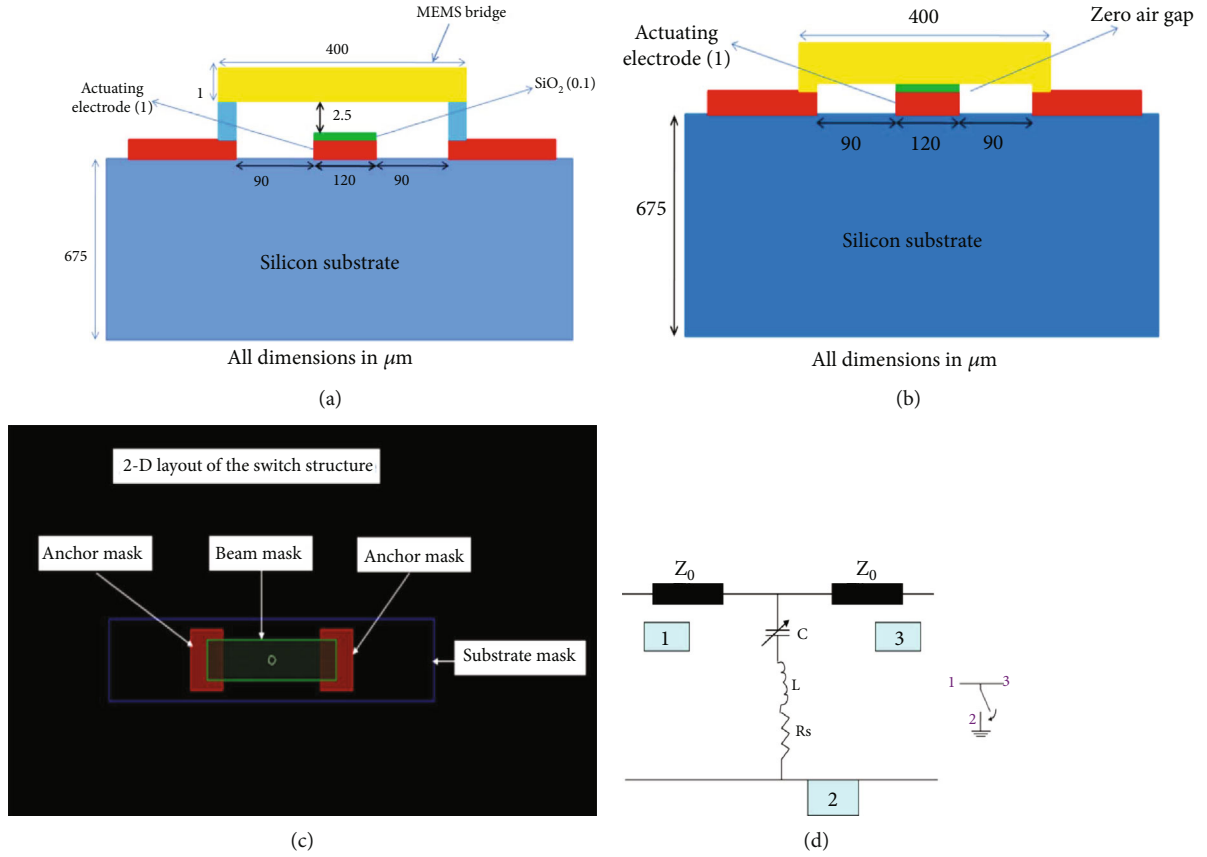


FIGURE 3: (a) Cross-section view of MEMS capacitive switch in upstate (b) in downstate position. (c) 2D layout of switch structure in Coventorware. (d) Electrical equivalent model of switch in downstate.

switch through the anchors. The material used for anchors, transmissions line, and bridge is gold because resistivity is higher than other conducting materials such as aluminum, silver, and copper. A thin dielectric layer is used above the center conductor transmission line, which is used to prevent the upper electrode and bottom electrode from short-circuit. The dielectric materials between both conducting electrodes are chosen in such a way that having high relatively permittivity results in the low losses and lower pull-in voltage. The proposed switch has been simulated using SiO<sub>2</sub> and AlN dielectric materials to study the impact on the RF performance of the switch.

The electrical actuation and mechanical actuation are two sections of the RF MES switch. To actuate the mechanical section, there are four types of actuation mechanism, i.e., piezoelectric, electrostatic, thermal, and electromagnetic mechanisms. The common approach used nowadays is the electrostatic actuation mechanism.

When there is no DC voltage applied between the beam and bottom electrode, the switch is in ON state and signal pass from one port to another port. On the other hand, when the DC voltage is applied between them, the switch is in the OFF state. Hence, membrane collapses on the dielectric layer which is above the center transmission. Due to electrostatics force between top and movable beam the signal pass from one port to another port blocks. This electrostatic force is

caused by actuation voltage applied between both electrodes and is given as [1, 2].

$$F = \frac{\epsilon_0 w W V_a^2}{2[g_0 + (t_d/\epsilon_r)]^2}, \quad (1)$$

where  $V_a$  is actuation voltage and is given by [1].

$$V_a = \sqrt{\frac{2kg^2(g_0 - g)}{\epsilon_0 w W}}, \quad (2)$$

where  $W$  is the width of the CPW transmission line,  $g_0$  and  $g$  are pre- and postair gap height from membrane,  $w$  is the beam width, and  $k$  is the spring constant of the beam in negative  $z$  direction and is given as [1, 5]

$$K = K' + K'', \quad (3)$$

$$K = 32Ew(t/l)^3(27/49) + 8\sigma(1 - \nu)w(t/l),$$

where  $E$  (GPa) is Young's modulus,  $\sigma$  (MPa) is biaxial residual stress due to fabrication process,  $K'$  is due to the stiffness of structure,  $K''$  is spring constant contribution due to residual stress, and  $\nu$  is Poisson's ratio of beam. The detailed

dimension and material used for the switch structure are given in Table 2.

Above a definite threshold voltage, the electrostatic force is increased due to an increase in charge and overcome the mechanical restoring force of the beam. An increase in electrostatic force results in a decrease in the beam gap height and at the same time which in turn enhances the downstate capacitance, and resulting beam becomes unstable and this threshold voltage is called pull-in voltage given as [1, 14]

$$V_p = V(2g_0/3) = \sqrt{\frac{8kg_0^3}{27\epsilon_0 w W}}. \quad (4)$$

#### 4. Electrical Model of Shunt Switch

The electrical equivalent model describes a shunt switch as CLR (capacitance, inductance, resistance) series resonant circuit as shown in Figure 3(d). The movable metallic beam of the MEMS shunt switch is sketched by switch variable capacitance, lumped resistance, and switch inductance. Depending upon the ON and OFF conditions of the switch, the variable capacitance is changed. When the switch is ON condition, the variable capacitance is represented by  $C_{up}$  and in OFF condition it is represent by  $C_{down}$ . From Eq. (6), if the frequency of operation is less than LC resonance frequency, the CLR model works as a capacitor, while it works as an inductor above LC resonant frequency. At the series LC resonant frequency, the CLR (capacitance, inductance, resistance) model reduces as series resistance and is represented by  $R_s$ . Capacitances in up- and downstate define the insertion and isolation of shunt switch, respectively. The following subsections explain these points elaborately. The impedance of the capacitive shunt switch is given as [5]

$$Z_s = R_s + j\omega L + \frac{1}{j\omega C}, \quad (5)$$

$$Z_s = \begin{cases} \frac{1}{j\omega C} & \text{for } f \ll f_0 \\ R_s & \text{for } f = f_0 \\ j\omega L & \text{for } f \gg f_0 \end{cases}, \quad (6)$$

where  $C$  is the capacitance of the switch it may be up capacitance ( $C_u$ ) and down capacitance ( $C_d$ ) depends upon the switch position,  $R_s$  is the bridge resistance and it depends upon the resistivity of bridge, and  $L$  is the bridge inductance and it depends upon the gap between signal line ground of CPW. The LC series resonant frequency of the capacitive shunt MEMS switch is given as [1]

$$f_0 = \frac{1}{2\pi\sqrt{LC_d C_u}}. \quad (7)$$

### 5. Result and Discussion

**5.1. Pull-In Analysis.** The modal analysis and pull-in voltage for fixed-fixed beam has been carried using the finite element

TABLE 2: Specific parameters of the proposed MEMS switch.

Parameters	Value
Beam length ( $L$ )	400 $\mu\text{m}$
Beam width ( $w$ )	120 $\mu\text{m}$
Center conductor width ( $W$ )	120 $\mu\text{m}$
Overlap area ( $A$ )	$120 \times 120 = 14400 \mu\text{m}^2$
Dielectric material and constant	AlN & 11
Beam thickness ( $t$ )	1 $\mu\text{m}$
Beam material	Gold
Dielectric thickness ( $t_d$ )	0.1 $\mu\text{m}$
Air-gap ( $g_0$ )	2.5 $\mu\text{m}$
Substrate thickness ( $h$ )	$675 \pm 20 \mu\text{m}$
CPW dimension	G/W/G-90 $\mu\text{m}/120 \mu\text{m}/90 \mu\text{m}$
CPW thickness	1 $\mu\text{m}$

method- (FEM-) based Coventorware software. At the pull-in voltage, the movable bridge/membrane suddenly collapses on the thin dielectric layer due to the mechanical action of electrostatic force and causing the system to unstable (Figure 4). The electromechanical analyses in Coventorware are shown in Figure 5. It can be seen from the plot as voltage increases on the center conductor the top movable metallic beam starts to snap down from the top in the negative  $z$  direction towards the dielectric layer due to electrostatic force. When the metallic beam travel  $1/3^{\text{rd}}$  gap of the total initial gap from the topside, the movable beam enters into the instable region/area, and at this condition, electrostatic force overcome the restoring force. Small diameters ( $10 \times 10 \mu\text{m}^2$ ) holes are introduced in the top metal membrane to reduce the stiction problem and residual stress during the release process as shown in Figure 4.

**5.2. Switching Time.** The switching time depends upon the mechanical resonant frequency of the movable beam, applied source voltage, and pull-in voltage. It is defined as a time taken by the movable metallic beam to toggle from actuated state to unactuated state and vice versa is called switch speed and is given as [1].

$$T_s = 3.67 \frac{V_p}{V_s \omega_0}, \quad (8)$$

where  $V_s$  is the source voltage and given by  $V_s = 1.35V_p$ ,  $\omega_0$  is the mechanical resonant frequency and given by as  $\omega_0 = \sqrt{k/m}$ ,  $m$  is the beam mass, and  $k$  is the spring constant in negative  $z$  direction. Figure 6 demonstrates the variation of switching speed/time with beam thickness to beam length ( $t/l$ ) ratio. The switching in gold membrane is three times slower compared to aluminum.

**5.3. RF Analysis.** The ANSYS HFSS software has been used to extract the RF performance of the designed fixed-fixed beam configuration-based MEMS switch. RF parameters such as insertion loss ( $S_{21}$  in dB) and return loss ( $S_{11}$  in dB) are defined in upstate, whereas isolation ( $S_{21}$  in dB) is defined

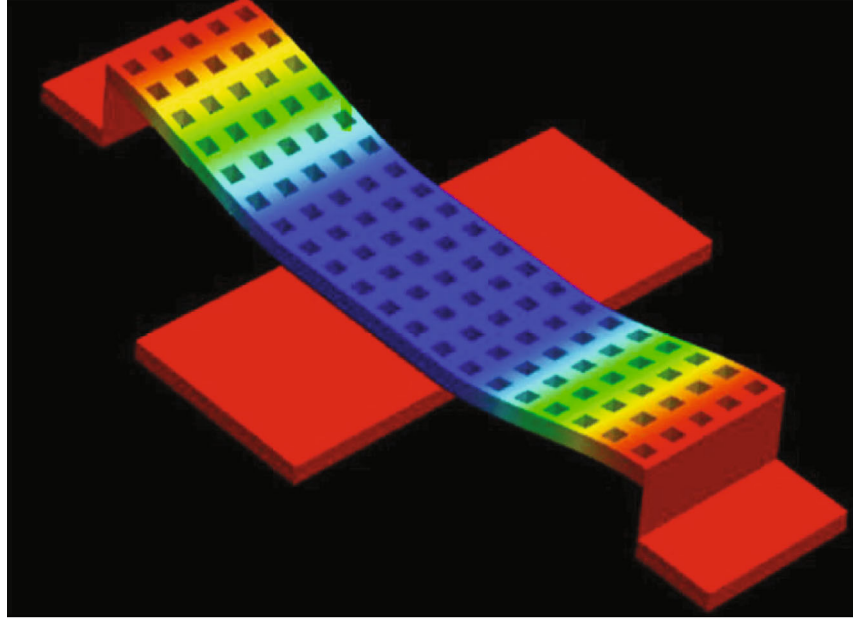
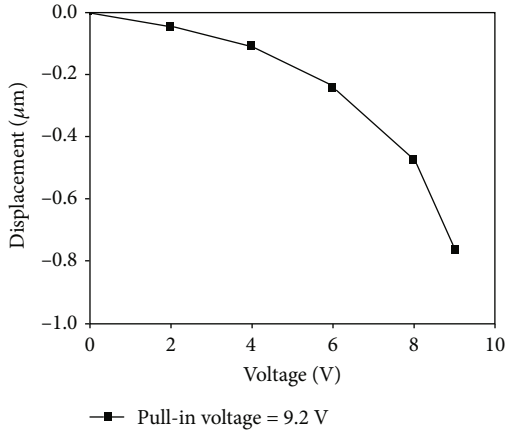
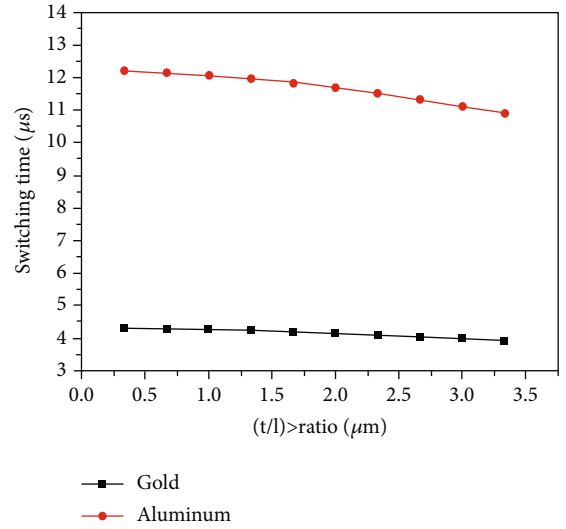


FIGURE 4: 3D view of proposed switch in Coventorware.



FIGURES 5: Variation of initial gap with applied voltage.

FIGURE 6: Variation of switching time ( $t_s$ ) with  $(t/l)$  ratio of RF-MEMS Shunt Switch.

in downstate. When there is no voltage applied to the bottom electrode, the switch is in unactuated state, and in this state, two RF parameters such as return loss and insertion loss of the switch have been analyzed. Return loss state that how much power is reflected back by the input/exciting port of coplanar waveguide transmission line. This is due to the improper impedance matching between switch and CPW line. Figure 7 shows the return loss or impedance matching as a function of frequency is better than 20 dB over whole frequency band. The return loss ( $S_{11}$ ) in the up state of the switch is mathematically calculated by [1]

$$|S_{11}|^2 \approx \frac{\omega_0^2 C_{up}^2 Z_0^2}{4}. \quad (9)$$

Insertion loss is also calculated in upstate and is it change the flow of RF signal between the input port and output port

to control the power dissipations in transmission line and is given as [1].

$$|S_{21}| = \left( \frac{1}{1 + j\omega_0 C_d Z_0 / 2} \right). \quad (10)$$

Insertion loss happens at low frequency due to the resistive loss between contact resistance region of the switch and finite resistance of CPW line while at high frequency is due to skin depth. Figure 8 shows the insertion loss better than 0.5 dB throughout the frequency band.



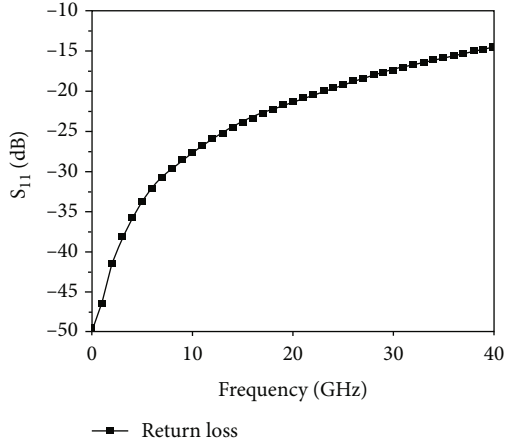


FIGURE 7: Return loss in upstate as a function of frequency.

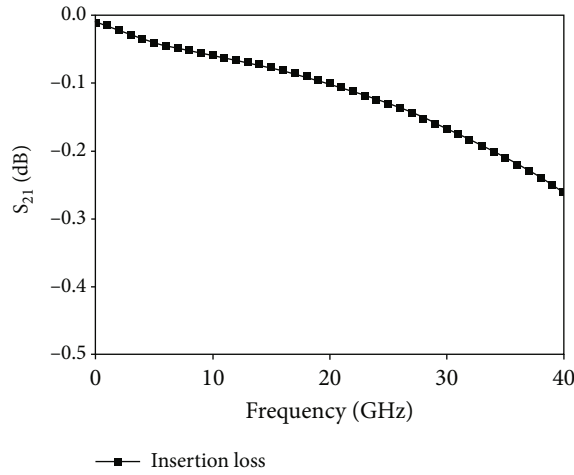


FIGURE 8: Insertion loss in upstate as a function of frequency.

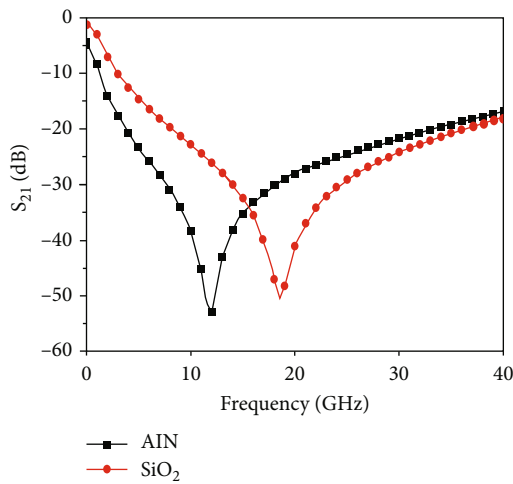


FIGURE 9: Isolation in downstate as a function of frequency.

When the proposed shunt MEMS switch is in an actuated state, switch capacitance is a large increase in downstate by factor 20-100 resulting in the good isolation. Isolation defines

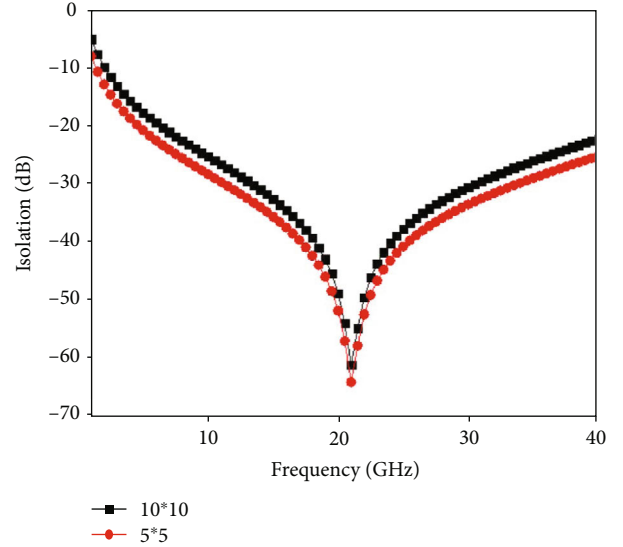


FIGURE 10: Effect of holes on isolation.

as how much power is present between port 1 and port 2 when the switch is in OFF state and is given as [2].

$$|S_{21}|^2 = \frac{4}{\omega_0^2 Z_0^2 C_{\text{down}}^2}, \quad (11)$$

where  $C_{\text{down}}$  is the downstate capacitance and is given by [1].

$$C_{\text{down}} = \frac{\epsilon_0 \epsilon_r A}{t_d}. \quad (12)$$

The ratio of capacitance in downstate to upstate is defined as the figure of merit (FOM). The FOM factor for the proposed switch is greater than 50. Figure 9 shows the isolation for the proposed switch is better than 20 dB for the entire frequency band and maximum isolation is 50 dB @18 GHz and 55 dB @12 GHz for  $\text{SiO}_2$  and  $\text{AlN}$  dielectric materials, respectively.

In MEMS shunt switch, small diameter holes play the vital role in RF performance as well as in mechanical performance. Minor diameters holes are inserted into the top movable beam to overcome the squeeze air film damping and improve the switching speed of the switch. The total holes area may be 65% of the whole structure. Therefore, holes discharge some of the residual stress in the membrane and decrease the young modules of the MEMS switch. The effect of holes is negligible in upstate if the holes sizes are less than the 3-5 initial air gap because the fringing field can fill the hole area. In downstate, the holes reduced capacitance as well as isolation of the switch. Figure 10 shows the for holes dimension  $5 \times 5 \mu\text{m}^2$  isolation is 65 dB and for  $10 \times 10 \mu\text{m}^2$  isolation is 60 dB.

## 6. Conclusion

In this work, a detailed analysis of a designed RF MEMS capacitive type shunt switch is outlined. Fixed-fixed beam configuration is chosen here for ease of realization. The

operating frequency is targeted for the 10 to 40 GHz band. MATLAB is used for all analytical calculation, whereas HFSS and Coventorware are used for the full-wave analysis of the switch structure. The proposed switch shows the pull-in voltage around 9.2 V for the gold membrane. The RF parameters such as isolation, insertion loss, and return loss are >20 dB, >0.5 dB, and >25 dB, respectively, over the whole frequency band for SiO<sub>2</sub> as a dielectric layer. Furthermore, to improve the RF parameters, here, an AlN dielectric material is used instead of SiO<sub>2</sub> because of the higher dielectric constant to increase the downstate capacitance and thus improve the isolation. The reported maximum isolation in downstate is 55 dB at 15 GHz.

### Data Availability

Data will be made available on request.

### Conflicts of Interest

The authors declare that there is no conflict of interest regarding the publication of this paper.

### References

- [1] G. G. M. Rebeiz, *RF MEMS Theory, Design and Technique*, Wiley, Hoboken, 2003.
- [2] H. Jaafar, K. S. Beh, N. A. Yunus, W. Z. W. Hasan, S. Shafic, and O. Sidek, "A comprehensive study on RF MEMS switch," *Microsystem Technologies*, vol. 20, no. 12, pp. 2109–2121, 2014.
- [3] K. V. Caekenbergh and K. Sarabandi, "A self-aligned fabrication process for capacitive fixed-fixed beam RF MEMS components," *Journal of Microelectromechanical Systems*, vol. 17, no. 3, pp. 747–754, 2008.
- [4] C. Goldsmith, J. Ehmke, A. Malczewski et al., "Lifetime characterization of capacitive Rf MEMS switches," in *2001 IEEE MTT-S International Microwave Symposium Digest (Cat. No.01CH37157)*, pp. 227–230, Phoenix, AZ, USA, May 2001.
- [5] C. L. Dai, H. J. Peng, M. C. Liu, C. C. Wu, and L. J. Yang, "Design and fabrication of RF MEMS switch by the CMOS process," *Tamkang Journal of Science and Engineering*, vol. 8, no. 3, pp. 197–202, 2005.
- [6] L. Y. Ma, A. N. Nordin, and N. Soin, "A novel design of a low-voltage low-loss T-match RF-MEMS capacitive switch," *Microsystem Technologies*, vol. 24, no. 1, pp. 561–574, 2018.
- [7] Y. W. Yu, J. Zhu, S. X. Jia, and Y. Shi, "A high isolation series-shunt RF MEMS switch," *Sensors*, vol. 9, no. 6, pp. 4455–4464, 2009.
- [8] A. Persano, A. Cola, G. de Angelis, A. Taurino, P. Siciliano, and F. Quaranta, "Capacitive RF MEMS switches with tantalum-based materials," *Journal Of Microelectromechanical Systems*, vol. 20, no. 2, pp. 365–370, 2011.
- [9] W. B. Zheng, Q. A. Huang, X. P. Liao, and F. X. Li, "RF MEMS membrane switches on GaAs substrates for X-band applications," *Journal of Microelectromechanical Systems*, vol. 14, no. 3, pp. 464–471, 2005.
- [10] H. R. Ansari and S. Khosroabadi, "Design and simulation of a novel RF MEMS shunt capacitive switch with a unique spring for Ka-band application," *Microsystem Technologies*, vol. 25, no. 2, pp. 531–540, 2019.
- [11] B. Pillans, J. Kleber, C. Goldsmith, and M. Eberly, "RF power handling of capacitive RF MEMS devices," in *2002 IEEE MTT-S International Microwave Symposium Digest (Cat. No.02CH37278)*, pp. 329–332, Seattle, WA, USA, June 2002.
- [12] A. Persano, A. Tazzoli, A. Cola, P. Siciliano, G. Meneghesso, and F. Quaranta, "Reliability enhancement by suitable actuation waveforms for capacitive RF MEMS switches in III–V technology," *Journal of Microelectromechanical Systems*, vol. 21, no. 2, pp. 414–419, 2012.
- [13] Q. Ma, Q. Tran, T. Kuan et al., *Metal Contact Reliability of RF MEMS Switches*, Intel Corporation, Santa Clara, CA, USA, 2007.
- [14] J. Innaci, "Reliability of MEMS: a perspective on failure mechanisms, improvement solutions and best practices at development level," *Displays*, vol. 37, pp. 62–71, 2015.
- [15] N. Kobayashi, A. Takano, and S. Kubono, "Measuring equipment and measurements of adhesion force between gold electrical contacts," *IEEE Transactions on Components, Packaging and Manufacturing Technology-Part A*, vol. 21, no. 1, pp. 46–53, 1998.
- [16] M. F. B. Badia, E. Buitrago, and A. M. Ionescu, "RF MEMS shunt capacitive switches using AlN compared to Si<sub>3</sub>N<sub>4</sub> dielectric," *Journal of Microelectromechanical Systems*, vol. 21, no. 5, pp. 1229–1240, 2012.
- [17] C. Chu and X. Liao, "One to 40 GHz ultra-wideband RF MEMS direct-contact switch based on GaAs MMIC technique," *IET Microwaves, Antennas & Propagation*, vol. 12, no. 6, pp. 879–884, 2017.
- [18] A. Ziaei, T. Dean, and Y. Mancuso, "Life time characterization of capacitive power RF MEMS switch," in *2005 European Microwave Conference*, Paris, France, October 2005.
- [19] J. Y. Park, G. H. Kim, K. W. Chung, and J. U. Bu, "Monolithically integrated micromachined RF MEMS capacitive switches," *Sensors and Actuators A: Physical*, vol. 89, no. 1–2, pp. 88–94, 2001.
- [20] C. L. Goldsmith, Z. Yao, S. Eshelman, and D. Denniston, "Performance of low-loss RF MEMS capacitive switches," *IEEE Microwave and Guided Wave Letters*, vol. 8, no. 8, pp. 269–271, 1998.
- [21] S. Fouladi and R. R. Mansour, "Capacitive RF MEMS switches fabricated in standard 0.35- $\mu$ m CMOS technology," *IEEE Transactions on Microwave Theory and Techniques*, vol. 58, no. 2, pp. 478–486, 2010.
- [22] K. Jairath, N. Singh, V. Jagota, and M. Shabaz, "Compact ultra-wide band metamaterial-inspired split ring resonator structure loaded band notched antenna," *Mathematical Problems in Engineering*, vol. 2021, Article ID 5174455, 12 pages, 2021.
- [23] Z. Deng, H. Wei, S. Fan, and J. Gan, "Design and analysis a novel RF MEMS switched capacitor for low pull-in voltage application," *Microsystem Technologies*, vol. 22, no. 8, pp. 2141–2149, 2016.
- [24] F. M. Guo, Z. Q. Zhu, Y. F. Long et al., "Study on low voltage actuated MEMS rf capacitive switches," *Sensors and Actuators A: Physical*, vol. 108, no. 1–3, pp. 128–133, 2003.

## Research Article

# Location and Layout of Common Storage and Multichannel Common Distribution considering Time Windows

**Biqin Hu** <sup>1</sup>, **Bin Yang** <sup>2</sup>, **Wei Jiang** <sup>3</sup>, **Zhe Yang** <sup>4</sup> and **Mohammed Abdella Kemal** <sup>5</sup>

<sup>1</sup>*Institute of Logistics Science and Engineering, Shanghai Maritime University, Shanghai Pudong, 201306, China*

<sup>2</sup>*Business School, Zhejiang Textile and Fashion College, Ningbo 315211, China*

<sup>3</sup>*CIM Department, Shanghai Advanced Semiconductor Manufacturing Co., Ltd., Shanghai Pudong, 201206, China*

<sup>4</sup>*School of Computer Science, University of Manchester, Oxford Road, Manchester, M13 9PL, UK*

<sup>5</sup>*Arba Minch University, Ethiopia*

Correspondence should be addressed to Mohammed Abdella Kemal; [abdella.kemal@amu.edu.et](mailto:abdella.kemal@amu.edu.et)

Received 10 May 2021; Accepted 15 June 2021; Published 6 July 2021

Academic Editor: Vimal Shanmuganathan

Copyright © 2021 Biqin Hu et al. This is an open access article distributed under the Creative Commons Attribution License, which permits unrestricted use, distribution, and reproduction in any medium, provided the original work is properly cited.

In the process of logistic activities of common storage and common distribution, due to problems such as urban traffic congestion period, parking restriction, working time restriction, and road restriction time, people often agree on the arrival time for customer orders, so that the receiving and delivering parties can connect in time and speed up unloading and distribution. Therefore, considering the actual distribution operation, it is necessary to consider the location and layout of common storage and multichannel common distribution in time windows. This paper takes multichannel common storage and common distribution as the research object, combines with the actual distribution situation, considers the location and distribution route optimization of the common storage and common distribution mode under the condition of time windows, takes the form of linking time windows with distribution time completion efficiency, and forms a reverse constraint on the objective function by time completion efficiency, thus realizing the double-objective optimization of “minimizing the total cost and satisfying the time windows.” In addition, through the comparison of various intelligent algorithms, find that the squirrel search algorithm (SSA) has more stable performance and better solution results.

## 1. Introduction

With the management and control of distribution vehicles in large cities becoming more and more strict, urban distribution vehicles are affected by high parking and loading charges, the shortage of vehicle entrance passes indexes and the like; meanwhile, a large number of cross distribution and personnel overlap among logistic enterprises cause the unnecessary urban end distribution cost, and the demand of end distribution among the logistic distribution enterprises is generated (see, e.g., [1]). Secondly, under the new retail trend, higher requirements are put forward for the timeliness of the logistic distribution, and the service requirements of hourly arrival, daily arrival, and next day arrival are common, which makes the new retail mode integrating online and offline urgently need an efficient common storage and distribution system as a support (see, e.g., [2]). Under

this background, the channel boundaries of the urban logistic distribution gradually show a trend of blurring and integration, and common storage effectively acts as the function of multichannel cargoes collection and distribution in the process of channel integration (see, e.g., [3]). Through common storage, joint holding of inventory and joint use of storage facilities and management personnel, inventory costs, and labor costs can be effectively reduced, and order response speed can be improved. At the same time, combined with the common distribution, the transportation distribution plan is formulated from the perspective of storage and distribution integration operation optimization, and the same destination-oriented cargoes are distributed with one vehicle, which not only reduces repeated distribution but also greatly saves limited transport resources (see, e.g., [4]).

In the literature of integrated optimization of storage and distribution, the storage location problem is a mixed

```

for i=1:length (Ware House) no_WH=Ware House(i);
no_WH_N=find (WH_N==i); [~,temp_p]=sort (x(no_WH_N,3));
no_WH_N=no_WH_N (temp_p); num_V=data.WareHouse (no_WH,4);
recording.V{i}=zeros (num_V,10); S_WH=data.WareHouse (no_WH,2);
for j=1:length (no_WH_N).
if no_WH_N(j)<=data.num_WH continue;
end no_N=no_WH_N(j);
Type_Cargoes=data.Demand (no_N,5); weight_Cargoes=
(data.Demand(no_N,2 : 3)); [~,priority_V]=sor t(x(no_N,4 : 3+num_V));

```

ALGORITHM 1

```

x=cell(option.popSize,1); fit=zeros(option.popSize,1); for j=1:option.popSize.
x{j,1}=creat_x_1(option,data); v{j,1}=rand(size(x{j,1}));
fit(j,1)=option.aimFcn(x{j,1},option,data);
end data.x=x; data.fit=fit; data.v=v;

```

ALGORITHM 2

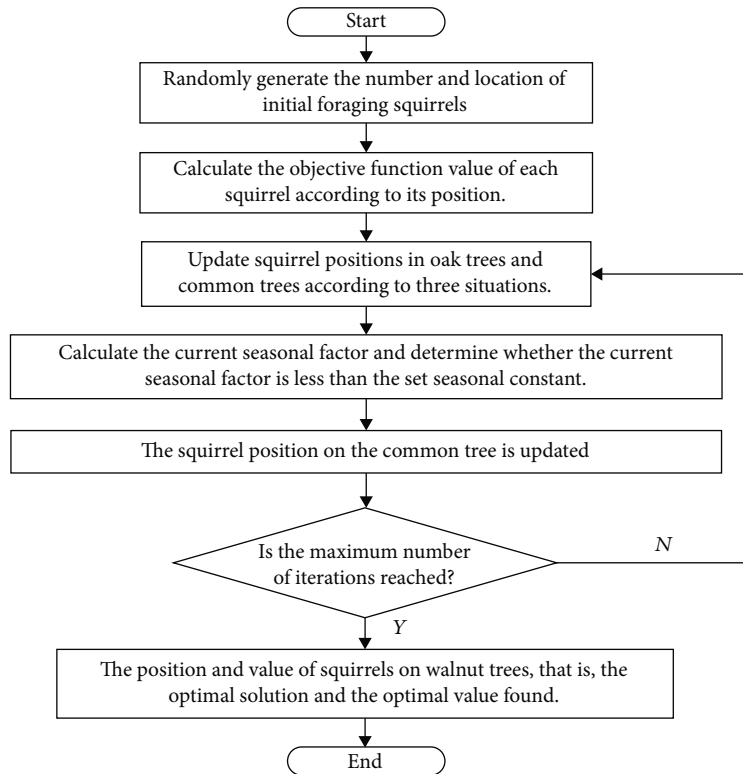


FIGURE 1: Solving steps of the squirrel search algorithm for the multichannel common storage and subchannel distribution with location and layout problem.

integer programming problem, while the distribution routing problem is a vehicle routing problem (VRP); so, it is a NP problem to combine the two problems. The traditional problem of warehouse location and distribution is generally solved by disassembly into two stages or consider the influence of production place, inventory level, and distribution channel when selecting warehouse

location, but most of them are not optimized together (see e.g. [5]). Most of the warehouse location models currently established are based on the freight or service level under single channel circulation mode, proposing the selection of warehouse location, but less research has been carried out from the perspective of storage and distribution integration.

TABLE 1: Time window plan for each demand point.

Demand point	$P = 1$ , pallet	$P = 2$ , items/parcels	Estimated unloading time	Hard time window 1	Soft time window 1	Soft time window 2	Soft time window 3
11	31	0	1	0.5	1	6	16
12	31	0	1	0.5	1	6	16
13	28	0	1	0.5	1	6	16
14	33	0	1	0.5	1	6	16
15	14	0	1	0.5	1	6	16
16	10	0	1	0.5	1	6	16
17	2	0	1	0.5	1	6	16
18	2	0	1	0.5	1	6	16
19	12	0	1	0.5	1	6	16
20	30	0	1	0.5	1	6	16
21	3	0	1	0.5	1	6	16
22	3	0	1	0.5	1	6	16
23	4	0	1	0.5	1	6	16
24	31	0	1	0.5	1	6	16
25	40	0	1	0.5	1	6	16
26	0	19	1	0.5	1	6	16
27	0	11	1	0.5	1	6	16
28	0	18	1	0.5	1	6	16
29	0	2	1	0.5	1	6	16
30	0	2	1	0.5	1	6	16
31	0	32	1	0.5	1	6	16
32	0	3	1	0.5	1	6	16
33	0	40	1	0.5	1	6	16
34	0	15	1	0.5	1	6	16
35	0	4	1	0.5	1	6	16
36	0	6	1	0.5	1	6	16
37	0	28	1	0.5	1	6	16
38	0	3	1	0.5	1	6	16
39	0	24	1	0.5	1	6	16
40	0	29	1	0.5	1	6	16
41	5	0	1	0.5	1	6	16
42	3	0	1	0.5	1	6	16
43	2	0	1	0.5	1	6	16

Multichannel means that the structure and mode of circulation are different. For example, the logistic demand of online channels is small-piece high-frequency mode, while the logistic demand of offline stores is large-piece low-frequency mode. The joint storage of online channels and offline channels can reduce the inventory of the same product and realize the joint storage and distribution of the two modes (see, e.g., [6]). However, this requires redesigning the distribution network and reasonably selecting the warehouse location and optimizing the distribution route according to the characteristics of multichannel integrated warehouse allocation. At present, there are few literatures on the research content of the integrated layout of common storage and distribution under the background of multichannel integration (see, e.g., [7]). Most of them expound the characteristics and development trend of multichannel

TABLE 2: Available area, rental, and vehicles of warehouse candidate points.

Warehouse No.	Area	Area rent	Number of vehicles
1	1000	2.5	5
2	1500	1.3	5
3	1600	0.8	5
4	1100	0.7	5
5	800	1.2	5
6	2000	1.1	5
7	1200	1.3	5
8	2800	1.0	5
9	3000	1.5	5
10	3200	0.6	5

TABLE 3: Results of distribution cargo types and transportation distance of vehicles corresponding to candidate warehouse No. 3.

Vehicle	Number of access nodes	Quantity of type 1 cargoes	Quantity of type 2 cargoes	Single distribution distance
1	4	57	0	44.51
2	4	35	34	73.39
3	4	101	0	74.12
4	2	3	3	54.14

TABLE 4: Distribution route points of vehicles corresponding to candidate warehouse No. 3.

Vehicle	Route point 1	Route point 2	Route point 3	Route point 4	Route point 5
1	12	18	15	16	0
2	43	37	36	14	0
3	20	19	11	13	0
4	38	42	0	0	0

TABLE 5: Results of distribution cargo types and transportation distance of vehicles corresponding to candidate warehouse No. 10.

Vehicle	Number of access nodes	Quantity of type 1 cargoes	Quantity of type 2 cargoes	Single distribution distance
1	4	35	6	55.83
2	5	0	96	37.55
3	5	8	40	30.26
4	5	45	57	36.78

storage and distribution services, but there are few researches on the cost of the multichannel logistic distribution and single-channel logistic distribution. Some scholars discussed the service mode of multichannel orders and store-based or warehouse-based distribution systems. Under the condition of limited space, professional order pickers and ordinary customers will influence each other in the store-based model; so, it is necessary to seek cooperative work strategies (see, e.g., [8]). Alptekinoglu and Tang (2005) proposed a model to analyze the multichannel distribution system and used the joint distribution system of two retailers to find a low-cost product distribution method. Relevant literatures show that there are many methods to solve the storage location or distribution routing problem. However, for the integrated optimization of storage and distribution, there is almost no very effective approximate optimal algorithm in a short period of time. squirrel search algorithm is a new algorithm inspired by squirrel's dynamic foraging behavior. Compared with existing algorithms, this algorithm has more accurate solution and fast convergence speed in big data experiments, but it has not yet been applied to storage and distribution optimization problems (see, e.g., [9]).

For the optimization of location and distribution route in the mode of common storage and common distribution under the condition of time windows, it is not only necessary to consider the reasonable location of warehouses under the condition of multichannel logistic demand, but also to consider the layout of the corresponding multichannel distribution network, and to study the cooperative operation and common optimization among warehouses, vehicles, and demand points. In the existing subchannel distribution pro-

cess, we need to combine the service time requirements, consider the optimization and operation of storage and distribution integration resources under the condition of time windows on the basis of common storage and common distribution, and study the warehouse location, distribution network layout, distribution plan formulation, and other contents of the multichannel common storage and distribution under the condition of time constraint (see, e.g., [10]).

On the basis of a common storage multichannel common distribution location and layout model, a demand point receiving time window is added to the problem, the earliest service time, the latest service time and the running time of a vehicle of each demand point are combined, the minimum total cost of distribution and storage is taken as a target, whether the arrival time of the vehicle is linked with the completion efficiency of the distribution time within the appointed receiving time is set as the reverse relation of a target function, the distribution route is optimized, the distribution vehicle resources are reasonably distributed, and the arrival time and the departure time of the vehicle to the demand point are as much as possible in accordance with the time interval of allowable cargoes receiving of each demand point, thus achieving the dual objectives of meeting the time window and the lowest cost.

## 2. Material and Methods

*2.1. Objective Function.* The objective function consists of the total cost of warehouse allocation and the time completion efficiency, and the total cost is divided into two parts. The first part is the distribution cost. The transportation distance

TABLE 6: Distribution route points of vehicles corresponding to candidate warehouse No. 10.

Vehicle	Route point 1	Route point 2	Route point 3	Route point 4	Route point 5
1	35	23	24	30	0
2	29	26	31	32	33
3	27	21	22	40	17
4	39	41	34	25	28

TABLE 7: Distribution time and time completion efficiency of each demand point.

Demand point	Distribution completion time	Time completion efficiency	Estimated unloading time	Hard time window 1	Soft time window 1	Soft time window 2	Soft time window 3
11	4.30	1.00	1	0.5	1	6	16
12	1.53	1.00	1	0.5	1	6	16
13	5.36	1.00	1	0.5	1	6	16
14	5.33	1.00	1	0.5	1	6	16
15	3.58	1.00	1	0.5	1	6	16
16	4.58	1.00	1	0.5	1	6	16
17	5.63	1.00	1	0.5	1	6	16
18	2.56	1.00	1	0.5	1	6	16
19	3.14	1.00	1	0.5	1	6	16
20	1.90	1.00	1	0.5	1	6	16
21	2.26	1.00	1	0.5	1	6	16
22	3.33	1.00	1	0.5	1	6	16
23	2.40	1.00	1	0.5	1	6	16
24	3.44	1.00	1	0.5	1	6	16
25	4.60	1.00	1	0.5	1	6	16
26	2.34	1.00	1	0.5	1	6	16
27	1.15	1.00	1	0.5	1	6	16
28	5.75	1.00	1	0.5	1	6	16
29	1.15	1.00	1	0.5	1	6	16
30	4.90	1.00	1	0.5	1	6	16
31	3.49	1.00	1	0.5	1	6	16
32	4.51	1.00	1	0.5	1	6	16
33	5.56	1.00	1	0.5	1	6	16
34	3.37	1.00	1	0.5	1	6	16
35	1.31	1.00	1	0.5	1	6	16
36	3.70	1.00	1	0.5	1	6	16
37	2.63	1.00	1	0.5	1	6	16
38	1.68	1.00	1	0.5	1	6	16
39	1.23	1.00	1	0.5	1	6	16
40	4.48	1.00	1	0.5	1	6	16
41	2.28	1.00	1	0.5	1	6	16
42	2.81	1.00	1	0.5	1	6	16
43	1.23	1.00	1	0.5	1	6	16

between all points on the route is multiplied by the unit distance transportation cost of the vehicles carried. The second part is the storage cost, the total rental cost of the warehouse candidate point  $i$  multiplied by whether to locate the site as the decision variable of the warehouse (see, e.g., [11]). Time

completion efficiency is the average time completion efficiency of distribution points. The higher the time completion efficiency, the smaller the objective function value, which can effectively achieve the dual requirements of minimum cost and meeting the distribution time window.

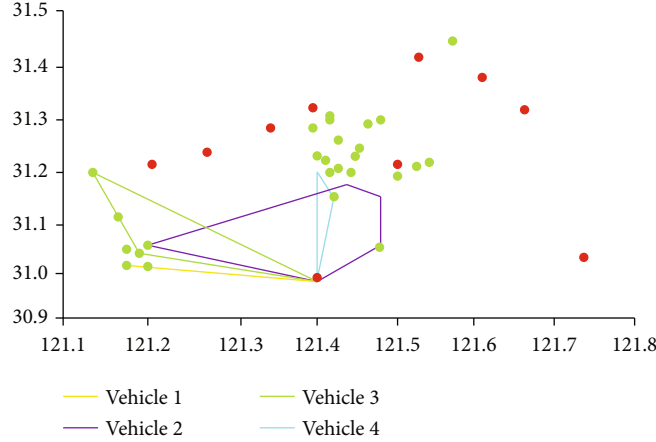


FIGURE 2: Distribution route diagram corresponding to candidate warehouse No. 3.

**2.2. Description of Time Window Restriction Conditions.** The restriction condition 1 refers to if the distribution vehicle corresponds to the service demand point, and then the completion time point of the distribution vehicle to the demand point is equal to the completion time point of the distribution vehicle to the demand point plus the service time of the distribution vehicle at the demand point and the travel time of the distribution vehicle to travel from the demand point to the demand point (see, e.g., [12]).

The restriction condition 2 is a piecewise function for calculating the service time completion efficiency of the distribution point related to the soft and hard time windows. If the completion time of the vehicle at the demand point is less than the earliest time point (hard time window) or greater than the latest time point (maximum soft time window), the time completion efficiency is 0. If the completion time of the vehicle at the demand point is greater than or equal to the earliest serviceable time point (hard time window) but less than the agreed start service time, the time completion efficiency is the deviation ratio of the current arrival time and the agreed start service time (see, e.g., [13]). If the completion time of the vehicle at the demand point is greater than the agreed end service time and less than the latest time point (maximum soft time window), the time completion efficiency is the deviation ratio between the completion time of the vehicle at the demand point and the agreed end service time. If the completion time of the vehicle at the demand point is between the agreed start service time and the agreed end service time, the time completion efficiency is 1.

The restriction condition 3 means that the total distribution time completion efficiency is the average value of the time completion efficiency of each distribution point.

The restriction condition 4 means that if the distribution vehicle corresponds to the service demand point, the travel time from point to point on the path is equal to the distance between the two points divided by the average speed of the distribution vehicle.

### 2.3. Squirrel Search Algorithm Solution Design

**2.3.1. Design Idea of the Squirrel Search Algorithm.** The squirrel search algorithm assumes that there are squirrels on trees

in the forest, and there is only one squirrel in each tree, and each squirrel forages for food and maximizes the available food resources through dynamic actions (see e.g. [14]). There are only three kinds of trees in the forest: Common tree, oak tree and walnut tree, of which oak tree and walnut tree are the food sources of squirrels, and only three oak trees and one walnut tree are set to exist in the forest area.

**2.3.2. Solving Steps of the Squirrel Search Algorithm for the Multichannel Common Storage and Subchannel Distribution with Location and Layout Problem.** Step 1. Randomly generate the position of squirrels. The position is represented by the dimensional independent variable matrix in the model, and the starting position is randomly generated as follows:

**2.4. Design of Independent Variables.** Randomly generates a matrix of independent variables  $X$ , for example, for 93 demand points and 10 warehouses, the generated  $X$  matrix has  $93 + 10 = 103$  rows and 8 columns, of which the first column value indicates the warehouse construction priority, the second column value indicates the corresponding relationship between the warehouse and the demand points, the third column value indicates the distribution route of the demand points, the fourth column value indicates that the demand points are responsible for distributing vehicles, and the fourth, fifth, sixth, seventh, and eighth column values indicate the sending sequence of vehicles.

**2.5. Determine the Design of the Construction Warehouse.** The  $X$  values generated in the random first column of the warehouse are sorted. If the number with the value less than 0.5 is found, the candidate points in the top few places will be selected as the warehouse. For example, after warehouses 1-10 are sorted, there are 3 values less than 0.5, and then the warehouse number corresponding to the 1-3 digits  $x$  value of the sorted  $B$ .

Determine the corresponding relationship design between warehouse and demand point:

For the second column of the independent variable  $X$  matrix, point multiplied by the number of built warehouses and rounded up. If the rounded value is greater than or equal



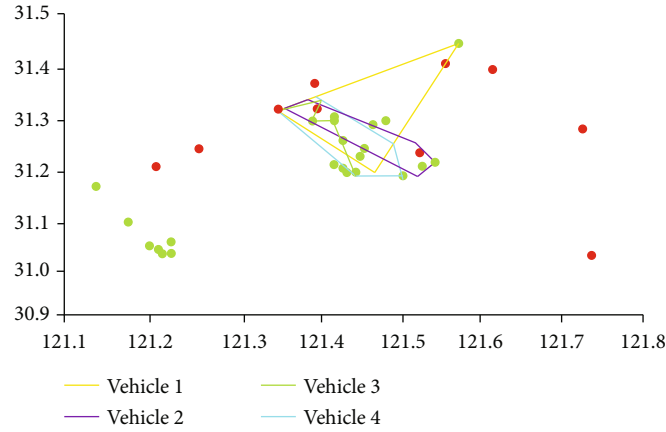


FIGURE 3: Distribution route diagram corresponding to candidate warehouse No. 10.

TABLE 8: Results of 5 algorithms under different data sizes.

Size	Result	SSA	APSO	AGA	CSO	WPA
$10 \times 13$	Best	225.75	229.02	227.62	226.66	227.15
	Mean	226.80	235.89	253.34	231.89	232.53
	Worst	229.24	244.17	285.51	240.05	240.59
	Median	226.62	237.39	260.09	231.84	231.86
	Time (10)	997.40	276.54	269.80	275.03	2216.26
$10 \times 33$	Best	1023.82	1045.34	1101.57	1045.78	1081.15
	Mean	1067.59	1101.01	1175.62	1073.25	1129.51
	Worst	1148.07	1152.34	1258.68	1130.05	1162.82
	Median	1061.26	1106.71	1174.83	1072.36	1136.22
	Time(10)	1111.50	301.15	335.55	359.67	2078.14
$10 \times 53$	Best	2099.66	2211.38	2303.31	2096.97	2389.61
	Mean	2191.58	2361.13	2427.04	2305.26	2461.44
	Worst	2297.26	2648.55	2643.81	2669.60	2595.11
	Median	2186.69	2342.83	2393.48	2265.50	2451.08
	Time (10)	1098.11	351.56	358.77	366.86	2471.37
$10 \times 73$	Best	3270.64	3611.38	3531.92	3547.04	3687.64
	Mean	3485.94	3786.80	3655.94	3863.75	3893.35
	Worst	3597.42	4103.18	3918.77	4165.65	4128.85
	Median	3501.19	3768.78	3604.21	3852.54	3916.60
	Time (10)	2866.76	973.84	972.20	968.80	6365.26
$10 \times 93$	Best	4789.20	5132.77	5311.89	5196.20	5618.54
	Mean	5160.04	5404.58	5648.84	5615.16	5847.26
	Worst	5461.17	5821.07	5910.29	5842.58	6128.73
	Median	5147.29	5320.58	5635.41	5632.35	5817.87
	Time (10)	3326.43	1116.46	1109.59	1105.34	7066.79

to the number of built warehouses, it means that the built warehouse is responsible for this demand point.

Design of distribution route, number of vehicles, and priority of vehicle distribution for each demand point are as follows:

Sort the values in the third column of the independent variable  $X$  matrix, obtain the order in which the points are

visited according to the sorting results, and eliminate the warehouse candidate points (see, e.g., [15]). And we give feedback to the 4th column value of the independent variable  $X$  matrix as the number of vehicles to be delivered and sort the column values from the 4th column to the “3 + number of vehicles” to indicate the priority of vehicles to be delivered.

Initial position call, value, and acceleration generation design of squirrel are as follows:

The initial population has been generated. The step of the squirrel search algorithm is shown in Figure 1.

### 3. Results

**3.1. Experimental Data.** The cargoes demand information, unloading time, the earliest service time point (hard time window 1), and the agreed service time point, i.e., soft time windows 1 and 2 and the latest reception time (soft time window) of each demand point are shown in Table 1. Table 2 shows the available area, current, and vehicles of warehouse candidate points.

**3.2. Example Results.** By using the solution steps of the squirrel search algorithm in the fifth part, the examples of the above 10 warehouse candidate points and 33 demand points are solved. According to 10 experiments, the best solution is obtained, and the No. 3 candidate point and No. 10 candidate point are selected to set up the warehouse, as shown in the following Tables 3–7. Table 3 shows the type of cargoes, number of access nodes, number of cargoes carried, and single distribution distance corresponding to candidate warehouse 3. Table 4 shows the vehicle distribution route corresponding to candidate warehouse 3. The specific route and longitude and latitude of route points are shown in Figure 2, and the warehouse 3 is equipped with 4 vehicles. Table 5 shows the type of cargoes, number of access nodes, number of cargoes carried, and single distribution distance corresponding to candidate warehouse No. 10. Table 6 shows the distribution route of vehicles corresponding to candidate warehouse No. 3. The specific route and longitude and latitude of route points are shown in Figure 3, and the warehouse No. 10 is equipped with 4 vehicles. The distribution time and time completion efficiency of each demand point are shown in Table 7. The objective function value (total cost) of the distribution scheme is 1023.82, and the time completion efficiency is 1.

The blue line in the figure represents the convergence trajectory of the squirrel search algorithm, red line represents adaptive particle swarm optimization, yellow line represents the adaptive genetic algorithm, purple line represents chicken swarm optimization, and green line represents the wolf pack algorithm. The results show that its convergence speed and convergence effect are better than other colored lines.

By running these five algorithms 10 times with 1000 iterations each time, in the data volume of  $10 \times 13$ ,  $10 \times 33$ ,  $10 \times 53$ ,  $10 \times 73$ , and  $10 \times 93$ , as shown in Table 8, the best solution, average solution, worst solution, and median solution of SSA are better than the other four algorithms, and the solution stability is also higher than other algorithms. And its running time ranks fourth among the five algorithms, less than WPA. Therefore, by comprehensively analyzing the solution results of five different scale examples, SSA is better than the other four algorithms to find the approximate optimal solution of the common storage and common distribution with location and layout model under the multichannel back-

ground, with more stable optimization ability and good optimization effect for large data volume examples.

### 4. Conclusion

In this paper, a multichannel common storage and common distribution location model considering time window constraints is established, and the allowable receiving and sending time period of each distribution point is taken as the constraint condition in the design of distribution routes, so as to solve the optimal warehouse location scheme with the minimum total cost and the optimal distribution routes of each channel that conform to the time window constraints. Through the comparison of various intelligent algorithms, it is found that the squirrel search algorithm has better solution effect when solving large data volume examples of the model.

### Data Availability

Data will be made available on request.

### Conflicts of Interest

The author(s) declare(s) that there is no conflict of interest regarding the publication of this paper.

### References

- [1] Y. He, X. Wang, Y. Lin, F. Zhou, and L. Zhou, "Sustainable decision making for joint distribution center location choice," *Transportation Research Part D: Transport and Environment*, vol. 55, no. 8, pp. 202–216, 2017.
- [2] L. N. Y. Wong, V. S. K. Lai, and T. P. Y. Tam, "Joint spacing distribution of granites in Hong Kong," *Engineering Geology*, vol. 245, no. 12, pp. 120–129, 2018.
- [3] H. Y. Xu, S. H. Kuo, G. Li, E. F. T. Legara, D. Zhao, and C. P. Monterola, "Generalized cross entropy method for estimating joint distribution from incomplete information," *Physica A: Statistical Mechanics and its Applications*, vol. 453, no. 6, pp. 162–172, 2016.
- [4] W. M. Kempa and R. Marjasz, "Distribution of the time to buffer overflow in the M/G/1/N-type queueing model with batch arrivals and multiple vacation policy," *Journal of the Operational Research Society*, vol. 71, no. 3, pp. 447–455, 2019.
- [5] L. Zhou, R. Baldacci, D. Vigo, and X. Wang, "A multi-depot two-echelon vehicle routing problem with delivery options arising in the last mile distribution," *European Journal of Operational Research*, vol. 265, no. 2, pp. 765–778, 2018.
- [6] J. C. Goodson, "A priori policy evaluation and cyclic-order-based simulated annealing for the multi-compartment vehicle routing problem with stochastic demands," *European Journal of Operational Research*, vol. 241, no. 2, pp. 361–369, 2015.
- [7] R. Spliet, S. Dabia, and T. van Woensel, "The time window assignment vehicle routing problem with time-dependent travel times," *Transportation Science*, vol. 52, no. 2, pp. 261–276, 2017.
- [8] L. Wei, Z. Zhang, D. Zhang, and S. C. H. Leung, "A simulated annealing algorithm for the capacitated vehicle routing problem with two-dimensional loading constraints," *European*

- Journal of Operational Research*, vol. 265, no. 3, pp. 843–859, 2018.
- [9] J. Rieck, C. Ehrenberg, and J. Zimmermann, “Many-to-many location-routing with inter-hub transport and multi-commodity pickup-and-delivery,” *European Journal of Operational Research*, vol. 236, no. 3, pp. 863–878, 2014.
- [10] J. M. Home-Ortiz, M. Pourakbari-Kasmaei, M. Lehtonen, and J. R. Sanches Mantovani, “Optimal location-allocation of storage devices and renewable-based DG in distribution systems,” *Electric Power Systems Research*, vol. 172, no. 6, pp. 11–21, 2019.
- [11] F. Ahmadizar, M. Zeynivand, and J. Arkat, “Two-level vehicle routing with cross-docking in a three-echelon supply chain: a genetic algorithm approach,” *Applied Mathematical Modelling*, vol. 39, no. 22, pp. 7065–7081, 2015.
- [12] N. Zhang, X. Zhao, T. Liu, M. Lei, C. Wang, and Y. Wang, “Layout planning of highway transportation environment monitoring network: The case of Xinjiang, China,” *Sustainability*, vol. 12, no. 1, p. 290, 2020.
- [13] K. Czarnecki, D. Fourer, F. Auger, and M. Rojewski, “A fast time-frequency multi-window analysis using a tuning directional kernel,” *Signal Processing*, vol. 147, no. 5, pp. 110–119, 2018.
- [14] L. W. Rizkallah, M. F. Ahmed, and N. M. Darwish, “SMT-LH: A new satisfiability modulo theory-based technique for solving vehicle routing problem with time window constraints,” *The Computer Journal*, vol. 63, no. 1, pp. 91–104, 2019.
- [15] H. F. Liang, “Prediction and simulation of short-term high-speed traffic flow based on wolf swarm algorithm,” *Computer Simulation*, vol. 37, no. 3, pp. 139–143, 2020.

## Research Article

# Scalable and Storage Efficient Dynamic Key Management Scheme for Wireless Sensor Network

Vipin Kumar <sup>1</sup>, Navneet Malik <sup>1</sup>, Gaurav Dhiman <sup>2</sup> and Tarun Kumar Lohani <sup>3</sup>

<sup>1</sup>Department of Computer Science Engineering, Lovely Professional University, India

<sup>2</sup>Department of Computer Science, Government Bikram College of Commerce, India

<sup>3</sup>Arba Minch University, Ethiopia

Correspondence should be addressed to Vipin Kumar; vipin.17730@lpu.co.in

Received 16 February 2021; Revised 4 March 2021; Accepted 21 June 2021; Published 1 July 2021

Academic Editor: Vimal Shanmuganathan

Copyright © 2021 Vipin Kumar et al. This is an open access article distributed under the Creative Commons Attribution License, which permits unrestricted use, distribution, and reproduction in any medium, provided the original work is properly cited.

Recently, there have been exploratory growth in the research of wireless sensor network due to wide applications like health monitoring, environment monitoring, and urban traffic management. Sensor network applications have been used in habitat monitoring, border monitoring, health care, and military surveillance. In some applications, the security of these networks is very essential and need robust support. For a network, it is very important that node in the network trust each other and malicious node should be discarded. Cryptography techniques are normally used to secure the networks. Key plays a very important role in network security. Other aspects of security such as integrity, authentication, and confidentiality also depend on keys. In wireless sensor network, it is very difficult to manage the keys as this includes distribution of key, generation of new session key as per requirements, and renewal or revoke the keys in case of attacks. In this paper, we proposed a scalable and storage efficient key management scheme (SSEKMS) for wireless sensor networks that establish the three types of keys for the network: a network key that is shared by all the nodes in the network, a cluster key shared for a cluster, and pairwise key for each pair of nodes. We analysed the resiliency of the scheme (that is the probability of key compromise against the node capture) and compared it with other existing schemes. SSEKMS is a dynamic key management system that also supports the inclusion of the new node and refreshes the keys as per requirements.

## 1. Introduction

Sensor networks are very popular for collecting information and monitoring activities in hostile areas. In sensor networks, small sensors collect the data like humidity, temperature, pressure, and movements from physical environment. Through a gateway, this information is sent to the sink [1]. A large number of sensors are implemented, and in account of its wireless nature, they easily work in different environmental conditions. Sensors may be deployed in a random manor so it is important to deploy them carefully. If there are a less number of nodes in the area, it may lead to the unattended area or less connectivity of network, and if more nodes are deployed, there will be high traffic in the network and high collision rate of interference between packets. While sending the information to the base station, the security of data is very important and should be implemented properly.

To implement the security for this network is a challenging task [2]. Key management is a part of the security technique for a network. The main objective of key management in a sensor network is to maintain the integrity of messages between the communication parties and help to authenticate the nodes in the network. Other than this, the key scheme should be able to deal with node compromise issues and maintain the resiliency of the network against node capture. It should also have a strong node authentication mechanism [3]. These requirements are very important because most of the attacks on wireless sensor networks involve either an inside compromise node or an unauthorized outsider node. In addition, there are other factors as energy and number of messages required for key setup process, scalability, and storage requirement [4]. The rest of the paper is organized as follows: Section 2 explains the security of wireless sensor network and the need of key management and classification

of key management. In Section 3, we have a literature survey of key management schemes for sensor network. Sections 4 and 5 have a network model proposed scheme followed by security analysis of presented work and conclusion at last.

## 2. Security of Wireless Sensor Network

There is no continuous energy source which powers the sensor nodes. Therefore, proposing energy efficient schemes, which enhance the network lifetime, is another major concern in sensor networks [5]. We proposed a novel storage efficient scheme for enhancing the security and the network lifetime of WSNs. In most of the research on wireless sensor network, security issues are divided into many categories including cryptography, location security, secure routing, secure data aggregation, and secure data fusion [6]. Securing a WSN is a challenging task. Many WSN attacks have been identified by researches which fall under these categories: (i) to manage the keys is an important task to implement and maintain the security of sensor network. Keys are used to encrypt and decrypt the data before sending and receiving. Key can be public and private but it is very important that it must be safe. Public key is known to all but it must be verified that a public key belongs to a legitimate user. Keys are essential to provide authentication, confidentiality, and integrity. Key management is used to allocate and manage keys between network nodes and allows the revocation, updating, and destruction of keys. (ii) Security of routing and routing protocol is also an issue in WSNs. Most of the attacks in network layer make use of authentication loopholes to disturb the processing of message routing [7, 8]. As a result, messages are unable to reach the destination. There are external attackers and internal attacker threats to the routing in WSNs [9]. It is very difficult to identify a compromised internal node because it can generate unauthenticated packets. (iii) To prevent the different attacks on the network like denial-of-service is the next issue. DoS is an organized attack that prevents the user to access the service. It can also increase the delay to access a service. These types of attacks are also very difficult to prevent as data is coming from many sources [10].

*2.1. Key Management and Its Need.* The distribution of keys is one of the basic problems when security is implemented in WSN. Key management is defined as the set of procedures and techniques to distribute, maintain, and establishment of private key between communication parties [11]. It also includes refresh or update the keys of compromised nodes. It also must maintain forward and backward secrecy. The key management schemes should satisfy the following three groups of metrics [12] which are security, efficiency, and flexibility. If assigned same key for every node and a node is compromised or captured by adversary, it will reveal the key for whole network, and if every node has a different key, then it is very difficult to manage all keys because there are a very big number of node. In case of pool key distribution, if the node has less number of keys, it will create the problem of network connectivity, and to give more number of key to every node, it decreases the resiliency of the network. Public

key cryptography usually has the disadvantage of huge resources in demand [13]. Some of the basic requirements of the key are

- (i) Public key is very inefficient because it consumes more computation power
- (ii) In case of symmetric key approach the main disadvantage is that compromising one node leads to the compromising of entire network
- (iii) A predistribution approach requires that pairwise keys are preloaded and then deployed the nodes in the target area. In this approach, every pair has the shared key but this is not found to be suitable for large networks
- (iv) There are a number of probabilistic schemes that have some probability of connectivity. In probabilistic scheme, a set of keys are assigned to every node from a large pool of keys and then the probability that two nodes share a common key that can be used as secret key between nodes. To find a compromise between the number of keys assign to each node and total number of keys in key pool is a challenge for large network. A smaller key pool decreases the resilience against node capture attacks while the bigger one reduces the connectivity between nodes because of the reduced probability of share a common key [14]
- (v) One challenge in key management is that if a new sensor node joins the network, then, it is difficult in key predistribution case. If it joins the network after key establishment phase, we have to repeat the process

*2.2. Types of Key Managements.* Many key management techniques have been proposed for WSNs in recent years that can be categorized on different bases like symmetric cryptography or asymmetric cryptography, and other bases are pairwise or GroupWise, centralized or distributed, and dynamic or static [15]. Figure 1 represents the classification of various key management schemes. Various categories of key management are found in literature survey for WSN key management schemes are as follows:

- (1) Based on whether to assign pairwise keys or group-wise keys
  - (a) Pair-wise key schemes vs (b) Group-wise key schemes
- (2) Based on whether keys in the nodes are updated or not in network lifetime
  - (a) Static schemes vs. (b) dynamic schemes
- (3) Depend upon the location is known to node or not
  - (a) Location-dependent vs. (b) location-independent
- (4) Based on cryptography techniques

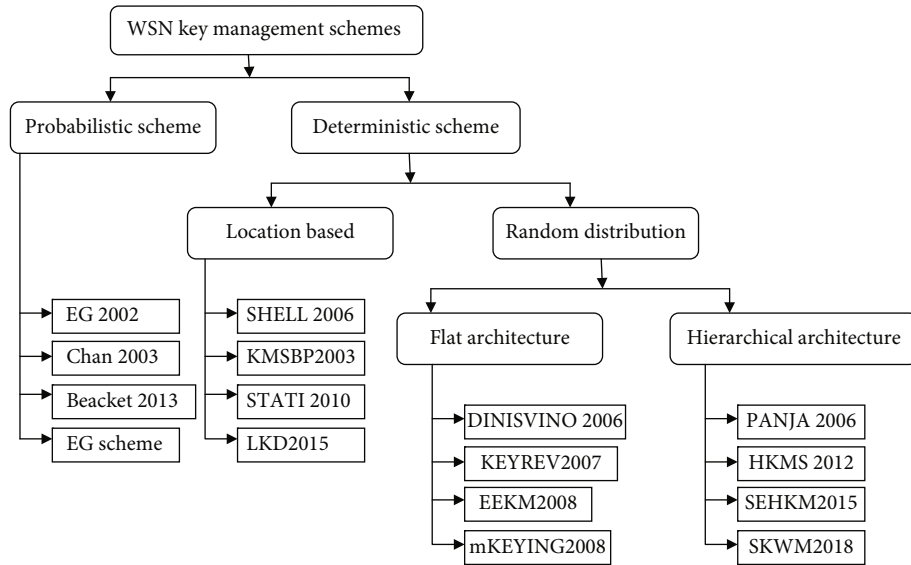


FIGURE 1: Key management schemes.

- (a) Symmetric key scheme vs. (b) asymmetric key scheme
- (5) Based on whether the responsibility of key management has been assigned to multiple nodes or a single node
- (a) Centralized schemes vs. (b) distributed schemes
- (6) Based on memory uses
- (a) Storage efficient vs. (b) storage inefficient

2.3. *Research Gap.* All the schemes for key management proposed in the literature consider the most of the requirements of key management but there is no scheme that considers all the aspects. All the key management schemes previously proposed are lacking in any of area resiliency, single point failure, or scalability. There are three main problems found that must be fulfilled by any key management structure:

*Single point failure:* scheme must be distributed and the responsibility must be divided to different nodes.

*Single key vs. resiliency:* if system operates on a single key or a set of keys, it normally does not provide good resiliency against node capture.

*Scalability:* scalability has been a major challenge for WSN as it consists of a huge number of small sensors. As the number of nodes increases old schemes do not provide support for scalability. In addition to these other challenges include storage efficiency, less energy consumption, and dynamic [16] to support change in network topology.

### 3. Related Work

Security issues in wireless sensor network achieve a good attention because of its different application [17]. Key management is a fundamental requirement for security of WSN [18, 19]. In this section, we provide work related to manage

the keys in sensor network. One of the first key predistribution scheme given by Eschenauer and Gligor known as the E-G scheme [20]. E-G scheme uses the concept of predistribution of keys as a number of keys are preloaded in every node from a common pool of keys. Every node takes a key ring of size  $m$  from a big key ring pool of size  $s$ . The values of  $m$  and  $s$  follow the condition  $m < s$  means  $m$  is very small compare to  $s$ . After deployment of sensor node, every node tries to find the common key to every neighbours. If a common key is found between nodes, that key is used as a secure symmetric key. If a common key not found, then, a new key discovery phase started the try to establish the path key using neighbour node. A path key can be established between two nodes if they share the key with third neighbour node. This scheme is very storage efficient and less complex if the values of  $m$  and  $s$  are chosen carefully. This key management with low processing and storage and complexity requirements is easy to achieve. In this scheme, security is not very good, and connectivity is very poor. It is based on some probability that lies the sharing of common key between nodes.

A new  $q$ -composite key scheme which is the extinction of E-G scheme is proposed by Chan et al. [21], says that two nodes can only communicate if they have at least  $q$  key common between them, i.e., node must share at-least  $q$  keys to communicate. The problem in this scheme is the connectivity as the probability of shared key is reduced. Also, the problem with scheme is if a few nodes compromise the whole network is no thread [22]. Bloom gives a scheme that establishes pairwise keys between nodes. This scheme uses a matrix row and column and by sharing the row and column node can compute common key. The major problem with this scheme is scalability, and matrix is prepared before deployment of node and depends on number of nodes. After deployment, the addition of new node and assignment of keys to new node is not possible. Also, for refreshing the keys, new matrix is needed [23]. These types of key schemes work for homogeneous sensor network that has the same types of node and

does not work for heterogeneous network. If an application requires high level of security; then, these schemes cannot be used as they have various bottleneck in their applications [24]. Therefore, it is of great importance to design an effective key management scheme for homogeneous network as well as heterogeneous sensor network by using the heterogeneity properties [25]. In 2005, Du et al. present a key scheme for pairwise key establishment [26]. This scheme combine the works of the E-G scheme and Blom's work [27] by using the same mechanism as the E-G scheme [20] except the use of individual keys. It uses the  $k$  key matrix for each node that is distributed randomly. This process is based on symmetric matrix multiplication, in which  $f(i, j)$  is deployment on  $f(j, i)$ . By sending, their identity or partial secret information node can calculate secret common key. Because the scheme preloads the secret information in node in the form of a matrix so this scheme is not supported to at a new node at later stage after deployment. This scheme is not scalable as it is compulsory to create the matrix by number of nodes. Once the matrix is created, it is not possible to add a new entry to the matrix.

A key protocol for the cluster-based network is introduced by Zhu et al.'s LEAP the localized encryption and authentication protocol [28] which is based on a mixed approach and establish the key for every pair of node and a group key for clustered sensor network. This protocol also provides a key that is shared by all the nodes. So for a sensor network, LEAP protocol provides four types of keys that are individual key, pairwise key, group key, and cluster key. Cluster key is the key shared by all the nodes in a cluster, whereas group key is used by sink node to broadcast a secret message to all nodes in the network. Every sensor node can communicate to sink secretly with the help of an individual key that is unique for each node. In this scheme,  $\mu$ TESLA authentication protocol [21] is used to authenticate a node when a message is broadcast by sink.  $\mu$ TESLA is a  $\mu$ Timed Efficient Streaming Loss-tolerant Authentication Protocol used in a broadcast authentication. Leap provides a very good security but it is not storage efficient as it takes a large memory to store the different keys. Also, there is a network key that is deleted after the establishment of a different key, but if at an early stage this key is compromised, every other generated key is known to the adversary.

In 2006, the SHELL protocol is proposed by Tuah et al. [29]. It is location aware and Scalable, Hierarchical, Efficient, and Light-weight (SHELL) protocol that takes the advantage of location awareness of a sensor node. LEAP is a location-based key management protocol, and keys are assigned to node depending on location of each node. This protocol also used multiple types of keys the same as LEAP. There is a key distributor entity for each cluster that has the responsibility for assign the key for each node in the cluster. This scheme has a better resiliency against node capture, but if the key distributor entity captured all the keys in the node revealed, so this protocol has a big drawback as single point failure. The main advantage of the SHELL protocol is high resiliency against node capture. If nodes are deployed randomly, either node has some mechanism to track its location; otherwise, this protocol does not work as it is a location-based protocol.

In 2006, Panja et al. [30] introduced a hierarchical group keying scheme using the Tree-based Group Diffie-Hellman (TGDH) protocol. This is a tree-based protocol, and each key used by the cluster head is made by partial keys of member nodes. This scheme provides an efficient mechanism for rekeying, but as the number of level increases a very high computation required, so this scheme works best for the heterogeneous network with increasing computation power and memory. Adding or removing a node is also a very efficient and simple task as keys are breaking into smaller components.

Das and Sengupta [31] proposed a scheme for a large-scale sensor network key establishment scheme. This scheme is a deterministic scheme and has fixed connectivity and depends on the topology of the hierarchical wireless sensor networks. Although, the storage requirement and computational overhead for this scheme depend on  $t$ -degree polynomial, which is a complex process and consume maximum energy. This scheme is very good to establish pairwise key between the neighbours using the same symmetric bivariate polynomials over a finite field.

In 2013, Bechkit et al. propose a new type of Hash-Chain-based key schemes for WSN that uses hash chain to generate new keys [13]. This scheme also needs key predistribution to nodes before deployment. After deployment, new keys are generated using a hash function stored in the nodes. In 2015, Zhang and Wang present a new key management scheme SEHKM that uses the concept of assistant node [32].

Many key schemes for hierarchical sensor network schemes have been proposed in recent years. Zhang and Wang [32] gave SEHKM a secure efficient hierarchical key management scheme. This scheme depends on the Diffie-Hellman key algorithm but it is not scalable as more computation is required for key computation. This scheme is inspired for given less computation and overhead. Messai et al. [33, 34] proposed EAHKM for clustered sensor network, and it is a hierarchical key scheme for clustered sensor network. This scheme is also energy efficient but work only for hierarchical network and does not provide pairwise keys between nodes. The cluster head shared the key with member nodes and not with the other cluster heads. A sequence-based key management scheme is also provided by Messai et al. that uses a sequence number and a not coherent function to generate new keys. It is a series-based key management scheme. In this technique, a big number of partial keys are used which has more storage and communication overhead used by each node.

#### 4. Network Model

The following properties are assumed in regard to the WSN model used in our research, each sensor node has a unique identifier, and all sensor nodes are of the same capability other than base station related to memory, processing unit, and spleen and sensing capabilities. The base station has higher capabilities than others and can communicate using higher range. The sensor node and BS are static after deployment and unaware of their location after deployment and communication is symmetric. If a node  $s_i$  can listen to  $s_j$ ,

TABLE 1: Notation.

Notation	Description
$N_i$	$i$ th sensor node in the network denotes the unique id
BS	Base station
$CH_i$	$i$ th cluster head
$k_i$	$i$ th key chain in key pool
$k_{ij}$	$j$ time hash key from $i$ th key chain
$h_n$	No of time key is hashed
$u_0$	First term for recursive formula

then,  $s_j$  is also able to listen  $s_i$  and may use multihop communication. The attacker is assumed to be intelligent and has limited potential. Before taking the full control of network, attacker captures some node and remains invisible. Security scheme must be such that if the behavior of any node is malicious then the key must be renewed from the network. Table 1 represents the notations of various network parameters.

## 5. Proposed Work

We proposed a decentralized scheme for homogeneous cluster-based architecture. All the key management previously proposed are lacking in any of area resiliency, single-point failure, or scalability. Our scheme is distributed, and there is no single point failure. The resiliency of the scheme is also very good as a set of keys is used by different nodes. Our scheme also supports scalability, and it is storage efficient and also consumes less energy. This is also dynamic and shows the exhibility as system topology change. In the proposed scheme, the base station has infinite memory and processing speed, and all sensor nodes are homogeneous and have the same memory and processing speed.

**5.1. Key Chain.** In our scheme, as shown in Figure 2, we have used the key chain as discussed in [13]. In this method, the base station has a key pool that consists of  $P$  noncolliding hash chain of  $L$  length and in a single chain every value is considered as potential key. In a chain, the next key is generated by taking the hash of the previous key.

BS randomly selects  $m$  chain and assigns  $m$  keys to each node before deployment. The key can be hashed at any number of time  $l(0 \leq l \leq L)$ . This process is divided into three phases as key predistribution and cluster formation, session key and cluster key generation, and refresh of keys after interval on demand. Two nodes can communicate to each other if they share the keychain.

For renewal of the key or regenerate the new key for new node, a sequence number is also used. Sequence-based key generation is used to generate the keys for those nodes who are not able to find a common key. Each node also has a seed value or first term and a mathematical formula of a sequence. A numerical sequence like  $(u_1, u_2, u_3, \dots)$  is a list of numbers generated for a series. It is a discrete function that, for any integer  $n$ , associates a number, denoted  $un$ . A recursive formula is used to generate the next term that is used as key.

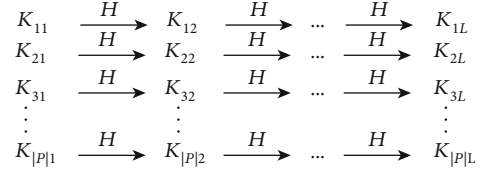


FIGURE 2: Key chain pool.

Series must be nonarithmetic and nongeometric that is also called nonconvergent series. In the case of nonconvergent series for an attacker, it is very difficult to deduce the values of the sequence terms.

**5.2. Key Predistribution and Initialization of Nodes.** Whenever setting up a sensor network, various operations need to be performed before and after the network starts its function. The initial network phase has to generate a hash function and hash chain key pool and also generate a nonconvergent recursive formula. Before randomly deployed the sensor network every node is preloaded with three information: a hash chain, first term of sequence, and a recursive function. Hash chain is used to setup a pairwise key to every node, but as key setup using key predistribution, it is a probabilistic scheme and not guarantees every pair shares a common key. If the key is not found between nodes, sequence number and recursive function are used to generate the common key. This phase involves the initialization of node parameters such as node identifiers, transmission range, and keying material. In this phase, all the network nodes are assigned unique identifiers. In addition, each node is assign  $m$  keys ( $m \ll P$ ) from big key pool  $P$  and a number  $u_0$  that tells how many times the key is hashed. A recursive formula is also stored in sensor. Once nodes are initialized, they will be deployed randomly into their target area which they need to monitor.

**5.3. Key Setup.** After randomly stored, every node sent their id and key chain id to all the neighbour node. If any keys chain matches in both the nodes, they setup the shared keys if no key chain match they use seed value and stored function to generate common key. To generate a common key by using seed value and function, the two nodes send their id and a random number nonce to each other. To maintain the integrity of message, the hash value of the message is also sent. The hash of the message is taken by  $u_0$  times. So a node  $S_i$  sends the message  $\{S_i \| N_i \| H_{u_0}(S_i \| N_i)\}$ , where  $N_i$  is the nonce generated by  $S_i$ , and  $u_0$  is the first term of nonconvergent formula stored in node  $S_i$ .  $H$  is the one way hash function. After receiving the message, node  $S_j$  generates the secret key by the following process:

- (i) Node  $S_i$  generates a nonce  $N_i$  and send the message  $\{S_i \| N_i \| H_{u_0}(S_i \| N_i)\}$  to  $S_j$
- (ii) Node  $S_j$ s generate a nonce  $N_j$  and send the message  $\{S_j \| N_j \| H_{u_0}(S_j \| N_j)\}$  to  $S_i$



**Require:** Network

1. Every node  $S_i$  broadcast a message  $S_i \rightarrow * : M\{S_i, k_i\}$
2. Upon receiving the  $M S_j$  do following:
  - for  $i$  and  $j$
  - if( $k_i == k_j$ )  $list = list + (S_i, k_i)$
  - else  $list = list + (S_i, 0)$
3. Every node  $S_i$  store the common key in the list else store 0
4. For every node  $S_j$  where  $K_j == 0$  Node  $S_i$  send a message  $S_i \rightarrow S_j : M\{S_i, u_i\}$
5. Upon receiving  $M S_j$  do the following
  - if( $k_i != 0$ )
  - if( $u_j < u_i$ )  $H(u_j - u_i)K_i$
  - else
    - generate  $x = H(u_0 \| u_{N1} \| u_{N2} \| S1 \| S2)$
    - $list = list + (N_i, x)$
6. The node with maximum degree is selected as CH
7. CH generate a group key and distribute to members
8. Every key stored in node is hashed by one more time  $K_i = H(k_i)$ ,  $u_0 = u_0 + 1$

ALGORITHM 1: Algorithm for cluster and key setup.

- (iii) After receiving the message  $S_i$  and  $S_j$  computes the  $u_{N_i}$  and  $u_{N_j}$  and generates the common key  $(u_{N_i} \| u_{N_j} \| S_i \| S_j)$

After setup, the pairwise key between every pair of node, a node can send the message to each other using the pairwise key. If the node wants to communicate with the base station, it can use any key of combination of keys and send message and id of keys so that base can use the key to decrypt the message. Once pairwise keys setup all the keys stored, the node is hashed by one more time and this has the same effect as keys are deleted from memory. In this phase node also select cluster head on the bases of node weight that difficult using minimum distance and maximum energy. After election of CH, it generates the group key or cluster key and distributes among the member nodes [29].

**5.4. Key Renewal.** To increase the life time of network, it is necessary to change the cluster head or change in the topology of network or cluster head is changed key refresh is required. If some node is capture than to isolate the node, we have to change the keys stored in that node. There are different processes to refresh the keys of member node or add a new node in the network. A cluster head refreshes the key any time or as per requirements. For this purpose, CH generates a new group key and distributes among the group nodes encrypted by pairwise key.

**5.4.1. If a New Node Is Added to the System.** After a long period of time, some node may lose all energy and stop working. New sensor nodes must be added or replace the previous dead node. Our scheme is exible to the addition of new sensor nodes in the network or replace an old node from network and maintain the key of new node. By using the SSEKMS, newly added node is able to share the common key with old node in the network that are previously

deployed and neighbours of new node. If a new node is added in the network or replace the old node a set of keys from key pool is loaded to the node and deployed in the field. As base station has the id of the node and list ok key that are loaded in the node it can assign the same key in case of node replacement or give a new set of key in case of new node is added. This node tries to find a common key with neighbour node. If a common key is found between nodes, that key is used as pairwise key, and if no key is found, sequence number and function is used to generate the shared key with neighbours.

**5.4.2. Key Refresh for the Node.** Whenever any node is compromise or the role of node is change and there is a change in network topology, BS can initiate the key refresh phase. Key can be refreshed for a specific node or for all nodes in the network. Whenever the keys of a specific node is refreshed, a new value of  $u_0$  is sent to node by base station, and this initial term is used to generate the new keys by using Algorithm 1. To refresh the keys for all node in the network base station initiate the key refresh process send a broadcast a message in the network. This message contains the level of node and energy of node and id of the node. Upon receiving of the message every node reset the initial value  $u_0$  according the level of node and execute Algorithm 1 to reset the key. In every round of key refresh, the value of level is start from max value of key chain length.

## 6. Performance Evaluation

We use the mathematical analysis and simulation process to evaluate the different parameters of our scheme. A theoretical analysis is done to evaluate the parameters, connectivity, storage overhead, and resiliency against node capture. Connectivity of network is given by, that two nodes within the range of each other can send the secure message to each

**Require:** Network

1. A set of  $m$  random keys from key pool  $S$  and loaded in the node
2. Recursive function and first term  $u_0$  is also stored and deploy
3. First node try to find a common key chain with neighbours by sending it's id  $S_i$  and key ids stored in this node
4. if node find common key use that as shared key else use random number and function to generate the key
5. Node choose the cluster head as per weightage of nodes

ALGORITHM 2: Algorithm to maintain the keys of newly added node.

**Require:** Network

1. BS initiate key refresh by brodcastion message  $BS \rightarrow M\{ \text{Hello, BS, Level}=0, \text{Energy}=\infty \}$
2. All the sensor node receiving the message set  $u_0=L$  and forword the message by increasing the level and seting their id and energy level.
3. After seting up the value of  $u_0$  all node execute algorithm 1
4. Node chose the cluster head as per weight

ALGORITHM 3: Refresh the key of node.

TABLE 2: Comparisons of various schemes.

	Key refresh	Node addition	Location based	Memory efficient
KMP	Yes	No	No	No
DKMM	Yes	Yes	Yes	Yes
EAHKM+	Yes	Yes	No	Yes
SSEKMS	Yes	Yes	No	Yes

other, i.e., they have a shared secret key. Storage overhead and computation overhead are given how much storage and computation power required to perform the operations. Resiliency is also the crucial parameter to check the impact of node capture. A simulation study of scheme is done in NS3 and compares the energy consumed by node or overall network compare to other schemes as shown in Table 2. We implement the scheme NS3 simulator with the following parameters number of nodes 50 to 500 in the area of  $300 \times 300$  meters with transmission range Tx Range 20DB and a Key pool 1000 key in which 50 keys are assigns to every node.

**6.1. Safety Analysis.** Sensor networks are also used in far flung areas and deployed in unattended areas to sense various parameters and collect data. So, wireless sensor networks are more prone to various attacks. Two famous attacks are replay attack and node replication. Our scheme is resistant to these attacks, and also resiliency is check against node capture. Resiliency is the probability to reveal the key if node is captured zero resiliency and keys are deleted.

**Node replication attack:** in node replication, an enemy deploys his own controlled sensor and disturbs the network traffic. For node authentication purpose adversary physically captures a sensor node and extracts all information from sensor. The secret credential stored in node is unveiled to adversary and if adversary captures a large number of nodes many key will be revealed. So key management scheme must be

resilient against node capture [35]. To avoid this attack, we deploy different key and key id in every node and base station have id of every allocated key. To apply this attack adversary must have all the keys and can be assign different set of keys to each node.

**Replay attack:** an active attacker who eavesdrop a valid message between the sender and receiver and send this message at a later time is known as playback attack or replay attack. This can be avoided by time stamp on every message. Every message includes the nonce and a timestamp values and encrypted by the shared key. Receiving node checks the timestamp and nonce value after decryption of message. Receiving node may reject the message if timestamp is not valid.

**6.2. Connectivity.** When key setup is completed, a connected graph is created. Two nodes consider as connected if they have a one common key or  $q$  common key for  $q$ -composite scheme [21]. If every pair in the network has shared key, it is considered as 100 percent connectivity. For probabilistic scheme, connectivity is computed as the probability that every pair in the network shared a key. In case of  $q$  composite scheme, each pair must share at least  $q$  key so more keys required to increase the connectivity of network. It may increase the resiliency of network but also increase the computation of node and traffic in the network and bandwidth required for message exchange. In the E-G scheme, the probability  $P_r$  of sharing at least one key [36] is given by  $1 - P$  (node do not share any key) is same as

$$P_r = 1 - \frac{\binom{P}{m} \binom{P-m}{m}}{\binom{P}{2m}}, \quad (1)$$

Where  $m$  keys are selected from a pool of  $P$  keys, as shown in Figure 3. For  $q$ -composite where node share at least

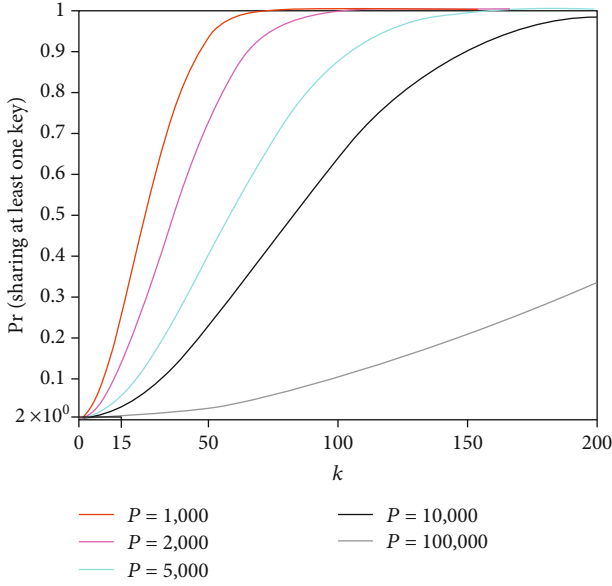


FIGURE 3: Probability of sharing at least one key when two nodes choose  $k$  keys from a pool of size [20].

$q$  keys Pr is given by  $1 - P(\text{node share keys less than } q)$ . The probability the node share exactly  $i$  keys is given by equation

$$P_{\text{SharedExactly}(i)} = \frac{\binom{P}{i} \binom{P-i}{2(m-i)} \binom{2(m-i)}{m-i}}{\binom{P}{m} \binom{P}{m}}, \quad (2)$$

and  $P_r$  the probability of shared at least  $q$  keys  $P_r$  is given by

$$P_r = 1 - (P(0) + P(1) + \dots + P(q-1)). \quad (3)$$

In our scheme, the probability that every pair of node shared one key is 100 percent as if common key is not found for any pair they can generate the key using seed and function stored in node.

**6.3. Communication and Storage Overhead.** Sensor node usually has limited memory, around 10 KB [37]. Hence, storing a large number of keys is not desirable. Although storing more number of keys in node increase connectivity of network but it also increase the probability of more key compromise if a node is capture. In over scheme node store only 10 to 20 keys and when common key establish key hashed are stored that have the same effect of key deleted. Other than this, node also stores a variable  $n$  and hash function that take negligible space but more secure the network.

**6.4. Resiliency of Scheme for Key Compromise.** Two important requirements of key management scheme are node authentication and resiliency of scheme. Resiliency is defined as probability of key revealed when a certain part or network is compromised. According to analysis given in [38], when two nodes have the key from same chain, they can share

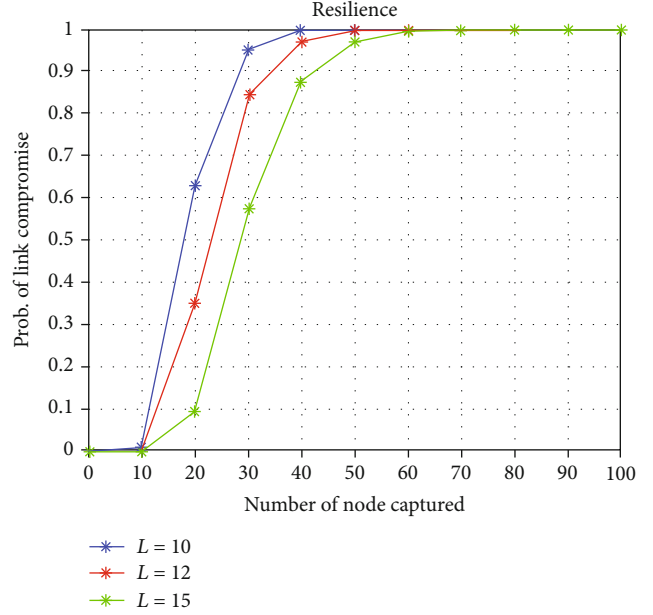


FIGURE 4: Resilience to node compromising attack.

the key with probability  $(2i-1)/L2$ . For a given key chain, the probability that  $i$ th key compromised is  $(m/P) * (i/L)$ . If this chain is compromised, the probability  $P_{\text{ChainComp}}$  is given by:

$$P_{\text{ChainComp}} = \sum_{i=1}^L \left( \frac{2i-1}{L^2} \right) \left( 1 - \left( 1 - \frac{m i}{P L} \right)^x \right). \quad (4)$$

If a chain is compromised than the fraction of link that uses the chain is given by the ratio of number of links uses that chain to total link establish. So the probability of link compromise is given by:

$$P_{\text{LinkComp}} = \sum_{i=q}^m (P_{\text{ChainComp}})^i \frac{P_{\text{Shared}(i)}}{P_{\text{LinkStablish}}}. \quad (5)$$

An important security parameter is the length of chain. The security of scheme is proportional to length of chain but may increase the computation. For better node capture resiliency, the length of chain should be chosen carefully. By increasing the key chain length, more computation is required but it improves resiliency. There is a trade-off between computation and resiliency similar to impact of processing on key chain.

**6.5. Expenditure of Energy.** We implement the scheme and measure expenditure of energy as shown in Figures 4–6. Due to survive on a battery life sensor nodes, key scheme must not use high energy and should utilize the energy effectively. In this scheme, energy consumption by calculating the average remaining energy in a sensor node and energy required for key establishment. In most schemes, a member node sends a message to head by using several hops which consume more energy than a single hope

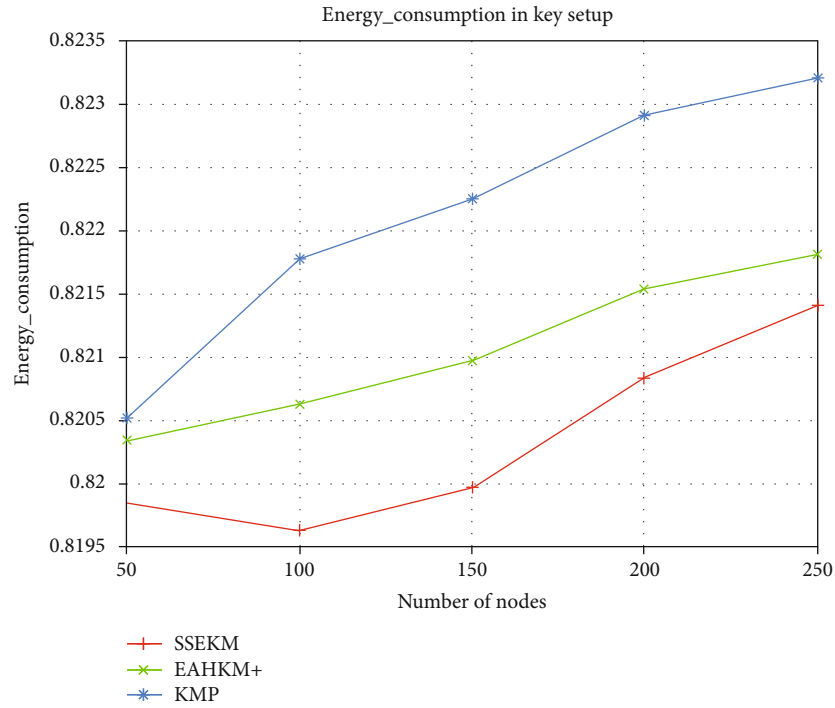


FIGURE 5: Energy consumption.

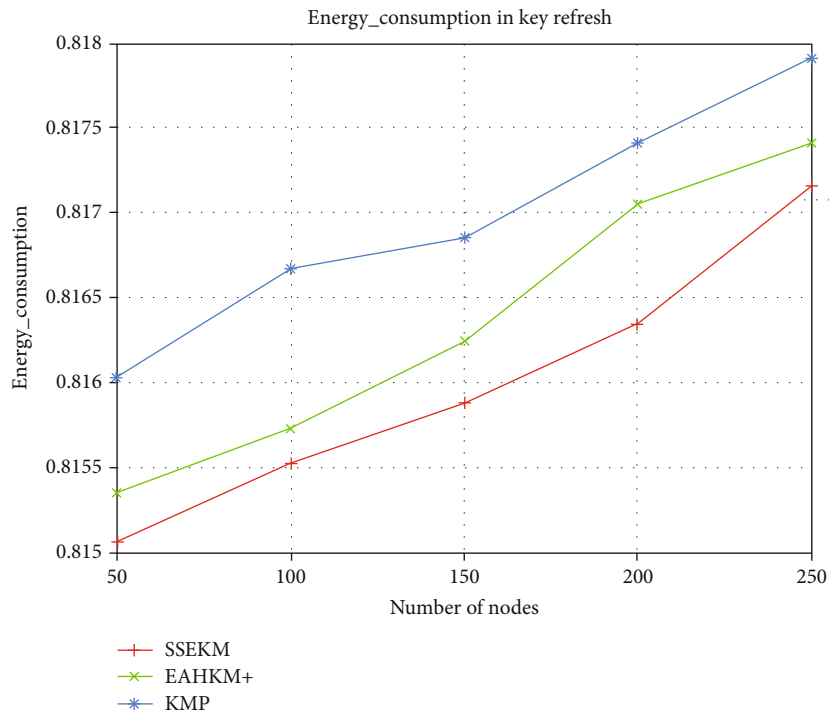


FIGURE 6: Energy consumption in key refresh.

transmission. In our scheme, some storage is used for storing the key, but to setup the key, only one message per node is required in most of the cases. If key is not setup by recursive formula, then some more energy is required in few of the case.

## 7. Conclusion

A key management scheme is a vital part of network security. To distribute and manage the key is very important in WSN. The proposed scheme may be extended for other networks

like IoT. In the paper, we presented a storage efficient dynamic key management technique (SSEKMS) for pairwise key distribution. These keys also support for secure cluster formation and secure connection with base station for each node. Additionally, SSEKMS supports key refreshment and key revoking in the network. SSEKMS has sequence-based key generation for refreshing the keys and used key predistribution with hash chain keys. With respect to other old schemes, our scheme is storage efficient and secure against node capture resiliency. It is also energy efficient compared to other schemes like LEAP, SKM, and SKWN. Unlike SHELL which is location-based and needs location information in advance, our scheme does not need any prior information and works for random distribution. This works in both the cases as pairwise key as well as groupwise key. In the future, we want to extend our scheme for heterogeneous systems and IoT security [39]. In the future, this technique can be extended to support modern networks, which could involve heterogeneous IoT networks [16]. Further use of artificial intelligence and optimization can be found in [36, 40–42].

## Data Availability

The data is open and shall be made available on request.

## Conflicts of Interest

The authors declare that they have no conflicts of interest.

## References

- [1] I. F. Akyildiz, W. Su, Y. Sankarasubramaniam, and E. Cayirci, "A survey on sensor networks," *IEEE Communications Magazine*, vol. 40, no. 8, pp. 102–114, 2002.
- [2] C. Karlof and D. Wagner, "Secure routing in wireless sensor networks: attacks and countermeasures," *Ad Hoc Networks*, vol. 1, no. 2-3, pp. 293–315, 2003.
- [3] D. W. Carman, P. S. Kruus, and B. J. Matt, "Constraints and approaches for distributed sensor network security (final)," *DARPA Project report*, vol. 1, Tech. Rep. 1, Cryptographic Technologies Group, Trusted Information System, NAI Labs, 2000.
- [4] W. R. Heinzelman, A. Chandrakasan, and H. Balakrishnan, "Energy-efficient communication protocol for wireless micro-sensor networks," in *Proceedings of the 33rd annual Hawaii international conference on system sciences*, p. 10, Maui, HI, USA, 2000.
- [5] X. Zhang, H. M. Heys, and C. Li, "Energy efficiency of symmetric key cryptographic algorithms in wireless sensor networks," in *2010 25th Biennial symposium on communications*, pp. 168–172, Kingston, ON, Canada, 2010.
- [6] A. K. Gautam and R. Kumar, "A comparative study of recently proposed key management schemes in wireless sensor network," in *2018 International Conference on Computing, Power and Communication Technologies (GUCON)*, pp. 512–517, Greater Noida, India, 2018.
- [7] G. Dhiman and M. Garg, "Mosse: a novel hybrid multi-objective meta-heuristic algorithm for engineering design problems," *Soft Computing*, vol. 24, no. 24, pp. 18379–18398, 2020.
- [8] H. Kaur, A. Rai, S. S. Bhatia, and G. Dhiman, "Moepo: a novel multi-objective emperor penguin optimizer for global optimization: special application in ranking of cloud service providers," *Engineering applications of Artificial Intelligence*, vol. 96, article 104008, 2020.
- [9] O. Younis and S. Fahmy, "Heed: a hybrid, energy-efficient, distributed clustering approach for ad hoc sensor networks," *IEEE Transactions on Mobile Computing*, vol. 3, no. 4, pp. 366–379, 2004.
- [10] M. Sharma, A. Tandon, S. Narayan, and B. Bhushan, "Classification and analysis of security attacks in wsn and ieee 802.15.4 standards: a survey," in *2017 3rd International Conference on Advances 21 in Computing, Communication & Automation (ICACCA)(Fall)*, pp. 1–5, Dehradun, India, 2017.
- [11] A. J. Menezes, P. C. Van Oorschot, and S. A. Vanstone, *Handbook of Applied Cryptography*, CRC press, 2018.
- [12] M. A. Simplício Jr., P. S. L. M. Barreto, C. B. Margi, and T. C. M. B. Carvalho, "A survey on key management mechanisms for distributed wireless sensor networks," *Computer networks*, vol. 54, no. 15, pp. 2591–2612, 2010.
- [13] W. Bechkit, Y. Challal, and A. Bouabdallah, "A new class of hash-chain based key pre-distribution schemes for wsn," *Computer Communications*, vol. 36, no. 3, pp. 243–255, 2013.
- [14] S. A. Camtepe and B. Yener, "Key Distribution Mechanisms for Wire-Less Sensor Networks: A Survey," Rensselaer Polytechnic Institute, Troy, New York, Technical Report, 2005.
- [15] J. Zhou, Z. Cao, X. Dong, N. Xiong, and A. V. Vasilakos, "4s: a secure and privacy-preserving key management scheme for cloud-assisted wireless body area network in m-healthcare social networks," *Information Sciences*, vol. 314, pp. 255–276, 2015.
- [16] G. Dhiman and V. Kumar, "Spotted hyena optimizer: a novel bio-inspired based metaheuristic technique for engineering applications," *Advances in Engineering Software*, vol. 114, pp. 48–70, 2017.
- [17] D. Qin, S. Jia, S. Yang, E. Wang, and Q. Ding, "Research on secure aggregation scheme based on stateful public key cryptography in wireless sensor networks," *Journal of Information Hiding and Multimedia Signal Processing*, vol. 7, pp. 938–948, 2016.
- [18] K. Lu, Y. Qian, M. Guizani, and H.-H. Chen, "A framework for a distributed key management scheme in heterogeneous wireless sensor networks," *IEEE Transactions on Wireless Communications*, vol. 7, no. 2, pp. 639–647, 2008.
- [19] J. Metan and K. N. N. Murthy, "Robust and secure key management in wsn using arbitrary key-deployment," in *2015 International Conference on Emerging Research in Electronics, Computer Science and Technology (ICERECT)*, pp. 246–250, Mandya, India, 2015.
- [20] L. Eschenauer and V. D. Gligor, "A key-management scheme for distributed sensor networks," in *Proceedings of the 9th ACM conference on Computer and communications security*, pp. 41–47, New York, NY, USA, 2002.
- [21] H. Chan, A. Perrig, and D. Song, "Random key predistribution schemes for sensor networks," in *2003 Symposium on Security and Privacy*, pp. 197–213, Berkeley, CA, USA, 2003.
- [22] M. Rahman, S. Sampalli, and S. Hussain, "A robust pair-wise and group key management protocol for wireless sensor network," in *2010 IEEE Globecom workshops*, pp. 1528–1532, Miami, FL, USA, 2010.
- [23] C. Yang, J. Zhou, W. Zhang, and J. Wong, "Pairwise key establishment for large-scale sensor networks: from identifier-based

- to location-based,” in *Proceedings of the 1st international conference on Scalable information systems*, p. 27, New York, NY, USA, 2006.
- [24] V. P. Mhatre, C. Rosenberg, D. Kofman, R. Mazumdar, and N. Shroff, “A minimum cost heterogeneous sensor network with a lifetime constraint,” *IEEE Transactions on Mobile Computing*, vol. 4, no. 1, pp. 4–15, 2005.
- [25] V. Sharma and M. Hussain, “Node authentication in wsn using key distribution mechanism,” in *2016 International Conference on ICT in Business Industry & Government (ICTBIG)*, pp. 1–7, Indore, India, 2016.
- [26] D. Wenliang, J. Deng, Y. S. Han, P. K. Varshney, J. Katz, and A. Khalili, “A pairwise key predistribution scheme for wireless sensor networks,” in *ACM Transactions on Information and System Security (TISSEC)*, vol. 8no. 2, pp. 228–258, New York, NY, USA, 2005.
- [27] R. Blom, “An optimal class of symmetric key generation systems,” in *Workshop on the Theory and Application of Cryptographic Techniques*, pp. 335–338, Springer, 1984.
- [28] S. Zhu, S. Setia, and S. Jajodia, “LEAP+,” *ACM Transactions on Sensor Networks*, vol. 2, no. 4, pp. 500–528, 2006.
- [29] N. Tuah, M. Ismail, and K. Jumari, “Evaluation of optimal cluster size in heterogenous energy wireless sensor networks,” in *2012 International Symposium on Telecommunication Technologies*, pp. 124–130, Kuala Lumpur, Malaysia, 2012.
- [30] B. Panja, S. K. Madria, and B. Bhargava, “Energy and communication efficient group key management protocol for hierarchical sensor networks,” in *IEEE International Conference on Sensor Networks, Ubiquitous, and Trustworthy Computing (SUTC’06)*, vol. 1, p. 8, Taichung, Taiwan, 2006.
- [31] A. K. Das and I. Sengupta, “An effective group-based key establishment scheme for large-scale wireless sensor networks using bivariate polynomials,” in *2008 3rd International Conference on Communication Systems Software and Middleware and Workshops (COMSWARE’08)*, pp. 9–16, Bangalore, India, 2008.
- [32] X. Zhang and J. Wang, “An efficient key management scheme in hierarchical wireless sensor networks,” in *2015 International Conference on Computing, Communication and Security (ICCCS)*, pp. 1–7, Pointe aux Piments, Mauritius, 2015.
- [33] M.-L. Messai and H. Seba, “Eahkm+: energy-aware secure clustering scheme in wireless sensor networks,” *International Journal of High Performance Computing and Networking*, vol. 11, no. 2, pp. 145–155, 2018.
- [34] M.-L. Messai, H. Seba, and M. Aliouat, “A new hierarchical key management scheme for secure clustering in wireless sensor networks,” in *International conference on wired/wireless internet communication*, pp. 411–424, Springer, 2015.
- [35] W. T. Zhu, J. Zhou, R. H. Deng, and F. Bao, “Detecting node replication attacks in wireless sensor networks: a survey,” *Journal of Network and Computer Applications*, vol. 35, no. 3, pp. 1022–1034, 2012.
- [36] G. Dhiman and V. Kumar, “Emperor penguin optimizer: a bio-inspired algorithm for engineering problems,” *Knowledge-Based Systems*, vol. 159, pp. 20–50, 2018.
- [37] T. Ian, “Downard. Simulating Sensor Networks in ns-2,” Technical report, Naval Research Lab, Washington DC, 2004.
- [38] V. Maty and P. Venda, “Two improvements of random key predistribution for wireless sensor networks,” in *International Conference on Security and Privacy in Communication Systems*, pp. 61–75, Springer, 2012.
- [39] S. Vimal, A. Suresh, P. Subbulakshmi, S. Pradeepa, and M. Kaliappan, “Edge computing-based intrusion detection system for smart cities development using iot in urban areas,” in *Internet of things in smart Technologies for Sustainable Urban Development*, pp. 219–237, Springer, 2020.
- [40] G. Dhiman and A. Kaur, “Stoa: a bio-inspired based optimization algorithm for industrial engineering problems,” *Engineering Applications of Artificial Intelligence*, vol. 82, pp. 148–174, 2019.
- [41] M. Garg and G. Dhiman, “Deep convolution neural network approach for defect inspection of textured surfaces,” *Journal of the Institute of Electronics and Computer*, vol. 2, no. 1, pp. 28–38, 2020.
- [42] P. Singh and G. Dhiman, “A hybrid fuzzy time series forecasting model based on granular computing and bio-inspired optimization approaches,” *Journal of Computational Science*, vol. 27, pp. 370–385, 2018.

## Research Article

# Nonholonomic Wheeled Mobile Robot Trajectory Tracking Control Based on Improved Sliding Mode Variable Structure

Hua Cen <sup>1</sup> and Bhupesh Kumar Singh <sup>2</sup>

<sup>1</sup>Department of Mechanical and Electrical Engineering, Guangxi Modern Polytechnic College, Hechi 547000, China

<sup>2</sup>Arba Minch Institute of Technology, Arba Minch University, Ethiopia

Correspondence should be addressed to Bhupesh Kumar Singh; [dr.bhupeshkumarsingh@amu.edu.et](mailto:dr.bhupeshkumarsingh@amu.edu.et)

Received 28 April 2021; Accepted 1 June 2021; Published 18 June 2021

Academic Editor: VIMAL SHANMUGANATHAN

Copyright © 2021 Hua Cen and Bhupesh Kumar Singh. This is an open access article distributed under the Creative Commons Attribution License, which permits unrestricted use, distribution, and reproduction in any medium, provided the original work is properly cited.

Several research studies are conducted based on the control of wheeled mobile robots. Nonholonomy constraints associated with wheeled mobile robots have encouraged the development of highly nonlinear control techniques. Nonholonomic wheeled mobile robot systems might be exposed to numerous payloads as per the application requirements. This can affect statically or dynamically the complete system mass, inertia, the location of the center of mass, and additional hardware constraints. Due to the nonholonomic and motion limited properties of wheeled mobile robots, the precision of trajectory tracking control is poor. The nonholonomic wheeled mobile robot tracking system is therefore being explored. The kinematic model and sliding mode control model are analyzed, and the trajectory tracking control of the robot is carried out using an enhanced variable structure based on sliding mode. The shear and sliding mode controls are designed, and the control stability is reviewed to control the trajectory of a nonholonomic wheeled mobile robot. The simulation outcomes show that the projected trajectory track control technique is able to improve the mobile robot's control, the error of a pose is small, and the linear velocity and angular speed can be controlled. Take the linear and angular velocity as the predicted trajectory.

## 1. Introduction

A mobile robot is a dynamic nonlinear device, with the benefits of unmanned driving and different controlling practices [1]. A wide range of applications covering survey, patrouille, emergency saving, recognition, and petrochemical features in automation industry, building structure, transport, health care, and other applications are being used by WMR from the last two decades. With the continuous improvement of robot performance, the application range of mobile robots is greatly expanded, and it is widely used in industry, agriculture, service industry, and other industries [2]. Therefore, it has become the hot spot of many scholars in recent years. Among them, wheeled mobile robot (WMR) has a wide range of practical application background [3]. This kind of system is a typical nonholonomic dynamic system because the rolling contact between the wheel and the ground must satisfy the nonholonomic constraint of pure rolling and no slipping. With the extensive feature of wheeled mobile robots

(WMR) in various fields, the precision requirements for the motion trajectory control of wheeled mobile robots are also higher and higher [4, 5]. Each application has specific constraints to the robot design process, which is minimized if all compromises are interpreted by choosing the most convenient drive configuration.

Pappalardo and Guida [6] analyzed the dynamics and control method of nonholonomic robots, studied the Udwadia kalaba equation and underactuated equivalent principle, and carried out corresponding motion control for the robot. Taking the dynamic model of a mobile robot as an example, numerical tests conducted to verify the effectiveness of the projected control method. In addition to preventing distinctiveness nonetheless also keeping the benefits of the mode control sliding system, Zhao et al. [7] have suggested an uncompressive wild nonsingular fatal sliding mode control for mobile robots. The experimental results show that the stability of the control method is high, and the tracking error of the robot trajectory is small.

Ernesto et al. [2] suggested that the response be improved through kinematic model when the robot is backward-oriented and with a short distance to reach the location. Spandan et al. [8] did a novel stability study for the time-related control and gave an empirical relation between the output of the control and the approximation error. In the case where the wheel velocity is not existing deprived in regard to parametrical uncertainty, Shi et al. [9] stated the controller for the case. Bessas et al. [10] have developed an integrated mode controller based on the system's kinematic model. In consideration of several kinematic models, Onat and Ozkan [11] designed an adaptive parameter recognition controller. Based on the tracking error, the controller is moved to different kinematic models. In a Cartesian Coordinate, Lee et al. [12] developed the SMC approach angle. The risk of a switching effect due to high switching gains is a significant drawback of the switching control strategy, which can in turn lead to high frequency unmodelled dynamics affecting the robotic system. In addition, determining the uncertainty limits requires a nominal modelling of the system which, for a complex system such as WMR, is another tedious process [13].

The parametric uncertainties in the actuator were approximated by the Arab and Fateh [14] fuzzy logic, while the core controller used the system's linearization approach to ignore system uncertainty. Application of response linearization-based control or converse dynamic control in real-life circumstances is not continually achievable because it needs a precise understanding of the hardware constraints. In view of the actuator limitation, Shojaei [15] recorded a strong controller with known uncertainty connection. Time-delayed control (TDC) [16] approximates all uncertainty's using immediate past-instant control input and state information. TDC output however is influenced by the TDE that occurs when the time is finite.

A large number of application domains extending from surveillance, planetary exploration, patrolling, emergency rescue operations, reconnaissance, petrochemical applications, industrial automation, construction, entertainment, museum guides, personal services, intervention in extreme environments, transportation, medical care, and other industrial and nonindustrial applications are making use of wheeled mobile robots since the past two decades. Each application faces unique limitations on the robot design procedure which is reduced by selecting the most convenient drive configuration interpreting all the compromises.

The shear feature and sliding mode controller were established in accordance with the sliding mode control theory in accordance with the study of the mobile robot kinematic model. The control stability is studied to diminish the posing fault, and the trajectory of nonholonomic mobile robot control is carried out.

## 2. Trajectory Tracking Control in accordance with Improved Sliding Mode Variable Structure

The trajectory tracking problem of nonholonomic WMR is to propose a virtual mobile robot model which can perfectly

track the ideal space trajectory and then let the actual robot track. Depending on the spatial coordinates, the desired movement of the nonholonomic robot can be expressed [6]. Different robot states, such as angular velocity, linear velocity, and spatial location, differ in time. The tracking trajectory not only included details about the spatial location but also the kinematic model and tracking trajectory feature of the nonholonomic mobile robot with wheels, as well as information on speeds and mobile angles [17]. As shown in Figure 1, the two driving wheels are autonomously determined through 2 DC motors. The follow-up wheel only plays a supporting role in the moving process, and its influence in the kinematic model can be ignored.

Figure 1 shows nonholonomic wheeled moving robot (WMR) powered by two engines attached to a radius  $r$  at distance  $b$  of the two wheels. The vehicle length is regarded as  $L$ . The  $x$ -axis of the axle of the robot in the center of mass is located by a moving body-fixed coordinate system, and the distance offset is supposed to apply. Let  $P$  also stands for the WMR mass deprived of the driving wheels, rotor, and gearbox rotors;  $w$  be each wheel's mass and the appropriate motor-rotor and gearbox rotor;  $I_w$  stands for the wheel MOI equivalent to the wheel axis; and  $I_m$  is the MOIs of each wheel with a rotor engine and gearbox that passes through the  $z$ -axis with a wheel diameter. Three generalized coordinates,  $x_c$ ,  $y_c$ , and  $\theta$ , will specify the location of the WMR. The COM location here  $(x_c, y_c)$  is the WMR heading angle, and  $\theta$  is the WMR heading angle. Again, two more variables  $\theta_r$  and  $\theta_l$ , indicating the rotation of the right-wing and left-wing wheels, are specified to identify some point on the wheels.

*2.1. Nonholonomic Constraints for Wheeled Mobile Robots.* As a characteristic nonholonomic control scheme, the motion of WMR is not only limited by the basic requirements of starting point and ending point but also meets the special requirements of velocity direction or trajectory shape. In addition, WMR is an essentially nonlinear under actuated drift-free dynamic system, which brings greater challenges to its control [18, 19]. However, nonintegrality makes the structure of the robot more flexible and reliable, such as allowing some joints of the robot to be driveless, which greatly reduces the manufacturing cost, quality, and energy consumption of the robot. The nonholonomic control system represented by nonholonomic wheeled mobile robot is a new type of subject, which has important practical value and theoretical significance.

The motion behavior of the mobile robot is constrained by kinematics, which is determined by the structural characteristics of the robot and its motion model. In practical applications, the system is always subject to various constraints, such as geometric constraints and motion constraints, steady and unsteady constraints, double-sided constraints and single-sided constraints, integrable constraints, and nonintegrable constraints [20–23]. Under different constraints, the motion of the control system shows different characteristics. From the essence of system motion, constraints are divided into complete constraints and nonholonomic constraints. Nonholonomic constraints restrict the driving



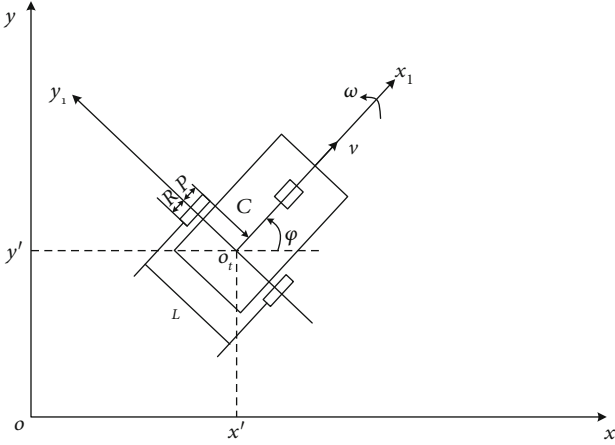


FIGURE 1: Representation of nonholonomic wheeled mobile robot.

direction of robots. Holonomic constraints are dimensions relative to the state description of the system. Suppose a constraint form:

$$f(\mathbf{q}, \dot{\mathbf{q}}, t) = 0, \quad (1)$$

where  $\mathbf{q} = [q_1, q_2, \dots, q_n]$  is the generated space vector.

If this form of constraint can be transformed into a form:

$$F(\mathbf{q}, t) = 0, \quad (2)$$

then the constraint form is integrable. Even if  $f$  in Equation (1) contains the differential quantity of generating space vector in time, it can be expressed by Equation (2), which is usually called complete constraint.

A nonholonomic constraint is defined as a time derivative including variables (coordinates) in the generating system and cannot be integrated. Nonholonomic constraint is a characteristic of the mechanical system. When the dimension of the control variable is lower than the state variable, the control variable can control the state variable [24, 25]. If the system has nonholonomic constraints, the system is nonholonomic, so it cannot move in any path (for example, the car will drive forward or backward, not side-by-side) [26]. The movement of this system is not arbitrary for nonholonomic systems; nonholonomic restrictions specify a subspace in the current time of the potential speed space. The return of internal variables to the initial value in a nonholonomic system does little to ensure that the system returns to the initial state. The condition of a nonholonomic system therefore depends on the route (a sequence set of internal variables that vary according to time). The coordinate dimension for the generated space is not reduced by nonholonomic restrictions excluding the generated speed space.

If the constraint of Equation (1) is integrable, its kinematic constraint is complete; that is, the velocity  $q_1, q_2, \dots, q_n$  can be eliminated from the equation. If the constraint of Equation (1) is not integrable, then the corresponding kinematic constraint is incomplete.

**2.2. Kinematic Model Analysis.** Mobile robots through nonholonomic components are called nonholonomic mobile robots. It belongs to the category of nonholonomic constraints, and its nonholonomic constraints mainly affect the motion characteristics of nonholonomic systems. The nonholonomic constraints received by wheeled mobile robots are generally expressed as first-order differential equations.

In the plane, the position and attitude of the robot can be represented by the following state vectors:

$$\mathbf{x}_m(t) = \begin{bmatrix} x_m(t) \\ y_m(t) \\ \theta_m(t) \end{bmatrix}. \quad (3)$$

$(x_m, y_m)$  represents the position of robot global coordinate system, and  $\theta_m$  represents the steering angle of robot global coordinate system.  $\mathbf{x}_m$  represents the pose state of the robot at time  $t$ .

To keep the balance in the plane, this type of robot usually has one or more castors as additional support only. The driving control is completed by motors which are separately distributed in two wheels. In the universal organize scheme, the motion equation of the robot can be formulated as:

$$\begin{bmatrix} \dot{x}_m(t) \\ \dot{y}_m(t) \\ \dot{\theta}_m(t) \end{bmatrix} = \begin{bmatrix} \cos \theta_m(t) & 0 \\ \sin \theta_m(t) & 0 \\ 0 & 1 \end{bmatrix} \begin{bmatrix} v(t) \\ w(t) \end{bmatrix}. \quad (4)$$

Its nonholonomic motion constraints are as follows:

$$-\dot{x}_m \sin \theta_m + \dot{y}_m \cos \theta_m = 0. \quad (5)$$

Equation (5) can be written in terms of the direction of motion that can be realized by the motion matrix

$$S = \begin{bmatrix} \cos \theta_m(t) & 0 \\ \sin \theta_m(t) & 0 \\ 0 & 1 \end{bmatrix}. \quad (6)$$

$v(t)$  and  $w(t)$  are usually regarded as control variables in robot motion research. After applying the Euler integral to Equation (4), it can be written as follows:

$$\begin{aligned} x_m(k+1) &= x_m(k) + v(k)\Delta t \cos(\theta_m(t)), \\ y_m(k+1) &= y_m(k) + v(k)\Delta t \sin(\theta_m(t)), \\ \theta_m(k+1) &= \theta_m(k) + w(k)\Delta t, \end{aligned} \quad (7)$$

where  $k$  is the discrete time constant and  $\Delta t$  is the time interval.

There are many ways to make the robot move to the ideal position by using the plane changing trajectory. The inverse kinematic challenge is easier for the robot to plane the target trajectory  $(x(t), y(t))$ , so that the direction of the robot is always tangent to the trajectory. If the initial pose of the

reference robot is on a certain trajectory, then there is a kinematic model corresponding to the physical quantity of the reference robot. It can be concluded that the control linear velocity is  $v(t)$ :

$$v(t) = \pm \sqrt{\dot{x}^2(t) + \dot{y}^2(t)}. \quad (8)$$

The positive and negative signs represent the ideal driving direction (+ is the forward direction, and - is the reverse direction). Every point on the track has a tangent angle defined as follows:

$$\theta(t) = \arctan 2(\dot{y}(t), \dot{x}(t)) + k\pi, \quad (9)$$

where  $k \in \{0, 1\}$  defines the ideal driving direction (0 is the forward direction, and 1 is the reverse direction). By calculating the differential of time in Equation (9), the angular velocity of the robot can be obtained:

$$\omega(t) = \frac{\dot{x}(t)\ddot{y}(t) - \dot{y}(t)\ddot{x}(t)}{\dot{x}^2(t) + \dot{y}^2(t)}. \quad (10)$$

By using the Equations (8) and (9), the ideal trajectory control is obtained.

**2.3. Sliding Mode Control Principle.** When the system does not satisfy the linear parameterization condition or when the system model has both structural and parametric uncertainties, a sliding mode control algorithm can be used. If the upper bound function can be found for the unknown dynamic characteristics, the sliding mode control algorithm can achieve the desired control effect by strengthening the control input, that is, using very strong control variables to deal with the unknown dynamic characteristics. Sliding mode control has strong control performance for nonlinear systems affected by uncertain dynamics, which makes the system move according to the designed sliding mode trajectory. The control method has the advantages of a simple calculation method and strong anti-interference ability.

Sliding mode control for nonlinear systems influenced by unknown factors is an easy and efficient way of control. The problem can be reduced to a complex one by simple sliding mode control. The nonlinear method for the single input output can be expressed as follows:

$$y^{(n)} = f(\bar{y}) + u. \quad (11)$$

$u \in R$  and  $y \in R$  are control input variables and system output variables, respectively, and  $\bar{y} = [y, \dot{y}, \dots, y^{(n-1)}]^T \in R^n$  is system state vector.

In order to make the trajectory tracking error  $\bar{e} = \bar{y} - \bar{y}_d = [e, \dot{e}, \dots, e^{(n-1)}]^T$  of the controlled system converge to zero, that is, the state variables of the closed-loop system can gradually track the reference trajectory  $\bar{y}_d = [y_d, \dot{y}_d, \dots, y_d^{(n-1)}]^T$ , a state feedback control law needs to be designed by using sliding mode controller. The PI sliding mode variable structure

controller is defined as follows:

$$s(y, t) = e(t) + \gamma \int_0^t e(\tau) d\tau. \quad (12)$$

Among them,  $\gamma > 0$ . When  $s(y, t) = 0$  is set,  $e = 0$  is the only solution to Equation (12). Then, the problem of tracking the desired trajectory  $y_d$  is equivalent to the problem of function  $s(y, t) = 0$ . At the same time, the selection of control law  $u$  should satisfy the following conditions:

$$\frac{1}{2} \frac{d}{dt} s^2 \leq -\rho |s|, \quad (13)$$

where  $\rho > 0$  is a constant. Equation (13) is called sliding condition, which guarantees that the error state can converge from the initial position far away from  $s(y, t) = 0$  surface to  $s(y, t) = 0$  surface.

The strategy of sliding mode controller mainly comprises 2 parts: the equivalent control variable  $u_{eq}$  is designed for the ideal sliding mode control, and the variable structure control variable  $u_{sw}$  is also designed for the nonlinear system affected by various uncertain factors. The design of sliding mode variable structure controller consists of two steps:

*Step 1.* Design  $s$  switching function to make sliding mode stable and dynamic.

*Step 2.* The sliding mode control law  $u$  is designed to form a sliding mode region on the switching surface  $s(y, t) = 0$  under the condition that the condition Equation (13) is satisfied [27].

For uncertain systems, using the sliding mode variable structure control method can often get the desired results. Compared with the traditional control algorithm, the sliding mode production variable structure control method is discrete; that means, the high-frequency switch control is used to switch between several control laws, which can make the system oscillate with small amplitude and high frequency near the set space surface. Such motion is defined as sliding mode motion. Since various control laws in the variable control method for sliding mode are set in advance and are not disturbed and do not rely on device parameters, this method is highly robust. Then, the concept of sliding mode control combines a trajectory tracking controller with global asymptotic stability.

#### 2.4. Design Shear Function

**Lemma 1.** Any  $x \in R$  and  $|x| < \infty$ , then  $\varphi(x) = x \sin(\arctan x) \geq 0$ , if and only if  $x = 0$ , the equal sign holds. The switching function of sliding mode variable structure control is designed based on backstepping method; firstly, the Lyapunov function is defined as  $V_y = (1/2)y_e^2$ ; suppose  $x_e = cf(k\omega)y_e$ , where  $f(k\omega) = (1 - \exp(-2k\omega))/(1 + \exp(-2k\omega))$  is a hyperbolic tangent function and  $cf(k\omega)y_e$  is a virtual feedback variable;  $c$  and  $k$  were normal. According to the characteristics of

hyperbolic tangent function, we can know  $\omega f(k\omega) \geq 0$ . Assuming  $\phi_e = -\arctan(u_r y_e)$ , then

$$\dot{\phi} = \frac{\partial \phi_e}{\partial u_r} + \frac{\partial \phi_e}{\partial y_e} = \frac{u_r + y_e}{1 + (u_r y_e)^2} < 0. \quad (14)$$

Based on Equation (14) and Lemma 1, the following equation can be given

$$\begin{aligned} \dot{V}_y &= y_e \dot{y}_e = y_e (-x_e \omega - a\omega + u_r \sin \phi_e + a\omega_r \cos \phi_e) \\ &= -y_e x_e \omega - y_e a\omega + u_r y_e \sin(-\arctan(u_r y_e)) \\ &\quad + y_e a\omega_r \cos(-\arctan(u_r y_e)) \leq -y_e x_e \omega - y_e a\omega \\ &\quad + y_e a\omega_r = -y_e^2 cf(k\omega)\omega + y_e a\dot{\phi}_e < 0. \end{aligned} \quad (15)$$

It is concluded that as long as  $x_e$  converges to  $cf(k\omega)y_e$  and  $\phi_e$  converges to  $-\arctan(u_r y_e)$ , the system state variable  $y_e$  will converge to 0. According to this conclusion, the switching function is designed as follows:

$$s = \begin{bmatrix} s_1 \\ s_2 \end{bmatrix} = \begin{bmatrix} x_e - cf(k\omega)y_e \\ \phi_e + \arctan(u_r y_e) \end{bmatrix}. \quad (16)$$

Through the design of sliding mode controller,  $s_1$  and  $s_2$  tend to 0, which means  $x_e$  converges to  $cf(k\omega)y_e$ ,  $\phi_e$  converges to 0, so the system state variable  $y_e$  also converges to 0.

$$\begin{bmatrix} u \\ \omega \end{bmatrix} = \begin{bmatrix} y_e + u_r \cos \phi_e - a\omega_r \sin \phi_e - ckf'(k\omega)\dot{\omega}y_e - cf(k\omega)\dot{y}_e + \varepsilon_1 \frac{1 - e^{-s_1}}{1 + e^{-s_1}} - h_1 s_1 \\ \omega_r + (\partial\alpha/\partial u_r)\dot{u}_r + (\partial\alpha/\partial y_e)(u_r \sin \phi_e + a\omega_r \cos \phi_e) + \varepsilon_2 ((1 - e^{-s_2})/(1 + e^{-s_2})) - h_2 s_2 \\ 1 + (\partial a/\partial y_e)(x_e + a) \end{bmatrix}. \quad (19)$$

When  $a = 0$  is chosen, the trajectory tracking control law of discrepancy drive nonholonomic wheeled mobile robot is as follows

$$\begin{bmatrix} u_0 \\ \omega_0 \end{bmatrix} = \begin{bmatrix} y_e \omega + u_r \cos \phi_e - ckf'(k\omega)\dot{\omega}y_e - cf(k\omega)\dot{y}_e + \varepsilon_1 \frac{1 - e^{-s_1}}{1 + e^{-s_1}} - h_1 s_1 \\ \omega_r + (\partial\alpha/\partial u_r)\dot{u}_r + (\partial\alpha/\partial y_e)(u_r \sin \phi_e) + \varepsilon_2 ((1 - e^{-s_2})/(1 + e^{-s_2})) - h_2 s_2 \\ 1 + (\partial a/\partial y_e)x_e \end{bmatrix}, \quad (20)$$

$$\frac{\partial \alpha}{\partial u_r} = \frac{y_e}{1 + (u_r y_e)^2}, \quad \frac{\partial \alpha}{\partial y_e} = \frac{u_r}{1 + (u_r y_e)^2}.$$

**2.6. Stability Analysis.** Because the sliding mode variable structure control requires that the state quantity of the motion on the sliding surface must be the end point, when the moving point reaches the sliding surface, it must meet the following requirements:  $\lim_{s \rightarrow 0} s\dot{s} \leq 0$ . The following Lyapunov

**2.5. Design of Sliding Mode Controller.** To weaken the jitter, the exponential reaching law  $\dot{s} = -\varepsilon \operatorname{sgn} s - hs$  is adopted, in which  $\varepsilon$  and  $h$  are greater than 0, and  $\varepsilon$  is a small positive number. The following equation can be obtained by using S type continuous function  $(1 - e^{-s})/(1 + e^{-s})$  instead of symbol function:

$$\dot{s}_i = -\varepsilon_i \frac{1 - e^{-s_i}}{1 + e^{-s_i}} - h_i s_i, \quad i = 1, 2. \quad (17)$$

$\varepsilon_i$  is a small positive number, and  $h_i$  is a normal number.

Suppose  $\alpha = \arctan(u_r y_e)$ , from Equation (16) and Equation (17), we can get the following results:

$$\begin{aligned} \dot{s}_i &= \begin{bmatrix} \dot{s}_1 \\ \dot{s}_2 \end{bmatrix} = \begin{bmatrix} -\varepsilon_1 \frac{1 - e^{-s_1}}{1 + e^{-s_1}} - h_1 s_1 \\ -\varepsilon_2 \frac{1 - e^{-s_2}}{1 + e^{-s_2}} - h_2 s_2 \end{bmatrix} = \begin{bmatrix} \dot{x} - ckf'(k\omega)\dot{\omega}y_e - cf(k\omega)\dot{y}_e \\ \dot{\phi}_e + \frac{\partial \alpha}{\partial u_r} \dot{u}_r + \frac{\partial \alpha}{\partial y_e} \dot{y}_e \end{bmatrix} \\ &= \begin{bmatrix} y_e \omega - u + u_r \cos \phi_e - a\omega_r \sin \phi_e - ckf'(k\omega)\dot{\omega}y_e - cf(k\omega)\dot{y}_e \\ \omega_r - \omega + \frac{\partial \alpha}{\partial u_r} \dot{u}_r + \frac{\partial \alpha}{\partial y_e} \dot{y}_e \end{bmatrix}. \end{aligned} \quad (18)$$

From Equation (18), the kinematic trajectory tracking control law of the nonholonomic wheeled mobile robot with discrepancy drive can be obtained

nov function is defined as [28, 29]

$$V = \frac{1}{2} s_1^2 + \frac{1}{2} s_2^2. \quad (21)$$

By deriving Equation (21) and substituting it into Equation (17), we can get the following results:

$$\dot{V} = -h_1 s_1^2 - h_2 s_2^2 - \varepsilon_1 s_1 \frac{1 - e^{-s_1}}{1 + e^{-s_1}} - \varepsilon_2 s_2 \frac{1 - e^{-s_2}}{1 + e^{-s_2}}. \quad (22)$$

Because  $\dot{V} \leq 0$ , so  $V$  is a monotone nonincreasing function;  $V_{t \leq 0}$ ,  $V_t$  is bounded on  $t \in [0, \infty)$ ; therefore, from Equations (16) and (21),  $x_e, y_e, \varphi_e$ , and  $\omega$  are bounded values; it is also known from Equation (19) that  $\dot{\omega}$  expected linear velocity  $u_r$  and angular velocity  $\omega_r$  are bounded quantities; from error Equation (13),  $\dot{x}_e, \dot{y}_e$ , and  $\dot{\varphi}_e$  are bounded; that is,  $x_e, y_e$ , and  $\varphi_e$  are consistent continuous variables; according to Barbat theorem,  $x_e, y_e$ , and  $\varphi_e$  converge to zero when  $t \rightarrow \infty$ .

**Theorem 2.** The Lyapunov function candidate be  $V(\mathbf{e}) = \mathbf{e}^T \mathbf{M} \mathbf{e}$ , where  $\mathbf{M}$  is the result of the Lyapunov equivalence. The stability aspects of the nonholonomic WMR are considered for diverse cases represented as follows:

Case 1. When  $\|s\| \geq \epsilon$ .

The time derivative of  $V$  gives,

$$\begin{aligned} V'(\mathbf{e}) &= \mathbf{e}^T \mathbf{M} \dot{\mathbf{e}} + \dot{\mathbf{e}}^T \mathbf{M} \mathbf{e} = \mathbf{e}^T (\mathbf{A}^T \mathbf{M} + \mathbf{M} \mathbf{A}) \mathbf{e} \\ &+ 2\mathbf{e}^T \mathbf{M} \mathbf{B} (\Delta \mathbf{u}_a + \delta) = -\mathbf{e}^T \mathbf{N} \mathbf{e} + 2s^T \left( -k \frac{s}{\|s\|} + \delta \right). \end{aligned} \quad (23)$$

Additional universalization of  $V'(\mathbf{e})$  produces:

$$\begin{aligned} V'(\mathbf{e}) &\leq -\mathbf{e}^T \mathbf{N} \mathbf{e} - 2\mathbf{k}' \|s\| + 2\|s\| \mathbf{k} \\ &\leq -\lambda_{\min}(\mathbf{N}) \|\mathbf{e}\|^2 + 2(\mathbf{k} - \mathbf{k}') \|s\| \\ &\leq -\|\mathbf{e}\| \left( \lambda_{\min}(\mathbf{N}) \|\mathbf{e}\| - 2(\mathbf{k} - \mathbf{k}') \|\mathbf{B}^T \mathbf{M}\| \right) \end{aligned} \quad (24)$$

So,  $V'(\mathbf{e}) < 0$  may be conventional if  $\|\mathbf{e}\| > (2(\mathbf{k} - \mathbf{k}') \|\mathbf{B}^T \mathbf{M}\|) / \lambda_{\min}(\mathbf{N}) := \omega_2$ . Consequently, the structure may be ultimate bound through subsequent:

$$\|\mathbf{e}\| \leq \frac{\sqrt{(\lambda_{\max}(\mathbf{M}) \omega_2)}}{\lambda_{\min}(\mathbf{M})}. \quad (25)$$

The time to range  $\omega_2$  can initiate as  $t_{r2} - t_0 \leq (V(\mathbf{e}(t_0)) - V(\omega_2)) / c_0$ .

Case 2. When  $\|s\| < \epsilon$ .

The term  $2s^T \delta$  may show as follows:

$$2s^T \delta \leq 2\|s\| \|\delta\| \leq 2\mathbf{k} \|s\| = 2\mathbf{k} \left( \frac{\mathbf{S}^T \mathbf{S}}{\|s\|} \right). \quad (26)$$

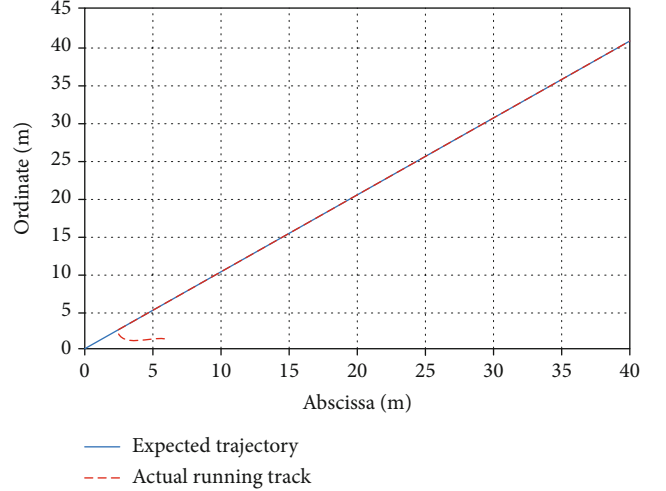


FIGURE 2: Track tracking effect.

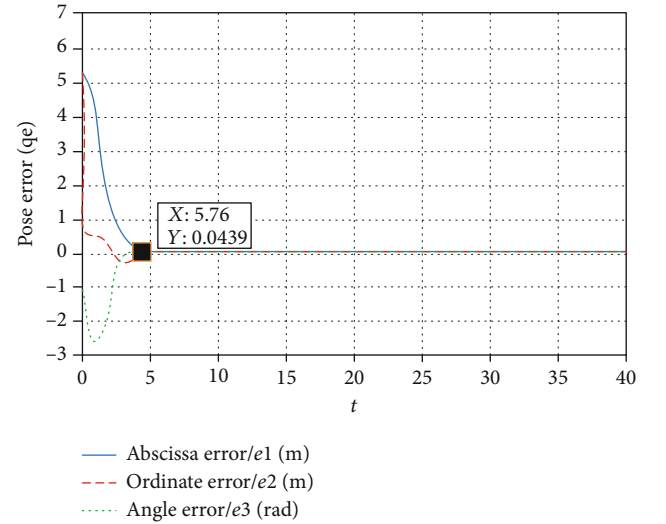


FIGURE 3: Change curve of pose error.

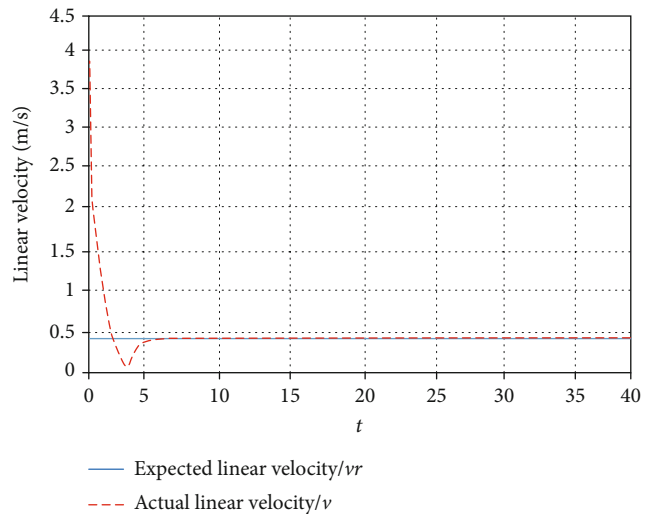


FIGURE 4: Linear velocity variation curve.

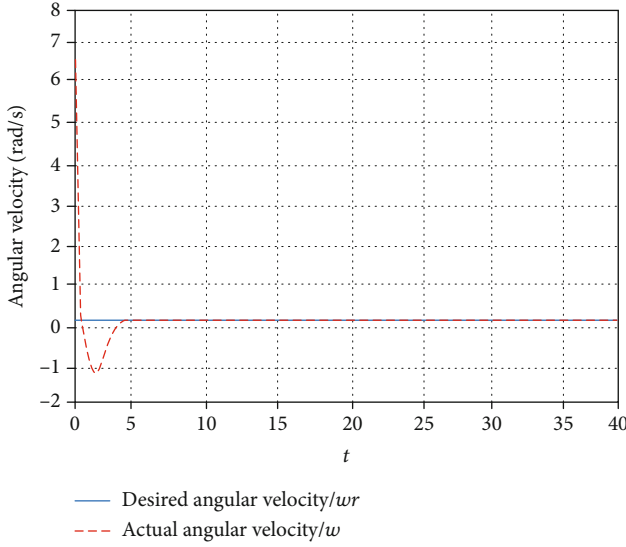


FIGURE 5: Variation curve of angular velocity.

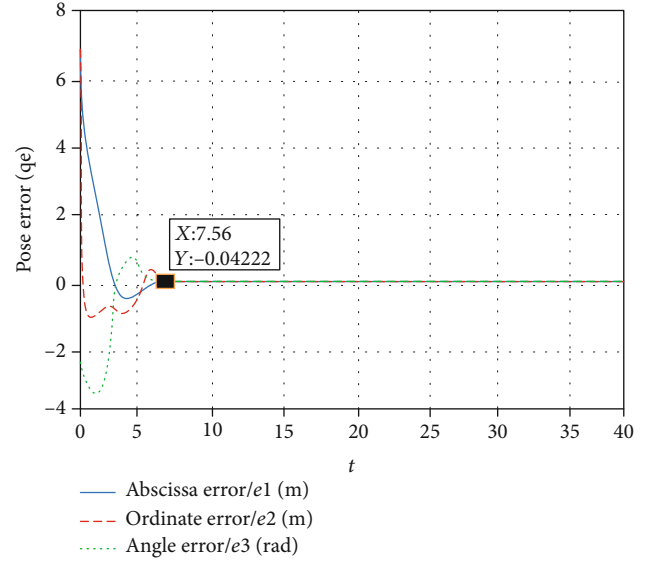


FIGURE 7: Change curve of pose error.

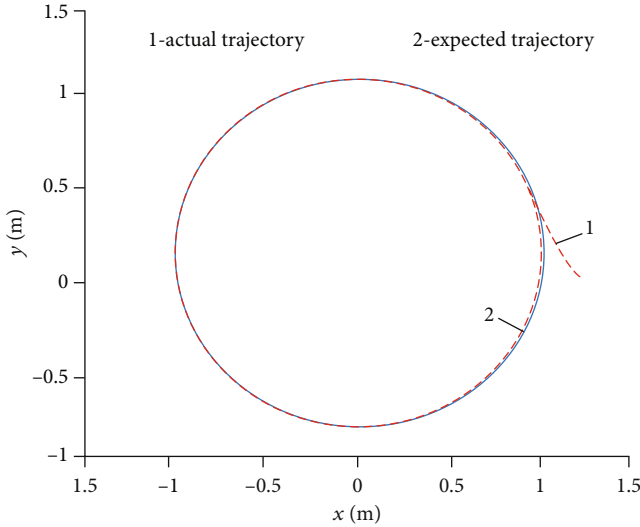


FIGURE 6: Track tracking effect.

By Equations (23) and (26), time directive  $\mathbf{V}(\mathbf{e})$  produces

$$\begin{aligned} \mathbf{V}(\mathbf{e}) &\leq -\mathbf{e}^T \mathbf{N} \mathbf{e} + 2\mathbf{s}^T \left( \Delta \mathbf{u}_a + \mathbf{k} \frac{\mathbf{S}}{\|\mathbf{S}\|} \right) \\ &\leq -\lambda_{\min}(\mathbf{N}) \|\mathbf{e}\|^2 + 2\mathbf{s}^T \left( -\mathbf{k} \frac{\mathbf{S}}{\epsilon} + \mathbf{k} \frac{\mathbf{S}}{\|\mathbf{S}\|} \right). \end{aligned} \quad (27)$$

Equation (27) computes more value  $(\epsilon \mathbf{k}^2)/(2\mathbf{k}')$  when  $\|\mathbf{S}\| = (\epsilon \mathbf{k})/(2\mathbf{k}')$ , so

$$\mathbf{V}(\mathbf{e}) \leq -\lambda_{\min}(\mathbf{N}) \|\mathbf{e}\|^2 + \frac{\epsilon \mathbf{k}^2}{2\mathbf{k}}. \quad (28)$$

Yet over,  $\mathbf{V}(\mathbf{e}) < 0$  may conventional if  $\|\mathbf{e}\| >$

$\sqrt{(\epsilon \mathbf{k}^2)/(2\mathbf{k}' \lambda_{\min}(\mathbf{Q}))} := \dot{\omega}_3$ . Consequently, the structure is ultimate bound with the subsequent:

$$\|\mathbf{e}\| \leq \sqrt{\frac{\lambda_{\max}(\mathbf{M}) \dot{\omega}_3}{\lambda_{\max}(\mathbf{M})}}. \quad (29)$$

Correspondingly, the time to influence  $\dot{\omega}_3$  can initiate as  $t_{r3} - t_0 \leq V(e(t_0)) - V(\dot{\omega}_3)/c_0$ .

Equations (23), (25), and (29) can easily be understood as  $\dot{\omega}_3 < \dot{\omega}_2 < \dot{\omega}_1$ . In addition,  $\epsilon$  is chosen very small in practice, and thus,  $\dot{\omega}_3$  can be minimized by correct tuning of  $\epsilon$  and  $N$  additionally.

### 3. Simulation Experiment Verification

Considering that line and circle are common expected trajectory forms in practical application, this paper selects linear and circular trajectories to simulate and verify the above tracking control law and carries out the corresponding trajectory tracking controller simulation for nonholonomic WMR. The excessive acceleration caused by excessive speed will destroy the nonholonomic constraints of the robot, which is easy to cause the lateral movement or longitudinal sliding of the mobile robot. To avoid the above problems, the speed of the mobile robot must be limited. The maximum speed is 1.5 m/s, and the extreme angular velocity is 1.5 rad/s. The experiments of WMR are considered as follows: the hardware components for the robotic stages are nominated as  $m = 34$  kg,  $d = 0.14$  m,  $r = 0.085$  m,  $b = 0.504$  m,  $I = 4.89$  kg m<sup>2</sup>,  $I_w = 0.08$  kg m<sup>2</sup>,  $k = 0.36$  kg m<sup>2</sup>,  $I = 6.13$  kg m<sup>2</sup>,  $I_w = 0.08$  kg m<sup>2</sup>, and  $K = 0.33$  kg m. Due to the communiqué interruption among the robot and control station and the related sensor suite and hardware, the sampling time  $h$  is considered judiciously 100 ms. In experimentation with wheel location and velocity, the wheel encoders (incremental encoder of square

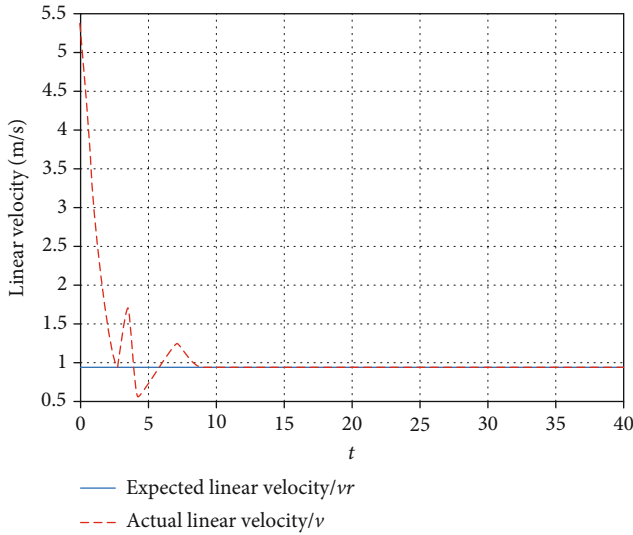


FIGURE 8: Linear velocity variation curve.

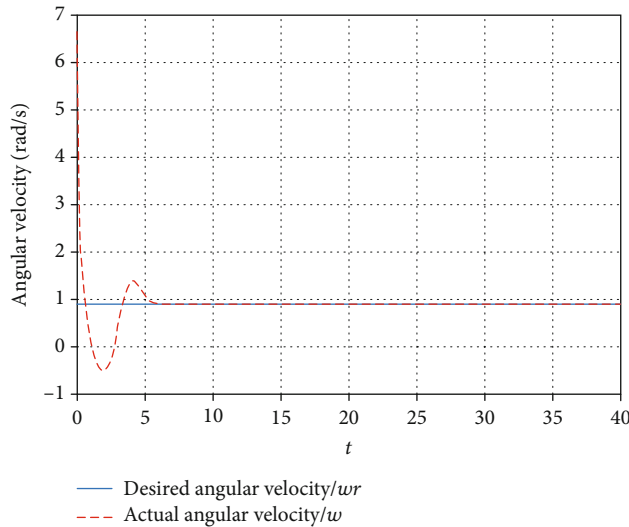


FIGURE 9: Variation curve of angular velocity.

design with 500 ppr) are used. Moreover, when the wheel velocities  $\theta_r$  and  $\theta_l$  are achieved, the following kinematic relationships integrate the remaining state variables.

**3.1. Straight Track.** When the trajectory is a straight line, the control input of the mobile robot is selected as follows: the primary linear velocity is 0.4 m/s, the angular velocity is 0.3 rad/s, and the controller parameters are set to 1.5. The simulation results are shown in Figures 2–5.

It can be seen from Figure 2 that under the action of the control law, the nonholonomic WMR system can realize the straight-line trajectory tracking at the abscissa of about 5 m and finally converge to the given linear reference trajectory. The pose error can eventually converge to 0 and can be seen in Figure 3. The nonholonomic wheeled mobile robot device will, as shown in Figures 4 and 5, converge the anticipated linear velocity and the expected angular velocity under the

control rule, which checks the effectiveness of the trajectory tracking process.

**3.2. Circular Trajectory.** When the trajectory is circular, the control input of the mobile robot is selected as follows: the primary linear velocity is 1 m/s, the angular velocity is 1 rad/s, and the controller parameters are set to 1. Figures 6–9 show the results of the simulation.

From Figures 6–9 that under the action of the designed control law, the circular motion trajectory always has a good fit with the expected trajectory, and the pose error can eventually converge to 0, and the linear velocity and angular velocity can also converge to the expected situation after different times. Therefore, the efficiency of the control law in tracking the circular trajectory of the nonholonomic WMR is verified.

In summary, it can be seen from the results of the above simulation of two tracking types on a nonholonomic mobile robot that the nonholonomic mobile robot system can progressively pursue the reference trajectory under the effect of a designed trajectory tracking law, the position error can converge to zero quickly, and the input of the speed control can converge also to the referee quickly. The efficacy of the proposed law on control is verified.

## 4. Conclusion

In this paper, the nonholonomic WMR trajectory control system based on improved variable structure of sliding mode is projected. Based on analyzing the principle of sliding mode control, the improved method is designed by adding stability analysis to reduce the pose error of trajectory tracking control. The experimental results verify the high control precision effect of the designed method and provide a basic theoretical reference for practical application.

## Data Availability

Data are available on request

## Conflicts of Interest

The authors declare no conflicts of interest.

## References

- [1] Y. Qiu, B. Li, W. Shi, and X. Zhang, “Visual servo tracking of wheeled mobile robots with unknown extrinsic parameters,” *IEEE Transactions on Industrial Electronics*, vol. 66, no. 11, pp. 8600–8609, 2019.
- [2] E. Fabregas, G. Farias, E. E. Aranda et al., “Simulation and experimental results of a new control strategy for point stabilization of nonholonomic mobile robots,” *IEEE Transactions on Industrial Electronics*, vol. 67, no. 8, pp. 6679–6687, 2020.
- [3] C. Della Santina, R. K. Katzschmann, A. Bicchi, and D. Rus, “Model-based dynamic feedback control of a planar soft robot: trajectory tracking and interaction with the environment,” *The International Journal of Robotics Research*, vol. 39, no. 4, pp. 490–513, 2020.

- [4] D. Saravanakumar, A. Thomas, and J. Jarvis, "Bacillus strains in the control of bacterial wilt in tomato," *Phytopathology*, vol. 108, no. 10, p. 143, 2018.
- [5] Y. Wang, M. Shan, Y. Yue, and D. Wang, "Vision-based flexible leader-follower formation tracking of multiple nonholonomic mobile robots in unknown obstacle environments," *IEEE Transactions on Control Systems Technology*, vol. 28, no. 3, pp. 1025–1033, 2020.
- [6] C. M. Pappalardo and D. Guida, "On the dynamics and control of underactuated nonholonomic mechanical systems and applications to mobile robots," *Archive of Applied Mechanics*, vol. 89, no. 4, pp. 669–698, 2019.
- [7] J. Y. Zhai and Z. B. Song, "Adaptive sliding mode trajectory tracking control for wheeled mobile robots," *International Journal of Control*, vol. 92, no. 10, pp. 1–16, 2018.
- [8] S. Roy, S. Nandy, I. N. Kar, R. Ray, and S. N. Shome, "Robust control of nonholonomic wheeled mobile robot with past information: theory and experiment," *Proceedings of the Institution of Mechanical Engineers Part I Journal of Systems and Control Engineering*, vol. 231, no. 3, pp. 178–188, 2017.
- [9] S. Shi, X. Yu, and S. Khoo, "Robust finite-time tracking control of nonholonomic mobile robots without velocity measurements," *International Journal of Control*, vol. 89, no. 2, pp. 411–423, 2016.
- [10] A. Bessas, A. Benalia, and F. Boudjema, "Integral sliding mode control for trajectory tracking of wheeled mobile robot in presence of uncertainties," *Journal of Control Science and Engineering*, vol. 2016, Article ID 7915375, 10 pages, 2016.
- [11] A. Onat and M. Ozkan, "Dynamic adaptive trajectory tracking control of nonholonomic mobile robots using multiple models approach," *Advanced Robotics*, vol. 29, no. 14, pp. 913–928, 2015.
- [12] J. K. Lee, Y. H. Choi, and J. B. Park, "Sliding mode tracking control of mobile robots with approach angle in Cartesian coordinates," *International Journal of Control, Automation*, vol. 13, no. 3, pp. 718–724, 2015.
- [13] M. Rakhra, R. Singh, T. K. Lohani, and M. Shabaz, "Metaheuristic and machine learning-based smart engine for renting and sharing of agriculture equipment," *Mathematical Problems in Engineering*, vol. 2021, Article ID 5561065, 13 pages, 2021.
- [14] A. Arab and M. M. Fateh, "An uncertainty compensator for robust control of wheeled mobile robots," *Advanced Robotics*, vol. 29, no. 20, pp. 1303–1313, 2015.
- [15] K. Shojaei, "Saturated output feedback control of uncertain nonholonomic wheeled mobile robots," *Robotica*, vol. 33, no. 1, pp. 87–105, 2015.
- [16] S. Roy, S. Nandy, R. Ray, and S. N. Shome, "Robust path tracking control of nonholonomic wheeled mobile robot: experimental validation," *International Journal of Control, Automation and Systems*, vol. 13, no. 4, pp. 897–905, 2015.
- [17] Q. Yao, M. Shabaz, T. K. Lohani, B. M. Wasim, G. S. Panesar, and R. K. Singh, "3D modelling and visualization for vision-based vibration signal processing and measurement," *Journal of Intelligent Systems*, vol. 30, no. 1, pp. 541–553, 2021.
- [18] S. J. Yoo and B. S. Park, "Connectivity-preserving approach for distributed adaptive synchronized tracking of networked uncertain nonholonomic mobile robots," *IEEE Transactions on Cybernetics*, vol. 48, no. 9, pp. 2598–2608, 2018.
- [19] V. Jagota, A. P. S. Sethi, and K. Kumar, "Finite element method: an overview," *Walailak Journal of Science & Technology*, vol. 10, no. 1, pp. 1–8, 2013.
- [20] A. Sgorbissa, "Integrated robot planning, path following, and obstacle avoidance in two and three dimensions: wheeled robots, underwater vehicles, and multicopters," *The International Journal of Robotics Research*, vol. 38, no. 7, pp. 853–876, 2019.
- [21] A. Kumar, V. Jagota, R. Q. Shawl et al., "Wire EDM process parameter optimization for D2 steel," *Materials Today: Proceedings*, vol. 37, no. 2, pp. 2478–2482, 2021.
- [22] S. Dogru and L. Marques, "A physics-based power model for skid-steered wheeled mobile robots," *IEEE Transactions on Robotics*, vol. 34, no. 2, pp. 421–433, 2018.
- [23] P. B. Dash, B. Naik, J. Nayak, and S. Vimal, "Deep belief network-based probabilistic generative model for detection of robotic manipulator failure execution," *Soft Computing*, 2021.
- [24] G. Dhiman and A. Kaur, "HKn-RVEA: a novel many-objective evolutionary algorithm for car side impact bar crashworthiness problem," *International Journal of Vehicle Design*, vol. 80, no. 2/3/4, pp. 257–284, 2019.
- [25] K. Albert, K. S. Phogat, F. Anhalt, R. N. Banavar, D. Chatterjee, and B. Lohmann, "Structure-preserving constrained optimal trajectory planning of a wheeled inverted pendulum," *IEEE Transactions on Robotics*, vol. 36, no. 3, pp. 910–923, 2020.
- [26] Y. A. Kapitanjuk, A. V. Proskurnikov, and M. Cao, "A guiding vector-field algorithm for path-following control of nonholonomic mobile robots," *IEEE Transactions on Control Systems Technology*, vol. 26, no. 4, pp. 1372–1385, 2018.
- [27] T. Yona and Y. Or, "The wheeled three-link snake model: singularities in nonholonomic constraints and stick-slip hybrid dynamics induced by Coulomb friction," *Nonlinear Dynamics*, vol. 95, no. 3, pp. 2307–2324, 2019.
- [28] L. Ding, L. Huang, S. Li et al., "Definition and application of variable resistance coefficient for wheeled mobile robots on deformable terrain," *IEEE Transactions on Robotics*, vol. 36, no. 3, pp. 894–909, 2020.
- [29] J. Alonso-Mora, P. Beardsley, and R. Siegwart, "Cooperative collision avoidance for nonholonomic robots," *IEEE Transactions on Robotics*, vol. 34, no. 2, pp. 404–420, 2018.

## Research Article

# Hybrid Resource Environmental Value Chain Model Based on a Discrete Time Algorithm

Wenting Cao <sup>1</sup>, Melkamu Teshome Ayana <sup>2</sup>, and Rongwei Gao <sup>3</sup>

<sup>1</sup>School of Economics and Management, Fuzhou University, Fuzhou 350108, China

<sup>2</sup>Department of Hydraulic and Water Resources Engineering, Arba Minch University, Ethiopia

<sup>3</sup>Planning and Design Institute 1, Fujian Provincial Institute of Architectural Design and Research Co. Ltd., Fuzhou 350001, China

Correspondence should be addressed to Melkamu Teshome Ayana; [melkamu.teshome@amu.edu.et](mailto:melkamu.teshome@amu.edu.et)

Received 27 March 2021; Accepted 29 May 2021; Published 15 June 2021

Academic Editor: Vimal Shanmuganathan

Copyright © 2021 Wenting Cao et al. This is an open access article distributed under the Creative Commons Attribution License, which permits unrestricted use, distribution, and reproduction in any medium, provided the original work is properly cited.

Due to the inconsistency between resource environment and value data types, the hybrid model of resource environment value chain cannot effectively coordinate the relationship among resources, environment, and value chain. The circulation of resource chain, ecological chain, and value chain is not completed independently; they are intertwined and promote each other. Therefore, this paper proposes a hybrid resource environmental value chain model based on a discrete time algorithm. Analyze the hybrid internal structure of resource chain, environment chain, and value chain model; integrate the natural resource information through the objective function of natural resource integration; obtain the indicators affecting the environment; and complete the analysis of the characteristics of environmental change. On this basis, the relationship between resources, environment, and economic value is analyzed, and the hybrid content of resources, environment, and value chain is determined. The discrete-time algorithm is introduced to transform the hybrid content into the same data format, obtain the objective function and constraints of the resource environment value chain hybrid model, and complete the construction of the resource environment value chain hybrid model based on the discrete-time algorithm. The simulation results show that the hybrid model designed in this paper can effectively improve the resource saving rate, up to 97%, and the error of resource environment value chain data fusion is the lowest, and the time is less than 1 min which was a considerable achievement.

## 1. Introduction

Since the 1990s, the problems of resources and environmental protection have become a hot topic in manufacturing industry, and the concept of green manufacturing has been put forward. This is a modern enterprise production mode based on environmental protection competition strategy. Mechanical engineering scholars mostly discuss the general theoretical system, special technology, and other aspects of green manufacturing, involving the concept and content of green design to a certain extent, mainly from the aspect of manufacturing technology, but these studies only examine the technical greenness of products and their manufacturing design schemes, which is not enough, and need further cost-benefit analysis [1]. In recent years, most of the production industries have formed an industrial model of “raw materials production processing sales.” Among them, raw materials are

mainly obtained from the natural environment, are produced into products through generation and processing technology, and obtained economic benefits through sales to achieve industrial value. Resources are all kinds of material elements such as material resources, financial resources, and human resources in a country or a certain area. It can be divided into natural resources and social resources. The environment includes not only the material factors including atmosphere, water, soil, plants, animals, and microorganisms but also the nonmaterial factors including ideas, systems, and codes of conduct; not only the natural factors but also the social factors; and not only the nonlife forms but also the life forms. The conditions for the existence and development of an industrial enterprise must create value for its shareholders and other interest groups. The process of creating value is divided into a series of different but interrelated economic activities, or “value-added activities,” which constitute the



enterprise “value chain” [2]. In the process of enterprise operation, we pay more attention to the economic benefits of the enterprise and ignore the environmental protection and the rational use of resources, so there are environmental pollution, resource shortage, and other problems. In order to solve this problem, researchers in this field have done a lot of research.

The hybrid model of resource environment value chain enables enterprises to pay attention to the value of products and the benefits of enterprises in operation and production, realize the rational use of resources, and minimize the damage to the natural environment. By nesting the three parts of resources, environment, and value chain, a coordinated and linked mechanism is formed, so as to balance the industrial economy and resource environment and the relationship between. Foreign research on the hybrid development of resource environment value chain mainly focuses on the development of environmental industry in developed countries, the driving force of industrial development, and the necessity of environmental industry development [3].

The literature [4] proposes a multilevel hybrid model based on resources, ecology, and value chain industrial circular economy system. Based on the idea of symbiotic circular economy, through literature review, theoretical analysis, practical research, and expert consultation, according to the logic of resource chain, ecological chain, and value chain, this model studies the ecological environment subsystem in a wider range. The core structure model of circular economy and its multilevel extended structure model of social economic subsystem can effectively reduce environmental pollution, but its analysis process is complex and time-consuming, which cannot be applied in practice. In reference [5], a zero model for hybrid decision of resource environment symbiotic network is proposed. The construction of the model is an important basis to determine the network nesting. By exploring the influence of matrix asymmetry on the network nesting based on different zero model construction methods, this paper attempts to provide a basis for the selection of the zero model of asymmetric network. The construction of the model can effectively reduce the deviation error of pairing overlap degree and improve the accuracy. However, the sensitivity of the model is insufficient in determining the nesting of highly asymmetric networks, and there are obvious problems of resource, environment, and value chain inconsistency.

In order to solve the problems in the traditional hybrid model of resource environment value chain, a discrete time algorithm is introduced. The discrete-time algorithm can consider the running time and cost of enterprise project comprehensively, which is more in line with the multiobjective characteristics of a hybrid model. Based on the traditional hybrid model of resource environment value chain, the discrete-time algorithm is used to deal with the three components of the model, and the hybrid structure is replanned to achieve the optimal design of the hybrid model. Coordinate resources, environment, and value chain in the same position in operation, and realize the protection of environmental resources on the basis of ensuring enterprise value and benefit.

## 2. Design of Hybrid Model of Resource Environment Value Chain

Ecological economy requires people to use ecological laws to guide human economic activities, reconstruct the economic system according to the laws of material circulation and energy flow of the natural ecosystem, integrate the economic system into the material circulation process of the natural ecosystem, and integrate clean production, comprehensive utilization of resources, ecosystem construction, sustainable consumption, and interest balance. Therefore, the economic model is a kind of economic development model to promote the coordination and harmony between human and nature. The economic system of most enterprises’ production industry chain itself spans the economic system and natural system and has the unique structure and green symbiosis characteristics that the general economy is not prepared for. The implementation process of enterprise production industry chain is shown in Figure 1.

Among them, the main driving factors of industrial development in the mature stage are economic stimulus, public environmental awareness, and corporate social responsibility. In the mature stage of the industry, due to the gradual improvement of environmental laws and regulations, the improvement of public environmental awareness, the improvement of the ability of enterprises to bear environmental responsibility, and the reduction of the role of environmental laws and regulations help in promoting the environmental industry [6]. Through the application of the hybrid model of resource environment value chain and the assistance of relevant laws and regulations, the balance of resource, environment, and enterprise value can be realized.

*2.1. Hybrid Structure Analysis of Resource Environment Value Chain.* A hybrid model is a kind of structural equation model. If all free parameters of a model are part of the same parameters in model B, a model is said to be hybrid in the model [7]. In the path graph, the path graph of model A can be obtained by removing some paths from the path graph of model B. Combined with the basic structure of the hybrid model, the planning of the hybrid model structure of resource environment value chain is realized from three aspects: resource chain, ecological environment chain, and value chain.

*2.1.1. Hybrid Structure of Resource Chain.* In the upstream of the resource chain, the extended structure model regards resource cultivation as the “first workshop” of product production, providing stable raw material source with low transaction cost and operation risk for the product production and processing process; the external market transaction channel with high transaction cost, high risk, and poor stability of the supply chain is only used as an auxiliary raw material source. In order to improve the utilization rate of natural resources, the natural raw material sources of the product industry also include “three residues,” i.e., cutting residues, wood making residues, and processing residues [8]. The production enterprise and its supply chain members invest in the raw material base to form a forest management cycle.

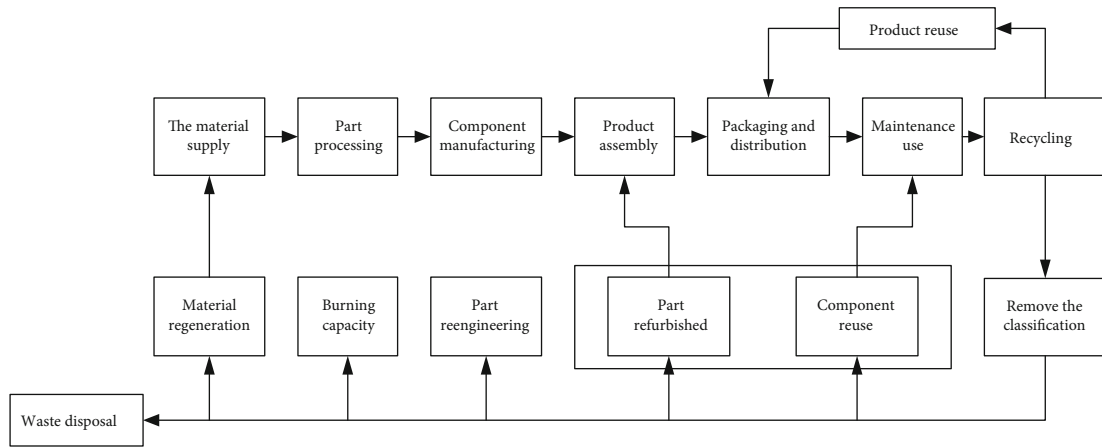


FIGURE 1: Flow chart of enterprise production industry chain.

In the downstream of the resource chain, the economic system can be extended to the recycling of waste in the consumption link, that is, reverse logistics industry or vein industry. The expanding fields mainly include chemical processing cycle and wood physical processing cycle. In the circulation chain, raw materials are used in a certain step of the technological process, and products are formed through a series of complex chemical processing processes for consumers to use. Then, the consumer's waste products after use are recycled and treated properly as product processing raw materials for recycling [9]. From the perspective of resource chain, economic system can be hybrid in product processing industry and comprehensive utilization of production process waste.

*2.1.2. Hybrid Structure of Environment Chain.* The structure of resource chain expansion provides the necessary biological basis for the further expansion of the enterprise economic system to the ecological environment subsystem. On this basis, according to the operation principle of ecosystem, the environment chain expansion structure of enterprise economic system is constructed, as shown in Figure 2.

In Figure 2, the environment chain is hybrid as a grey box of “CE resource chain extension structure,” in which the directed solid line is the main resource chain. Outside the grey box, each box represents the process of promoting the healthy development of the ecosystem, which is called “ecological process” for short; connecting each box with the directional dotted line represents the ecological flow, which is called “ecological force” for short. Different from resource flow, ecological flow has gone beyond the scope of material flow and energy flow. It forms ecological forces through material flow, energy flow, capital flow, technology flow, process flow, and other “fluids.” In this paper, the environmental chain is composed of ecological process and ecological flow.

In product manufacturing and its horizontal expansion of supply chain enterprises, ecological chain circulation is formed through the ways: first, under the guidance of resource processing integration strategy, industrial raw material construction is carried out to solve the problem of enterprise raw material supply on the one hand and make

contribution to the construction of natural ecosystem on the other hand [10, 11]. Under the guidance of green marketing strategy, carry out a forest certification work and implement sustainable management of natural resources. After the treatment of processing wastewater, after removing harmful substances, there are rich organic substances left, which can be used to irrigate natural resources, which is conducive to the growth and construction of natural resources. In addition, sludge and separated elements are rich in organic matter, N, P, K, and other substances that are conducive to the growth of natural resources, which can be used to develop special compound fertilizers and soil improvers for quick natural resources.

If we want to make the environment have good ecological benefits, the process not only should have good ecological functions but also depends on the input ecological power. The positive direction of ecological input will play a role in promoting ecological benefits, while the negative direction will play a role in destroying the ecology. Therefore, only through the virtuous cycle of the whole ecological chain system can we finally achieve the management objectives of ecological construction and environmental protection.

*2.1.3. Hybrid Structure of Value Chain.* Using the same structure as the environment chain, the environment chain structure is hybrid into the value chain structure. In value chain planning, the optimization and coordination of supply chain benefit distribution are an important part of value chain and a process of supply chain management. Reasonable benefit distribution can mobilize the enthusiasm of each subject of circular economy, and then a series of benign cycle processes will take place: promoting the coordination and effective operation of value chain itself, encouraging the economic subject of relevant enterprises, making continuous input to the cultivation of natural resources, realizing value feedback, and then promoting the benign cycle of resource chain and environmental chain of economic system and the health of resource chain and environmental chain. In turn, healthy development supports the healthy growth of the value chain and ultimately promotes the sustainable development of the entire economic system [12].

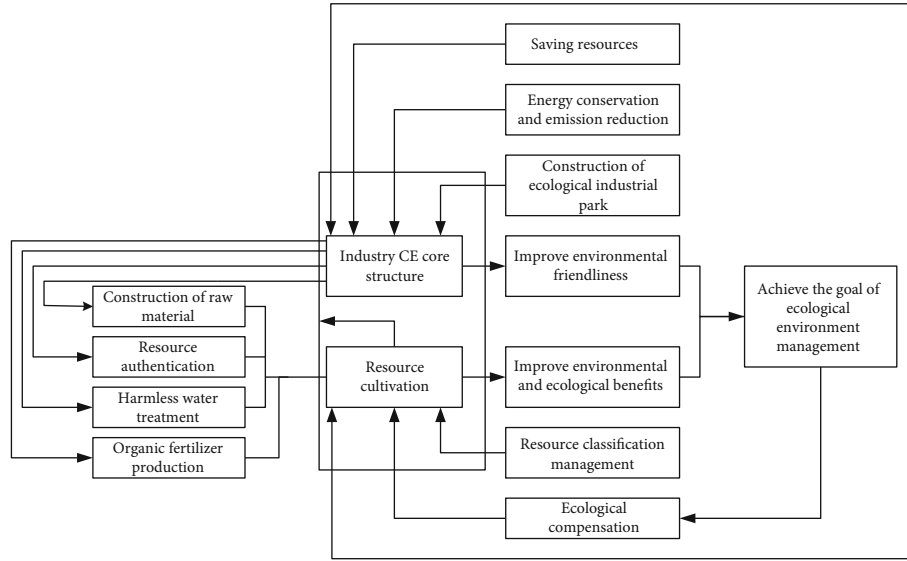


FIGURE 2: Hybrid structure of environment chain.

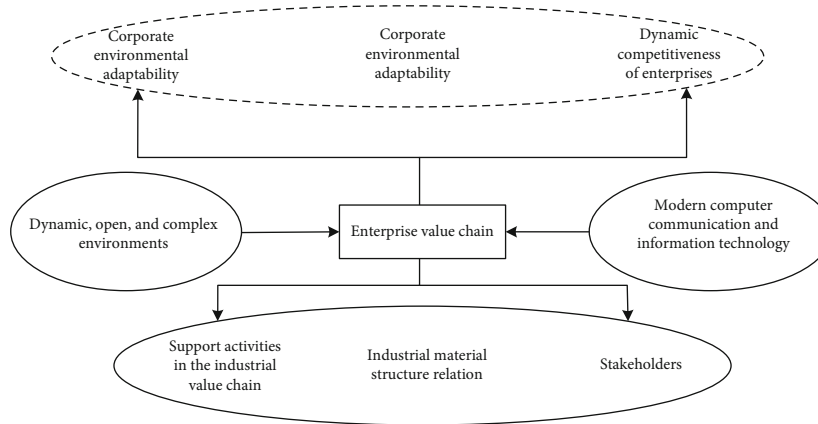


FIGURE 3: Industrial value chain structure.

In addition to value distribution and factor input, another important way for value chain to promote the virtuous cycle of resource chain and environment chain is the realization process of market transaction value. It is divided into two types of value chain links: resource chain and environment chain. Through the market mechanism, we can realize their value distribution of the economic system, make up for the lack of administrative measures and the unreasonable initial value distribution, and then use the system self-organization mechanism to realize the internal construction of the value chain.

The construction of an enterprise cost value chain system is to divide the enterprise into several value activities from the perspective of enterprise competitive advantage and then connect them organically. Through the analysis of the main value chain activities, we can achieve the competitive advantage of the enterprise and finally achieve the strategic goal of the enterprise. The structure of enterprise industrial value chain is shown in Figure 3.

An industrial value chain can be divided into raw material purchase cost value chain, production and processing cost value chain, and sales and after sales service cost value chain. In the actual operation process, it presents a dynamic state of change. Among them, raw material procurement refers to various activities related to product production, such as purchase, receiving, storage, and distribution [13]. The value chain of raw material purchase cost is formed. It consists of five value activities: purchase, transportation, handling, sorting, inventory, and inventory control.

2.2. *Integration of Natural Resources and Acquisition of Environmental Pollution Indicators.* After the analysis of the hybrid structure of the resource chain, environment chain, and value chain models, it is necessary to integrate the natural resources to lay the foundation for the construction of the model. The integration of natural resources is mainly the integration of raw materials and

processing materials. The objective function of natural resource integration is as shown in

$$F(x) = \text{Max} \left( \sum B_i * V_i \right). \quad (1)$$

In the formula,  $B_i$  is the type and quantity of natural resources to be used in the production process of the enterprise and  $V_i$  represents the quantity of natural resources of a single type to be used. According to the objective function, the raw materials needed for enterprise production are integrated, and the hybrid content of resources in the hybrid model of resources environment value chain is obtained.

The hybrid model of resource environment value chain is designed to realize the unification of environmental, economic, and social benefits. From the perspective of providing material products and services, there is no difference between the environment and general material production departments and service provision departments. In addition to the environmental industry, the production process of other material production departments is to obtain natural resources and turn them into means of life and means of production through processing natural resources. The purpose of production is to change the material form of the labor object, so as to meet the needs of human beings. When commodities enter the consumption domain, it marks the end of the production process [14]. Not only the production process needs to consume resources and energy, but also after the commodity enters the consumption process, it will continue to consume resources. After the commodity is consumed, it will enter the environment in the form of waste. The production process and consumption process show that people's unilateral demand for resources, reducing the stock of natural resources and reducing the capacity of environmental self-purification, cannot make economic benefits and environmental benefits unified. The connotation of environmental industry lies in the protection of natural resources, the rational use of resources, the treatment of environmental pollution, the removal of other material production departments, and consumers of environmental damage, and its production purpose highlights environmental benefits. Environmental change is mainly affected by human factors, among which the impact of enterprise production on the environment is the main factor leading to environmental change. Combined with the whole life cycle of enterprise products, the environmental cost measurement method is obtained, shown in

$$T_c = M + C_r + C_o + C_s + C_B + C_n + C_{co2}. \quad (2)$$

In the formula,  $T_c$  represents the total environmental cost of the whole life cycle of the enterprise,  $M$  represents the cost of resource depletion,  $C_r$  represents the impact loss of resource consumption,  $C_o$  represents the loss of air pollution,  $C_s$  is the environmental loss caused by water pollution,  $C_B$  is the pollution loss of solid waste,  $C_n$  represents the loss of the impact of noise on the environment, and  $C_{co2}$  is the loss of external environmental impact.

In the specific environmental cost measurement process, each environmental cost is measured. That is, the values of  $M$ ,  $C_r$ ,  $C_o$ ,  $C_s$ ,  $C_B$ ,  $C_n$ , and  $C_{co2}$  are not fixed. According to the production projects of different enterprises, carry out specific calculation. Taking the resource consumption impact loss index as an example, the calculation formula of the index is as shown in

$$C_r = \Delta L_r \times Q_r, \quad (3)$$

where  $\Delta L_r$  is the unit resource consumption loss and  $Q_r$  is the total loss of resource consumption. Similarly, it can be concluded that the calculation method of corresponding indicators of water pollution environmental loss is shown in

$$C_s = V_1 + V_2 = Q_s \times f_s + \sum \left( \frac{Q_1}{Q_0 \times p_i} \right). \quad (4)$$

In the formula,  $V_1$  and  $V_2$  are the recovery cost and pollution discharge cost, respectively,  $f_s$  is the unit governance cost,  $Q_s$  and  $Q_0$  are the sewage discharge,  $Q_1$  is the emission amount and equivalent of a pollutant, and  $p_i$  is the collection standard of each pollution equivalent. By using the same method, all environmental impact indicators can be obtained, so as to realize the analysis and rectification of environmental change characteristics.

*2.3. Analysis of the Relationship between Resources, Environment, and Economic Value.* Natural resources and environment are indispensable natural conditions for human survival and development and the basis of human activities. From the economic point of view, natural resources are a kind of multifunctional assets, which provide human with the shown four services:

- (1) Provide human with natural resources. The natural environment provides natural resources for all kinds of economic activities of human beings, as the input of human production activities. Natural resources include all kinds of raw materials and energy needed by economic activities. Raw materials are transformed into consumer goods through the production process, and energy provides the necessary power for the production of commodities
- (2) Provide public consumer goods for human beings. The natural environment provides public consumer goods for human beings, including free use of air, scenery, and people's leisure places
- (3) Accept human waste. Human activities will produce a variety of wastes, which are discharged into people's environment. Some wastes are partially decomposed, collected, or transferred to other places. Waste discharge in the natural environment will become a pollutant through the diffusion process
- (4) It provides space for human survival. The environment provides the location space of economic activities for the economic system, such as industrial land,

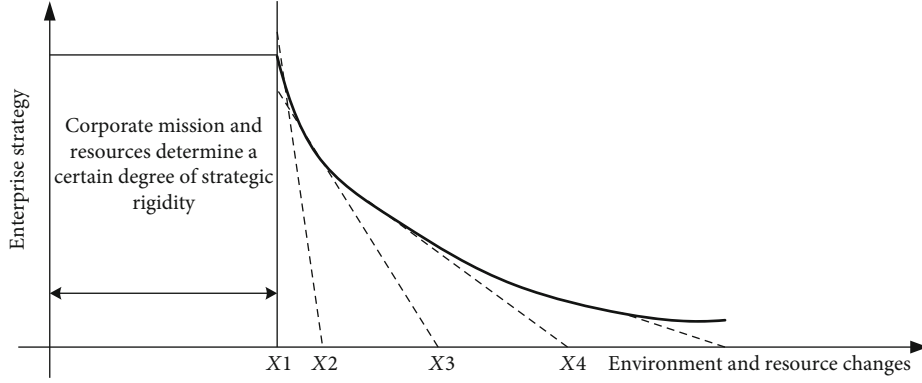


FIGURE 4: Development curve of enterprise economic value with the change of resources and environment.

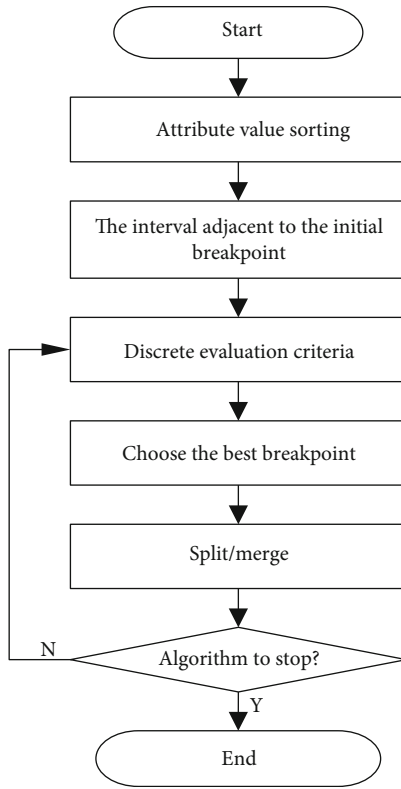


FIGURE 5: Flow chart of discrete time algorithm processing.

residential land, leisure land, agricultural land, and infrastructure land

A resource environment economy hybrid model is a complex model. Its complexity is mainly reflected in the diversity of model elements, the dynamics of model correlation, the dynamic existence of material circulation, energy flow, and information transmission and value-added in the model and between the model and environment. The relationship between enterprise economic value and resource environment is shown in Figure 4.

**2.4. Content Determination of Industrial Value Chain.** Production refers to the activities related to the transformation

of inputs into final products. The resulting production cost value chain consists of six value activities: raw material handling, production products, finished product inspection, finished product handling, finished product abandonment, and finished product inventory. The cost accounting formula of the enterprise value chain at this stage can be expressed as shown in

$$C_z = (M + W + R) * (1 + r) + \frac{F}{Q}. \quad (5)$$

In the formula,  $M$  represents unit product material cost,  $w$  represents unit product labor wage cost,  $R$  represents unit product energy consumption expenditure,  $R$  represents the proportion of general management cost of the enterprise,  $F$  represents fixed asset depreciation, and  $Q$  represents product output.

In the production process, in addition to the enterprise's own cost, the environment cost also needs to be calculated. The cost calculation formula is as shown in

$$C_h = \frac{(C_{e1} + C_{e2} + C_{e3} + C_{e4})}{Q}. \quad (6)$$

The environmental cost is mainly divided into four parts: pollution emission control cost, waste disposal cost, ecological environment tax, and pollution penalty cost. The calculation method of each index is as shown in

$$\begin{cases} C_{e1} = (F + Q) * C_v, \\ C_{e2} = \text{Num} \times \text{Mon}, \\ C_{e3} = Q', \\ C_{e4} = Y. \end{cases} \quad (7)$$

In the formula,  $F$  and  $C_v$  are the fixed cost and variable cost, respectively, Num and Mon are the standard unit prices of waste disposal volume and waste disposal charges, and  $Q'$  and  $Y$  represent the standard unit price of environmental tax and pollution charge for regulating the behavior of damaging environment and resources.

Sales refers to various activities that guide customers to buy enterprise products and deliver them to their hands

TABLE 1: Experimental parameters.

Variable factors of	Details of variable	Description of measurement items
Cost synergies	Y1	It helps enterprises in the circular economy industry chain to pursue the common goal of cost reduction
	Y2	It can improve the utilization of resources and reduce the cost of raw materials
	Y3	It is helpful to reduce the cost of internal production and operation
	Y4	It is helpful to reduce the environmental cost and improve the environmental management efficiency and ecological efficiency
	Y5	It helps to reduce the transaction cost between enterprises and improve the internal operation efficiency
Core enterprise internal collaboration	X1	The company's internal procurement, production, sales, and logistics departments to participate in the product ecological design
	X2	R&D designers should be familiar with cost control, environmental protection, and resource recycling technologies
	X3	The whole process cost control should be implemented in the whole life cycle of the product
	X4	The production process of an enterprise shall implement cleaner production techniques
Collaboration with profit and waste enterprises	X5	Build the material circulation system with waste enterprises
	X6	Share special equipment and other resources with waste enterprises
	X7	Develop market and share marketing network in cooperation with waste enterprises
	X8	To provide technical, production, and environmental support for waste enterprises

[15–17]. After sales service refers to the activities of providing services to increase or maintain the value of products after the sale of products. The resulting cost value chain of sales and after sales service consists of eight value activities: advertising, establishing distribution channels, order processing, commodity handling, commodity transportation, customer maintenance, customer training, and customer relationship management. Through the cost accounting of each environment of enterprise production and sales, the value and value chain analysis results of enterprise products are obtained, which are regarded as resource environment–value chain nesting content in the value chain nesting model.

### 3. Hybrid Resource Environmental Value Chain Model Based on a Discrete Time Algorithm

**3.1. Model Continuous Attribute Analysis.** The purpose of discretization of model continuous attributes is to transform three different types of data in the hybrid model, resources, environment, and value chain, into discrete form and individual data, so as to realize the transformation of three information formats. Through optimal synthesis, the coupling relationship among the three components of the model can be guaranteed. The processing flow of the discrete-time algorithm is shown in Figure 5.

The state of linear discrete time can be expressed as shown in

$$x(k) = \varphi(k, k-1)x(k-1) + w(k-1). \quad (8)$$

In the formula, system noise  $w(k)$  is a white noise sequence with zero mean. The random vector whose initial

state  $x(0)$  is mean  $m(0)$  and variance matrix  $\Sigma_0$  is defined. There are  $l$  observation stations to evaluate the model independently as shown in

$$z_i(k) = C_i(k)x(k) + v_i(k). \quad (9)$$

In the formula, measurement noise is  $v_i(k)$  white noise sequence with zero mean. In the centralized processing, all measurement data  $z_i(j)$  are fed to the central processor, to obtain the optimal estimation of the linear minimum variance of the overall state  $x(k)$ , shown in

$$\hat{x} = (k|k) = \hat{E}\{x(k)|z_i(j)\}. \quad (10)$$

In the formula,  $E\{x_i(k)|z_i(j)\}$  is the orthogonal projection operator. In the decentralized processing, each local processor will provide local measurement data  $\{z_i(j)\}$  according to its own observation station. According to Equation (10), the optimal estimation of the linear minimum variance of the local state  $x_i(k)$  is obtained. Then, the discrete decomposition of the local model can be expressed as shown in

$$C_i(k) = H_i(x_i(k)). \quad (11)$$

In the formula,  $H(\cdot)$  is a discrete-time processing function. The three hybrid contents of resources, environment, and value chain are, respectively, substituted into the above formula to realize the discretization of each module content. Using Equation (12) to achieve the optimal synthesis of

discrete content, namely,

$$\hat{x}(k|k) = \xi(k) + \sum_{i=1}^L G_i(k) \hat{x}_i(k|k). \quad (12)$$

In the formula,  $G_i(k)$  is the corresponding expression of synthesizer and  $\xi(k)$  represents three hybrid content states.

**3.2. Resource Environment Economy Hybrid Model Implementation.** On the basis of planning resource environment economy hybrid model structure, discrete data synthesis hybrid content will be processed, respectively. The hybrid operation of models is realized by the relationship among them. In the process of running the resource environment economy hybrid model, it is necessary to allocate the cost consumption reasonably, realize the collaborative matching of each module, and optimize the information scheduling between discrete time and cost balance [18–20]. From the two aspects of equilibrium index and nesting strength of hybrid models, the constraints of the model are set, shown in

$$\begin{cases} \text{GVCEVA\_Balance Ratio} = \frac{\text{EVA}_{kj} - \text{EVA}_{jk}}{E_j + E_k}, \\ \text{GVCEVA\_Link} = \frac{\text{EVA}_{kj} + \text{EVA}_{jk}}{E_j + E_k}. \end{cases} \quad (13)$$

In the formula,  $\text{EVA}_{jk}$  and  $\text{EVA}_{kj}$  are the values added between any two hybrid cells in the model. Set the parameter value and constraint threshold of constraint conditions in the model to realize the nesting of resource environment economy.

## 4. Experimental Analysis

**4.1. Experimental Environment.** In order to verify the comprehensive effectiveness of the design model, simulation experiments are carried out. The experiment is carried out on MATLAB 6.0, and SPSS 13.0 software is used for data processing.

**4.2. Experimental Parameters.** Because the hybrid model of resource environment value chain needs a certain period of time in the process of operation and the experiment period is long, in order to better carry out the experiment, the environmental data of a laboratory in the past three years is selected as the experimental sample data. There are 3000 pieces of economic information and current state data of resources and environment collected by the laboratory, including 1000 pieces of environmental pollution data, 1000 pieces of resource related data, and 1000 pieces of impact data after the realization of enterprise value. In order to verify the scientific validity of the design model, 3000 data were analyzed. The specific experimental parameters are shown in Table 1.

**4.3. Experimental Scheme.** The experiment adopts the method of comparison, comparing the model of this paper, the model of literature [4], and the model of literature [5]. The data

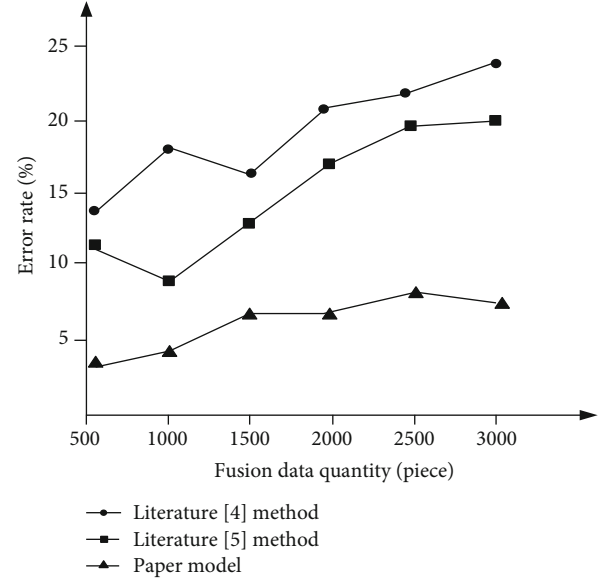


FIGURE 6: Comparison of data fusion errors of different models.

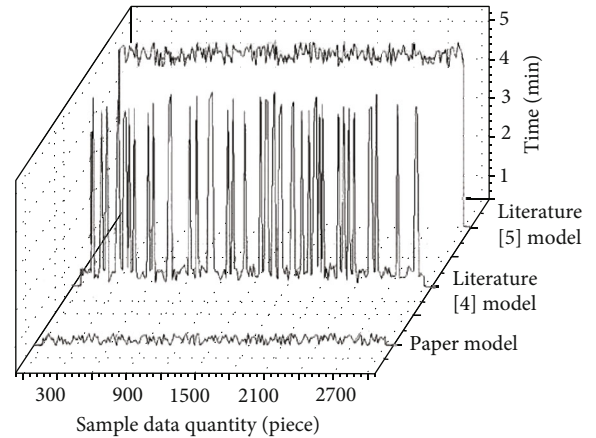


FIGURE 7: Comparison of evaluation time of different models.

TABLE 2: Comparison of resource saving rate of different models (%).

Iterations/time	Paper model	Literature [4] model	Literature [5] model
2	94	89	85
4	95	85	86
6	94	87	83
8	96	82	80
10	97	80	75

fusion degree of the model, the time to complete the evaluation of the model, and the resource saving rate of the model are selected as the experimental indicators for verification.

### 4.4. Analysis of Experimental Results

**4.4.1. Error Analysis of Data Fusion of Different Models.** In order to verify the scientific validity of the proposed model,

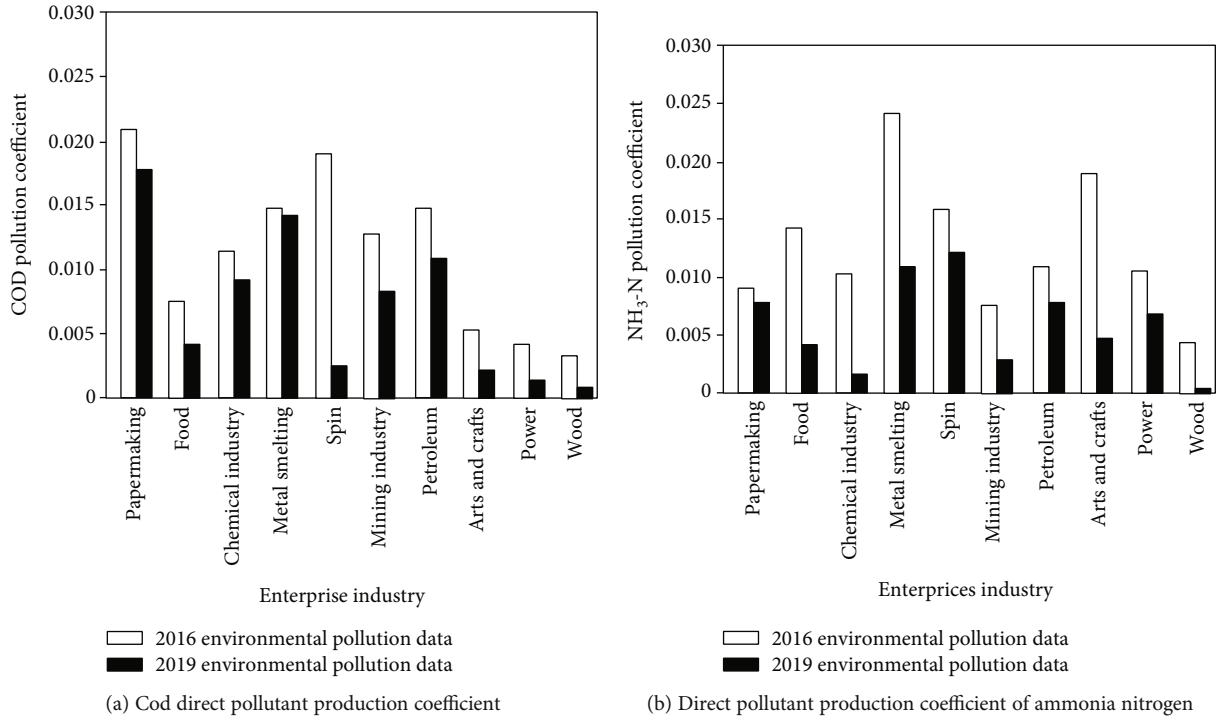


FIGURE 8: (a, b) Comparison results of environmental protection functions [21].

the fusion errors of the model, document [4] model, and document [5] model to the data of resources, environment, and value chain are studied. Among them, the lower the error result, the better the fusion degree of the representative model to the data. The experimental results are shown in Figure 6.

From the analysis of Figure 6, it can be seen that there is a certain gap in the error of data fusion of resources, environment and value chain with three models under the same conditions. Among them, when the data volume is 1500, the error rate of document [4] model fusion is about 15%, the error rate of document [5] model fusion is about 13%, and the error rate of this model fusion is about 7%; when the data volume is 3000, the error rate of document [4] model fusion is about 18%, the error rate of document [5] model fusion is about 13%, and the error rate of this model fusion is about 6%. Compared with the other two models, the data fusion error of this model is increased by 7% and 12%, respectively. This is because the proposed model analyzes the structure of resource, environment, and value chain data and integrates the natural resource data with discrete-time algorithm, which improves the accuracy of data fusion.

**4.4.2. Time-Consuming Analysis of Different Models.** In order to verify the scientific validity of the proposed method, the time consumption of resource, environment, and value chain data evaluation of this model, literature models [4, 5] are analyzed. Among them, the shortest time used indicates the faster processing speed. The experimental results are shown in Figure 7.

From the analysis of Figure 7, it can be seen that the time consumption of three methods for resource, environment, and value chain data evaluation is not the same. Among

them, the evaluation time of this model is always less than 1 min, the evaluation time of literature [4] model is about 2.9 min, and the evaluation time of literature [5] model is about 4.2 min. In contrast, the time consumption of this model is saved by 1.9 min and 3.2 min, respectively, which verifies the feasibility of this model.

**4.4.3. Analysis of Resource Savings in Different Models.** In order to verify the comprehensive effectiveness of the model in this paper, the rate of three models is analyzed experimentally. The experimental results are shown in Table 2.

According to the data in Table 2, the saving rate of environmental resources with three models is different. Among them, the resource saving rate of the model in this paper is up to 97%, the resource saving rate of the model in literature [4] is up to 89%, and the resource saving rate of the model in literature [5] is 86%. In contrast, the resource saving rate of the model in this paper is the highest, which verifies the scientific effectiveness of the proposed method.

**4.4.4. Environmental Protection Functions.** The verification of the environmental protection function is to compare the environmental pollution around the enterprise before and after the application of the model. In this verification, the environmental pollution index sets for comparison are cod direct pollution production coefficient, ammonia nitrogen direct pollution production coefficient, SO<sub>2</sub> direct pollution production coefficient, nitrogen oxide direct product coefficient, and smoke dust direct product coefficient. Among them, the comparison of COD direct pollution generation coefficient and ammonia nitrogen direct pollution generation coefficient is shown in Figure 8.



From the analysis of Figure 8, it can be seen that after applying the hybrid model of resource environment value chain based on the discrete-time algorithm, both the COD direct pollution generation coefficient and the ammonia nitrogen direct pollution generation coefficient have decreased, and COD can be calculated quantitatively. The direct pollution coefficient is reduced by 0.0396, while the direct ammonia nitrogen pollution coefficient is reduced by 0.065. Through the calculation of all environmental pollution coefficients, it can be found that the hybrid resource environment value chain model can be applied to the operation of the enterprise, which can control the enterprise value and reduce the environmental pollution degree of the product production to a certain extent, so as to realize the environmental protection.

## 5. Conclusions

The circulation of resource chain, ecological chain, and value chain is not completed independently; they are intertwined and promote each other, so this paper proposes a hybrid resource environmental value chain model based on a discrete time algorithm. By analyzing the structure of resource chain, ecological chain, and value chain, the interaction among resource chain, ecological chain, and value chain is obtained. Based on the traditional hybrid model, the discrete-time algorithm is introduced to construct the hybrid model of resource environment value chain. Its overall structure model can make clear the relationship between complex natural environment and value, facilitate the development of ideas in the process of enterprise economic construction, and facilitate the scientific formulation of national and regional circular economy strategic planning. The experiment is carried out on MATLAB 6.0. According to the simulation results, the error rate of the proposed model fusion is about 6%. Compared with the other two models, the data fusion error of the proposed model is increased by 7% and 12%, respectively. With respect to time-consuming analysis, the evaluation time of proposed model is always less than 1 min compared to the other two existing models. The saving rate of environmental resources with three models is different. Among them, the resource saving rate of the proposed model is up to 97%, and those of the remaining two models are up to 89% and 86%. It proved that the resource saving rate of the model in this paper is the highest. Finally, it can be found that the hybrid resource environment for the COD pollution is reduced by 0.0396 and the NH<sub>3</sub>-N pollution is reduced by 0.065.

This model is conducive to the decision-making bodies such as the relevant industry associations of production enterprises and the relevant management departments of governments at all levels. When making the decision of different levels of enterprises, according to their different requirements and concerns, it is not only able to get what they need but also easy to understand the relationship between the local structure and the overall system and also conducive to coordinating the interaction of various stakeholders.

## Data Availability

Data are available on request.

## Conflicts of Interest

The authors declare no conflicts of interest.

## References

- [1] M. Chen, M. Fan, C. B. Xie, A. L. Peace, and H. Wang, "Stoichiometric food chain model on discrete time scale," *Mathematical Biosciences & Engineering Mbe*, vol. 16, no. 1, pp. 101–118, 2019.
- [2] J. H. S. Chong, Y. K. Wan, and V. Andiappan, "Synthesis of a sustainable sago-based value chain via fuzzy optimisation approach," in *MATEC Web of Conferences*, vol. 152, p. 01004, Selango, Malaysia, 2018.
- [3] Y. H. Qu, A. N. Wang, and S. Lin, "A novel stable value iteration-based approximate dynamic programming algorithm for discrete-time nonlinear systems," *Chinese Physics B*, vol. 27, no. 1, pp. 010203–010203, 2018.
- [4] Y. F. Liu and Y. W. Wang, "Analysis of market operation of enterprise annuity from the perspective of value chain," *West Forum on Economy and Management (Journal of Sichuan Economic Management Institute)*, vol. 30, no. 4, pp. 71–80, 2019.
- [5] R. Huang, H. Q. Zhang, and D. X. Chang, "A backup and recovery mechanism for security service chain fault in network function virtualization environment," *Journal of Computer Research & Development*, vol. 55, no. 4, pp. 768–781, 2018.
- [6] X. Xu, H. Chen, C. Q. Lian, and D. Z. Li, "Learning-based predictive control for discrete-time nonlinear systems with stochastic disturbances," *IEEE Transactions on Neural Networks & Learning Systems*, vol. 29, no. 12, pp. 6202–6213, 2018.
- [7] C. Y. Zhang, J. B. Li, and S. S. Wang, "Encrypted image retrieval algorithm based on discrete wavelet transform and perceptual hash," *Journal of Computer Applications*, vol. 38, no. 2, pp. 539–544, 2018.
- [8] Z. Dai, H. Zhou, and F. Wen, "Efficient predictability of stock return volatility: the role of stock market implied volatility," *North American Journal of Economics and Finance*, vol. 52, p. 101174, 2020.
- [9] K. U. Shang-qi, Z. H. Chao, L. I. Shuo, Y. A. Hai-gui, H. U. Tong-lin, and Z. H. Hong-jun, "Design and fabrication of broadband discrete extreme-ultraviolet multilayer based on quantum state genetic algorithm," *Acta Photonica Sinica*, vol. 47, no. 4, article 431001, 2018.
- [10] Q. Jiao and D. Xu, "A discrete bat algorithm for disassembly sequence planning," *Journal of Shanghai Jiaotong University*, vol. 23, no. 2, pp. 276–285, 2018.
- [11] Z. C. Zhang, W. Han, and B. Mao, "Adaptive discrete cuckoo algorithm based on simulated annealing for solving TSP," *Acta Electronica Sinica*, vol. 46, no. 8, pp. 1849–1857, 2018.
- [12] F. H. Wen, Y. P. Zhao, M. Z. Zhang, and C. Y. Hu, "Forecasting realized volatility of crude oil futures with equity market uncertainty," *Applied Economics*, vol. 51, no. 59, pp. 6411–6427, 2019.
- [13] Q. Sun, X. H. Zhang, H. W. Zhang, and H. P. Niu, "Coordinated development of a coupled social economy and resource environment system: a case study in Henan Province," *China, Environment Development & Sustainability*, vol. 20, no. 1, pp. 1–20, 2018.

- [14] E. K. Rousham, L. Unicomb, and M. A. Islam, "Human, animal and environmental contributors to antibiotic resistance in low-resource settings: integrating behavioral," *Proceedings of the Royal Society B: Biological Sciences*, vol. 285, no. 1876, article 20180332, 2018.
- [15] G. X. Xiao, B. Yang, and W. Li, "Big data resource planning for food safety: a preliminary exploration of the "environment, food and health" information chain," *Journal of Resources and Ecology*, vol. 9, no. 1, pp. 22–27, 2018.
- [16] C. Yan and M. Lin, "Coordination of the "economy-society-environment" triad in the transition development of resource-based cities in Northeast China," *Geographical Research*, vol. 37, no. 2, pp. 307–318, 2018.
- [17] A. J. Benjamin and S. M. McDermott, "Health impacts of invasive species through an altered natural environment: assessing air pollution sinks as a causal pathway," *Environmental & Resource Economics*, vol. 71, no. 1, pp. 23–43, 2018.
- [18] D. Howard, A. F. R. T. Mirjam, and D. Mercy, "Advanced value chain collaboration in Ghana's cocoa sector: an entry point for integrated landscape approaches," *Environmental Management*, vol. 62, no. 1, pp. 143–156, 2018.
- [19] Y. S. Chen and L. L. Wang, "Simulation of multi-source information resource fully homomorphic encryption under cloud computing environment," *Computer Simulation*, vol. 35, no. 7, pp. 117–120, 2018.
- [20] B. W. William and A. E. Edward, "Welfare impact of wheat farmers participation in the value chain in Tanzania," *Modern Economy*, vol. 9, no. 4, pp. 853–887, 2018.
- [21] A. Miskowska, A. Siczka, and E. Koda, "Levels of organic pollution indicators in groundwater at the old landfill and waste management sit," *Applied Science*, vol. 7, no. 638, pp. 1–22, 2017.

## Research Article

# A New Hybrid Deep Learning Algorithm for Prediction of Wide Traffic Congestion in Smart Cities

G. Kothai <sup>1</sup>, E. Poovammal,<sup>1</sup> Gaurav Dhiman <sup>2</sup>, Kadiyala Ramana <sup>3</sup>,  
Ashutosh Sharma <sup>4</sup>, Mohammed A. AlZain,<sup>5</sup> Gurjot Singh Gaba <sup>6</sup>, and Mehedi Masud <sup>7</sup>

<sup>1</sup>Department of Computer Science and Engineering, SRMIST, Chennai, India

<sup>2</sup>Department of Computer Science, Government Bikram College of Commerce, Patiala, India

<sup>3</sup>Department of Artificial Intelligence & Data Science, AITS, Rajampet, India

<sup>4</sup>Institute of Computer Technology and Information Security, Southern Federal University, Rostov Oblast 344006, Russia

<sup>5</sup>Department of Information Technology, College of Computers and Information Technology, Taif University, P.O. Box 11099, Taif 21944, Saudi Arabia

<sup>6</sup>School of Electronics and Electrical Engineering, Lovely Professional University, Punjab 144411, India

<sup>7</sup>Department of Computer Science, College of Computers and Information Technology, Taif University, P.O. Box 11099, Taif 21944, Saudi Arabia

Correspondence should be addressed to Mehedi Masud; mmasud@tu.edu.sa

Received 8 February 2021; Revised 22 March 2021; Accepted 24 April 2021; Published 20 May 2021

Academic Editor: VIMAL SHANMUGANATHAN

Copyright © 2021 G. Kothai et al. This is an open access article distributed under the Creative Commons Attribution License, which permits unrestricted use, distribution, and reproduction in any medium, provided the original work is properly cited.

The vehicular adhoc network (VANET) is an emerging research topic in the intelligent transportation system that furnishes essential information to the vehicles in the network. Nearly 150 thousand people are affected by the road accidents that must be minimized, and improving safety is required in VANET. The prediction of traffic congestions plays a momentous role in minimizing accidents in roads and improving traffic management for people. However, the dynamic behavior of the vehicles in the network degrades the rendition of deep learning models in predicting the traffic congestion on roads. To overcome the congestion problem, this paper proposes a new hybrid boosted long short-term memory ensemble (BLSTME) and convolutional neural network (CNN) model that ensemble the powerful features of CNN with BLSTME to negotiate the dynamic behavior of the vehicle and to predict the congestion in traffic effectively on roads. The CNN extracts the features from traffic images, and the proposed BLSTME trains and strengthens the weak classifiers for the prediction of congestion. The proposed model is developed using Tensor flow python libraries and are tested in real traffic scenario simulated using SUMO and OMNeT++. The extensive experimentations are carried out, and the model is measured with the performance metrics likely prediction accuracy, precision, and recall. Thus, the experimental result shows 98% of accuracy, 96% of precision, and 94% of recall. The results complies that the proposed model clobbers the other existing algorithms by furnishing 10% higher than deep learning models in terms of stability and performance.

## 1. Introduction

The vehicular adhoc network is one among the puissant research applications in the intelligent transportation system (ITS) that furnishes the information to prevent or reduce the traffic congestion. For exchanging the information in a network, the vehicular adhoc network has vehicle-to-vehicle (V2V) and vehicle-to-infrastructure (V2I) communication. When a conveyance directly communicates with other con-

veyance in a network is V2V communication and when a conveyance directly communicates with roadside units (RSU), then, it is V2I communication [1]. The momentous standards of VANET are the dedicated short-range communication (DSRC) protocol, IEEE 802.11 [2], and wireless access in vehicular environment (WAVE) [3, 4]. Delays due to traffic, traffic that leads to congestion, consumption of energy, and the emission of pollution are the disputable in traffic management for smart cities [5–9]. The traffic

management must effectuate the smart system for parking, an intelligent system for vehicles in routing management, and an intelligent system that predicts the traffic [10–16].

In recent years, there is a higher death rate in road accidents which must be conquered to save the lives of people. User behavior, infrastructure, environmental factors, and mechanical error in roads are the important factors that cause accidents on the road [17, 18]. Traffic congestion is one among predicaments that need to be mutated in the transportation system [19]. As stirring of population accelerated, there is an increase in the number of vehicles on road that steer to traffic congestion, accidents, and pollution [20].

Collision in traffics is caused due to bad traffic management, poor law enforcements, poor infrastructure, and failure of signals [17, 21]. Averting of transportation fatalities ahead is an open aftereffect in vehicular traffic on highways, cities, and urban areas [22]. Ammunition on the road comprehends traffic monitoring and channeling that begets which consist of various technology riveting alert systems, digital maps. The vehicle active safety is a consequential part in collision warning systems [23].

The congestion can be minimized by identifying traffic jams, attaining the estimation of congestion levels, relaying the information about prevailing traffic state, and proposing new routes [24, 25]. Hence, to reduce the congestion level of traffic, the methodology mandatorily needed to predict the traffic jams. Prognosticating the prevalence of crashes that pertains to the count of crashes jotted down for a unit of time at a concrete location is benignant in monitoring highways [26, 27]. Evading auguring collisions will have high strike on reducing road concussion [28]. The demurrer in vehicular networks comprehends the vehicles' rapid stirring and communication disassociation and conjunctions [29–34].

The various techniques for predicting the traffic collisions in machine learning are sampling, regressions, correlations [35], clustering algorithms [36, 37],  $k$ -nearest neighbor (kNN) algorithm [38], and artificial neural network (ANN) [39] are clobbered by the deep learning (DL) models in terms of accuracy in predicting the collision. CNN [40], transpose CNN [41], and long short-term Memory (LSTM) [42] are some of the deep learning techniques [43–48] used for predicting the collision [41]. The systematic random sampling ameliorates in getting the automobilist samples, samples of the commuter, and samples of arid for reducing the hazards of bias. Purposive sampling ameliorates in electing the respondents of traffic officers that cynosure on the authentic traffic officer inaugurates at the sedulous streets [35].

Congestion cluster furnishes the advertent amount of flexibility in disparate needs in applications. These clusters vary dynamically in the network. These clusters accomplish intracluster similarity to disport the analogous development of driving speeds in the road segment over time [36]. The kNN inaugurates in classifying the conditions of the traffic and imputes the advertence to the class for receiving the considerable vote among the neighbors. This method identifies the accident betides due to traffic by utilizing the condition of traffics and constraining the factors of environments [38]. The ANN substantiates in extracting the features and dredging the incidents that furnishes and smashes the warn-

ing to the commuters and operator [39]. The features of images are extracted by a feedforward neural network called CNN by applying convolution operations. A conventional recurrent neural network called LSTM contains the cell state, the memory part, and three gates to predict the collision based on the time series sequence of images in traffic. The transpose convolutional neural network produces the predicted images of collision [41].

These deep learning algorithms produce the high spatial resolution that leads to the overfitting problem and disaccords the access and amalgamate in vehicle stirring patterns and conditions in traffic. Exploration of accidents at junctions must be included, and visualizing the emission and dispersion of traffic must substantiate in evaluating the real-time environment. This paper establishes the hybrid BLSTME and CNN for overcoming the overfitting problem and in predicting the traffic collision. This paper squarely fractionalized into five segments. The related work has been elaborated in Section 2. The proposed methodology in this paper has been deliberated in Section 3 along with the equation. Section 4 demonstrates the implementation of the model that is proposed and compared the accuracy with the existing models. Finally, this paper is concluded in Section 5.

## 2. Related Work

A systematic random sampling approach by Onyeneke et al. [35] supports in reducing the chance of bias by getting the samples of allonges, travelers, and pedestrians. The purposive sampling focuses in recruiting the respondents from the right traffic officers. The simple linear regression canvasses the relationship to place the dependent and independent variables in data. Based on the casualties that are intended as a dependent variable and an independent variable is the number of registered vehicle; the future values are interpreted. This model examines the independent effects of manufacturing and enables the concrete absorption of causes and effects of congestion in traffic. The model fails in evaluating the accuracy, precision, and recall.

Wang et al. [49] studied the strike of congestion in traffic by using the spatial analysis technique for finding the frequency of accidents in the road. Poisson-lognormal, Poisson-gamma, and Poisson-lognormal with car priors for first- and second-order neighbors are the models to inquire the relationship amide congestion of traffic and the prevalence of distinct accidents on road. Accidents can be mapped to the veracious motorway segment, and the congestion index is evaluated to reckon the segment-level congestion of traffic. The Poisson-lognormal and Poisson-gamma models test the heterogeneity effects and exclude the spatial correlation effects, but the Poisson-lognormal car model holds up the effects of heterogeneity and spatial correlation. These models are consistent and confronted that congestion on traffic has no strike on the frequency of accidents. Exploration of congestion effects at junction on roads is required. The analysis is made by containing only the road segments in London from the M25 motorway.

Hao et al. [50] develop a system that conveys some intimation to the operators for transportation and officials of

public health to ease the imminence of air pollutant. The authors proposed a model that blends the traffic state model, emission model, and dispersion model. The traffic condition from mobile data nourishes in reckoning the traffic state-like link average speed and traffic volume. Whence, with traffic conditions to emission and from emission to dispersion for preparing the data and estimating traffic state, a low-frequency problem is harnessed by extending stochastic arterial trajectory estimation model to freeways. Reliable real traffic volume information is furnished for a low penetration problem. Vehicular emissions and short-range dispersion of air pollutant emissions are estimated. A real-time environmental evaluation system must be entrenched to envision the traffic emission and dispersion.

Rempe et al. [36] determine the congestion clusters that furnish the significant amount of flexibility for different applications by the clustering algorithm technique. A congestion cluster is identified by dynamic congestion pockets and construction of static congestion clusters. In the case study of the Munich road network in Germany, the clusters that are the static road network of Munich and discriminating amide days of regular and irregular are taken for cluster congestion analysis. The resulting cluster countenances in identifying the weekdays that do not bear systematically. Reckoning the times and variance of the congestion and quantifying the distinct clusters for correlating the congestion behavior are obtained. This model postulates the implementation and testing in an online traffic forecast system.

The CNN model outperforms the other deep learning algorithm as it inaugurates in furnishing the prognostication of flow in traffic by prying the features of traffic images and classifies the data of traffic based on any feature from traffic data. The convolutional and pooling layers are the two important layers that inaugurate in learning the feature representation of the input traffic images. The LSTM model trains and tests the feature and solves the dematerializing and detonating of the gradient problem in training the neural network.

Song et al. [51] aim to prognosticate the traffic speed and analogize the performance with the existing prediction models by exploiting the CNN. The CNN captures the local dependencies of data and is lesser inclined to clatter in traffic data. This method requires five input layers where one input layer is for furnishing the temporal data and the remaining layers are for the speed profile of links one, two, three, and four. Attaining the local dependencies and capitalizing on the strong relationship for proximate data or nodes in the convolutional layer catenates to a fraction of nodes in the antecedent layer. This algorithm serves to attain the local dependencies and is less sensitive to noises in data. For outperforming the existing models, there is a need for multiple submodels.

Hebert et al. [52] creates the high-resolution accident prediction model for prognosticating the circumstance of an accident within hours on segments of roads delineated by intersections through exploiting big data analytics. Big data analytics is an intended approach that permits data scientists for prying the significant information from large amount of heterogeneous and complex data. The balanced

random forest algorithm exploits in amending or sampling the imbalance of data, and several machine learning algorithms like decision trees, artificial neural networks, and Bayesian networks abet in prognosticating the circumstance of road accidents. By exploiting the features and parameters such as weather attributes, attributes from arterial segment, and attributes from date and time in the dataset, the circumstance of road accidents can be successfully prognosticated. Various features like location and date of erection work on roads and population density must be added to the dataset for excelling the performance.

The hybrid multimodel deep learning framework (HMDLF) by Du et al. [53] is aimed at forecasting the traffic flow. This model incorporates gated recurrent units (GRU) and one-dimensional CNN for attaining the features of correlation amid drifts and elongate dependencies of any one modal traffic data, by incorporating the CNN with GRU delves and ascertaining the deep nonlinear correlation attributes of multimodal input data. The end-to-end multimodel communes the traffic sequential data processing framework that rivets on features of spatial locally, features that have long dependency, and correlations of spatial-temporal. The CNN-GRU dopes out the traffic flow auguring issues by ascertaining the long temporal dependencies and features of spatial-temporal correlation for determining the correlation between speed flow journeys' time in multimodality traffic data. Recasting in number of vehicles at the advertence point is awaited. Encompassing the ascertaining of time series precipitate, bouncing match with error tolerance, and spatial and temporal interdependence of multimodality input data are exploited. Collecting potent traffic data in a short epoch of time is a hindrance. The information that was congregated from the highways of England is traffic flow, speed, and passing time as they face rigor by traffic fatalities and ultimate weather events.

Building a potent model for prognosticating the traffic abundance based on features that effectuate the hidden insights in vehicular stirs is the intent of Moses and Parvathi [54]. The author exploits the support vector regression that maps the input using nonlinear mapping on  $m$ -dimensional features. The mean square error approach estimates the performance by scaling the average squares of errors. The linear regression model erects in scaling the relation between scalar response and independent variables. The decision tree learning algorithm reckons the entropy or information gain. Efficient in identifying the optimal model to the open data that are available is the biggest profit. This model is generic; hence, integrating with existing agencies for doping out the traffic knot in real time is arduous.

Bang and Lee [25] redict the awaited position in stirrings and direction of each conveyance for avoiding amalgamate or access of collision between vehicles. The vector-based mobility prognosticate model in the TDMA-based VANET avoids the collision by apportioning the time slots and prognosticates the mobility of proximate vehicles through exploiting the habitation information of the control time slot, vehicle ID, direction of the vehicle stir, hop information, and latitude and longitude of a vehicle. The gain in performance of the algorithm is amended in the road ambient where the

firmness of the traffic is high and the conveyances have high stirring and recasting the directions for travel constantly. Access and amalgamate collisions betide due to vehicle stir patterns and the condition of traffic.

Wei et al. [55] steer in ameliorating the prognosticate accuracy in the flow of traffic. In the autoencoder long short-term memory (AE-LSTM) approach, the autoencoder endorses the internal accordance of the flow in traffic by plucking the characteristics of the stream data in the traffic flow. The LSTM network cannibalizes the attained characteristic data and the historical data to prognosticate the baroque linear data in the traffic flow. This approach is arduous to implement and has a sober applicability. It also furnishes the exalted performance in prognosticating the traffic flow. But the strike is this study only esteems the time patterns and simple spatial patterns.

Sellami and Alaya [56] inquest the unpredictable density of conveyance and also furnish the attestation in the determinate load balance and other resources attainable between the distinct VANET networks for conveyances. The self-adaptive multikernel clustering for urban VANET (SAMNET) approach is postulated on a designated data that can be measured by depicting the ambivalent density of conveyance nodes, deceleration, acceleration, and bounded radio ranges for communication. It undergoes three stages, and they are the initialization stage of clusters, adaption stage of clusters, and fusion stage of clusters. It poses preeminent resultant alluded to the other distinct algorithms for any densities of traffic in the urban environment with the deduction of the arrant transmitted packets that was not unanimous at the destination. The incommmodity in the adaption of the proposed algorithm parameters to concede the wielding of SAMNET is more complex in the road for distinct scenarios, and for optimizing the performance in distinct scenarios, there is bearing of the machine learning technique.

Ranjan et al. [41] redict the congestion level of a transportation network by integrating the CNN, transpose CNN, and LSTM. The convolutional encoder as a spatial feature extraction network encodes the input image into a low-resolution latent state. The temporal or time series information on data is ascertained by a recurrent network hackneyed as long short-term memory. The reconstruction network postulates the convolutional decoder and transposes operation on data by the transpose convolutional neural network to consequence the predicted image. The PredNet and ConvLSTM models attain the towering accuracy, precision, and recall in predicting the traffic congestion by associating the spatial and temporal features. For learning the background area, the huge number of resources and computing time is debilitated [41].

By incorporating the CNN and BLSTME models, the prognostication of the traffic flow is acquired. The proposed model does not necessitate higher resource that may lead to higher computational time [41]. The hybrid does not furnish multiple submodels of CNN for extracting the features that reduces the imbalance in collecting the data [53], and BLSTME is integrating the LSTM. The AdaBoost algorithm is used for strengthening the weak classifiers that resolve the overfitting problem with stir patterns of vehicles [25] and fur-

nish higher performance in prognosticating the flow of traffic in real time [54] with higher density of population [52].

The recent survey on VANET is tabulated in Table 1. The gap diagnosed from the above survey table is optimizing the performance and arduous in inferring the traffic problem in real time that is conquered by our proposed system that combines the CNN and BLSTME.

### 3. Methodology

Section 3 includes the proposed architecture for predicting the traffic congestion. The proposed hybrid incorporated CNN and BLSTME models prognosticate the traffic flow. The features of input traffic images are extracted by CNN, and the extracted features are trained based on the classes for prognosticating the traffic flow by BLSTME through strengthening the weak classifiers.

*3.1. Proposed Architecture.* A high spatial resolution is produced by the long short-term memory (LSTM) technique. Hence, to avoid this problem, a hybrid deep learning algorithm BLSTME-CNN is proposed, and the architecture is shown in Figure 1.

*3.2. Convolutional Neural Network.* The CNN has the pulverized adroitness in the representation of a feature of an input image with nonpareil aspects as local connectivity to the neuron and sharing of the weight. The layers of CNN are the convolutional layer that learns in representing the feature of the input image and pooling layer that accomplishes the shift invariance. In the convolutional layer, the neurons will receive the inputs from its previous layer's neuron of the local group for the output layer. The distinct feature representations were erudite by convoluting several kernels from the previous layer. The convolution layer is incurred by equation (1) [41].

$$y_f^l = \sigma \left( \sum_{k=1}^{f_{l+1}} y_k^{l-1}, W1_{kf}^l + b1_f^l \right), f \in [1, f_l]. \quad (1)$$

Equation (1) infers the  $f^{\text{th}}$  activation map of the  $l^{\text{th}}$  convolution layer which is denoted by  $y_f^l$ ,  $k^{\text{th}}$  activation map of  $(l-1)^{\text{th}}$  layer is represented by  $y_k^{l-1}$ , and  $W1_{kf}^l$  and  $b1_f^l$  refer to the weight that connects the  $f^{\text{th}}$  activation map of the  $l^{\text{th}}$  layer at position  $k$ . The several filters in  $l^{\text{th}}$  layer can be represented by  $f_f$ , and the elementwise nonlinear activation function is signified by [41].

The spatial size of the activation map can be subdued by the pooling operations, but these operations possess the vital information.  $y_f^l(i, j)$  in equation (2) [41] can be obtained by coiling the output of previous layer with the size  $(m, n)$  in the convolution filter and touching bitwise nonlinear activation is imparted [41]. a1 and b1 is kernel location.

$$y_f^l(i, j) = \sigma \left( \sum_{k=1}^{f_{l+1}} \sum_{a1=0}^{m-1} \sum_{b1=0}^{m-1} (W1_{kf}^l(a1, b1) \otimes y_k^{l-1}(i+a1, j+b1) + b1_f^l) \right), f \in [1, f_l]. \quad (2)$$

TABLE 1: Recent survey on VANET computational techniques.

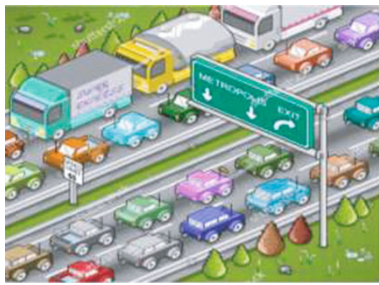
Author and year	Methods	Objective	Limitations
Wang et al. [49] 2009	Spatial analysis approach	To scout the strike of congestion in traffic on the prevalence of distinct accidents in road	To cruise the effectuate of congestions at junctions on smash-up
Rempe [36] 2016	Clustering algorithm	To decree congestion clusters that furnishes an allusive quantum of flexibility to confront the covenants for distinct applications	The composed method must be enforced and tested in an online form of a forecast system of traffic
Song et al. [51] 2017	Convolutional neural network	To prognosticate the speed in traffic and analogize the performances with the existing prognosticate models	The multiple submodels are persistent
Hao et al. [50] 2017	(1) Sparse mobile crowd (2) Integrating traffic state model, emission model, and dispersion model	To forge a system that furnishes suggestions to the respective officials to alleviate the exposure of air pollutant	A system must be demonstrated to visualize the dispersion and emission of traffic
Onyeneke et al. [35] 2018	(1) Systematic random sampling (2) Purposive sampling (3) Simple linear regression (4) Correlation	To audit the effects that is independent of withal fabricating or importing conveyance in the United States	Perception of performance metric is persistent
Hebert et al. [52] 2019	(1) Balanced random forest algorithm (2) XG boost algorithm	To nurture high-resolution accident prognosticate model using big data analytics	More features and a dataset with population density are persistent for delicate performance
Wei et al. [55] 2019	Autoencoder long short-term memory (AE-LSTM)	To ameliorate the prognosticate accuracy in flow of traffic	Simple spatial patterns and time patterns are only premeditated in this study
Du et al. [53] 2020	Hybrid multimodel deep learning framework for traffic flow forecasting (HMDLF)	To portent the short-term traffic flow	Confound in competent collection of data on accidents and baroque weather events in shorter time period
Moses and Parvathi [54] 2020	(1) Support vector regression (2) Mean squared error (3) Linear regression model (4) Decision tree learning	To prefabricate an efficient model for prognosticating the traffic volume and for effectuating out the hidden insights in vehicular stirrings	Arduous in inferring the traffic problem in real time
Bang and Lee [25] 2020	(1) Vector-based mobility prediction model (2) TDMA-based VANET	To avert blending or access collision between conveyances by prognosticating the delinquent stirring position and direction of each conveyance	Radical access and merging fracasas intervene due to conveyance patterns in the movement and conditions of traffic
Ranjan et al. [41] 2020	(1) Convolutional neural network (CNN) (2) Long short-term memory (LSTM) (3) Transpose CNN	To prognosticate the congestion level by grasping the chronological ramification of input images	Abundance of resources and computational time are indulgent in ascertaining the background area
Sellami and Alaya [56] 2021	Self-adaptive multikernel clustering for urban VANET (SAMNET)	To strike the unpredictable density and to stipulate a certain balance load	Adopting this approach is complex in road scenarios, and optimizing the performance is difficult

The convolution layer supervised by the location of the  $f^{\text{th}}$  activation map of  $l + 1^{\text{th}}$  pooling layer, by coiling the outcome of the previous layer with the filter of size  $(2, 2)$ ;  $y_f^{l+1}(i, j)$  is obtained, and then, the bitwise nonlinear activation is applied and postulated in (3) [41].

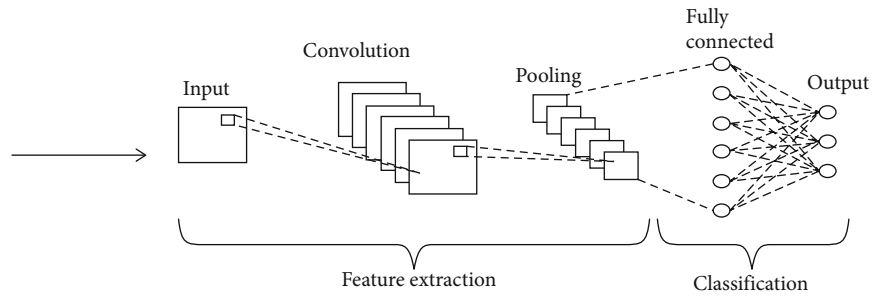
$$y_f^{l+1}(i, j) = \sigma \left( \sum_{k=1}^{f_i} \sum_{a=0}^{m-1} \sum_{b=0}^{m-1} \left( W 1_{kf}^{l+1}(a, b) \otimes y_k^l(2i + a, j + b) + b 1_f^{l+1} \right) \right), f \in [1, f_{l+1}] \quad (3)$$

3.3. *Long Short-Term Memory*. LSTM has been extensively used in many fields such as in generating music, captioning images, recognition of speech, and machine translation for improving the hidden layer cell on the basis of the recurrent neural network (RNN) [55]. The network consists of a cell to commemorate the values aloft the time intervals from LSTM memories and the gates [57, 58]. The LSTM network is the RNN that consorts with LSTM units which is paraded in Figure 2.

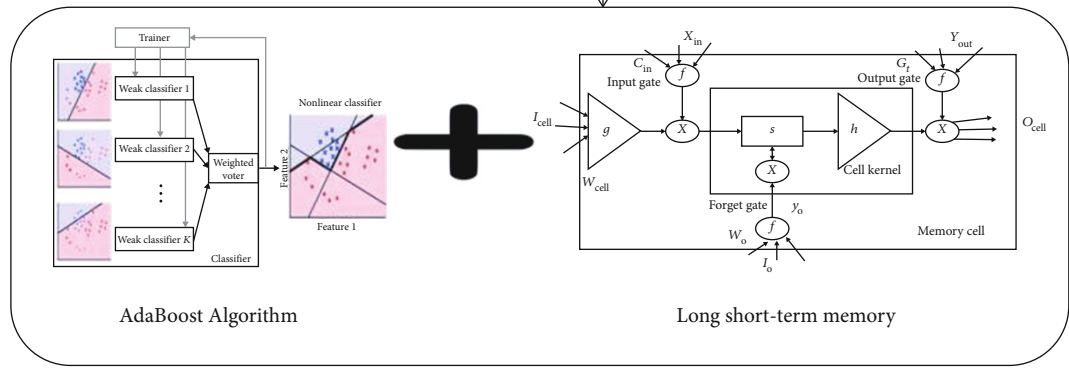
Figure 2 reminisces the output for the hidden layer as  $h_t$ , preceding output as  $h_t - 1$ , input of a cell, and output and preceding state as  $C_t$ ,  $G_t$  and  $G_t - 1$ , respectively.  $J_t$ ,  $T_f$ , and  $T_o$  are



Traffic images



Convolutional neural network



Proposed boosted long short-term memory ensemble

Prediction of traffic congestion

FIGURE 1: Architecture for the proposed BLSTME-CNN algorithm.

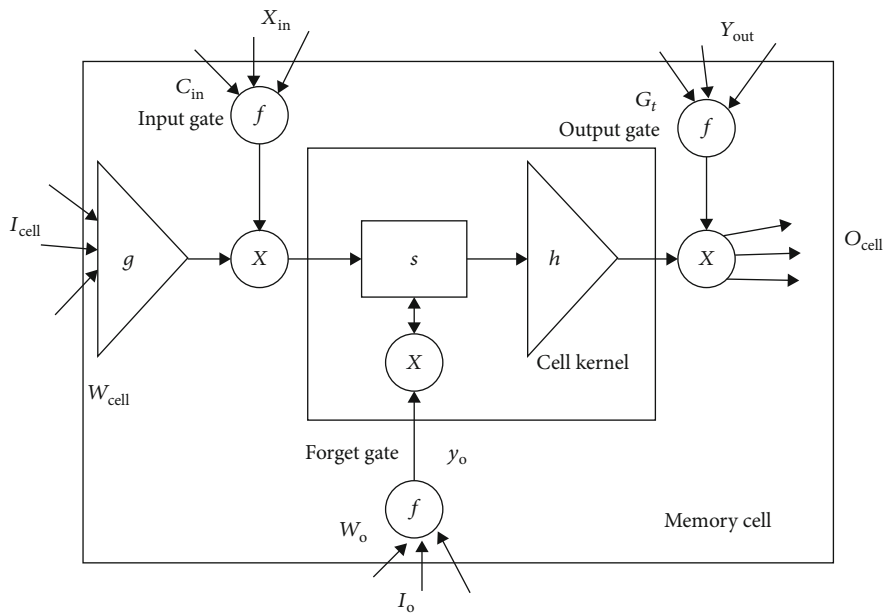


FIGURE 2: LSTM structure [57].



1. Inputs sample training sets  $\{p_i, q_i\}$  where  $p = \{p_1, p_2, p_3, \dots, p_n\}$  where  $n =$  no of input samples and  $q_i \in \{1, 2, 3\}$  where  $q_i$  is a multi-class label associated with  $p$
2. Initialize  $D(k) = n$
3. For  $k = 1, 2, 3, \dots, K$
4.     Train the LSTM classifier using the distribution  $Dk$
5.     Get the hypothesis with error function with respect to  $Dk$
6.     Error function is calculated at each stage which is then weighted  $Dk$
7.     Choose  $\alpha_k = 0.5 \{\ln(1 - e_k)/e_k\}$ -network parameter calculation
8. Update the  $Dk + 1(i)$
9.     Calculate the error function and repeat step 4
10. If error is less than  $e_k$
11. Then, ensemble all the outputs  $H(x) = H(x) = \text{sign}(\sum \alpha_k T_k)/\alpha_k$
12. Else
13. Go to step 4
14. End
15. End

PSEUDOCODE 1: Pseudocode for the boosted LSTM predictor.

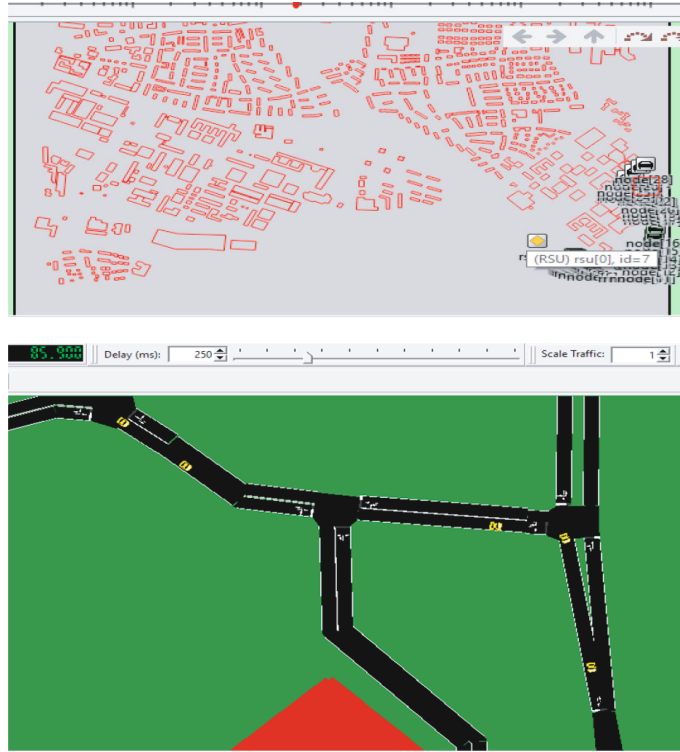


FIGURE 3: Real-time scenario for the data congregate module using SUMO-OMNeT++ interfaces.

three gate states in the network. LSTM cells  $G_t$  and  $h_t$  are calculated by evaluating the three gate states and cell input state and can be transmitted to the next neural network [57].

The input gate is given in equation (4) [57].

$$j_t = \Phi(G_t^i \cdot O_t + G_h^i \cdot e_{t-1} + s_i). \quad (4)$$

The forget gate is given in equation (5) [57].

$$T_f = \Phi(G_t^f \cdot O_t + G_h^f \cdot e_{t-1} + s_f). \quad (5)$$

The output gate is calculated by using equation (6) [57].

$$T_o = \Phi(G_t^o \cdot O_t + G_h^o \cdot e_{t-1} + s_o). \quad (6)$$

The cell input is given in equation (7) [57].

$$\widetilde{T}_C = \tanh(G_t^c \cdot O_t + G_h^c \cdot e_{t-1} + s_c). \quad (7)$$

The matrices of weight are  $G_t^0, G_t^f, G_t^i, G_t^c$  connected to the input gates of the output layers and are the weight matrices  $G_h^i, G_h^f, G_h^o, G_h^c$  that are connected by the gate inputs for



```
((524, 1360),
array ([[0.62745098, 0.94117647, 0.94117647, ...,
0.94117647, 0.94117647],
[0.62745098, 0.94117647, 0.94117647, ..., 0.41602275,
0.41602275,
0.41602275],
[0.62745098, 0.94117647, 0.94117647, ..., 0.41602275,
0.41602275,
0.41602275],
...,
[0.62745098, 0.94117647, 0.94117647, ..., 0.41602275,
0.41602275,
0.41602275],
[0.62745098, 0.94117647, 0.94117647, ..., 0.41602275,
0.41602275,
0.41602275],
[0.62745098, 0.94117647, 0.94117647, ..., 0.41602275,
0.41602275,
0.41602275]]))
```

FIGURE 4: Image shape representation.

TABLE 2: Computing density and class of the network.

Pixel value	Density	Class
11	1	0
27	2	0
33	2	0
43	2	0
63	3	0
76	4	1
82	5	1
97	3	0
106	6	1
110	4	1
152	7	2
167	8	2
178	8	2
240	8	2
252	10	2

the hidden layers [R14]. The bias vector network is  $s_i, s_f, s_o, s_c$ , and the hyperbolic function for the network is  $\tanh$  [57].

The calculated output state of a cell is given in equation (8) [57].

$$T_C = k_t * \widetilde{T}_C + T_f * T_{t-1}. \quad (8)$$

The calculated hidden layer output is given in equation (9) [57].

$$e_t = T_o * \tanh(T_C). \quad (9)$$

The number of concatenated cells designates the number of observations of the data that are regarded before making

the prediction. Generally, more layers of LSTM cells are strong in predicting the collision but induce the overfitting problem. The boosted LSTM ensemble approach solves the problem by boosting LSTM for an effective traffic flow prediction.

**3.4. AdaBoost Algorithms.** In the AdaBoost approach, hybrid ensemble learning algorithms are established by integrating the LSTM networks with AdaBoost learning algorithms for strengthening the weak classifiers. Normally, by updating its weights, the AdaBoost algorithm strengthens the weak classifiers until classification or prediction accuracy obtains a maximum value [59]. The proposed model is a strong model where each weak classifier satisfies the performance.

**3.5. Boosted LSTM Ensemble.** In this approach, the hybrid neural network aggregates BLSTME and CNN to reduce overfitting for the prediction of traffic congestion. The CNN extracts the features of the image, and the feature is trained using BLSTME. The pseudocode and mathematical expression of BLSTME are given below.

The LSTM network is trained using  $D_k(i)$  over the training set of traffic data at iteration  $k$ . At first,  $D(i)$  is set equally,  $D_1(i) = 1/n$ . By using mathematical equation (6), the weak LSTM predictor computes the network for the first iteration. The modified output cell is given in equation (10):

$$T_k = \sum_{k=0}^n [\Phi(G_k^0 \cdot O_k + G_k^o \cdot e_{k-1} + s_k)]. \quad (10)$$

A user-defined error function is identified to describe the boosting outputs by the mathematical expression in equation (11):

$$e_k = (T_{\text{actual}} - T_k). \quad (11)$$

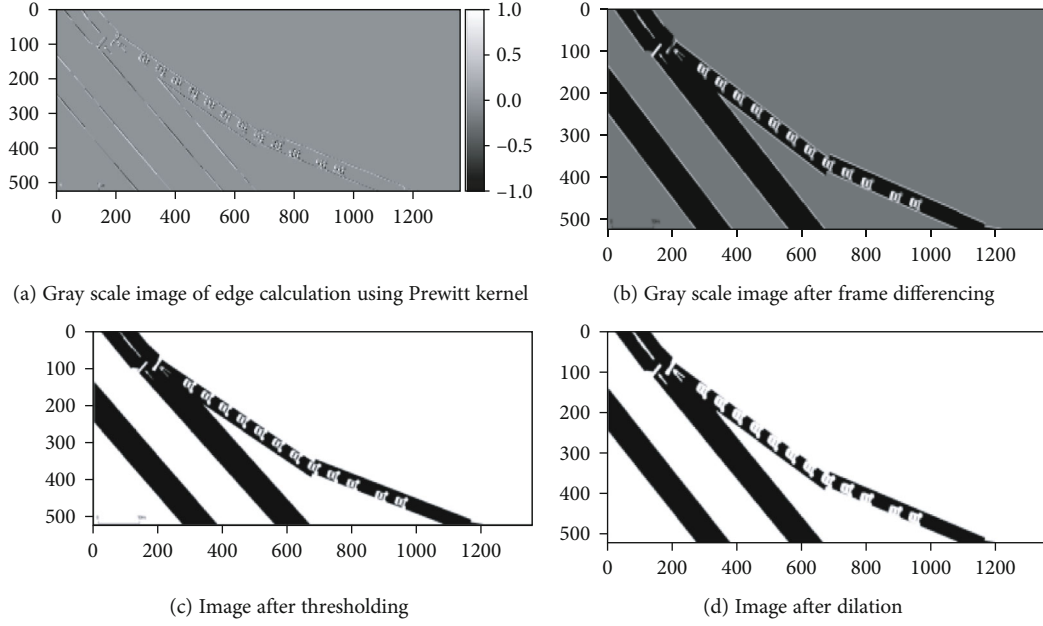


FIGURE 5: Feature extraction.

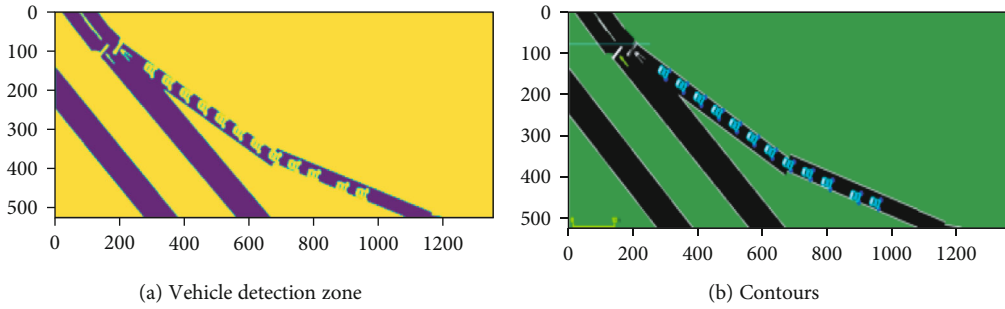


FIGURE 6: Vehicle detection zone and contours.

By the expression  $\alpha_k$ , the network parameter has been calculated and is given by equation (12):

$$a_k = 0.5 \left\{ \ln \frac{(1 - e_k)}{e_k} \right\}. \quad (12)$$

$e_k$  and the final ensemble boosted output is calculated for every iteration when error is zero, and the mathematical expression is given by equation (13)

$$Y_k = \sum_{k=0}^n. \quad (13)$$

The complete pseudocode for the proposed BLSTME is rendered below.

#### 4. Results and Discussion

For a potent perpetration of prognosticate models in the networks, the real-time data are congregated from the arterial network of Seoul city. To utensil the real-time data congregate mechanism, we have incorporated SUMO platforms

that run in the OMNeT++ environment. The separate python API has been developed to interface with data collection unit which runs on the SUMO-OMNeT++ platforms to utensil the continuous simulation. However, the simulation analysis has been done using Python Tensor Flow API running on the Intel i3.

Figure 3 flourishes the real-time scenario of the arterial system and the vehicles are surveilled in the SUMO. They are alchemized into vehicular nodes by catenate effectuated using the C++ programming for an apparent perpetration in OMNeT++ for the foster annotations and modeling.

**4.1. Feature Extraction.** The images are collected from SUMO-OMNeT++ interfaces, and their shape variations of real-time dynamic scenarios are represented in Figure 4.

Around 125 images are deliberated for the feature analysis. The classes are classified based on the density, and the computed values are represented in Table 2.

From Table 2, it is inferred that the density value is based on the pixel value of the input image. If pixel values get increased then automatically density values of an image get increased. Based on the density, the classes are classified.

TABLE 3: Computed convolutional neural network for input images.

Layer (type)	Output shape	Param #
conv2d (Conv2D)	(none, 32, 32, 32)	896
activation (Activation)	(none, 32, 32, 32)	0
conv2d_1 (Conv2D)	(none, 32, 32, 32)	9248
dropout (Dropout)	(none, 32, 32, 32)	0
batch_normalization (BatchNo)	(none, 32, 32, 32)	128
conv2d_2 (Conv2D)	(none, 32, 32, 64)	18496
Activation_1 (Activation)	(none, 32, 32, 64)	0
max_pooling2d (MaxPooling2D)	(none, 16, 16, 64)	0
dropout_1(Dropout)	(none, 16, 16, 64)	0
batch_normalization_1 (BatchNo)	(none, 16, 16, 64)	256
conv2d_3 (Conv2D)	(none, 16, 16, 64)	36928
activation_2 (Activation)	(none, 16, 16, 64)	0
max_pooling2d_1 (MaxPooling2D)	(none, 8, 8, 64)	0
dropout_2 (Dropout)	(none, 8, 8, 64)	0
batch_normalization_2 (BatchNo)	(none, 8, 8, 64)	256
conv2d_4 (Conv2D)	(none, 8, 8, 128)	73856
activation_3 (Activation)	(none, 8, 8, 128)	0
dropout_3 (Dropout)	(none, 8, 8, 128)	0
batch_normalization_3 (BatchNo)	(none, 8, 8, 128)	512
flatten (Flatten)	(none, 8192)	0
dropout_4 (Dropout)	(none, 8192)	0
dense (Dense)	(none, 256)	2097408
activation_4 (Activation)	(none, 256)	0
dropout_5 (Dropout)	(none, 256)	0
batch_normalization_4 (BatchNo)	(none, 256)	1024
dense_1 (Dense)	(none, 128)	32896
activation_5 (Activation)	(none, 128)	0
dropout_6 (Dropout)	(none, 128)	0
batch_normalization_5 (BatchNo)	(none, 128)	512
dense_2 (Dense)	(none, 10)	1290
activation_6 (Activation)	(none, 10)	0

TABLE 4: Performance analysis of the prediction models.

Prediction models	Precision	Recall	Accuracy
Autoencoder [41, 60]	0.74	0.71	0.75
ConvLSTM [41, 60]	0.80	0.78	0.82
PredNet [41]	0.86	0.85	0.86
BLSTME-CNN	0.96	0.94	0.98

When the density ranges from 1 to 3, it comes under Class 0. When the density ranges from 4 to 6, it is Class1, and if the density ranges higher than 6, then it is Class 2.

Based on the traffic density, the different image data are gathered and the image dilation and image thresholding are performed. The frames are converted into gray scale, and the images are plotted after frame differencing. The density is obtained by calculating the horizontal and vertical edges by using Prewitt kernel as shown in Figure 5.

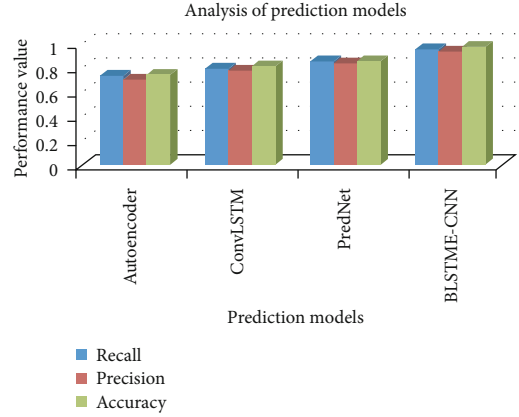


FIGURE 7: Performance analysis of the prediction models.

Figure 5(a) depicts the gray scale image of edge calculation using Prewitt kernel; Figure 5(b) portrays the gray scale image after frame differencing; Figure 5(c) represents the image after thresholding, and Figure 5(d) describes the image after dilation.

The vehicle detection zone and the contours of the vehicle in the road network are shown in Figure 6. Figure 6(a) expresses the vehicle detection zone, and Figure 6(b) denotes the contours.

The convolutional neural network extracts the features from the input images, and the results are represented in Table 3.

The total parameters computed in CNN from the input data is 2,273,706. The trainable and nontrainable parameters for training the dataset in the network are 2,272,362 and 1,344 from the total parameters, respectively. The features that are extracted from the CNN are trained by BLSTME. It has higher computational load by handling 2,272,362 trainable parameters.

**4.2. Performance Analysis.** The proposed predicted BLSTME model is analyzed based on the performance metrics. The performance standards of the proposed DL algorithm are calculated, and the parameters such as accuracy, precision, and recall are applicative and estimated in training datasets and by using equations (14), (15), and (16) [41].

$$\text{Accuracy} = \frac{\text{Detected Results}}{\text{Total no.of iterations}}, \quad (14)$$

$$\text{Precision} = \frac{\text{True Positive}}{\text{True Positive} + \text{True Negative}}, \quad (15)$$

$$\text{Recall} = \frac{\text{True Negative}}{\text{True Positive} + \text{True Negative}}. \quad (16)$$

The performance analysis of the proposed BLSTME-CNN and the existing models such as the autoencoder, convolutional long short-term memory (ConvLSTM), and PredNet are tabulated in Table 4. The data of the existing prediction models such as the autoencoder, ConvLSTM,

and PredNet are collected from [41, 60] for the statistical analysis of performance.

The performance analysis of distinct performance metrics is evaluated for the various prediction models such as the autoencoder, ConvLSTM, PredNet, and proposed BLSTME-CNN and is represented in Figure 7.

Figure 7 flaunts that the existing autoencoder model has 0.74 precision value, ConvLSTM has 0.86 precision value, and PredNet has 0.86 precision value. The proposed BLSTME-CNN model has 0.96 precision value that is 10% higher than the autoencoder, ConvLSTM, and PredNet.

Figure 7 flaunts that the existing autoencoder model has 0.71 recall value, ConvLSTM has 0.78 recall value, and PredNet has 0.85 recall value. The proposed BLSTME-CNN model has 0.94 recall value that is around 10% higher than the autoencoder, ConvLSTM, and PredNet.

Figure 7 flaunts that the existing autoencoder model has 0.75 accuracy value, ConvLSTM has 0.82 accuracy value, and PredNet has 0.86 accuracy value. The proposed BLSTME-CNN model has 0.98 accuracy value that is around 10% higher than the autoencoder, ConvLSTM, and PredNet.

## 5. Conclusions and Future Work

The hybrid deep learning model is evolved by assimilating the CNN and BLSTME. The models can apprehend effectively based on the relation of both the temporal and spatial of the input images. It inaugurates in prognosticating the congestion of traffic for traffic management in smart cities that reduces delays which occurred by traffic, consuming energy, and travel management for passengers. By prognosticating the flow of traffic, the recurring and nonrecurring congestion of traffics are directed by smart traffic management by computing the density, calculating the edges, and frame differencing. Incorporating the CNN and BLSTME inaugurates for smart city traffic management by thresholding, dilation, contours, and detecting the vehicle zone. The CNN method extracts both spatial and temporal features from the traffic images, and BLSTME trains the features and strengthens the weak classifiers for predicting the traffic flow. Our proposed model is analogized with the existing models such as the autoencoder, ConvLSTM, and PredNet for predicting the traffic collision. The proposed model BLSTME-CNN achieves more than 10% higher accuracy, precision, and recall in predicting the collision than the existing models by strengthening the weak classifiers. Therefore, the proposed BLSTME-CNN algorithm produces the higher performance and computational efficiency in predicting the congestion. The future direction of our research work is to propose a hybrid incorporation of predictors with the attainment during collision in the network.

Another subject worth mentioning is real-time prediction. It plays an important role in modern cities and puts greater demands on the capacity of available prediction methods to forecast in real time. In the future, we will consider a more complex model architecture, especially for modeling temporal closeness, cycles, and patterns, in order to better capture temporal dependencies. We will also look at how to deal with sparse spatial traffic flow matrix inputs

in order to minimize training time and maintain topological relationships.

Future research will concentrate on using larger datasets, exploring different combinations of flow, occupancy, speed, and other road traffic characteristics to improve prediction accuracy, improving prediction methodologies and analytics, using various types of road traffic datasets, fusing multiple datasets, and using multiple deep learning models.

## Data Availability

The data used to support the findings of this study are available from the author upon request (gdhiman0001@gmail.com).

## Conflicts of Interest

The authors declare that they have no conflicts of interest.

## Acknowledgments

We are thankful for the support from the Taif University Researchers Supporting Project number (TURSP-2020/98).

## References

- [1] K. Arthi and S. Rani, "Secured message transmission between vehicles for reducing delay and collision in VANET," *International Journal of Innovative Technology and Exploring Engineering*, vol. 8, no. 8, pp. 2853–2857, 2019.
- [2] M. Aydemir and K. Cengiz, "A potential architecture and next generation technologies for 5G wireless networks," in *IEEE 24th Signal Processing and Communication Application Conference (SIU)*, pp. 277–280, Zonguldak, Turkey, 2016.
- [3] Z. Lu, G. Qu, and Z. Liu, "A survey on recent advances in vehicular network security, trust, and privacy," *IEEE Transactions on Intelligent Transportation Systems*, vol. 20, no. 2, pp. 760–776, 2019.
- [4] H. Faris and S. Yazid, "Development of communication technology on VANET with a combination of ad-hoc, cellular and GPS signals as a solution traffic problems," in *2019 7th International Conference on Information and Communication Technology (ICoICT)*, pp. 1–9, Kuala Lumpur, Malaysia, 2019.
- [5] P. Singh, G. Dhiman, and A. Kaur, "A quantum approach for time series data based on graph and Schrödinger equations methods," *Modern Physics Letters A*, vol. 33, no. 35, p. 1850208, 2018.
- [6] G. Dhiman and V. Kumar, "Astrophysics inspired multi-objective approach for automatic clustering and feature selection in real-life environment," *Modern Physics Letters B*, vol. 32, no. 31, p. 1850385, 2018.
- [7] M. Garg and G. Dhiman, "Deep convolution neural network approach for defect inspection of textured surfaces," *Journal of the Institute of Electronics and Computer*, vol. 2, no. 1, pp. 28–38, 2020.
- [8] G. Dhiman, M. Soni, H. M. Pandey, A. Slowik, and H. Kaur, "A novel hybrid hypervolume indicator and reference vector adaptation strategies based evolutionary algorithm for many-objective optimization," *Engineering with Computers*, pp. 1–19, 2020.
- [9] G. Dhiman, M. Garg, A. Nagar, V. Kumar, and M. Dehghani, "A novel algorithm for global optimization: rat swarm

- optimizer,” *Journal of Ambient Intelligence and Humanized Computing*, pp. 1–26, 2020.
- [10] F. Malik, M. A. Shah, and H. A. Khattak, “Intelligent transport system: an important aspect of emergency management in smart cities,” in *2018 24th International Conference on Automation and Computing (ICAC)*, pp. 1–6, Newcastle upon Tyne, United Kingdom, 2018.
  - [11] G. M. Lingani, D. B. Rawat, and M. Garuba, “Smart traffic management system using deep learning for smart city applications,” in *2019 IEEE 9th Annual Computing and Communication Workshop and Conference (CCWC)*, pp. 0101–0106, Las Vegas, NV, USA, 2019.
  - [12] G. Dhiman and V. Kumar, “Spotted hyena optimizer: a novel bio-inspired based metaheuristic technique for engineering applications,” *Advances in Engineering Software*, vol. 114, pp. 48–70, 2017.
  - [13] G. Dhiman and V. Kumar, “Emperor penguin optimizer: a bio-inspired algorithm for engineering problems,” *Knowledge-Based Systems*, vol. 159, pp. 20–50, 2018.
  - [14] G. Dhiman and V. Kumar, “Multi-objective spotted hyena optimizer: a multi-objective optimization algorithm for engineering problems,” *Knowledge-Based Systems*, vol. 150, pp. 175–197, 2018.
  - [15] G. Dhiman and V. Kumar, “Seagull optimization algorithm: theory and its applications for large-scale industrial engineering problems,” *Knowledge-Based Systems*, vol. 165, pp. 169–196, 2019.
  - [16] P. Singh and G. Dhiman, “A hybrid fuzzy time series forecasting model based on granular computing and bio-inspired optimization approaches,” *Journal of computational science*, vol. 27, pp. 370–385, 2018.
  - [17] M. Divyaprabha, M. Thangavel, and P. Varalakshmi, “A comparative study on road safety problems,” in *2018 IEEE International Conference on Computational Intelligence and Computing Research (ICCIC)*, pp. 1–7, Madurai, India, 2018.
  - [18] S. Jat, R. S. Tomar, and M. S. P. Sharma, “Traffic Analysis for Accidents Reduction in VANETs,” in *2019 International Conference on Computational Intelligence and Knowledge Economy (ICCIKE)*, pp. 115–118, Dubai, United Arab Emirates, 2019.
  - [19] C. Jayapal and S. S. Roy, “Road traffic congestion management using VANET,” in *2016 International Conference on Advances in Human Machine Interaction (HMI)*, pp. 1–7, Doddaballapur, 2016.
  - [20] Y. R. B. Al-Mayouf, O. A. Mahdi, N. A. Taha, N. F. Abdullah, S. Khan, and M. Alam, “Accident management system based on vehicular network for an intelligent transportation system in urban environments,” *Journal of Advanced Transportation*, vol. 2018, 11 pages, 2018.
  - [21] A. Ghazy and T. Ozkul, “Design and simulation of an artificially intelligent VANET for solving traffic congestion,” in *2009 6th International Symposium on Mechatronics and its Applications*, pp. 1–6, Sharjah, 2009.
  - [22] P. G. Shinde and M. M. Dongre, “Traffic congestion detection with complex event processing in VANET,” in *2017 Fourteenth International Conference on Wireless and Optical Communications Networks (WOCN)*, pp. 1–5, Mumbai, 2017.
  - [23] S. B. Raut and L. G. Malik, “Survey on vehicle collision prediction in VANET,” in *2014 IEEE International Conference on Computational Intelligence and Computing Research*, pp. 1–5, Coimbatore, 2014.
  - [24] G. B. Araújo, M. M. Queiroz, F. de LP Duarte-Figueiredo, A. I. J. Tostes, and A. A. F. Loureiro, “CARTIM: A proposal toward identification and minimization of vehicular traffic congestion for VANET,” in *2014 IEEE Symposium on Computers and Communications (ISCC)*, pp. 1–6, Funchal, 2014.
  - [25] J.-H. Bang and J.-R. Lee, “Collision avoidance method using vector-based mobility model in TDMA-based vehicular ad hoc networks,” *Applied Sciences*, vol. 10, no. 12, p. 4181, 2020.
  - [26] K. Pandey, P. Fulzele, R. Singh, P. Kumar, and S. Singh, “Predicting and preventing fatal crashes,” in *2019 Twelfth International Conference on Contemporary Computing (IC3)*, pp. 1–6, Noida, India, 2019.
  - [27] M. H. Ahmadzadegan, H. A. Deilami, M. Izadyar, and H. Ghorbani, “Implementation and evaluation of the impact of traffic congestion on the detection of the missing packets in VANET,” in *2019 Third International conference on I-SMAC (IoT in Social, Mobile, Analytics and Cloud) (I-SMAC)*, pp. 169–172, Palladam, India, 2019.
  - [28] N. Aljeri and A. Boukerche, “A predictive collision detection protocol using vehicular networks,” in *2017 IEEE 28th Annual International Symposium on Personal, Indoor, and Mobile Radio Communications (PIMRC)*, pp. 1–5, Montreal, QC, 2017.
  - [29] G. Tuna and K. Cengiz, “Telematics and mobile internet: current situation and 5G networks,” *Principles and Applications of Narrowband Internet of Things (NBloT)*, IGI Global, pp. 373–396, 2021.
  - [30] S. Kaur, L. K. Awasthi, A. L. Sangal, and G. Dhiman, “Tunicate swarm algorithm: a new bio-inspired based metaheuristic paradigm for global optimization,” *Engineering Applications of Artificial Intelligence*, vol. 90, article 103541, 2020.
  - [31] G. Dhiman and A. Kaur, “STOA: a bio-inspired based optimization algorithm for industrial engineering problems,” *Engineering Applications of Artificial Intelligence*, vol. 82, pp. 148–174, 2019.
  - [32] G. Dhiman and V. Kumar, “Spotted hyena optimizer for solving complex and non-linear constrained engineering problems,” in *Harmony Search and Nature Inspired Optimization Algorithms*, pp. 857–867, Springer, Singapore, 2019.
  - [33] P. Singh and G. Dhiman, “Uncertainty representation using fuzzy-entropy approach: special application in remotely sensed high-resolution satellite images (RSHRSIs),” *Applied Soft Computing*, vol. 72, pp. 121–139, 2018.
  - [34] P. Singh and G. Dhiman, “A fuzzy-LP approach in time series forecasting,” in *International conference on pattern recognition and machine intelligence*, pp. 243–253, Cham, 2017.
  - [35] C. Onyeneke, C. Eguzouwa, and C. Mutabazi, “Modeling the effects of traffic congestion on economic activities-accidents, fatalities and casualties,” *Biomedical Statistics and Informatics*, vol. 3, no. 2, pp. 7–14, 2018.
  - [36] F. Rempe, G. Huber, and K. Bogenberger, “Spatio-temporal congestion patterns in urban traffic networks,” *Transportation Research Procedia*, vol. 15, pp. 513–524, 2016.
  - [37] A. Jesudoss, S. K. Raja, and A. Sulaiman, “Stimulating truth-telling and cooperation among nodes in VANETs through payment and punishment scheme,” *Ad Hoc Networks*, vol. 24, pp. 250–263, 2015.
  - [38] Y. Lv, S. Tang, and H. Zhao, “Real-time highway traffic accident prediction based on the k-nearest neighbor method,” in *2009 International Conference on Measuring Technology and Mechatronics Automation*, pp. 547–550, Zhangjiajie, Hunan, 2009.

- [39] Y. Ki, W. Jeong, H. Kwon, and M. Kim, "An algorithm for incident detection using artificial neural networks," in *2019 25th Conference of Open Innovations Association (FRUCT)*, pp. 162–167, Helsinki, Finland, 2019.
- [40] H. Zhao, H. Cheng, T. Mao, and C. He, "Research on traffic accident prediction model based on convolutional neural networks in VANET," in *2019 2nd International Conference on Artificial Intelligence and Big Data (ICAIBD)*, pp. 79–84, Chengdu, China, 2019.
- [41] N. Ranjan, S. Bhandari, H. P. Zhao, H. Kim, and P. Khan, "City-wide traffic congestion prediction based on CNN, LSTM and transpose CNN," *IEEE Access*, vol. 8, pp. 81606–81620, 2020.
- [42] Y. Jeong and K. Yi, "Bidirectional long short-term memory-based interactive motion prediction of cut-in vehicles in urban environments," *IEEE Access*, vol. 8, pp. 106183–106197, 2020.
- [43] G. Dhiman and V. Kumar, "KnRVEA: a hybrid evolutionary algorithm based on knee points and reference vector adaptation strategies for many-objective optimization," *Applied Intelligence*, vol. 49, no. 7, pp. 2434–2460, 2019.
- [44] G. Dhiman, S. Guo, and S. Kaur, "ED-SHO: a framework for solving nonlinear economic load power dispatch problem using spotted hyena optimizer," *Modern Physics Letters A*, vol. 33, no. 40, p. 1850239, 2018.
- [45] P. Singh, K. Rabadiya, and G. Dhiman, "A four-way decision-making system for the Indian summer monsoon rainfall," *Modern Physics Letters B*, vol. 32, no. 25, p. 1850304, 2018.
- [46] G. Dhiman, "MOSHEPO: a hybrid multi-objective approach to solve economic load dispatch and micro grid problems," *Applied Intelligence*, vol. 50, no. 1, pp. 119–137, 2020.
- [47] G. Dhiman, "ESA: a hybrid bio-inspired metaheuristic optimization approach for engineering problems," *Engineering with Computers*, pp. 1–31, 2019.
- [48] A. Kaur, S. Kaur, and G. Dhiman, "A quantum method for dynamic nonlinear programming technique using Schrödinger equation and Monte Carlo approach," *Modern Physics Letters B*, vol. 32, no. 30, p. 1850374, 2018.
- [49] C. Wang, M. A. Quddus, and S. G. Ison, "Impact of traffic congestion on road accidents: a spatial analysis of the M25 motorway in England," *Accident Analysis & Prevention*, vol. 41, no. 4, pp. 798–808, 2009.
- [50] P. Hao, C. Wang, G. Wu, K. Boriboonsomsin, and M. Barth, "Evaluating the environmental impact of traffic congestion based on sparse mobile crowd-sourced data," in *2017 IEEE Conference on Technologies for Sustainability (Sus Tech)*, pp. 1–6, Phoenix, AZ, 2017.
- [51] C. Song, H. Lee, C. Kang, W. Lee, Y. B. Kim, and S. W. Cha, "Traffic speed prediction under weekday using convolutional neural networks concepts," in *2017 IEEE Intelligent Vehicles Symposium (IV)*, pp. 1293–1298, Los Angeles, CA, 2017.
- [52] A. Hébert, T. Guédon, T. Glatard, and B. Jaumard, "High-resolution road vehicle collision prediction for the city of Montreal," in *2019 IEEE International Conference on Big Data (Big Data)*, pp. 1804–1813, Los Angeles, CA, USA, 2019.
- [53] D. Shengdong, T. Li, X. Gong, and S.-J. Horng, "A hybrid method for traffic flow forecasting using multimodal deep learning," *International journal of computational intelligence systems*, vol. 13, pp. 85–97, 2020.
- [54] A. Moses and R. Parvathi, "Vehicular traffic analysis and prediction using machine learning algorithms," in *2020 International Conference on Emerging Trends in Information Technology and Engineering (ic-ETITE)*, pp. 1–4, Vellore, India, 2020.
- [55] W. Wei, H. Wu, and H. Ma, "An auto encoder and LSTM-based traffic flow prediction method," *Sensors*, vol. 19, no. 13, article 2946, 2019.
- [56] L. Sellami and B. Alaya, "SAMNET: self-adaptative multi-kernel clustering algorithm for urban VANETs," *Vehicular Communications*, vol. 29, article 100332, 2021.
- [57] S. Amudha and M. Murali, "Deep learning based energy efficient novel scheduling algorithms for body-fog-cloud in smart hospital," *Journal of Ambient Intelligence and Humanized Computing*, 2020.
- [58] B. Tian, G. Wang, Z. Xu, Y. Zhang, and X. Zhao, "Communication delay compensation for string stability of CACC system using LSTM prediction," *Vehicular Communications*, vol. 29, article 100333, 2021.
- [59] Y. Zhang, M. Ni, C. Zhang et al., "Research and application of AdaBoost algorithm based on SVM," in *2019 IEEE 8th Joint International Information Technology and Artificial Intelligence Conference (ITAIC)*, pp. 662–666, Chongqing, China, 2019.
- [60] S. Zhang, Y. Yao, J. Hu, Y. Zhao, S. Li, and J. Hu, "Deep auto-encoder neural networks for short-term traffic congestion prediction of transportation networks," *Sensors*, vol. 19, no. 10, article 2229, 2019.

## Research Article

# CPIDM: A Clustering-Based Profound Iterating Deep Learning Model for HSI Segmentation

Kriti Mahajan <sup>1</sup>, Urvashi Garg <sup>1</sup>, and Mohammad Shabaz <sup>2</sup>

<sup>1</sup>Department of Computer Science and Engineering, Chandigarh University, India

<sup>2</sup>Arba Minch University, Ethiopia

Correspondence should be addressed to Mohammad Shabaz; [mohammad.shabaz@amu.edu.et](mailto:mohammad.shabaz@amu.edu.et)

Received 6 April 2021; Revised 23 April 2021; Accepted 30 April 2021; Published 13 May 2021

Academic Editor: Vimal Shanmuganathan

Copyright © 2021 Kriti Mahajan et al. This is an open access article distributed under the Creative Commons Attribution License, which permits unrestricted use, distribution, and reproduction in any medium, provided the original work is properly cited.

The existing work on unsupervised segmentation frequently does not present any statistical extent to estimating and equating procedures, gratifying a qualitative calculation. Furthermore, regardless of the datum that enormous research is dedicated to the advancement of a novel segmentation approach and upgrading the deep learning techniques, there is an absence of research comprehending the assessment of eminent conventional segmentation methodologies for HSI. In this paper, to moderately fill this gap, we propose a direct method that diminishes the issues to some extent with the deep learning methods in the arena of a HSI space and evaluate the proposed segmentation techniques based on the method of the clustering-based profound iterating deep learning model for HSI segmentation termed as CPIDM. The proposed model is an unsupervised HSI clustering technique centered on the density of pixels in the spectral interplanetary space and the distance concerning the pixels. Furthermore, CPIDM is a fully convolutional neural network. In general, fully convolutional nets remain spatially invariant preventing them from modeling position-reliant outlines. The proposed network maneuvers this by encompassing an innovative position inclined convolutional stratum. The anticipated unique edifice of deep unsupervised segmentation deciphers the delinquency of oversegmentation and nonlinearity of data due to noise and outliers. The spectrum efficacy is erudite and incidental from united feedback via deep hierarchy with pooling and convolutional strata; as a consequence, it formulates an affiliation among class dissemination and spectra along with three-dimensional features. Moreover, the anticipated deep learning model has revealed that it is conceivable to expressively accelerate the segmentation process without substantive quality loss due to the existence of noise and outliers. The proposed CPIDM approach outperforms many state-of-the-art segmentation approaches that include watershed transform and neuro-fuzzy approach as validated by the experimental consequences.

## 1. Introduction

Recent progress partakes intended for evolving HSI sensors that devour advanced three-dimensional and spectral resolution involving innumerable airborne, UAV, satellite, and pulverized procurement platforms. The effectual exploration of improved continuums and three-dimensional statistics can upgrade recognition of substantial and object acknowledgment applications suggestively by demonstrating and illuminating the elusive dissimilarities in spectral signatures for numerous objects. Distinguishing numerous objects, constituents, and topography terrestrial cover classes constructed on the property of their reflectance can be regarded as the undertaking of classification; i.e., imagery pixel is categorized

based on their spectral physiognomies. However, for an extensive assortment of applications such as astrophysics, scrutiny, agricultural science, and biomedical imaging, HSI is used extensively and has its peculiar inimitable challenges that embrace (i) data partaking extraordinary dimension, (ii) labeled illustrations inadequate in quantity, and (iii) spectral signatures devouring huge three-dimensional inconsistency [1]. The taxonomy of HSI data in the present work surveys unadventurously the archetype of image acknowledgment entailing twofold phases; initially, the computation of multifaceted handcrafted topographies is prepared from the contribution of raw statistics and the features acquired are used for the erudition of classifiers, such as SVM and NN. Particularly, for statistics with a great aspect and the



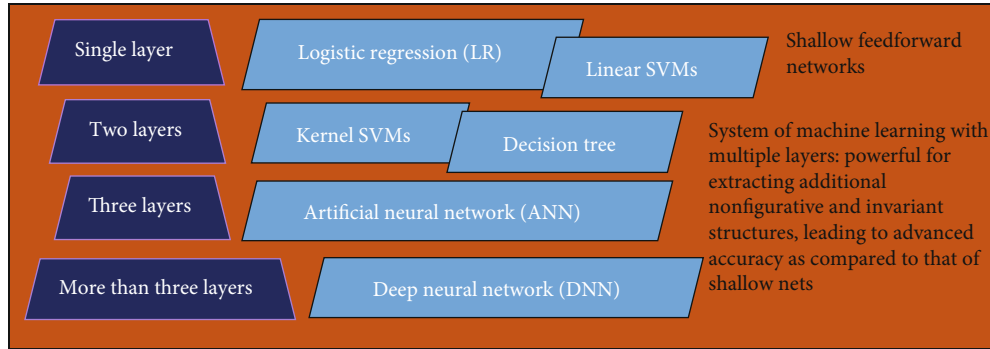


FIGURE 1: From the neural net perception, classifiers are categorized on the basis of layers [4].

obtainability of limited training samples, the engagement of arithmetical erudition approaches is prepared for undertaking the heterogeneity and great dimensionality of HSI data. Nevertheless, for the illustrated substantiality owing to its rich assortment, the prominence of the features is infrequently acknowledged for the undertaking of classification. For the band acknowledgment, in contradiction to the conservative archetype, prototypes of deep learning [2] are a class of machinery that are proficient in erudition of a hierarchy of features as it constructs extraordinary features from low-level ones, in which it programs the feature erection practice for the delinquent imminence. Besides, intended for the datasets that are greater and imageries enormous in magnitude partaking great spectral and three-dimensional firmness, the agenda of deep learning appears to be adequate and address the delinquency of taxonomy efficiently [3]. The encouraging outcomes are presented by methods that were based on deep learning both for precise object discovery, like synthetic ones, and for the HSI data arrangement [3]. A deep learning structure explicitly was engaged in [3] to the HSI data taxonomy presenting relatively favorable outcomes. In particular, autoencoders are preserved as building blocks, and the conception of acquisitive stratum-wise preparation is explored for fabricating a profound structural design to construct a hierarchy of great-level spectral topographies for every pixel. In an isolated step, spectral features were united with three-dimensional subjugated data and then provided to a logistic regression classifier as input.

Intended for the identical scene, the HSI comprises numerous amounts of spectral information. For HSI sensors, the influence to distinguish constituents of concern precisely is delivered by exhaustive spectral statistics with the augmentation in the accurateness of classification. Furthermore, with the progress in HSI technology, for the recently functioned sensors, the adequate three-dimensional resolution benefits from analyzing trivial three-dimensional constructions in imageries. For a widespread application, an expedient tool is the HSI data in the abovementioned progress. The dimensionality of the imageries is amplified in the spectral dominion that contributes to applied and hypothetical complications. The predictable procedure established for multi-spectral data in this way is no longer competent to practice data of high dimensionality typically because of the curse of dimensionality. A vital phase to address the profanity of

dimensionality in HSI dispensation is feature extraction (FE). However, HSI FE is still a perplexing undertaking due to the realistic discrepancy of spectral signatures. For HSI FE, in its initial periods, the emphasis was on spectral-centered procedures. The lined transformation is smeared by these systems for mining features hypothetically for the input data in the new dominion. Concerning the contrivance of multifaceted light smattering of environment objects, intrinsic nonlinearity is unveiled by HSI statistics creating the technique of lined transformation not that appropriate to scrutinize such data. Also, manifold erudition endeavors to determine the essential edifice of data that is circulated nonlinearly, which is auxiliary predictable to be exceedingly convenient for HSI feature abstraction. Instead, the delinquency of nonlinearity is addressed for statistical illustration by kernel-based events. The inventive data is plotted by the kernel techniques into the Hilbert space of extraordinary dimension and proposes likelihood to transform a deviating delinquency to an undeviating one. Contemporary studies partake acclaimed to integrate the three-dimensional statistics into a structure of spectral-based FE. The HSI sensors with the development of imaging expertise can convey virtuous three-dimensional tenacity. The inclusive three-dimensional measurements consequently have turned to be accessible. The process for spectral-spatial FE is established to deliver virtuous advance in terms of enactment in classification as shown in Figure 1. In [4], the three-dimensional measurements besides spectral statistics are mined by the projected structure that customs active learning and loopy belief proliferation. For the protracted morphological attribute silhouette, the sparse illustration [5] is explored integrating three-dimensional data in the taxonomy of HSI in [6] that progresses the accurateness of taxonomy further. In the community of HSI, only solitary stratum dispensation is measured by most of the existing FE approaches that demote the feature erudition dimensions. Maximum classification and FE methods are not constructed in a “deep” way. The solitary layer erudition approaches extensively used are PCA (principal component analysis) and ICA (independent component analysis) [4].

In neuroscience conversely, the graphic structure of a primate humanoid is categorized by a structure of dispensation at a diverse levels and the erudition structure of this kind is achieved appropriately well in the entity acknowledgment

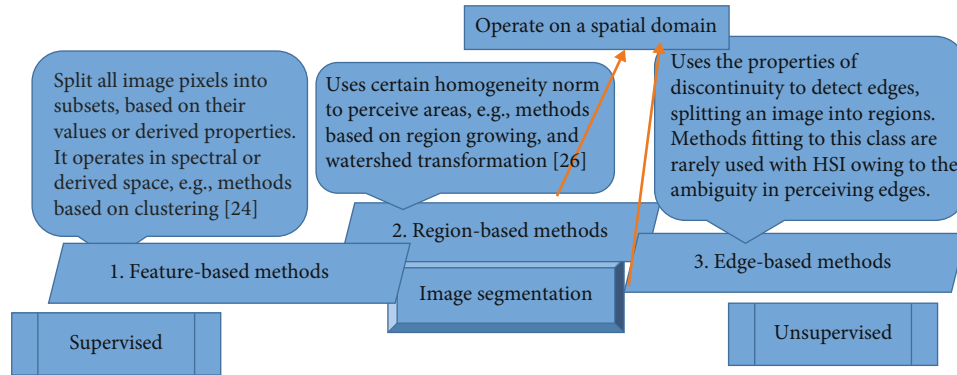


FIGURE 2: Image segmentation method categorization [20].

tasks [7]. The systems established on deep learning comprise two or additional layers for mining new features intended for simulating the method, and these constructions of deep learning have the prospective of acquiescent great performances in target discovery and imagery classification. From the other objects, the undesired sprinkling may distort spectral features of the object of concern. Likewise, aspects like infraclass inconsistency and diverse atmospheric scattering circumstances make it enormously problematic for mining the HSI data topographies efficiently. The deep architecture is acknowledged to be an encouraging choice to address such concerns by a principal to extra-abstract topographies possibly at great intensities that are usually invariant and vigorous. The article is systematized in this manner. Section 2 outlines the common segmentation methods and the era of deep learning in the field of HSI. Section 3 comprehends the followed approach. Sections 4 and 5 encompass experimental outcomes and discussion followed by a conclusion.

## 2. Segmentation in HSI

Image segmentation is the practice of apportioning imagery into associated expanses with standardized properties. Image segmentation intends to abstract areas by isolating imagery into separate arrays of pixel fragments as shown in Figure 2. In the arena of HSI, it accelerates the tranquil exploration of HSI statistics. It can likewise be exploited to perceive uncharacteristic objects and improve HSI data compression enactment [8]. Convex conduit exploration is anticipated in [9] to segment HSI. Multithresholding, isocustering, and histogram-centered methods of the subdivision are smeared to the spectral index illustration [10]. An eigen expanse-centered splitting up is projected in [11] for the persistence of compression. The separation of HSI statistics into fragments centered on the histogram of the primary elements is undertaken in [12]. Unsupervised HSI data itemization by subjective incremental NN cantered neuro-fuzzy structures is recommended in [13]. The  $K$ -means process is an engrained unsupervised way for imagery breakdown, and the exploitation of the  $K$ -means reassembling process for HSI subdivision is offered in [14]. HSI separation by a multi-constituent veiled Markov chain archetype is recommended in [15]. An arithmetical HSI division tactic created on Gaussian assortment prototypes is undertaken in [16]. In [17], the

texture data is anticipated to append through filter arrays to upsurge HSI segmentation precision. Bayesian separation of HSI via hidden Markov forming is undertaken in [18]. Recently, it is presented that the level correspondence of sub-tested visualizations denoted as adapted phase association is successfully used to differentiate analogous and disparate imageries and, consequently, delivers a proficient methodology for firm amended exposure in documenting film systems pretentious by noise and supplementary artifacts, and the subsampling of imageries progresses vigor counter to noise along with worldwide and native disparities [19].

Segmentation is a comprehensive segregation of the participating imageries into standardized expanses. Segmentation procedures are a prevailing tool to delineate three-dimensional necessities. Unsupervised breakdown of HSI is exploited to outline three-dimensional structures using watershed, partitioned clustering, and hierarchical subdivision practices [21]. A watershed transmute [22] cogitates a grayscale illustration as a topographic liberation. The water bases are situated at the extremity facts of purported catchment sinks. To subdivide an image by this transmute, begin by probing the native minima of the incline. Though a huge volume of clustering procedures is projected, the eminent  $k$ -means process [23] is the furthestmost regularly used methodology. In [24], it is used with the aligned Euclidean expanse degree. To reset cluster epicenters, the  $k$ -means++ algorithm is used. It is revealed that it accomplishes earlier conjunction to an inferior native minimum. By devouring frontiers, an image hike practice is exploited to abstract associated expanses inside precincts. Lastly, the respective periphery pixel is categorized to one of the contiguous areas by adjacent neighbor imperative. The foremost concern of this transmute for HSI entails gradient calculation [25]. Segmentation and pixel astute taxonomy are accomplished autonomously, and the products are united by a popular elective imperative. Thus, each expanse commencing a separation plot is reflected as an adaptive consistent region for entirely the pixels in this area. This method led to a significant enhancement of organization precisions and delivered additional consistent taxonomy plots when associated with taxonomy practices by native regions to embrace three-dimensional data into a classifier as shown in Figure 3. Nevertheless, an unsupervised imagery subdivision is a stimulating undertaking. Subdivision purposes at isolating an image into identical

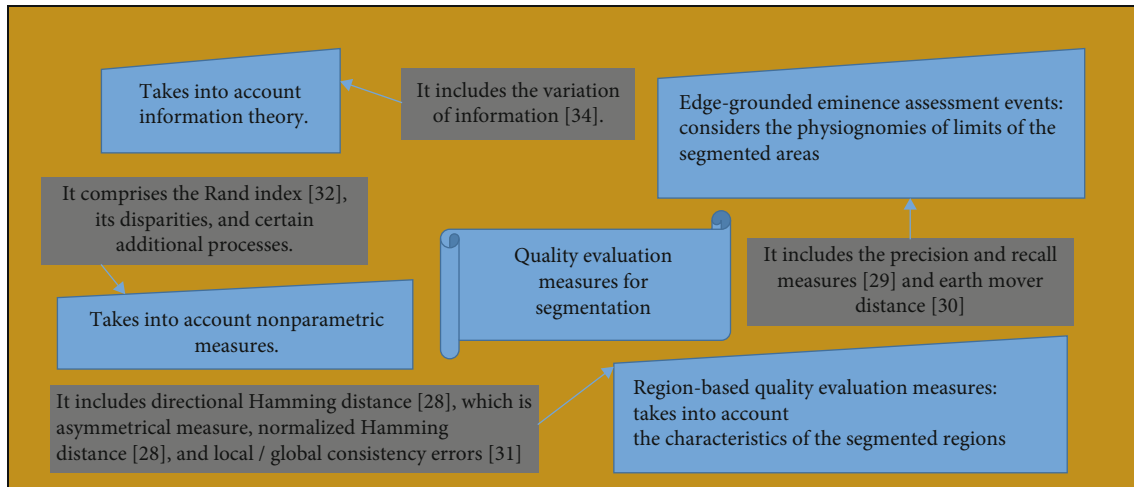


FIGURE 3: Quality evaluation measurement for segment images on different constraints.

areas; however, the extent of homogeneousness is image reliant [26]. Conditional on this quota, the practice results in undersegmentation; i.e., numerous areas are perceived as one or over segmentation; i.e., a single area is perceived as numerous ones of the image. In [27], oversegmentation is favored over undersegmentation to avoid omitting entities in the taxonomy plot. Further to reduce oversegmentation, markers or area seeds are used [28]. In the aforementioned studies, an interior marker is demarcated as an allied constituent owing to the illustration and concomitant with an entity of importance [29].

**2.1. DL in HSI.** Ever since the initial period of the sixties, while Robert's verge operative was presented, computer visualization investigators were operational on planning numerous object acknowledgment structures. The objective is to project an endways mechanized structure merely consenting two-dimensional, three-dimensional, or video contributions and give the class labels or physiognomy of objects. Commencement with template equivalent tactics in the seventies, techniques established on inclusive and native silhouette descriptors was established. Also, procedures constructed on demonstrations for instance Fourier descriptors, instants, Markov prototypes, and arithmetical array recognizers were established. In the initial years, the prerequisite for creating the global acknowledgment methodologies be invariant to numerous alterations such as scale, rotation, etc. are documented. Contrasting these comprehensive descriptors, native descriptors founded on primitives like contour fragments, arches, etc. are used in both physical and syntactic array acknowledgment machines. In the eighties, arithmetical array acknowledgment approaches controlled constrictions and symmetrical illustrations. Graph equivalent or relaxation methods became standard for exploiting complications such as fractional entity equivalent. In the mid of this phase, three-dimensional assortment data of entities became accessible prominent to apparently centered descriptors, hedge limits, and crumple edges. These illustrations certainly directed to graph centered or physical equivalent procedures. Additional methods centered on elucidation trees generated a class of

processes for entity acknowledgment. The philosophy of invariants is widespread to distinguishing entities over enormous perspectives. Although these methodologies were being industrialized, techniques built on ANNs came into existence. The occurrence of ANNs is essentially encouraged by the anticipation engendered by the Hopfield complex's capability to explore the peripatetic salesman delinquency and the reawakening of the back proliferation process for training the ANNs. Computer visualization researchers conveyed the perception that demonstrations resulting from symmetrical, photometric along with human revelation arguments of interpretation are precarious for the accomplishment of entity acknowledgment structures. The tactic of merely feeding imageries into a three-layer ANN and receiving the labels obtainable by training data is not alluring to furthestmost computer visualization researchers. Moreover, computer visualization researchers are further concerned with three-dimensional entity acknowledgment complications and not in areas where the ANNs are functional.

A nonintrusive method is the HSI that accumulates profuse three-dimensional and spectral statistics concurrently of pragmatic expanses. For the HSI statistics, correctness of classification is vital for numerous applications. Though, the eminent dimensionality curse resulting from the tremendously enormous spectral channels making the classification considerably stronger than multispectral imageries. The enactment of customary classification structure is depreciated by the inadequate labeling illustrations and the spectral signature that differs radically. A foremost revolution is perceived by the last era on neural computing especially in the area of deep learning. The objective of this process is to acquire manifold altitudes of illustration that are typically cavernous than 3 layers, and the plotting is done commencing input to output unswervingly from the statistics. To vintage prodigious enactment, deep structural designs are employed and verified in several areas as discussed in Figure 4. DL is a recently established method aiming for artificial intelligence. DNN can epitomize convoluted data. Nevertheless, it is appropriately challenging to train the network. Owing to the deficiency of an appropriate training procedure,

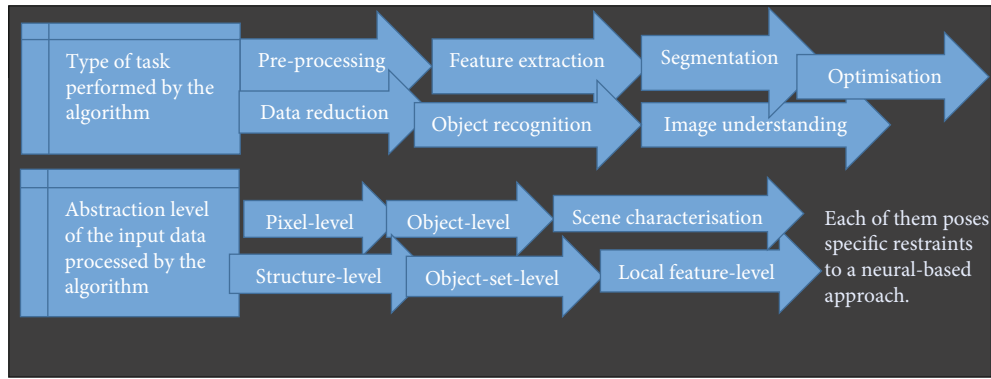


FIGURE 4: A new two-dimensional categorization for imagery dispensation procedures categorized on various applications.

it was challenging to confer this influential archetypal until the notion of deep learning was projected. It encompasses a class of prototypes that attempt to acquire manifold stages of data illustration, which benefits yielding the gain of input data. This benevolence of erudition signifies the abstraction and invariant topographies, favorable for an extensive assortment of tasks. DL is a fragment of an extensive family of machine erudition procedures based on erudition demonstrations of statistics. A reflection is epitomized in sundry customs such as a vector of concentration tenets per pixel, or a more intangible manner as a customary of edges, regions of a specific shape, etc. It pursues to explore the anonymous edifice in the input dispersal to determine virtuous depictions, frequently at manifold levels, by advanced level erudite features demarcated in terms of inferior level topographies. The aim is to make them additionally abstract, with their distinct features [2]. Then, these revealed features are extra invariant to utmost disparities that are archetypally existent in the training dispersal, while mutually conserving copiously the data in the input. DL processes like CNN and convolutional AE have been successfully applied in computer vision. CNN was developed by LeCun and its allies. CNN [30] is encompassed of single or additional convolutional stratum and then followed by solitary or extra effusively allied layers as in a regular multilayer NN. The architecture of a CNN is intended to yield the benefit of the 2D edifice of an input image. This is accomplished with local associates and tangled weights tailed by certain custom of pooling that consequences in paraphrase invariant features. Additional advantage of CNNs is that they are tranquil to train and have various scarcer constraints than fully allied networks with the similar amount of hidden units. In [29] the solicitation of supervised CNN is explored, one of the deep prototypes in HSI FE, and a 3-D CNN archetypal is established for operational spectral and three-dimensional HSI arrangement. Smearing deep learning to HSI is perplexing as the quantity of training illustrations is inadequate and the statistics structure is multifaceted. The quantity of training illustrations in computer visualization diverges from thousands to millions; however, in HSI remote sensing taxonomy, it is not common to partake such a huge amount of training illustrations. Overall, an influential demonstration ability is presented by a NN with copious training sections. The difficulty of “overfitting”

is encountered by the NN, lacking adequate training illustrations which means that performance of taxonomy for the test statistics will be relegated. Once deep learning is smeared to data tenuously sensed, this delinquency is anticipated; however, an elucidation is offered to create such tactics viable to conditions when the accessibility of training illustrations is inadequate. A process of DL-based taxonomy is projected contrary to these methodologies that create extraordinary level structures hierarchically in a computerized manner. It explores CNN for encrypting pixels three-dimensional and spectral statistics and a Multilayer Perceptron for piloting the undertaking of classification. [31].

The mechanism of multifaceted light scattering in regular entities, the situation of diverse atmospheric scattering, and intraclass inconsistency make the process of HSI fundamentally nonlinear. The deep architecture as assumed leads to additional intellectual features gradually at advanced layers of topographies and the topographies that are further intellectual are invariant all together to furthestmost local variations of the input. The design of DNN typifies deep learning. DNN delivers a classified portrayal if premeditated and proficient appropriately for the input statistics in terms of tranquil to deduce and pertinent topographies at each layer. In [32], for the taxonomy of HSI data, a DBN-based feature abstraction is projected. For obtaining power weights, there is a prerequisite for an allocation of training trials in the training process [33]. Several samples are necessitated by the practice of conformist feature assortment to evaluate statistics precisely [34]. Furthermore, the extensive pursuit customs the foundation of utmost methods to discover the finest feature set amongst the entire dimensionality that entails a massive CPU time and many RAMs to primarily conclude efficaciously [34]. The abovementioned concerns are addressed with the innovative feature assortment inclination based on the methods of evolutionary-based optimization like PSO and GA [35]. In [36], the custom of GA is done to normalize hyperplane constraints of an SVM, while discovering effectual topographies to be served to the classifier. PSO has a drawback of precipitate conjunction of the swarm because of the following reasons: the conjunction of the element to a solitary point situated on a line concerning the personal preeminent and the global finest locations. Nevertheless, this point is not assured to be a native optimum,

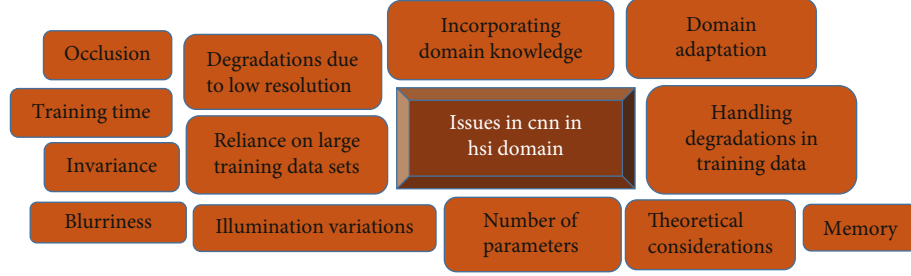


FIGURE 5: Issues in CNN.

and the debauched level of data drift prominent to the formation of analogous elements, resultant in the loss in assortment [34]. In [37], for feature assortment, a procedure is projected centered on fractional order Darwinian PSO (FODPSO) to determine the chief limitation of the PSO which is the same as that of PSO. Still, many issues remain to be addressed as shown in Figure 3 to make the CNN-based recognition systems robust and practical. These are briefly discussed below in Figure 5.

The dominant concern among HSI solicitation is classification. Nevertheless, utmost approaches agonize from the curse of dimensionality owing to the eminent Hughes phenomenon and depend intensely on the outmoded dimensional decline like PCA. To conflict with the Hughes phenomenon, several researchers have published their methodologies; every pixel is preserved distinctly by the traditional methods [38] and is characterized solitary by continuum signatures. For the taxonomy, a proficient method (SVM) is undertaken [39], which later ascertained to be a standard system for classification. The technique established on deep learning is initially smeared into HSI taxonomy, and favorable outcomes are accomplished amongst contemporary methods [3]. However, in a model centered on SAE, for keeping a truncated simplification and restoration error, an elongated epoch period is a prerequisite for the stages of pretraining and adequate regulation. CNN in contrast has stimulating dynamics for mining local feature plots from inferior strata and then allocate them for dispensation of advanced layers. The anticipated structure could remedy the trainable constraints with rising size and sinking the time prominently for adequate tuning lacking classification precision cost. To contemplate three-dimensional statistics mutually for HSI and advancing the precision auxiliary for the sorting tasks, [40], the process of spectral assembling is employed in HSI and some favorable outcomes are already presented on classification applications as shown in Figure 6.

### 3. Proposed Framework for Segmentation Using CNN

A subdivision procedure constructed on a clustering system is relatively forthright. It entails twofold phases. At first, a gathering of imagery pixels is accomplished in an abbreviated space. At this phase, an assembling set of rules divides a customary of imagery pixels into a specific amount of subgroups, rendering to pixels topographies. At the subsequent phase, an

imagery rise process abstracts associated sections of an imagery comprehending pixels of analogous clusters. There are numerous clustering procedures appropriate for the subsequent classes [41]: hierarchical, density-centered, spectral clustering, etc. An unsupervised clustering technique is anticipated established on the pixels density in the spectral interplanetary and the remoteness among pixels in compliance to the profligate concentration uttermost assembling. Aimed at the metric of the compactness, we present an acclimatize bandwidth likelihood thickness utility by pixel quantities as the feedback and the premeditated pixel native thickness as the production, which regulates the bandwidth centered at the Gaussian postulation. For the region, the distance metric is exploited with Euclidean distance to acquire a pixel equivalent spectral distance amid pixel vectors from the manifold bands. The local density  $d_x$  is calculated between every data point.

$$d_x = \sum_y (\rho_{xy} \rho_e), \quad (1)$$

$$\rho_{xy} = \sqrt{(\mathbf{i}_x - \mathbf{i}_y)^2 + (\mathbf{j}_x - \mathbf{j}_y)^2}, \quad (2)$$

where  $\rho_{xy}$  is the Euclidian distance among point  $i$  and the additional points,  $\rho_e$  is the amended distance, and  $d$  and  $\partial$  are the density and distance, respectively, which are prerequisites to be calculated. The shortest distance is calculated owing to the point where it is superior to its local density  $\partial_x$ .

$$\partial_x = \min (\rho_{xy}). \quad (3)$$

Beginning from the twofold variables, the CPIDM process contemplates that the points with an advanced density and a superior distance are cluster epicenters. CPIDM does not essentially postulate a preliminary reiteration midpoint to discover a cluster core, nevertheless in an effusively instinctive manner. The human factors in the CPIDM process, i.e., the threshold  $\rho_e$ , is an empirical assessment, and the purpose of the cluster epicenters is labor-intensive, causing missing data and erroneous points. To improve CPIDM, two problems are solved using CNN. A Gaussian kernel utility is pragmatic in the process. Under the hypothesis, there is a dataset  $I(i_1, i_2, i_3, \dots, i_n)$ ; the frequently explored Gaussian kernel likelihood compactness

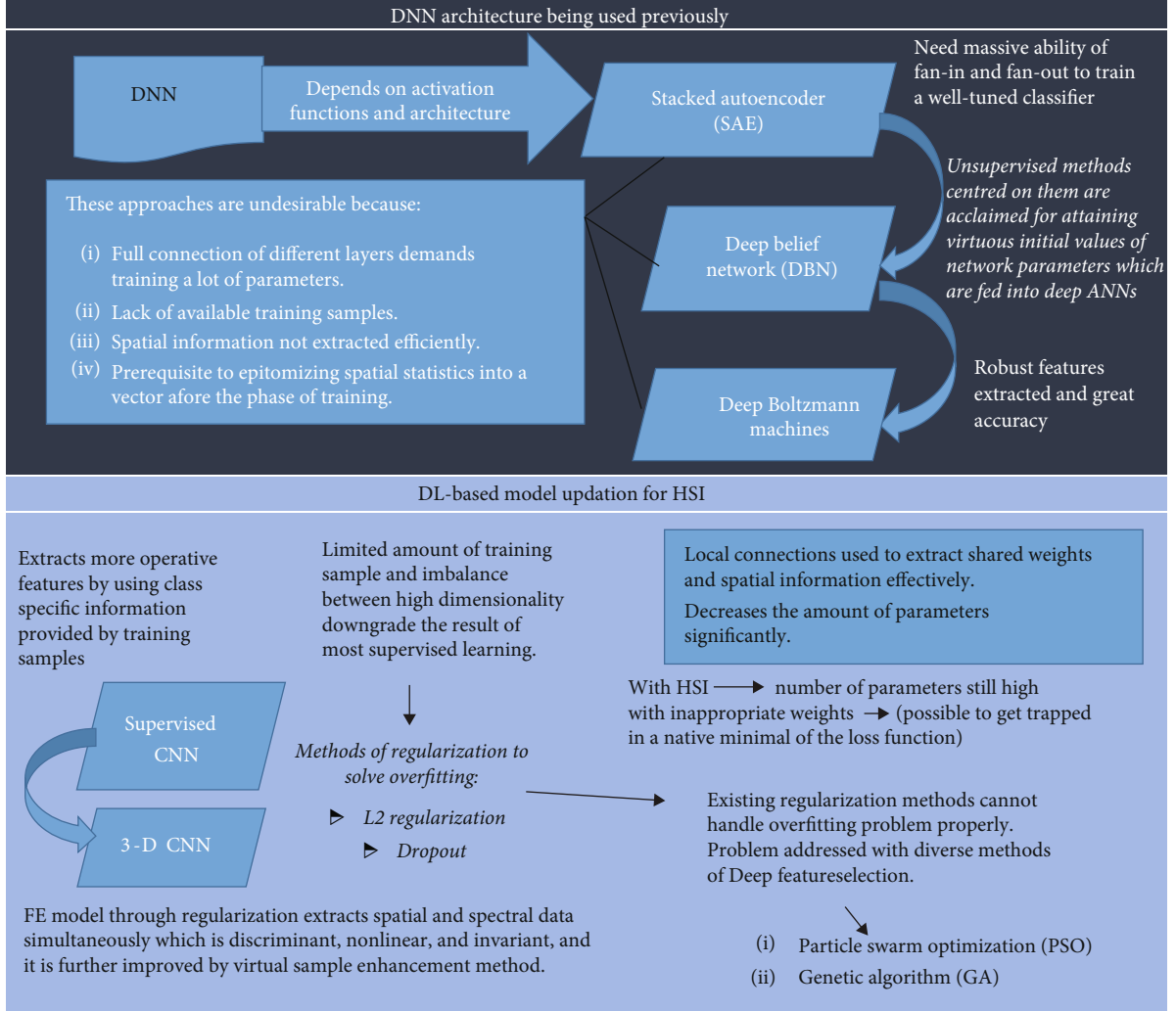


FIGURE 6: The CNN hierarchy in the arena of HSI.

approximation utility, which is assessed by the kernel thickness of the data, is determined as

$$h_{\ell}(\mathbf{i}) = \frac{1}{n\ell} \sum_{x=1}^n \mathfrak{B} \left\langle \frac{\mathbf{i} - \mathbf{i}_x}{\ell} \right\rangle, \quad (4)$$

where  $K(\cdot)$  is the Gaussian kernel utility and  $\ell$  denotes the bandwidth equivalent to the amended expanse  $\mathcal{P}_e$  of the CPIDM. Generally, the  $K(\cdot)$  exploits the assortment of the significance of  $h_{\ell}(\mathbf{i})$  at point  $\mathbf{i}_x$ . The assessment of  $K(\cdot)$  is frequently resolute by the bandwidth  $\ell$ . Inappropriately, the projected segmentation method can yield oversegmented imagery in conformity to the defined causes: an unnecessary amount of clusters and a disproportionate quantity of local minima in the image. To conquer the delinquency of oversegmentation CPIDM employs the spectrum efficacy as it erudite and incidental from united feedback via deep hierarchy with pooling and convolutional strata, as a consequence, it formulates an affiliation among class dissemination and spectral along with three-dimensional features. The central notion of the CPIDM is

to unite contiguous expanses with analogous physiognomies, preliminary by the utmost comparable areas. In the amalgamation process, we customized the neighboring provinces, encompassing statistics on altogether exclusive sets of contiguous areas. Consequently, we determine the correspondence of sections for every pair. Afterward, we situate entirely mined sets into a precedence queue so that sets of analogous expanses have advance primacy in the queue. Lastly, we reiteratively eliminate sets with uppermost precedence from the queue, combine equivalent expanses of imagery, and update statistics in the queue. Let  $\mathcal{E}_{\mathbf{r}}$  epitomize weights of  $\mathbf{r}^{\text{th}}$  filter in a convolutional layer and  $z_{\mathbf{r}}$  denote its preconceived notion. Let the feature vector at three-dimensional position  $(\mathcal{P}, \mathcal{Q})$  in the input splotch to this layer be  $\mathcal{A}(\mathcal{P}, \mathcal{Q})$  and the  $\mathbf{r}^{\text{th}}$  filter's response be  $\mathcal{U}_{\mathbf{r}}(\mathcal{P}, \mathcal{Q})$ . Therein the convolution maneuver is exemplified as

$$\mathcal{U}_{\mathbf{r}}(\mathcal{P}, \mathcal{Q}) = \mathbf{u} \left( \sum_{a, \beta} (\mathcal{A}(\mathcal{P} + a, \mathcal{Q} + \beta) \bullet \mathcal{E}_{\mathbf{r}}(a, \beta) + z_{\mathbf{r}}) \right), \quad (5)$$

TABLE 1: Number of training in addition to the test samples employed for the University of Pavia dataset.

Class name	Number	Training	Testing	Watershed transform [22]	NN cantered neuro-fuzzy approach [13]	Proposed CPIDM
Asphalt	6631	2210	4421	77.70	86.46	89.26
Meadows	18649	6216	12433	75.30	90.17	91.49
Gravel	2099	699	1400	77.27	85.04	88.37
Trees	3064	1021	2043	92.46	96.64	96.24
Painted metal sheets	1345	448	897	99.63	99.78	99.81
Bare soil	5029	1676	3353	79.50	92.39	94.89
Bitumen	1330	443	887	92.86	94.95	95.94
Self-blocking bricks	3682	1227	2455	76.45	85.36	90.44
Shadows	947	14291	28521	99.62	99.65	99.89

where  $\bullet$  symbolizes the dot product and  $\mathbf{U}$  denotes the ReLU nonlinearity. Now, the weights  $\mathcal{G}_r$  and the bias  $z_r$  are entirely autonomous of the position  $(p, q)$  on which they function, exploiting the convolutional maneuver position invariant. Familiarizing three-dimensional enslavement unswervingly by exploring the filter weights a utility of the three-dimensional coordinates will upsurge the number of stratum constraints intensely. Position precise intricacy where kernels are a utility of position functions virtuous for circumstances has unswerving advent at every position. Nevertheless, no such evenness of appearance embraces saliency. It correspondingly serves contrary to the norm of encumbrance partaking in CPIDM which is reflected as an imperative motive for its efficacy in image segmentation. We resolve this delinquency by concatenating a data autonomous and position explicit feature  $\mathcal{S}(p, q)$  to the prevailing input feature  $\mathcal{A}(p, q)$ . This upshot a great intensification in the number of stratum constraints and is independent of the input splotch's three-dimensional dimensions.

$$\mathcal{U}(\mathcal{A}(p, q)) = \mathbf{U} \left( \sum_{a, b} \left( \mathcal{A}(p+a, q+b) \bullet \mathcal{G}_r(a, b) + \mathcal{S}(p+a, q+b) \bullet \mathcal{G}'_r(a, b) + z_r \right) \right). \quad (6)$$

While the position explicit features,  $\mathcal{S}(p, q)$  endure persistent over the whole training process, the weights of a filter operational on it,  $\mathcal{G}'_r$ , are erudite overtraining. This qualifies the system to superlatively syndicate feedback impetuses with its position statistics for prophesying the concluding saliency plot.

#### 4. Results

CPIDM, is a fully convolutional structural design for extravagant image dispensation entrenching, an erudition framework that is validated in this section for effectually exploring deep learning for HSI segmentation. It is reciprocated to devour great consistency, precision, and speed. In this segment, we delineate the consequences of the investigational study rendering to the wide-ranging arrangement

demarcated in the third segment. In our experimentations, we exploited vulnerable and eminent HSI remote sensing prospects. Here we deliver investigational outcomes for the Indian Pines scene, assimilated by AVIRIS sensor and University of Pavia dataset. Indian Pines imagery encompasses  $145 \times 145$  pixels in 224 spectral bands. Only 180 bands were elected by eradicating bands with the truncated level of noise in addition to the outlier. The University of Pavia dataset contains  $610 \times 340$  pixels with 115 spectral bands. The wavelength assortment is 0.537 to 0.91. Owing to issues for instance noise and atmospheric concentration, 23 bands were eliminated and 123 bands were reserved by the unmixing process. The imageries asylums 9 categories of features as depicted in Table 1, based on the University of Pavia dataset, the identical experimental structure is trailed for training set illustrations and test set trials. The dataset, with magnitudes of  $640 * 340$  pixels, covers the Engineering School at the University of Pavia and entails of diverse classes, comprising trees, asphalt, bitumen, gravel, metal sheet, shadow, bricks, meadow, and soil (see Table 1). To evade the institution of surplus noise in the data segregating procedure that can influence the concluding product, the separation of the training and test arrays upholds the uniformity of the data dispersal in a sufficiently potential way. This dataset has comparatively pure images at every band and the illustrations are reasonably even. To attain an adequate elucidation, we speckled the quantity of clusters from 12 to 120. For every quantified quantity of clusters we modified and contended clustering with Monte Carlo runs 15 times (iterations) to acquire the superlative prearrangement obtainable of initializations. Thus, the customary clustering tactic is prolonged for HSI dispensation in a usual manner. This is certified by the capability of assembling systems to exertion in great dimensional spaces. So the vital concerns are the eminence of assembling in a HSI space, and the interval of dispensation, as assembling is a period of intense practice.

#### 5. Discussion

For the permanence of the investigational consequences, the supreme quantity of iterations is scrutinized in this experiment. Moreover, the outcomes of the training archetypal are evaluated via the precision and computational rate of

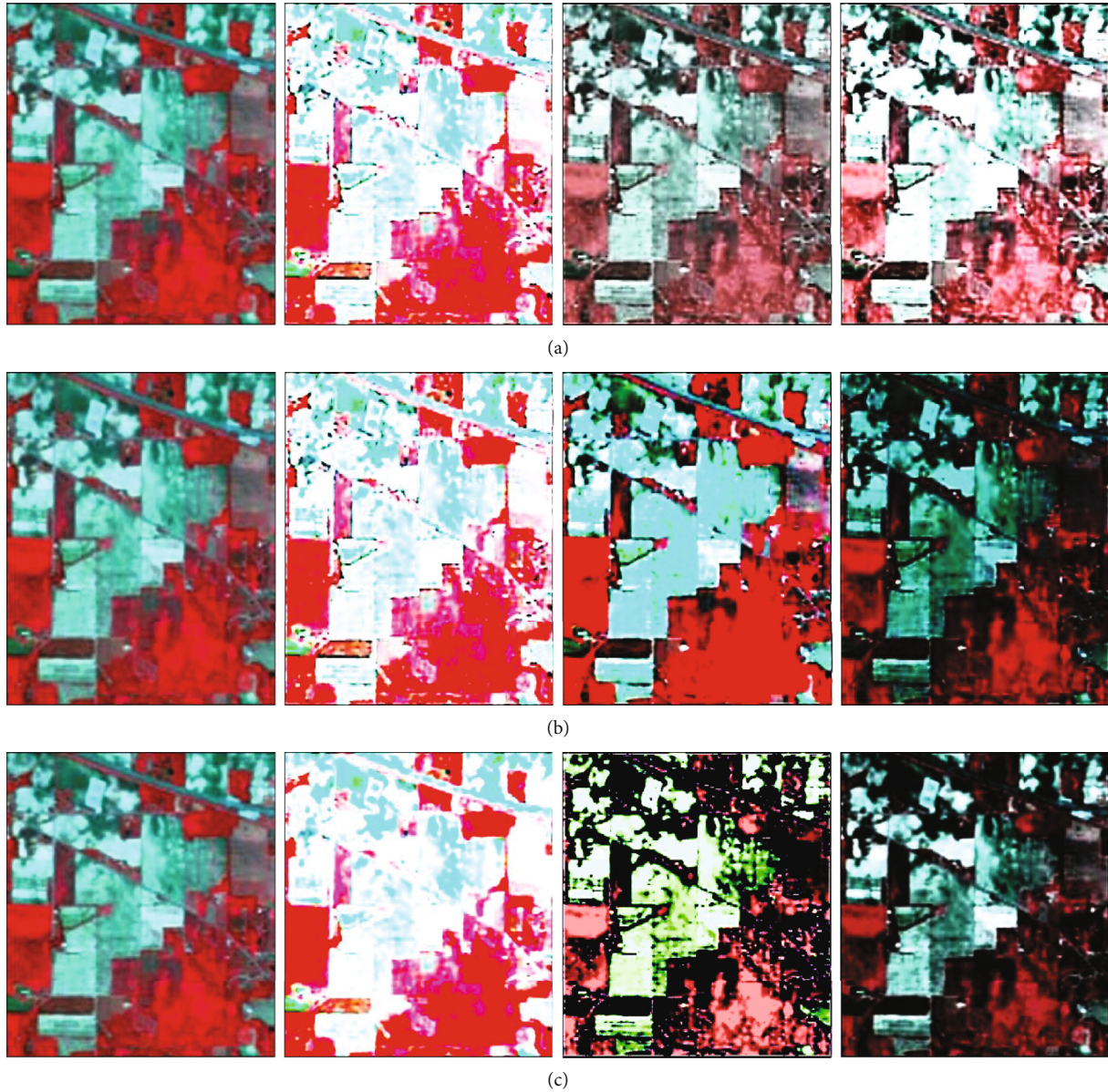


FIGURE 7: Segmentation outcomes attained by diverse approaches for the AVIRIS Indian Pines dataset: (a) watershed transform [22]; (b) NN cantered neuro-fuzzy approach [13]; (c) proposed CPIDM.

the authenticated set. Rendering to numerical examination, as the amount of iterations intensifies, the segmentation accurateness level continues to proliferate, and at that point, it reaches a firm rate. Conferring to the investigational consequences, the correctness inclines to alleviate after 10,850 iterations. Subsequently, for the number of iterations to be 16,500, the accurateness level is flat and the training archetypal had ultimately reached the optimum state, demonstrating that 18,000 iterations are adequate to satisfy the training prerequisites. Therefore, the supreme count of iterations is customized to 18000 times throughout the successive experimentation.

In the experimental procedure as shown in Figures 7(a)–7(c) and 8(a)–8(c), the assessment index of segmentation precision predominantly embraces overall accuracy (OA), average accuracy (AA), and computational time. OA charac-

terizes the proportion of illustrations that are appropriately segmented; AA symbolizes the mediocre of the measurements of appropriately segmented samples in every cluster. To explore the preeminence and subservience of CPIDM and traditional segmentation approaches in extraordinary dimensional, no sample data, such as HSI remote sensing data, we set up relative experiments and compares two regularly used traditional methods, such as watershed transform [22] and NN cantered neuro-fuzzy approach [13]. The training trials are verified in an unbiased manner in a diversity of ways as discussed in Table 2.

## 6. Conclusion

Alongside the spectrum, the spectral interpretations in numerous narrow spectral bands through HSI have delivered



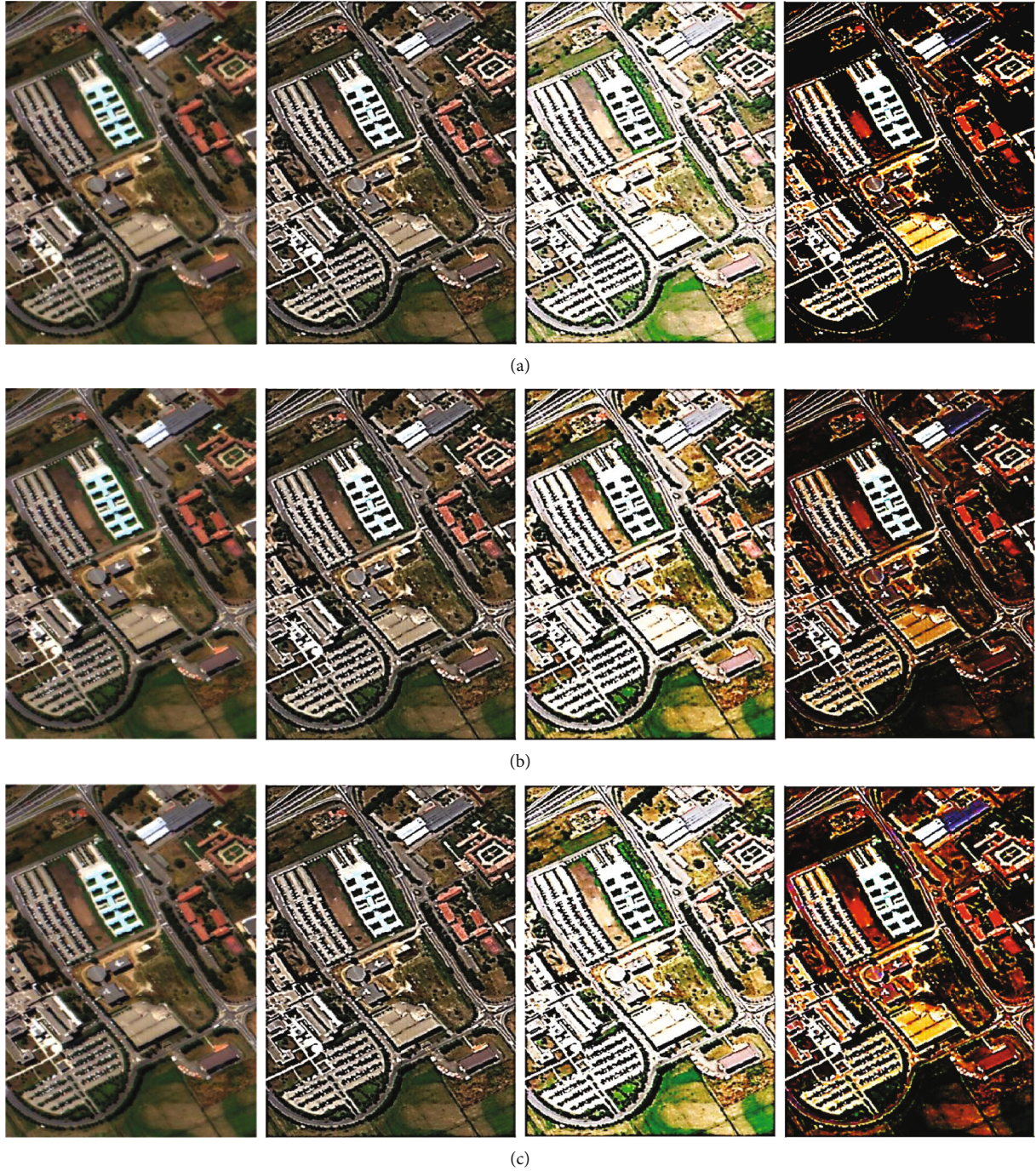


FIGURE 8: Segmentation outcomes attained by diverse approaches for the University of Pavia dataset: (a) watershed transform [22]; (b) NN centered neuro-fuzzy approach [13]; (c) proposed CPIDM.

TABLE 2: Performance evaluation of HSI datasets on various parameters.

Monte Carlo runs = 15	AVIRIS Indian Pines dataset			University of Pavia dataset		
	Watershed transform [22]	Neuro-fuzzy approach [13]	CPIDM	Watershed transform [22]	Neuro-fuzzy approach [13]	CPIDM
OA	86.37	89.58	92.23	86.19	88.09	91.21
AA	78.94	81.02	82.86	70.22	73.52	78.14
Time (s)	0.845	0.765	0.327	0.635	0.596	0.525

privileged information to the entity and physical acknowledgment that can be acknowledged as a segmentation task. A synthesis is prepared for the studies allied to the solicitation of imagery segmentation methods in HSI dispensation and precisely to the solicitation of NN. Lastly, we extend an outlook into the imminent application of neural networks and associate them with innovative advances of CPIDM. In the proposed approach, (1) the unsupervised clustering technique is anticipated established on the pixel density in the spectral interplanetary space and the remoteness among pixels in compliance with the profligate concentration uttermost assembling [42]; (2) the CPIDM process contemplates that the points with an advanced density and a superior distance are cluster epicenters; (3) to conquer the delinquency of oversegmentation, CPIDM employs the spectrum efficacy as it is erudite and incidental from united feedback via deep hierarchy; (4) qualify the system to superlatively syndicate feedback impetuses. Moreover, the deep learning model illustrates that it is potentially favorable to expressively expedite the segmentation process without significant quality loss owing to the occurrence of noise and outliers.

## Data Availability

The data shall be made available on request.

## Conflicts of Interest

The authors declare that they have no conflicts of interest.

## References

- [1] G. Camps-Valls and L. Bruzzone, "Kernel-based methods for hyperspectral image classification," *IEEE Transactions on Geoscience and Remote Sensing*, vol. 43, no. 6, pp. 1351–1362, 2005.
- [2] Y. Lecun, L. Bottou, Y. Bengio, and P. Haffner, "Gradient-based learning applied to document recognition," *Proceedings of the IEEE*, vol. 86, no. 11, pp. 2278–2324, 1998.
- [3] Y. Chen, Z. Lin, X. Zhao, G. Wang, and Y. Gu, "Deep learning-based classification of hyperspectral data," *IEEE Journal of Selected Topics in Applied Earth Observations and Remote Sensing*, vol. 7, no. 6, pp. 2094–2107, 2014.
- [4] Y. Bengio, A. Courville, and P. Vincent, "Representation learning: a review and new perspectives," *IEEE Transactions on Pattern Analysis and Machine Intelligence*, vol. 35, no. 8, pp. 1798–1828, 2013.
- [5] Y. Chen, N. M. Nasrabadi, and T. D. Tran, "Hyperspectral image classification using dictionary-based sparse representation," *IEEE Transactions on Geoscience and Remote Sensing*, vol. 49, no. 10, pp. 3973–3985, 2011.
- [6] B. Song, J. Li, M. D. Mura et al., "Remotely sensed image classification using sparse representations of morphological attribute profiles," *IEEE Transactions on Geoscience and Remote Sensing*, vol. 52, no. 8, pp. 5122–5136, 2014.
- [7] N. Kruger, P. Janssen, S. Kalkan et al., "Deep hierarchies in the primate visual cortex: what can we learn for computer vision?," *IEEE Transactions on Pattern Analysis and Machine Intelligence*, vol. 35, no. 8, pp. 1847–1871, 2013.
- [8] M. Cagnazzo, G. Poggi, and L. Verdoliva, "A comparison of flat and object-based transform coding techniques for the compression of multispectral images," in *IEEE International Conference on Image Processing 2005*, pp. 657–660, Genova, Italy, 2005.
- [9] A. Ifarraguerri and C.-I. Chang, "Multispectral and hyperspectral image analysis with convex cones," *IEEE Transactions on Geoscience and Remote Sensing*, vol. 37, no. 2, pp. 756–770, 1999.
- [10] S.-E. Qian, A. B. Hollinger, D. Williams, and D. Manak, "Vector quantization using spectral index-based multiple subcodebooks for hyperspectral data compression," *IEEE Transactions on Geoscience and Remote Sensing*, vol. 38, no. 3, pp. 1183–1190, 2000.
- [11] L. Chang, "Multispectral image compression using eigenregion-based segmentation," *Pattern Recognition*, vol. 37, no. 6, pp. 1233–1243, 2004.
- [12] J. Silvermann, S. R. Rotman, and C. E. Cafer, "Segmentation of hyperspectral images from the histograms of principle components," in *Imaging Spectrometry VIII*, vol. 4816, pp. 270–277, Nov. 2002.
- [13] H. H. Muhammed, "Unsupervised hyperspectral image segmentation using a new class of neuro-fuzzy systems based on weighted incremental neural networks," in *Applied Imagery Pattern Recognition Workshop, 2002. Proceedings*, pp. 171–177, Washington, DC, USA, Oct. 2002.
- [14] A. Sharma, M. D. Ansari, and R. Kumar, "A comparative study of edge detectors in digital image processing," in *2017 4th International Conference on Signal Processing, Computing and Control (ISPCC)*, pp. 246–250, Solan, India, 2017.
- [15] G. Mercier, S. Derrode, and M. Lennon, "Hyperspectral image segmentation with Markov chain model," in *IGARSS 2003. 2003 IEEE International Geoscience and Remote Sensing Symposium. Proceedings (IEEE Cat. No.03CH37477)*, vol. 6, pp. 3766–3768, Toulouse, France, Jul. 2003.
- [16] N. Acito, G. Corsini, and M. Diani, "An unsupervised algorithm for hyperspectral image segmentation based on the Gaussian mixture model," *IGARSS 2003. 2003 IEEE International Geoscience and Remote Sensing Symposium. Proceedings (IEEE Cat. No.03CH37477)*, vol. 6, pp. 3745–3747, 2003.
- [17] P. S. Hong, L. M. Kaplan, and M. J. T. Smith, "Hyperspectral image segmentation using filter banks for texture augmentation," in *IEEE Workshop on Advances in Techniques for Analysis of Remotely Sensed Data, 2003*, pp. 254–258, Greenbelt, MD, USA, 2003.
- [18] A. Mohammadpour, O. Féron, and A. Mohammad-Djafari, "Bayesian segmentation of hyperspectral images," in *AIP Conference Proceedings*, pp. 541–548, Maxent Workshop, Jul. 2004.
- [19] C. Sharma, A. Bagga, B. K. Singh, and M. Shabaz, "A novel optimized graph-based transform watermarking technique to address security issues in real-time application," *Mathematical Problems in Engineering*, V. Kumar, Ed., vol. 2021, Article ID 5580098, 27 pages, 2021.
- [20] K. S. Fu and J. K. Mui, "A survey on image segmentation," *Pattern Recognition*, vol. 13, no. 1, pp. 3–16, 1981.
- [21] Y. Tarabalka, J. Chanussot, J. A. Benediktsson, J. Angulo, and M. Fauvel, "Segmentation and classification of hyperspectral data using watershed," in *IGARSS 2008 - 2008 IEEE International Geoscience and Remote Sensing Symposium*, pp. III-652–III-655, Boston, MA, 2008.

- [22] S. Beucher and C. Lantuejoul, *Use of Watersheds in Contour Detection*, International Workshop Image Processing, Real Time Edge and Motion Detection/Estimation, 1979.
- [23] S. P. Lloyd, "Least squares quantization in PCM," *IEEE Transactions on Information Theory*, vol. 28, no. 2, pp. 129–137, 1982.
- [24] D. Arthur and S. Vassilvitskii, "K-means++: the advantages of careful seeding," in *SODA'07 Proceedings of the Eighteenth Annual ACM-SIAM Symposium on Discrete Algorithms 2007*, pp. 1027–1035, 2007.
- [25] M. Meil m, K. Warmuth, "Comparing clusterings by the variation of information," *Learning Theory and Kernel Machines*, LNCS, B. Sch olkopf, Ed., p. 2777, 2003.
- [26] R. Gonzalez and R. Woods, *Digital Image Processing*, Prentice-Hall, Englewood Cliffs, NJ, 2nd Edition edition, 2002.
- [27] J. Dogra, S. Jain, A. Sharma, R. Kumar, and M. Sood, "Brain tumor detection from MR images employing fuzzy graph cut technique," *Recent Advances in Computer Science and Communications*, vol. 13, no. 3, pp. 362–369, 2020.
- [28] P. Soille, *Morphological Image Analysis*, Springer Verlag, New York, 2nd Edition edition, 2003.
- [29] G. Noyel, J. Angulo, and D. Jeulin, "Morphological segmentation of hyperspectral images," *Image Analysis & Stereology*, vol. 26, no. 3, pp. 101–109, 2007.
- [30] T. Han and D. G. Goodenough, "Investigation of nonlinearity in hyperspectral imagery using surrogate data methods," *IEEE Transactions on Geoscience and Remote Sensing*, vol. 46, no. 10, pp. 2840–2847, 2008.
- [31] K. Makantasis, K. Karantzas, A. Doulamis, and N. Doulamis, "Deep supervised learning for hyperspectral data classification through convolutional neural networks," in *2015 IEEE International Geoscience and Remote Sensing Symposium (IGARSS)*, pp. 4959–4962, Milan, Italy, Jul 2015.
- [32] Y. Chen, X. Zhao, and X. Jia, "Spectral-spatial classification of hyperspectral data based on deep belief network," *IEEE Journal of Selected Topics in Applied Earth Observations and Remote Sensing*, vol. 8, no. 6, pp. 2381–2392, 2015.
- [33] A. Krizhevsky, I. Sutskever, and G. E. Hinton, "ImageNet classification with deep convolutional neural networks," *Communications of the ACM*, vol. 60, no. 6, pp. 84–90, 2012.
- [34] J. A. Benediktsson and P. Ghamisi, *Spectral-Spatial Classification of Hyperspectral Remote Sensing Images*, Artech House, Boston, MA, USA, 2015.
- [35] P. Ghamisi and J. A. Benediktsson, "Feature selection based on hybridization of genetic algorithm and particle swarm optimization," *IEEE Geoscience and Remote Sensing Letters*, vol. 12, no. 2, pp. 309–313, 2015.
- [36] Y. Bazi and F. Melgani, "Toward an optimal SVM classification system for hyperspectral remote sensing images," *IEEE Transactions on Geoscience and Remote Sensing*, vol. 44, no. 11, pp. 3374–3385, 2006.
- [37] P. Ghamisi, M. S. Couceiro, and J. A. Benediktsson, "A novel feature selection approach based on FODPSO and SVM," *IEEE Transactions on Geoscience and Remote Sensing*, vol. 53, no. 5, pp. 2935–2947, 2015.
- [38] G. Camps-Valls, D. Tuia, L. Bruzzone, and J. A. Benediktsson, "Advances in hyperspectral image classification: earth monitoring with statistical learning methods," *IEEE Signal Processing Magazine*, vol. 31, no. 1, pp. 45–54, 2014.
- [39] F. Melgani and L. Bruzzone, "Classification of hyperspectral remote sensing images with support vector machines," *IEEE Transactions on Geoscience and Remote Sensing*, vol. 42, no. 8, pp. 1778–1790, 2004.
- [40] N. D. Cahill, W. Czaja, and D. W. Messinger, "Schroedinger eigenmaps with nondiagonal potentials for spatial-spectral clustering of hyperspectral imagery," *Algorithms and Technologies for Multispectral, Hyperspectral, and Ultraspectral Imagery XX*, M. Velez-Reyes and F. A. Kruse, Eds., vol. 9088, p. 908804, 2014.
- [41] F. C. Monteiro and A. C. Campilho, "Distance measures for image segmentation evaluation. Numerical analysis and applied mathematics ICNAAM 2012," *AIP Conference Proceedings*, vol. 1479, pp. 794–797, 2012.
- [42] C. Sharma, B. Amandeep, R. Sobti, T. K. Lohani, and M. Shabaz, "A secured frame selection based video watermarking technique to address quality loss of data: combining graph based transform, singular valued decomposition, and hyperchaotic encryption," *Security and Communication Networks*, vol. 2021, 19 pages, 2021.